



UNIVERSITY OF PRETORIA
UNIVERSITEIT VAN PRETORIA

Qualitative and quantitative gas chromatography-mass
spectrometry analysis of the principal toxic constituents of some
South African plants in human biological fluid

by

Willem Johannes Rudolph

Submitted in fulfilment of the requirements for the degree

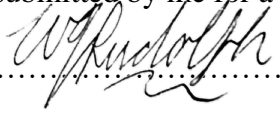
MAGISTER SCIENTIA CHEMISTRY

in the Faculty of Natural & Agricultural Sciences
University of Pretoria
Pretoria
15 December 2020

Supervisors:
Dr JB Laurens
Prof VJ Maharaj

Declaration

I, Willem Johannes Rudolph, declare that the dissertation, which I hereby submit for the degree Magister Scientia in Chemistry at the University of Pretoria, is my own work and has not previously been submitted by me for a degree at this or any other tertiary institution.

SIGNATURE:

DATE: 2020-12-15

Dedication

I dedicate this research to my family (Fanie, Alta and Nardus) who introduced me to the world of natural sciences.

Acknowledgements

To have achieved this milestone in my life, I would like to express my sincere gratitude to the following people:

- My supervisors: Dr JB Laurens and Prof VJ Maharaj.
- My family, for every late night you stayed up and supported me
- The staff of the Chemistry Department at the University of Pretoria for their aid in using the instrumentation and data analysis systems.
- The honours students I mentored during my project.
- Profs. CJ Botha and N Duncan, from the Faculty of Veterinary Sciences, for advice on plants that have a significant impact on agriculture.
- Ms Lettie Nortjie, for allowing me to use her cultivated *G. superba* in my research.
- Dr Hester Oosthuizen for her editorial work in my thesis.
- All those who have supported me in my work and given me hope and encouragement.

Abstract

In South Africa there are regular cases of human and animal poisoning where plants used in ethnic medicine are suspected to be the source of the poison. This project aims to develop methods for identifying *and* quantifying the principal toxins of four such plants in human urine. In this way a steppingstone for further research and development on this subject is produced.

This project focuses on toxins from four plants that fall into two broad classes of compounds: cardiac glycosides (*Acokanthera oppositifolia* and *Urginea sanguinea*) and alkaloids (*Boophane disticha* and *Gloriosa superba*). The principal toxic compounds within the respective plants are: acovenoside A, scillaren A, buphanidrine and colchicine. In this study, buphanidrine was isolated from a dichloromethane-methanol plant extract of *B. disticha*, through the utilisation of multiple chromatographic techniques, and its structure confirmed by nuclear magnetic resonance spectroscopy and high-resolution mass spectrometry.

Samples of known analyte concentrations were prepared by spiking blank urine samples with specific amounts of analyte stock solution. Extraction of colchicine and cardiac glycosides from urine was accomplished by solid-phase extraction. The extracted cardiac glycosides were hydrolysed in hydrochloric acid and the reaction products extracted via liquid-liquid extraction. Following extraction, the products of the hydrolysis reaction were silylated for gas chromatography-mass spectrometry analysis.

Extracts from urine samples containing colchicine were prepared without a hydrolysis process. Urine samples spiked with buphanidrine were prepared by buffering to alkaline pH, and subsequently conducting a liquid-liquid extraction. The organic phase extracts for both alkaloids were concentrated by evaporation and reconstitution in a small volume of an organic solvent. Both alkaloids were analysed without derivatisation following up-concentration.

Response models were generated by duplicate analyses of three batches of each analyte in a de-ionised aqueous solution and urine, respectively. The applicability of the linear response models to the measured data was evaluated for each respective analyte. The relative standard deviation was evaluated to establish the variance in the linear models. The response models, developed for colchicine, acovenoside A and scillaren A, were problematic and further investigated to determine the contributing factors. In the case of colchicine and acovenoside A, the utilisation of log-linear response models was less problematic in describing the trends in the data.

In analysing the trends in the processed data, the limits of detection and quantification were calculated statistically for buphanidrine, acovenoside A and colchicine. These were then compared to limits observed in the qualitative analysis of the analytes based on ion ratios. For each analyte five characteristic ion ratios were selected, considering the molecular ion signal area, relative to that of the base peak ion for each analyte. Applying multivariate Gaussian statistical analysis techniques, the correlation of ion ratios and their dependence upon analyte concentration was established. This proved insightful regarding the mechanism of analyte fragmentation.

Suggested further work, following this project, should look at factors concerning the optimisation of sample preparation methods, especially the purification via solid-phase extraction. The project provided an opportunity for the investigation of trends in ion ratios, to determine the fundamental limits of identification.

Key terms:

Poisonous plants, cardiac glycosides, alkaloids, traditional medicine, preparative HPLC, forensic toxicology, GC-MS.

Ethical Clearance and Permits

3.1 NAS016/2019 – Approved by the Faculties of Natural- and Agricultural Sciences and Health Sciences.

3.2 NAS029/2020 – Approved by the Faculties of Natural- and Agricultural Sciences, Health Sciences, and Veterinary Sciences

List of Abbreviations

Abbreviation	Expansion
ACN	Acetonitrile
ANOVA	Analysis of variance
ATP	Adenosine triphosphate
CI	Confidence interval
CID	Chemically induced dissociation
CNS	Central nervous system
CRM	Certified reference material
CV	Coefficient of variance
DAD	Diode array detector
DCM	Dichloromethane
dH ₂ O	De-ionised water
EtOAc	Ethyl acetate
EtOH	Ethanol
FID	Flame ionisation detector
GC	Gas chromatography
HPLC	High performance (pressure) liquid chromatography
HSQC	Heteronuclear semi-quantum coupling
IS	Internal standard
LC	Liquid chromatography
MDMA	3,4-Methylenedioxymethamphetamine
MeOH	Methanol
MFA	Monofluoroacetic acid (Fluoroacetic acid)
MS	Mass spectrometry
NEMBA	National Environmental Management: Biodiversity Act (10 of 2004)
n-Hex	n-Hexane
NIM	Negative ionisation mode
PDA	Photodiode array detector
PIM	Positive ionisation mode
q-TOF (MS)	Quadrupole tandem Time-of-flight mass spectrometry
RSD	Relative standard deviation
SD	Standard deviation

spp.	Species
TPIC	Tygerberg Poison Information Centre
UPLC	Ultra-high performance (pressure) liquid chromatography

Table of Contents

Declaration	i
Dedication	ii
Acknowledgements	iii
Abstract	iv
Ethical Clearance and Permits	vi
List of Abbreviations	vii
Chapter I	1
1. Background information	2
2. Problem identification	2
3. Aims and objectives for the project	2
4. Introduction to plant toxins	4
4.1 Poisonous plants of today.....	4
4.2 Ethnic medicine and poisonous plants	4
4.3 Poisons from plants for hunting purposes	4
4.4 Statistics of plant poisoning cases in South Africa	5
5. Selection of plants for this study	6
5.1 Rationale in selecting plants.....	6
5.2 Plants selected based on the rationale	7
6. Separation and analysis techniques	8
6.1 Solid-phase extraction (SPE)	8
6.2 Derivatisation by silylation	9
6.3 Gas chromatography-Mass spectrometry (GC-MS)	10
6.3.1 <i>Gas chromatography</i>	10
6.3.2 <i>Low resolution electron impact mass spectrometry</i>	11
6.4 Liquid chromatography-High resolution mass spectrometry (LC-HRMS)	13
6.4.1 <i>Liquid chromatography (LC)</i>	13

6.4.2	<i>High-resolution mass spectrometry (HRMS)</i>	14
7.	Statistical tools, methodology, and approaches	15
7.1	Confidence intervals in measurement	15
7.2	Statistical techniques applied in this project	16
7.2.1	<i>Multivariate analysis of ion ratios – key matrices and vectors</i>	16
7.2.2	<i>Hypotheses testing for significant difference</i>	18
7.2.3	<i>Univariate Analysis of variance (ANOVA)</i>	19
7.2.4	<i>Multivariate Analysis of Variance (MANOVA)</i>	21
7.3	Quantitative analysis of analyte signals detected in urine as physiological matrix ..	22
7.3.1	<i>Regression analysis</i>	22
7.3.2	<i>Measurement uncertainty in the regression model – sources of uncertainty</i>	23
7.3.3	<i>Measurement uncertainty in regression – the top-down approach</i>	23
7.3.4	<i>Measurement uncertainty in regression analysis – the bottom-up approach</i>	24
7.4	Figures of merit in method validation	25
7.4.1	<i>Selectivity in analyte identification</i>	25
7.4.2	<i>Limit of analyte detection (LoD)</i>	25
7.4.3	<i>Limit of analyte quantification (LoQ)</i>	26
7.4.4	<i>Linearity in the measured data</i>	27
7.4.5	<i>Precision in measurements</i>	28
7.4.6	<i>Accuracy of quantification and analyte recovery</i>	29
7.4.7	<i>Analytical range of a developed method</i>	30
7.4.8	<i>Robustness of a method</i>	30
7.4.9	<i>Stability of sample solutions</i>	30
7.4.10	<i>Carry-over of analyte between samples</i>	30
8.	Limitations of the project	31
	References	31
	Chapter II	38

1.	Background and information.....	39
1.1	Ethnopharmacology of <i>Boophane disticha</i>	39
1.2	Alkaloids of <i>B. disticha</i>	39
1.3	Notable cases of poisoning with <i>B. disticha</i>	41
1.4	Physiological symptoms observed in cases of Amaryllidaceae-alkaloid toxicosis...41	
1.5	Detection of buphanidrine.....	42
2.	Experimental.....	42
2.1	List of reagents used in the methods of this chapter	42
2.2	Isolation of buphanidrine from <i>B. disticha</i>	44
2.2.1	<i>Preparation and extraction of plant material</i>	44
2.2.2	<i>Concentration of alkaloids from crude extract</i>	45
2.2.3	<i>UPLC-qTOF-MSqTOF-MS analysis of the crude extract from B. disticha</i>	46
2.2.4	<i>Isolation of buphanidrine from the alkaloid fraction</i>	47
2.3	GC-MS analysis of samples spiked with buphanidrine	53
2.3.1	<i>Preparation of a concentrated sodium hydroxide solution</i>	53
2.3.2	<i>Preparation of an alkaline phosphate buffer</i>	53
2.3.3	<i>Preparation of stock standard solutions</i>	53
2.3.4	<i>Preparation method and parameters for GC-MS analysis of samples containing buphanidrine</i>	54
2.3.5	<i>Replicate analysis of samples for method validation</i>	55
3.	Results and discussion.....	55
3.1	Analysis of the extracts from <i>B. disticha</i>	55
3.1.1	<i>Plant extraction</i>	55
3.1.2	<i>UPLC-qTOF-MS analysis of the crude extract and alkaloid fraction from B. disticha</i>	56
3.1.3	<i>TLC-analysis and comparison of crude extract and alkaloid fraction</i>	60
3.2	Isolation of buphanidrine from the alkaloid fraction	61
3.2.1	<i>Column chromatography of the alkaloid fraction</i>	61

3.2.2	<i>Preparative thin layer chromatography (prep-TLC)</i>	62
3.2.3	<i>Semi-preparative HPLC purification of buphanidrine</i>	64
3.2.4	<i>Confirmation of the identity and purity of isolated buphanidrine</i>	65
3.3	Quantification of buphanidrine in spiked samples -Validation figures of merit.....	72
3.3.1	<i>Matrix matched samples – Urine</i>	72
3.3.2	<i>Analysis of spiked de-ionised aqueous samples</i>	78
3.3.3	<i>A comparison of response models generated for samples prepared in urine and de-ionised water</i>	82
3.4	Qualitative analysis of buphanidrine in spiked matrices.....	83
3.4.1	<i>Matrix matched samples</i>	83
3.4.2	<i>De-ionised aqueous samples</i>	87
3.4.3	<i>Calculation of a limit of detection from the ion ratios</i>	90
4.	Conclusion to Chapter II	91
	References	92
	Chapter III	95
1.	Background and information	96
1.1	Medicinal applications of <i>Gloriosa superba</i>	96
1.2	Known chemical constituents of <i>G. superba</i>	96
1.3	Recorded cases of poisoning with colchicine and <i>G. superba</i>	98
1.4	Physiological effect	99
1.4.1	<i>Relief of gout inflammation</i>	99
1.4.2	<i>Neurotoxicity</i>	100
1.4.3	<i>Systemic toxicosis</i>	100
1.5	The metabolic pathway of colchicine.....	102
1.6	Methods cited in literature for the detection of colchicine.....	104
2.	Experimental	104
2.1	List of chemicals used for experimental work in this chapter.....	104

2.2	Preparation of a crude extract.....	105
2.3	UPLC-qTOF MS analysis of the crude extract	106
2.4	GC-MS method and parameters for quantitative analysis of samples containing colchicine	107
2.4.1	<i>Preparation of stock solutions.....</i>	<i>107</i>
2.4.2	<i>Preparation of the bicarbonate buffer</i>	<i>107</i>
2.4.3	<i>Analysis of samples spiked with colchicine.....</i>	<i>107</i>
2.4.4	<i>Preparation of SPE-cartridges and analyte elution.....</i>	<i>108</i>
2.4.5	<i>Liquid-liquid extraction of colchicine and 5-α-cholestane</i>	<i>108</i>
2.4.6	<i>GC-MS analysis of the prepared samples</i>	<i>108</i>
3.	Results and discussion.....	109
3.1	UPLC-qTOF MS analysis of the crude extract	109
3.2	Mass spectral analysis of colchicine	113
3.2.1	<i>Electron impact-Mass spectrum.....</i>	<i>113</i>
3.2.2	<i>Electrospray ionisation-Mass spectrum.....</i>	<i>116</i>
3.3	Assessment of quantitative figures of merit in the generated response model	118
3.3.1	<i>Linearity in the response models generated from measured data</i>	<i>118</i>
3.3.2	<i>Repeatability of the analytical method and response models</i>	<i>126</i>
3.3.3	<i>Accuracy in the measurement of the concentration of colchicine in a sample</i>	<i>128</i>
3.4	Assessment of qualitative figures of merit in the analysis of samples for colchicine...	131
3.4.1	<i>The relationship between measured ion ratios and analyte concentration</i>	<i>132</i>
3.4.2	<i>Repeatability of ion ratios between individual batches</i>	<i>138</i>
4.	Conclusion to Chapter III	139
	References.....	140
	Chapter IV.....	145
1.	Introduction to <i>Acokanthera oppositifolia</i> and acovenoside A	146

1.1	Ethnobotanical applications of <i>Acokanthera oppositifolia</i>	146
1.2	Applications of acovenoside A in modern medicine	146
1.3	Occurrence of <i>A. oppositifolia</i> poisoning.....	146
1.4	Toxic chemical constituents of <i>A. oppositifolia</i>	147
1.5	The physiological actions of cardiac glycosides	150
1.6	Proposed metabolic pathways for acovenoside A.....	150
1.7	Detection of cardenolides.....	153
1.7.1	<i>Radioimmuno assay</i>	153
1.7.2	<i>Liquid chromatography – Mass spectrometry</i>	153
1.7.3	<i>Gas chromatography – Mass Spectrometry</i>	154
1.7.4	<i>Liquid chromatography-Diode array detection</i>	155
2.	Experimental methods	155
2.1	Reagents and chemicals utilised in this chapter	155
2.2	Preparation of crude extract from <i>A. oppositifolia</i>	157
2.3	UPLC-qTOF MS analysis of extracts	157
2.4	UPLC-qTOF MS analysis of hydrolysed acovenoside A	158
2.5	Analytical method for the analysis of urine samples for acovenoside A	160
2.5.1	<i>Preparation of acovenoside A stock solution</i>	160
2.5.2	<i>Preparation of internal standard stock solution</i>	160
2.5.3	<i>Preparation of acetate buffer</i>	160
2.5.4	<i>Preparation of the alkaline phosphate buffer</i>	160
2.5.5	<i>Initial sample preparation and extraction via SPE</i>	161
2.5.6	<i>Microwave assisted hydrolysis of eluted samples</i>	161
2.5.7	<i>Liquid-liquid extraction of analytes from the hydrolysis solution</i>	162
2.5.8	<i>Microwave assisted silylation of analytes</i>	162
2.5.9	<i>GC-MS analysis of derivatised samples</i>	162
2.5.10	<i>Approach in analysis of detected chromatograms</i>	163

2.6	Validation of the analytical method	164
3.	Results and discussion.....	164
3.1	UPLC-qTOF MS analysis of crude extracts from plant material	165
3.2	Determining the purity of commercially sourced acovenoside A.....	169
3.3	Analysis of hydrolysed acovenoside A	170
3.3.1	<i>UPLC-qTOF MS analysis of the hydrolysis products of acovenoside A.....</i>	<i>170</i>
3.3.2	<i>Inter-ion ratio relationships of fragment ions.....</i>	<i>180</i>
3.4	Validation of quantitative GC-MS method	183
3.4.1	<i>Linearity and precision in measured data</i>	<i>183</i>
3.4.2	<i>Limits of analyte detection and quantitation.....</i>	<i>190</i>
3.4.3	<i>Selectivity (Specificity) of the analytical method</i>	<i>192</i>
3.4.4	<i>Recovery of the analyte and accuracy in measurement</i>	<i>192</i>
3.5	Validation of qualitative figures of merit in the analytical method	193
3.5.1	<i>Variation of ion ratios over the modelled calibration range in de-ionised aqueous samples</i>	<i>194</i>
3.5.2	<i>Variation of ion ratios over the modelled calibration range in urine samples.....</i>	<i>196</i>
3.5.3	<i>Between-batch variation of ion ratios at a single concentration</i>	<i>198</i>
4.	Conclusion to Chapter IV.....	199
	References.....	200
	Chapter V.....	206
1.	Background and information.....	207
1.1	Ethnic applications of <i>Urginea sanguinea</i>	207
1.2	Toxic chemical constituents of <i>U. sanguinea</i>	207
1.3	Physiological effects following intoxication.....	209
1.4	Proposed metabolic pathways of scillaren A	210
1.5	Cases and statistics of <i>U. sanguinea</i> poisoning	213
1.5.1	<i>Cases and statistics regarding bufadienolide poisoning in humans.....</i>	<i>213</i>

1.5.2	<i>Cases and statistics regarding bufadienolide poisoning in animals</i>	213
1.6	Methods for the detection of bufadienolides cited in literature	213
1.6.1	<i>Radioimmuno assay</i>	213
1.6.2	<i>Fluorescence polarisation immunoassay</i>	214
1.6.3	<i>Liquid chromatography-Mass spectrometry</i>	214
2.	Experimental methods	215
2.1	List of reagents and chemicals utilised in the experimental work	215
2.2	Preparation of a crude extract from <i>U. sanguinea</i>	216
2.3	UPLC-qTOF-MS analysis of the crude extract.....	217
2.4	Sample preparation method for the GC-MS analysis of physiological samples.....	218
2.4.1	<i>Preparation of a scillaren A stock solution and an internal standard stock solution</i>	218
2.4.2	<i>Spiking of urine and de-ionised aqueous samples for analysis</i>	218
2.4.3	<i>Solid phase extraction of scillaren A from samples</i>	218
2.4.4	<i>Preparation of eluted samples and temperature program for GC-MS analysis</i>	219
2.5	Validation of qualitative analysis of urine samples for scillaren A	220
2.5.1	<i>Evaluation of the method linearity and precision</i>	220
2.5.2	<i>Evaluation of the method accuracy and recovery</i>	221
2.5.3	<i>Selection of ion ratios for the identification of analytes</i>	221
3.	Results and discussion	222
3.1	UPLC-qTOF-MS analysis of the crude extract.....	222
3.2	GC-MS analysis of samples for scillaren A	226
3.3.1	<i>Identification of the derivatised hydrolysis products of scillaren A</i>	226
3.3.2	<i>Ion ratio relationships observed for urine samples spiked with scillaren A</i>	229
3.3	Assessment of quantitative figures of merit in the generated response model	230
3.4	Assessment of qualitative figures of merit in the generated response model	234
3.4.1	<i>Change in ion ratios over the concentration range</i>	234

3.4.2	<i>Comparison of precision in ion ratios from two matrices</i>	238
4.	Conclusion to Chapter V	239
	References	241
	Chapter VI	245
1.	Isolation of a reference standard of buphanidrine from <i>B. disticha</i>	246
2.	Limitations of developed quantitative analytical methods	246
2.1	Linearity of the developed methods	246
2.2	Precision in measurement and analysis	247
3.	Applicability of developed quantitative methods in the routine setting	248
4.	Planned and suggested future research on the topic of this project	248
	Appendix to Chapter I	249
A.	Additional molecular structures	249
B.	Gas chromatography-Mass spectrometry diagrams	249
C.	Liquid chromatography-High Resolution Mass Spectrometry diagrams.....	251
D.	Additional formulas used in statistical data analysis	251
	Appendix to Chapter II	253
A.	Library mass spectra from the Wiley-NIST spectral registry	253
B.	NMR-spectra recorded for isolated buphanidrine	255
C.	Photographs of <i>B. disticha</i>	258
D.	Method for the preparation of Dragendorff reagent.....	258
	Appendix to Chapter III	259
A.	Photographs of <i>G. superba</i>	259
B.	Library mass spectrum from the NIST mass spectral library.....	260
	Appendix to Chapter IV	261
A.	Methods for preparing arrow poison from <i>A. oppositifolia</i>	261
B.	Photographs of <i>A. oppositifolia</i>	263

C. GC-MS data related to the analysis of derivatised hydrolysis products263

Appendix to Chapter V264

A. Photographs of *U. sanguinea*264

Chapter I

Introduction

1. Background information

Alternative and traditional medicine is a deeply engraved part of culture and life in most African countries, to which South Africa is no exception. Despite the long history of its practice, traditional medicine still carries immense risks as any plants used as a source of medication are extremely poisonous.¹ They are also easily obtained from centralised markets (e.g. Faraday Muti Market, Johannesburg) and small stores devoted to the sale of medicinal herbs. This ease of availability and the high cost of private healthcare makes traditional medicine a common alternative for low-income populations worldwide.²

A recurring issue in cases of poisoning, where traditional medicine is suspected as the source of the poison, is the unwillingness of patients to indicate whether they have used traditional medicine and, if they did use alternative treatment, what they used.³ In some cases, the traditional healers have been alleged to also withhold information for of fear of prosecution.⁴

2. Problem identification

Some plants, used in traditional medicine, exhibit symptoms of toxicosis that are almost indistinguishable from natural illnesses. This may result in diagnoses being based on misinformation, leading to the incorrect treatment of an intoxicated individual. An example of this is intoxication with cardiac glycosides from *Urginea sanguinea* when taken orally.⁵ Initial symptoms may relate to those of a gastrointestinal disorder, whereas myocardial symptoms are not necessarily observed.

A method for rapid qualitative, and quantitative, analysis of physiological fluid for the presence of poisons, frequently encountered by users of ethnic medicine and participants in traditional rituals, could provide a higher degree of certainty in determining a cause of death. Such a method can also be used in a clinical environment to improve the diagnosis of a patient presenting symptoms related to toxicosis.

3. Aims and objectives for the project

In this study, the overall aim is the development of analytical methods for the identification and quantification of plant toxins in human urine. To attain this overall aim, various objectives must be achieved. The analysis of physiological samples required the development and optimisation of sample preparation procedures for analysis, via gas chromatography-mass spectrometry (GC-MS). The differences in chemical properties of the different analyte classes,

addressed within this project, required the development of different sample preparation procedures for each class of analyte. Since each chapter will discuss the primary toxic constituent of a different plant, the objectives were similar for the chapters, however, the outcomes in achieving the objectives of each chapter differed.

In chapter II, the component of the study focussed on *Boophane disticha* and its primary toxic constituent, buphanidrine, the objectives were:

- Development and analysis of a crude extract, with a suitable broad-spectrum extraction solvent system, from the dried plant material.
- Isolation of buphanidrine from this crude extract.
- Development of a suitable sample preparation method, via an optimised liquid-liquid extraction process, for the GC-MS analysis of urine samples, spiked with isolated buphanidrine.
- Optimisation and validation of the method for application in the routine quantitative and qualitative analysis of buphanidrine in human urine samples.

The objectives for chapter III, the project component focussed on the primary toxic constituent of *Gloriosa superba*, namely colchicine, were:

- Development of a polar crude extract from dried plant material, with a suitable solvent system, and analysis for confirmation of the presence of colchicine in the plant material.
- Development of a suitable sample preparation method, via an optimised solid phase extraction-process, for the GC-MS analysis of urine samples, spiked with commercially sourced colchicine.
- Optimisation and validation of the developed method for application in the routine quantitative and qualitative analysis of colchicine in human urine samples.

In both chapters IV and V cardiac glycosides are present as the primary toxic constituents of the respective host plants, *Acokanthera oppositifolia* and *Uriginia sanguinea*. For both these chapters the following objectives had to be met:

- Development of crude extracts, with suitable broad-spectrum extraction solvent systems, and analysis for confirmation of the presence of the respective primary toxic constituents of the individual plants, as cited in literature.

- Development of a suitable method for the preparation of human urine samples, containing cardiac glycosides, for hydrolysis of the analytes and validation of the method for applicability in the routine quantitative and qualitative analysis setting.
- Optimisation of the hydrolysis conditions for the deconjugation of the cardiac glycosides, to obtain the aglycones of the analytes.
- Optimisation of the extraction of hydrolysis products, from the reaction mixture, and subsequent aglycone derivatisation.
- Development and optimisation of a GC-MS temperature program for the separation of the target analytes from endogenous steroids in human urine.
- Validation of the developed and optimised method to determine its suitability to application in routine toxicological analyses (qualitative and quantitative) of human urine samples.

4. Introduction to plant toxins

4.1 Poisonous plants of today

Many toxins from antiquity are still in use today. Some are used to commit suicide or criminal acts, while the hallucinogenic properties of some are exploited for ritualistic or recreational purposes. In chemical and pharmaceutical research, toxic extracts from plants are utilised in the development of new drugs.⁶ Today, the plants implicated in suicides and homicides in South Africa include *A. oppositifolia* (Bushman's poison bush), *B. disticha* (Bushman's poison bulb), *G. superba* (Flame lily), and *Strophanthus speciosus* (Common poison rope).⁷⁻¹² Plants, such as *U. sanguinea* ('Slangkop') and *Moraea* spp. ('Tulp') are notorious for causing poisoning among grazing livestock.¹³

4.2 Ethnic medicine and poisonous plants

An easily overlooked source of plant poisoning in humans is ethnic medication. Botha and Penrith¹³ claim cases such as these are mostly unintentional and typically the result of accidental overdose. They indicate that in South Africa, *U. sanguinea* is particularly infamous for this.¹³ From 1987 to 1992, Ga-Rankuwa Hospital (now Dr. George Mukari Hospital) reported 14 cases of poisoning possibly by *U. sanguinea*.¹⁴

4.3 Poisons from plants for hunting purposes

Hunting poisons have been in use since antiquity. Notable users of these toxins include the San hunter-gatherers of Southern Africa.^{15,16} The San hunter-gatherers have, according to

Bradfield, et al.¹⁷, been using arrows laced with plant toxins for at least 12 000 years. Some of these plant toxins are now used in medical applications.¹⁸ Traditional poisons used by the San contain compounds such as ouabain, buphanidrine, strophanthidin, ingenol, and tetraphyllin B.^{16,19}

4.4 Statistics of plant poisoning cases in South Africa

From 1981 to 1985, 1 164 cases of poisoning were admitted to the Ga-Rankuwa hospital. Of these, 17.5% (204 cases) were the result of poisoning with traditional medicine. In the five years, 1987-1992, 313 cases (9.2%) of poisoning by traditional medicine were documented by the Ga-Rankuwa hospital.¹⁴ In the period from 1996 to 2000, 98 cases of acute poisoning from traditional medicine were documented at the same hospital (**Figure I-1**).²⁰

A general decline in the number of cases reported for traditional medicine poisoning is noticeable. From 1987 to 2000, the overall number of deaths as a result of traditional medicine poisoning decreased from 42 (1987-1992) to 5 (1996-2000).²⁰ A possible reason for this decline is the improvement in the treatment of patients in such instances. (**Figure I-1**)

During the Tygerberg Poison Information Centre's (TPIC's) 2011-2013 survey,²¹ the number of poisoning cases directly attributed to ethnic medicine started to increase. In the 2014 Annual Report of the TPIC,²² 95 cases of intoxication by traditional medicine were recorded. This is close to the value recorded at Ga-Rankuwa during the 1996-2000 period.²⁰

Based on the August 2008-July 2009 Toxicovigilance-survey results of the South African Medical Journal,²³ from the 4 771 cases dealt with by the Tygerberg Poison Information Centre (TPIC), in 96 cases plants were the suspected source of poisoning. A small decrease in cases reported at the TPIC was observed for the 2011-2013 period.²¹ The number increased to 123 during 2014, based on the TPIC's 2014 Annual Report (See **Figure I-2**).²²

A contributing factor to this increase may be the additional poisoning cases from outside the borders of South Africa that were dealt with by the TPIC, and additional calls from other provinces where Poison Information Centres were closed down.²² The systematic increase in the number of cases where ethnic medicine was specified as the cause of poisoning, could be partly attributed to this as well. Overall, following the decrease in the incidence of poisoning by ethnic medicine from 1981 to 2000, the incidence of such cases has been rising since 2011 (See **Figure I-2**).^{20,21}

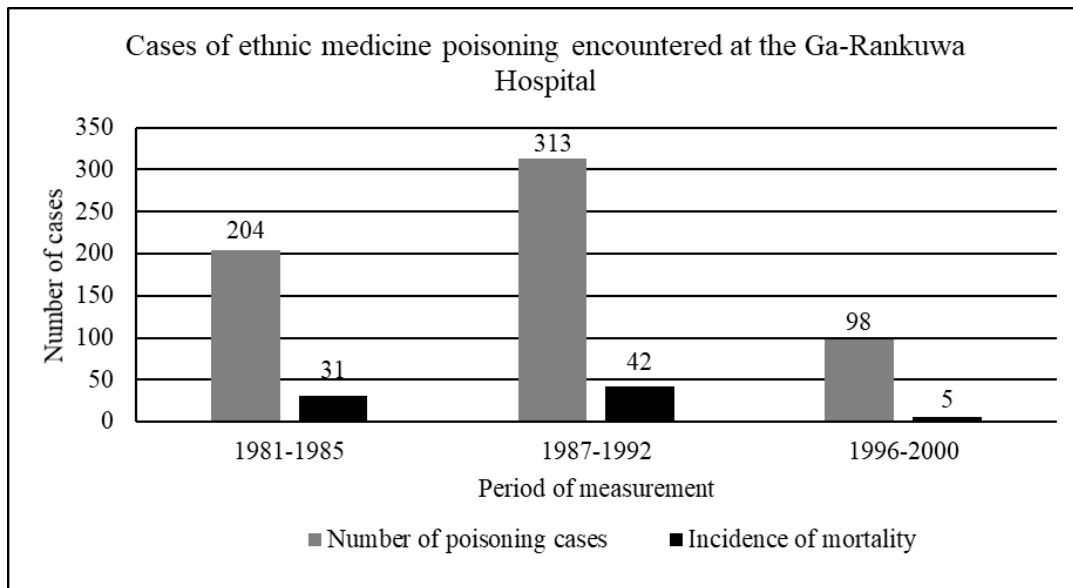


Figure I-1. Cases of poisoning by ethnic medicine encountered at the Ga-Rankuwa Hospital from 1981 to 2000.^{14,20}

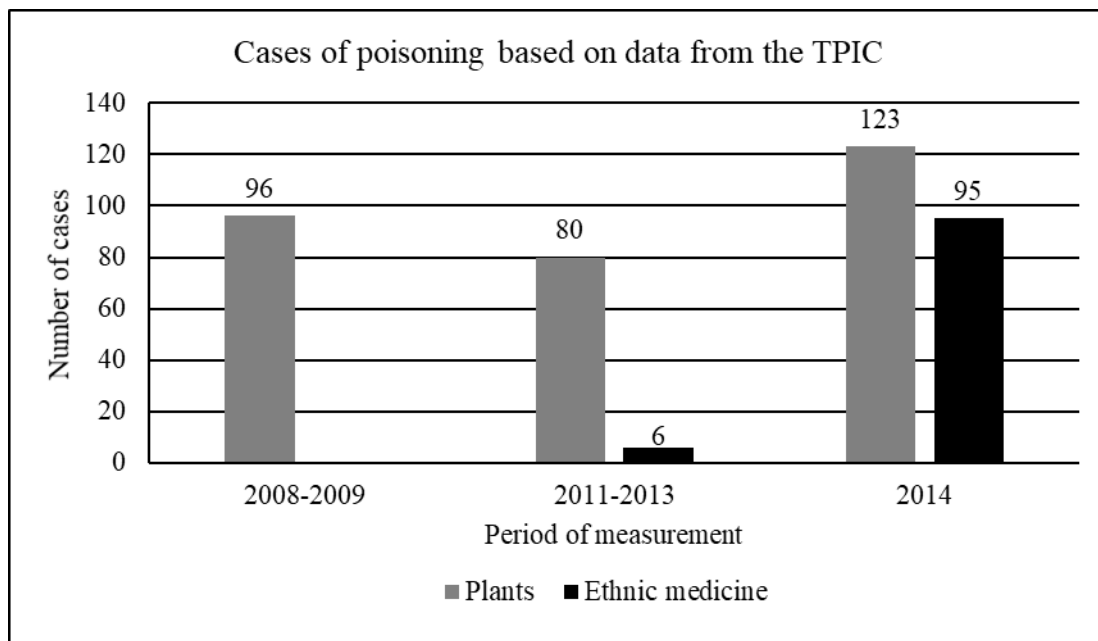


Figure I-2. Cases of plant and ethnic medicine poisoning reported to the Tygerberg Poison Information Centre (TPIC) between August 2008 and December 2014. No data was recorded on ethnic medicine related cases in the 2008/2009 survey.²¹⁻²⁴

5. Selection of plants for this study

5.1 Rationale in selecting plants

It was important to select plants that are used in ethnic medicine and have contributed to cases of poisoning in both humans and agricultural livestock. These plants impact the daily lives of

individuals and animals and pose a threat to their health and safety. Some of the plants have been suspected of being used in committing homicide and suicide.

Other factors considered in choosing the plants were their geographical distribution, their vulnerability to extinction, their indigeneity, and their primary toxic constituents. Plants growing in a wide range of habitats are more likely to be encountered by humans and agricultural livestock. Those that are also used in ethnic medicine would be sourced by a greater proportion of the population. The same holds for plants that are not at risk of becoming extinct or reaching population levels low enough for them to be considered endangered.

In this project, the aim was to emphasise on the poisonous plants that are indigenous to South Africa. In this way, some of the plants that cause poisoning, but go unnoticed, could be studied.

The primary toxic constituents of the plants, according to literature, was considered in terms of the research that has been done on the detection of these compounds in physiological fluids. The primary toxic constituents of three of the four selected plants were available commercially. In one case, the primary constituent had to be isolated from the plant material.

5.2 Plants selected based on the rationale

Based on information obtained from peer reviewed articles and discussions with academic professionals in the fields of Veterinary Pathology, Toxicology and Natural Products Research, the above rationale was applied in selecting four plants for this study as indicated in

Table I-1. Plants covered in this project, with herbarium specimen numbers.

Family	Genus	Species	Component utilised in this project
Apocynaceae	Acokanthera	Oppositifolia (Lam.) ²⁶	Leaves
Amaryllidaceae	Boophane	Disticha (L. f.) Herb. ³¹	Bulb scales
Colchicaceae	Gloriosa	Superba Linné ⁴⁷	Rhizomes
Hyacinthaceae	Urginea	Sanguinea Schinz ⁴⁸	Bulb scales

Acokanthera oppositifolia was selected for this study based on its use in ethnic medicine, as an arrow poison and its suspected use in homicides.^{8,13,25-27} It contains cardiac glycosides as primary toxic constituents.²⁸ This class of compounds is notorious for its narrow therapeutic indices and cases of unintentional overdose when used medicinally. It is rare that grazing

livestock ingest material from *A. oppositifolia*. However, if ingested or introduced into the bloodstream, it can cause fatal toxicosis.^{13,29}

Boophane disticha is a prominent plant in Southern African ethnic medicine. Its use as both medicine and arrow poison has been recorded in ethnobotanical studies.^{16,17,30-32} The utilisation of *B. disticha* in ethnic religion to induce trances creates a major risk for unintentional overdosage that can lead to death.³¹⁻³³ Cases of this have been recorded in literature, as well as cases of suicide where *B. disticha* was used as a source of poison.^{30,34} Its potent toxicity is attributed to the large amount of neurotoxic Amaryllidaceae-alkaloids present in the plant material.^{9,30} When sourced at an ethnic medicine market, the author was warned about the potency of the plant extract by vendors.

As has been recorded in literature, colchicine and its natural sources are extremely toxic in small doses. *Gloriosa superba* has been used in suicide attempts and in suicides that were successful for this very reason.^{35,36} It is also used in ethnic, South African, medicine to treat problems related to fertility and virility.^{37,38} Colchicine in physiological fluids is primarily detected by liquid chromatography-mass spectrometry.³⁹⁻⁴³ The inclusion of *G. superba* in the study accommodates the further development of detection methods for Colchicine in physiological fluids via gas chromatography-mass spectrometry.

Urginea sanguinea is used extensively in ethnic medicine and is a well-known cause of fatalities amongst livestock.^{13,29,44} Ethnic medicine has been suspected as the cause of many overdoses, some fatal.^{20,45} In some cases, the patients were misdiagnosed with gastrointestinal illness, based on the symptoms they present when they arrived at the hospital.⁴ Its primary toxic constituents are cardiac glycosides. However, belonging to a different subgroup as those in *A. oppositifolia*.^{4,45,46} By including *U. sanguinea* in this study, a significant contribution is made to the healthcare sector for both humans and animals.

6. Separation and analysis techniques

6.1 Solid-phase extraction (SPE)

In preparing urine samples for GC-MS analysis, solid-phase extraction (SPE) techniques were introduced into the methods for this project. SPE provides many benefits in sample preparation and clean-up. In this project, a key benefit of SPE over liquid-liquid extraction (LLE) was the decrease in the volume of organic solvents required to extract the analyte from a large sample volume (10.0-20.0 mL).

SPE provides better selectivity than LLE, or at the very least, an additional level of selectivity. In this project a C18-stationary phase was used as sorbent for SPE. Many matrix components in urine are both hydrophilic and lipophobic and are eluted through the SPE cartridge without retention. By buffering the sample solution, the analytes are maintained in a neutral state and trapped by the sorbent (equilibrated with the buffer solution). The analytes are eluted by aspirating organic solvents through the column. Since the organic solvents have high vapour pressures, the eluted samples' volumes can be reduced further for up-concentration of the analyte.⁴⁹⁻⁵¹

Since the solvents used in eluting analytes from SPE cartridges are compatible with liquid chromatography columns, little to no further sample preparation is required for liquid chromatographic analysis. For gas chromatography, however, further sample preparation may be required (e.g. derivatisation and reconstitution in a compatible solvent).^{49,50}

6.2 Derivatisation by silylation

Gas chromatography is, to a large extent, dependent on the vapor pressure of analytes. Non-volatile analytes are not readily vaporised in the sample inlet and, as a result, only small amounts might reach the column. The vapor pressure and volatility of the analytes are related to the strength of their intermolecular forces.⁵² Active hydrogen functionalities (e.g. **-OH**, **-SH**, and **-NH**) produce strong intermolecular hydrogen bonds between the analytes and a polar stationary phase and within the sample, thereby decreasing volatility and subsequently, method sensitivity.⁵³

Derivatisation is accomplished by de-solvating and reconstituting the extracted analytes in excess derivatising reagent and a compatible solvent or catalyst. Two very popular routes of derivatisation include alkylation and silylation.^{53,54} Both these processes aim to substitute active hydrogen atoms with bulkier functional groups, thereby significantly decreasing the strength of the intermolecular interactions and increasing analyte volatility.⁵³

In this project, derivatisation by silylation was used in the analysis of cardiac glycosides. The reagent used was *N*-methyl-*N*-(trimethylsilyl)trifluoroacetamide (MSTFA) with pyridine as a catalyst. During derivatisation, the active hydrogens in the analyte are displaced by the trimethylsilyl (TMS)-group according to the following mechanism:⁵⁴

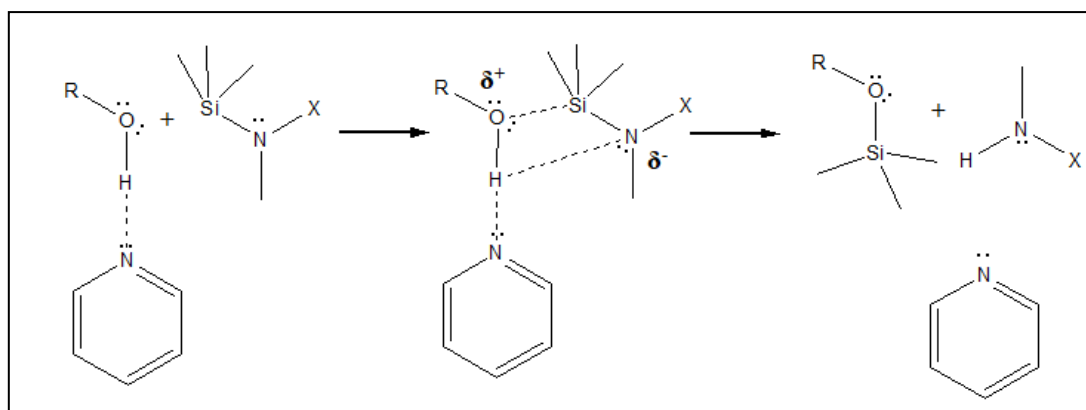


Figure I-3. A mechanism for silylation of a hydroxy group. The mechanism is the same for amines and thiols.⁵⁴

In this suggested mechanism, the derivatising reagent forms an activated complex with the active hydrogen functional group where the silicon atom accepts electron density from the oxygen atom (hydroxyl functionality) into its empty 3d-orbitals during the nucleophilic attack by oxygen. Simultaneously, the pyridine interacts with the active hydrogen via a hydrogen bond.

This combined interaction draws electron density away from the hydroxyl-oxygen atom, thereby giving it a partial positive charge. The opposite is achieved by the amide nitrogen atom that draws electron density, through its σ -bond with silicon, to itself. This induces a partial negative charge on the nitrogen atom that is stabilised by delocalisation of the lone pair over the amide conjugated system (for MSTFA, X = $-\text{C}(\text{O})\text{CF}_3$, for TMSI, X = imidazole).⁵⁴⁻⁵⁶

The interchange of the two units, proton and TMS, is facilitated by electron transfer in the activated complex. The partial negative charge on the nitrogen atom attracts the electron-deficient proton of the hydroxyl group, regenerating the free pyridine. The acceptance of electrons from oxygen by silicon stabilises the loss of the proton and the resulting negative charge. By dissociating from the amide, the positive charge on the amide-nitrogen atom is neutralised. The products are then the silylated analyte and the secondary amide.⁵⁴

6.3 Gas chromatography-Mass spectrometry (GC-MS)

6.3.1 Gas chromatography

In gas chromatography, separation of the analytes occurs based on their boiling point and the strength of the adsorption interactions of the analytes with the column stationary phase. Samples are injected rapidly through an inlet, kept at high temperature, and then loaded onto an open tubular column by a stream of carrier gas. In this project, a splitless inlet mode was

used to maximise the amount of analyte loaded onto the column.⁵⁷ The carrier gas acts as the mobile phase and is an inert gas such as nitrogen or helium⁵⁸ (See Appendix to Chapter I, Figure A (I) - 2).

In this project, helium was used as carrier gas and is beneficial to method development since its flattened van Deemter curve allows for faster flow rates to be applied to the analytical method, whilst maintaining optimal theoretical plate height conditions for analyte separation. The optimal flow rates for separation when nitrogen is used, are lower than when helium is used, which increase the amount of time required to analyse a sample with optimal separation.⁵⁸

In the process of being carried through the column by the carrier gas, the analytes in the sample are brought regularly into contact with the column stationary phase by random motion and diffusion along a concentration gradient. The narrow internal diameter of open tubular columns allows the analytes to rapidly diffuse from the carrier gas to the stationary phase adsorbed to the column walls. Analytes that experience stronger intermolecular attraction forces to the stationary phase are retained longer than those that are attracted by weaker forces. The rate of analyte diffusion from the stationary to the mobile phase is increased by increasing the temperature.⁵⁹

Solvent focussing is a technique employed in GC-analysis to focus the applied sample band into a narrow band at the column head. To achieve this, the GC-analysis is initiated at a low temperature which is maintained for about one minute to condense the sample in the column in a narrow band. To increase the rate of diffusion for the analytes between the stationary and mobile phases, the temperature is increased along a gradient in a process referred to as ‘temperature programming’. The analyte bands separate and elute as sharp bands of high intensity since the focussing process concentrated the analytes into narrower band than the initial applied band at the column head.^{57,60}

Through temperature programming, less band broadening occurs for the more retained analytes, and the chromatographic analysis requires less time. By increasing the column temperature during the analysis, the rates of diffusion from the stationary phase for the less volatile analytes increases, increasing the time spent in the mobile phase. Less band broadening occurs and the analytes elute earlier, producing shorter run times.^{61,62}

6.3.2 Low resolution electron impact mass spectrometry

The analysis of analytes from the GC-system is accomplished, in this project, by low resolution mass spectrometry. To maintain the vapour phase of the analytes in the GC-column with

minimal retention, the column is passed through an auxiliary transfer line kept at high temperature. At the column end, the analytes elute directly into the heated electron impact source kept under a high vacuum. Here a beam of electrons is emitted from a filament and accelerated across a potential difference of 70 V to obtain a kinetic energy of 70 eV (See Appendix to Chapter I, Figure A (I)- 3).⁶³

This beam of high kinetic energy electrons is directed at a right angle at the incoming stream of analytes eluting from the GC-column. The high kinetic energy of the electrons ensure that enough energy is imparted on these analyte molecules during a collision to cause ionisation. If the energy transferred during the collision is high enough in magnitude, the ionised analyte will absorb the excess energy and vibrate beyond the limits of its chemical bonds, leading to fragmentation. Conventionally, acceleration of the electrons to a kinetic energy of 70. eV is performed to obtain a fragmentation pattern from the ionised analyte that can be compared to a library of mass spectra developed at this kinetic energy level.⁶³

Once generated in the ion source, the ions are repelled by a repelling plate set to a positive voltage and accelerated toward an ion lens, set to a less positive voltage. Acceleration of the ions under high vacuum through accelerator and ion lens components, set to successively less-positive voltages, focuses the beam of newly generated ions into the mass analyser⁶³ (See Appendix to Chapter I, Figure A (I)- 3).

For low resolution (nominal mass) analysis, a quadrupole mass analyser is used. In a quadrupole mass analyser, the ions are separated based on their integer (nominal) mass-to-charge ratios (m/z). The selection of m/z -ratios in the analyser is achieved by applying a combination of a direct current (DC) voltage and a radio frequency (RF) voltage to the four rods of the analyser such that opposite rods have the same sign voltage. The polarity of the rods is rapidly altered, whilst keeping the DC/RF-ratio constant. The rapid transitions of polarity in the quadrupole, place the ions on specific paths. Based on the applied RF-voltage, a single m/z -ratio ion will reach the detector. The others are removed directly by the vacuum or after colliding with the analyser rods.^{63,64}

By rapidly scanning the voltages over a range, a full mass spectrum is obtained. The analyser can be programmed to selectively detect specific ions in the selected ion monitoring (SIM) mode. This allows the analyser to spend more time allowing specific ions to reach the detector, thereby increasing sensitivity.^{63,64} It must be kept in mind that this action influences ion ratios in detected spectra. Data for identification via the fragmentation pattern's characteristic ratios

in full scan mode should not be recklessly interchanged with data for identification in the SIM-mode.

Ions are detected via a high energy dynode electron multiplier (HED-EM) detector (see Appendix to Chapter I, Figure A (I)-4) consisting of a conversion dynode and a single continuous dynode. When an ion hits the conversion dynode, set to a high negative potential, high energy electrons are released from its surface and accelerated toward the continuous dynode of less negative potential. The secondary electrons accelerate towards the narrow end of the curved dynode where a positive, near-ground potential is applied. This electron current is further amplified and recorded by the data capture system. The more ions that strike the detector, the more electrons are released and multiplied, thereby producing a current of greater magnitude at the sensing plate. A greater current will register as a higher intensity peak on the total ion current (TIC) chromatogram.^{63,65}

Through SIM and extracted ion chromatograms (EIC), the hyphenation of mass spectrometry to gas chromatography enhances the selective detection of analytes. When two components cannot be effectively separated by chromatographic techniques and adjustments to the temperature programs used, ‘separation by ions’ can be considered.^{63,66}

6.4 Liquid chromatography-High resolution mass spectrometry (LC-HRMS)

6.4.1 *Liquid chromatography (LC)*

In contrast to the open tubular capillary tubes used in gas chromatography, packed columns of larger internal diameters are used in liquid chromatography.⁶⁷ This allows for the greater sample volumes required by LC-MS analysis. The stationary phase is adsorbed onto the surface of the packing particles.⁶⁷ The tight packing of the stationary phase particles creates interstitial channels with narrow internal diameters, thereby increasing the rate of analyte partitioning between the phases and improving chromatographic performance.⁶⁸

The column stationary phase employed in this project was of the type C18 (i.e. reversed phase). C18 stationary phases increase the retention of non-polar compounds and allow the polar analytes to elute first. In liquid chromatography, analytes are separated based on their polarity and the strength of their interactions with the stationary *and* mobile phases.^{67,69,70}

The analytes diffuse between the stationary and mobile phases in a dynamic equilibrium. When the sample is applied to the instrument, the sample is transported to the column head by the mobile phase. Inside the column, the analytes distribute between the two phases down a

concentration gradient. The direction of the concentration gradient depends on the analyte concentration in the mobile and stationary phases at the site of partitioning.^{69,70}

If the analyte experiences weak intermolecular attraction forces in the mobile phase, it will diffuse at a more rapid rate from the mobile phase than analytes that experience greater intermolecular attraction forces in the mobile phase. In the latter case, the analytes will tend to remain in the mobile phase and will elute more rapidly. The analyte-mobile phase interactions can be altered by changing the composition of the mobile phase along a gradient during the analysis (comparable to a GC temperature program). By changing the mobile phase composition along a gradient, both polar and non-polar analytes can be eluted with narrow bands and with good chromatographic resolution.^{69,70}

6.4.2 High-resolution mass spectrometry (HRMS)

In this project, following liquid chromatographic separation of the analytes in the crude extracts of their host plants, high-resolution mass spectrometry was used to identify the target analytes. Since exact elemental masses are unique, their combinations are also unique. Therefore, the specific exact monoisotopic mass of an ion can be linked to a specific elemental composition. However, since exact masses are measured values, there is uncertainty and possibly errors in their values. Calibration of the mass analyser and detector with samples of known accurate monoisotopic mass corrects for some of the errors in detected masses.^{71,72}

In coupling a liquid chromatography system to a mass spectrometer, the capacity of the ion source must be considered. The high output volume from the LC-column can flood a conventional electron impact ion source. LC-MS systems, therefore, use methods such as electrospray ionisation (ESI) and corona discharges to de-solvate and ionise samples.⁶⁷ The fragmentation patterns produced by these sources cannot be compared to the conventional 70 eV mass spectral libraries.⁷³

Repeatability of CI-fragmentation patterns is hard to obtain. Some degree of control can be obtained by controlling the pressure inside the ionisation chamber. If a quadrupole is used to induce fragmentation by collision-induced dissociation (CID), the degree of fragmentation can be controlled by the voltages to which the quadrupole is set.⁷⁴

High-resolution mass spectrometry was employed in this project, with a quadrupole-time-of-flight (qTOF) mass analysis system. The quadrupole selects nominal masses that are then further resolved to an accurate mass level by the time-of-flight (TOF) mass analyser. In the TOF-analyser, sections of the ion beam from the quadrupole are pulsed into a chamber under

high vacuum conditions at a right angle by a large repulsion force^{71,72} (See Appendix to Chapter I, Figure A (I)- 6).

Inside the high vacuum chamber, the ions do not experience any further attractive or repulsive forces and retain all the components of their momentum. Since a single force of known value was applied to accelerate the ions, and no other forces act upon the ions, the acceleration experienced from the repelling plate is inversely related to the masses of the ions.⁶³ For the single force, heavier ions are accelerated less than the lighter ions. Therefore, each mass is accelerated to a different velocity and traverses a fixed distance in a different time interval. Provided with enough distance, these ions will separate from each other and arrive at significantly different times at the ion detector.^{71,72}

The resolution is improved for a TOF-chamber by adding a reflectron (ion mirror) at the end to reverse the ion path without stopping them or colliding them. This effectively doubles the flight path length.⁶³ A greater contribution by the reflectrons is the refocussing of bands of ions with the same accurate m/z-ratio. This correction of the kinetic energy dispersion greatly improves mass resolution^{71,72} (See Appendix to Chapter I, Figure A (I)- 6).

7. Statistical tools, methodology, and approaches

7.1 Confidence intervals in measurement

Uncertainty and random variation are inherent to measurement. The standard deviation of the measurements around their mean value provides an estimate of the region wherein measured values are distributed due to random variation. If greater confidence is associated with the measured values, the region wherein a value may fall, without differing significantly from the mean, will be wider. The probability that a measured value is significantly different from the mean decreases. This probability is represented by the percentage area under a distribution function that is excluded from the confidence region.

In this project, two confidence levels have been used, a 99.7% and a 95.4% confidence interval. The former has been applied to compare ion ratios measured from samples that were spiked with the analyte to the corresponding mean ion ratios measured for samples prepared at the median concentration level in the response model. The 95.4% confidence level has been applied in the quantitative analysis of spiked samples where the uncertainty associated with a calculated analyte concentration was reported. This confidence level has also been applied to determine the repeatability of the method for quantitative analysis.

In explaining the confidence interval, assume a known measurement \tilde{x}_i . If the same measurement was made 1 000 times ($n = 1\ 000$), then a mean of all the measurements (μ) can be calculated. In assuming a random distribution of \tilde{x}_i about μ , a specific percentage of the measurements will lie within a specific distance from μ . At a 95.4% confidence interval, assuming a two-tailed distribution, 954 of the \tilde{x}_i will lie within two standard deviations to either side of μ . The probability that a measurement will fall outside the two standard deviations, to either side of μ , is 4.6%. In assessing precision and linearity, this 95.4% confidence interval was used.⁷⁵

In this project, the wide confidence interval of 99.7% was associated with measurements of ion ratios and retention time to reduce the risk of wrongly assuming the presence of the analyte in a sample known to be spiked with the analyte. The concept is similar for the 99.7% confidence interval where the measurements are expected to fall within three standard deviations of the mean 997 times out of 1 000 measurements. The probability that a measured concentration is rejected as an outlier is, therefore, greater than the probability that the analyte ion ratios are wrongly rejected.⁷⁵

7.2 Statistical techniques applied in this project

7.2.1 *Multivariate analysis of ion ratios – key matrices and vectors*

For identifying the analytes, characteristic ion ratios have been calculated from the absolute chromatographic signal areas. These signal areas have been calculated from the extracted ion chromatograms of the selected, characteristic ions in the analyte mass spectra. All the selected ion ratios must simultaneously correspond to a predetermined confidence interval around the respective means of each ion ratio. In this project the signal areas of the individual ions have been assumed to be normally distributed. Through the propagation of uncertainty, the ion ratios were also assumed to be normally distributed. Since the intensities of the ions may also be interdependent, a *multivariate* Gaussian approach was applied to analyse the ratios.

In multivariate analysis, each ion ratio is considered a variable that can be measured along an axis of values. Multiple measurements of the variables are made simultaneously by analysing multiple samples of reference material of known purity. These measurements are used to build up historical data for comparison to sample data.

Multivariate data analysis was used in this project for evaluating the simultaneous distribution of characteristic ion ratios around their multi-dimensional mean vector. Each measurement of k ion ratios can be represented as a k -dimensional column vector, therefore, a point in a k -

dimensional space.^{76,77} The multivariate mean of the n measurements made ($\bar{\mu}$) is then determined based on the same algorithm as in univariate Gaussian statistics^{77,78} but as a k -dimensional column vector with the individual means of the variables as its elements.^{76,77}

In a multivariate distribution, each variable has an intrinsic random error and is susceptible to external effects, but the interaction of variables adds further dimensionality to the distribution of measurements about their mean. The random error in one variable affects the distribution of a second and so on for all k variables in all combinations of the variables. The variances of the variable measurements around their means, due to these interactions, are referred to as the covariances of the variables.

The covariance of two variables with respect to their means is given by:^{77,79}

$$\sigma_{xy} = \frac{1}{N} \sum_{i=1}^N (x_i - \mu_x)(y_i - \mu_y) \quad (1)$$

where x and y are measurements of variables one and two, respectively. For three variables, the variances and covariances are calculated for each combination of two variables. The variances and covariances are calculated simultaneously, using vector and matrix algebra. For each measurement, the deviation vector, $(\bar{x}_i - \bar{\mu})$, is multiplied with its transpose, $(\bar{x}_i - \bar{\mu})^T$. The sum of the resultant 3×3 matrices, divided by the number of measurements, N , yields the distribution matrix (\mathcal{D}). Therefore, \mathcal{D} is given by:^{76,77}

$$\mathcal{D} = \frac{1}{N} \sum_{i=1}^N (\bar{x}_i - \bar{\mu})(\bar{x}_i - \bar{\mu})^T \quad (2)$$

The diagonal elements of this matrix correspond to the variances of each variable when viewed as independent variables. The off-diagonal elements are the covariances of the individual pairs of variables. Taking the square root of the diagonal elements of \mathcal{D} , the standard deviations for the individual variables can be obtained^{76,77} and will have the same form as in the univariate case.⁷⁸

Interaction between variables is visible in the covariances and correlations between them. To determine these correlations, a correlation matrix (\mathcal{R}) can be computed from the distribution matrix. This algorithm normalises the elements of \mathcal{D} by dividing each element d_{ij} (element of \mathcal{D} in the i -th row and j -th column) by the product of the square roots of the corresponding diagonal elements, d_{ii} , and d_{jj} .^{76,77}

If there exists an interaction between variables, the corresponding off-diagonal elements of the correlation matrix will be non-zero.^{76,77,79} The greater the magnitude of the element, the stronger the interaction. The nature of the interaction can be deduced from the sign of the element. A negative sign implies that the two variables interact in such a way that as one decreases, the other increases. In the case of a positive sign, the two variables change in the same direction, that is as one increases, so does the other, and vice versa.

As per the definition of \mathcal{R} , the diagonal elements of the correlation matrix are unity and non-negative. As the variables tend towards complete independence (spherical distribution) from each other, \mathcal{R} tends toward the identity matrix, I_p , for the p-variate case.⁸⁰

In all these cases, a *normal* multivariate Gaussian distribution was assumed. As in the case of univariate Gaussian statistics, the degrees of freedom must be corrected when small samples (typically $N < 30$) are studied. In such cases, the calculated mean vector, \bar{m} , is calculated in the same manner as ($\bar{\mu}$) the true mean but is referred to as the sample mean vector.^{76,77}

The distribution of the measured data about the sample mean vector now becomes an estimate of the distribution of the measured data about the true mean since the sample mean vector itself is an estimate of the true mean vector. Then \mathcal{D} becomes \mathbf{D} , the sample covariance matrix:^{76,77}

$$\mathbf{D} = \frac{N}{N-1} \mathcal{D} \quad (4)$$

The sample standard deviations are then the square roots of the diagonal entries of \mathbf{D} and the sample covariances the off-diagonal elements of \mathbf{D} .⁷⁶⁻⁷⁹ The definition of the correlation matrix remains the same, but as it is based on an estimated distribution matrix, \mathbf{D} , it becomes the sample correlation matrix, \mathbf{R} .⁷⁶

7.2.2 Hypotheses testing for significant difference

In this project, three types of hypothesis tests were applied: The Student's t-test (student t-test), the F-test, the analysis of variance (ANOVA) F-tests, and Hotelling's T²-test (a special type of F-test whereby the t-test is extended to the multivariate case). The basic approach in hypothesis testing remains the same and can be explained in a logical argument.

The null hypothesis (H_0) is defined as the assumption that there is no significant difference between the measured value, x_m , and the true value, x_T . The alternative hypothesis (H_1) is defined as the assumption that there is a significant difference between x_m and x_T . These

conclusions are drawn from the comparison of a calculated statistic (t-value, F-value)^a to the critical tabulated statistic value at the corresponding degrees of freedom. If the calculated value is less than or equal to this statistical value, the conclusion may be assumed to be H_0 , since the probability that the measured value does not differ significantly from the true value, is greater than the probability that it falls in the rejection region. Otherwise, the conclusion is assumed to be H_1 . It must be noted that the conclusion cannot be to accept both H_0 and H_1 as true.⁸¹

7.2.3 Univariate Analysis of variance (ANOVA)

Analysis of variance is required to determine whether there exists a significant difference between the variances contained within groups of data and the variances between the individual groups of data. This technique was applied in this project to compare the variances associated with mean concentration levels measured in the precision study and in the evaluation of the variance of the mean residuals for regression analyses of linear response models.

There are multiple variations of ANOVA calculations that can be performed, based on the arrangement of the raw data. By far the most frequently applied variation is ‘One-way’ ANOVA or Single-factor ANOVA. This variation of ANOVA is used when the data, that is to be analysed, can be grouped according to only one variable or factor. In chemometrics, it would be applied to determine whether the means of replicate analyses at different concentration levels are significantly different from each other, or whether their distribution can be attributed to random error. The hypotheses for ANOVA are then defined:^{82,83}

$$H_0: \mu_1 = \mu_2 = \dots = \mu_p$$

$$H_1: \mu_i \neq \mu_j; i, j \in [1, 2, \dots, p] \in \mathbb{N} \quad (5)$$

$$H_0 \leftrightarrow F_{test} \leq F_{crit}$$

In ‘One-way’ ANOVA, the variation within each concentration level (i) is averaged by first determining the sum of squares of deviations (S_W) of the n data points within each group from that group’s mean value (\bar{x}_i):^{82,83}

$$S_W = \sum_{i=1, p} \sum_{k=1, n} (\bar{x}_i - x_{ik})^2 \quad (7)$$

Dividing S_W by the sum of the degrees of freedom within each group ($N - p$, for a total of N data points and p groups), produces the mean square for the data points within the individual

^a For the formulae of these statistical values, see the Appendix to Chapter I - D.

groups (M_W). To determine the mean square value for variance between groups, the distribution between all the data, as if in one group (S_{TOT}), needs to be determined:^{82,83}

$$S_{TOT} = \sum_{i=1,p;k=1,n} (\bar{x} - x_{ik})^2 \quad (8)$$

The sum of squares for the between-group variation (S_B) is the difference between S_{TOT} and S_W , with degrees of freedom, $p - 1$. Dividing S_B by its degrees of freedom, the mean square for the between-group variation is obtained (M_B).^{82,83}

The average variance within each group is assumed to be a good estimation of the true within-group variance. The average variance between groups contains variance due to the intergroup changes and the random variance within each group. These statements define the mean square values as:^{82,83}

$$M_W = \sigma_W^2 \quad (9)$$

$$M_B = \sigma_W^2 + n\sigma_B^2 > M_W \quad (10)$$

The hypotheses for comparing these mean squares are:

$$H_2: M_B = M_W \quad (11)$$

$$H_3: M_B > M_W \quad (12)$$

A classic one-tailed F-test is then applied to compare the mean squares for significant difference.^{82,83} This calculated value is then compared to the appropriate one-tailed F -distribution value for the specified degrees of freedom and confidence level, F_{N-p}^{p-1} . The one-tailed distribution is used since the alternative hypothesis can only consider $M_B > M_W$ based on their definitions. If $F > F_{N-p}^{p-1}$, then H_3 (implying H_1) is assumed, and the variation of data between groups is greater than can be attributed to random variation. If the variances differ significantly, then the dataset cannot be pooled.^{82,83}

This basic ‘One-way’ ANOVA can be extrapolated to cases where there are two factors by which the data can be grouped. Depending on how the grouping is done, and whether replicate measurements are made, different approaches of Two-factor ANOVA become applicable.^{82,83}

7.2.4 *Multivariate Analysis of Variance (MANOVA)*

In MANOVA, the aim remains to determine whether or not there exists a significant difference between the means of different populations based on whether the variance between the populations can be wholly attributed to random variance contained within each population.^{84,85} In its simplest form, MANOVA is an extension of univariate ‘One-way’ ANOVA, where the measured values are vectors in several dimensions.

In this project, MANOVA was applied in the evaluation of the precision and repeatability of the methods. The measurements of the interrelated ion ratios are represented as vector variables. The interrelated nature of ion ratios in fragmentation patterns discourages the application of classical single factor ANOVA in comparing the contributions of the ‘within-group’ and ‘between-group’ variances. Starting from the single factor case of ANOVA, the algorithm for MANOVA can be constructed.

Consider the univariate case for single factor ANOVA. Now consider each measured value a column vector in m -dimensions ($m \in \mathbb{N}$). Then assume there are N such vectors, grouped by a single factor into p groups. Each group then contains n vectors, denoted \bar{x}_{ik} for the k^{th} vector variable \bar{x} in the i^{th} group. As in the univariate case, we define the within-group sum of squares (\mathbf{W}), total sum of squares (\mathbf{T}), and between-group sum of squares (\mathbf{A}). \mathbf{W} , \mathbf{T} , and \mathbf{A} are $m \times m$ -matrices for m -dimensional vector variables. As in the univariate case, $\mathbf{T} = \mathbf{W} + \mathbf{A}$. Each one of these matrices has an associated number of degrees of freedom, corresponding to the univariate case. \mathbf{W} has $(N - p)$, \mathbf{T} has $(N - 1)$ and \mathbf{A} has $(p - 1)$.^{84,85}

Corresponding to the mean squares in the univariate case, multiplying \mathbf{W} and \mathbf{A} with the inverse of their respective degrees of freedom give an estimate of the variance within each population (\mathbf{D}_W) and between the populations (\mathbf{D}_A).⁸⁵ The additional covariance of variables, in multivariate statistics, however, influences the comparison of variances and means. In MANOVA, the variances are compared in a Wilks’ Lambda test. Here the test statistic is calculated as the ratio of the determinant of \mathbf{W} to the determinant of \mathbf{T} :^{84,85}

$$\Lambda = \frac{|\mathbf{W}|}{|\mathbf{T}|} \quad (13)$$

^b For the explicit definitions also see: (85) Cooley, W. W. & Lohnes, P. R. 1971. *Multivariate Analysis of Variance*. In: JORDAN, J. F. & ST. JOHN, R. (eds.) *Multivariate Data Analysis*. New York: John Wiley & Sons, Inc., pp. 223-242.

From Λ , the F -distribution is approximated with Rao's approximation.⁸⁵ To determine the appropriate degrees of freedom for the approximating F -distribution's critical statistic, special equations are used (See Appendix to Chapter I -Section D)^b. The test statistic is then calculated as:⁸⁴

$$F = \left(\frac{1 - \Lambda^{\frac{1}{b}}}{\Lambda^{\frac{1}{b}}} \right) \left(\frac{ab - c}{n(p - 1)} \right) \quad (14)$$

The constants in the right-hand group, a , b and c , are given in the Appendix to Chapter I – Section D.⁸⁴ n and p are the number of measurements in a group and the number of groups, respectively. The left-hand side fraction estimates the relative sum of squares term. Multiplying this term with the inverse of the degrees of freedom associated with each sum of squares, generates an equation of the form like that of the conventional F -test applied in univariate ANOVA. Following the same rationale as in the univariate case, the hypothesis test can be performed, keeping in mind the centroids are now vectors.^{82,83}

7.3 Quantitative analysis of analyte signals detected in urine as physiological matrix

7.3.1 Regression analysis

Once the analytes were selectively identified, quantification could proceed. For quantitative analysis, the aim was to first establish a linear response model for the relative analyte response with respect to the internal standard signal area over the range of analyte concentration levels.

Assuming the presence of a linear trend in data is dangerous and should be confirmed with an analysis of y -residuals and their variance and the value of the product-moment correlation coefficient (r^2). If there are noticeable trends in the deviation of the observed y -values from the calculated \hat{y} -values, then it is likely the case that the data follows an exponential or polynomial trend and not a linear trend.^{79,86}

Ideally, the y -residuals should be as small as possible. This implies a close correlation between the linear regression model of calculated y -values and the experimental y -values. In such a case r^2 would be close to 1. However, the significance of r^2 should be determined, as it can be misleading regarding the trend of the data points. This is determined by a t-test where the null hypothesis assumes that there is no correlation between the data points and the calculated trendline ($r^2 \rightarrow 0.000$).⁷⁹

7.3.2 Measurement uncertainty in the regression model – sources of uncertainty

In the regression model it is assumed that there is no variance in the given x -values (i.e. the spiked sample concentration levels). However, a variance is assumed to be present in the observed y -values. The variance produced by their measurement generates variance in the interpolation of a measured y -value to a calculated x -value (i.e. a calculated concentration level of the analyte in a sample). This uncertainty is then influenced by the repeatability of sample preparation, the repeatability of sample chromatography, and the repeatability of manual signal integration. The repeatability of manual signal integration contains the random variation in the signal area due to the matrix background signal. Chromatographic bands were defined for integration between local minima adjacent to the apex of the band.⁸⁷

7.3.3 Measurement uncertainty in regression – the top-down approach

In the top-down approach, measurement uncertainty is determined from the distribution of results obtained when measured relative responses are interpolated from the regression equation to a corresponding analyte concentration.⁸⁸

To simplify the process of interpolation of the calculated x -values from a set of measured y -values from a specific sample, the measured y -values are averaged (y_0) and the variance between them determined. This variance is assumed to account for the individual sources of variance within sample preparation, chromatography, mass spectrometry, and data analysis. The x -value corresponding to the mean y -value (x_0) is then calculated from the equation of the linear regression model.

The error in the mean y -value is propagated with the error in the regression model to give an uncertainty range connected to the calculated x -value. This error in the regression model from the random distribution of measured y -values around the linear equation is incorporated into the standard deviation of the gradient (s_b) and that of the y -intercept (s_a) of the regression line ($\hat{y} = b\hat{x} + a$).⁷⁹

These standard deviations are calculated based on the residuals in the y -direction ($s_{y/x}$), that is the distances in the y -direction between the observed and calculated y -values (y_i and \hat{y}_i respectively at the theoretical concentration level) at each concentration level, and the distances of the respective concentration levels from the mean level (also see Appendix to Chapter I – Section D). Dividing this error in the y -direction by the distribution of points in the x -direction around the centroid of specified x -values, the standard deviation for the slope of the linear model is obtained:⁷⁹

$$s_b = \frac{s_{y/x}}{\sqrt{\sum_{i=1}^P (x_i - \bar{x})^2}} \quad (26)$$

Here P is the number of concentration levels used to set up the response model. By including the error in the y -direction, the degrees of freedom are retained. \bar{x} is the mean, or centroid, of the concentration levels used to set up the model, and x_i is the i^{th} level.

For the intercept of the regression line, the standard deviation is calculated from the equation:⁷⁹

$$s_a = s_{y/x} \sqrt{\frac{\sum_{i=1}^P x_i^2}{P \sum_{i=1}^P (x_i - \bar{x})^2}} \quad (27)$$

These standard deviations are used to calculate the confidence limits of the regression model. Keeping in mind that since less than 30 points are used to set up the model and only one unique line can be drawn through any set of two points, the degrees of freedom in the t -distribution become $(N - 2)$ for N concentration levels in the model.⁷⁹

Thus, the regression line's equation is defined as: $y = bx + a$ with a standard deviation of s_b in the gradient and s_a in the intercept.

The additional uncertainty from instrument repeatability, accounted for by performing multiple analyses of the same sample, makes the calculation of the standard deviation in the calculated x -value more complex. An approximation can be made by using a derived formula (see Appendix to Chapter I – Section D), or by error propagation.⁷⁹

7.3.4 Measurement uncertainty in regression analysis – the bottom-up approach

Measurement uncertainty, when calculated via the bottom-up approach, can be determined following the steps outlined in the Eurachem/CITAC guide (CG4).⁸⁹ In this approach, the measurement uncertainty is determined from first principles. Every step of sample preparation and analysis that carries uncertainty must be accounted for. All the contributing factors for this approach can be illustrated in a cause-and-effect diagram for each method.⁹⁰ The causes for each uncertainty source are elaborated to the point where further branching of causes no longer produces sources of uncertainty with significant effect. The uncertainties generated in each step are then propagated to determine the overall measurement uncertainty as the standard deviation of the result. This uncertainty is then multiplied with a factor, k , to obtain the confidence range corresponding to a specific confidence level.⁸⁹

7.4 Figures of merit in method validation

7.4.1 *Selectivity in analyte identification*

Selective identification of analytes in this project were based on guidelines provided by the European Commission's Directorate-General for Health and Food Safety in SANTE/12682/2019.⁹¹ In this protocol for pesticide analysis in foodstuff by gas chromatography-low resolution mass spectrometry, at least three characteristic ion ratios are required to fall within a defined confidence interval around their respective mean values.⁹¹ In our project, four ratios and the relative chromatographic retention time (w.r.t. the retention time of the internal standard) of the analyte have been used for identification. A 99.7% confidence interval has been associated with the mean of each variable.

The importance of selective identification of an analyte cannot be ignored. Chromatographically, the aim is to isolate the analyte during sample analysis such that no background or other analyte signals co-elute with the analyte signal, or significantly interfere with the target analyte signal. Significant interference with the analyte signal would cause its ion ratios to shift outside the confidence limits associated with the variable means.

If the chromatographic resolution is not possible, 'separation by ions' can be used. Herein the aim is to determine which ion signals can be attributed to the sample matrix and which are produced by the analyte. By theoretically 'subtracting' the matrix signals from the sample signals, the contribution of the analyte to the mass spectrum can be determined.⁶⁶

7.4.2 *Limit of analyte detection (LoD)*

There are two main routes to determine the limit of detection of an analyte in a specific sample matrix: quantitatively and qualitatively. Both routes must be investigated during method validation. In this project, the qualitative limit of detection carried more weight in interpretation, than the quantitative limit, that is both the analyte and internal standard had to be positively identified before they could be quantified.

The variables, described in the section on the selectivity of analyte identification, are all measurements with inherent random variation. The normal distribution of this variation follows from the normal variation assumed in the measured areas of the chromatographic bands in the extracted ion chromatograms. Therefore, a confidence interval (of known confidence level) was calculated for each of the analyte ion ratios during method validation. All the selected ion ratios must simultaneously fall within their respective confidence ranges for positive identification to hold. At low levels of the analyte, noise from the sample matrix and

background interfered with the ion signals and with the ability to determine the corrected retention time. This might have caused false-positive identification or the wrongful assumption that the analyte is absent (see Section 7.5.1).

For the quantitative component of the limit of detection, the U.S. Department of Health and Human Services define three possible limits.⁹² In this project the definition used calculates the relative response at the limit of detection as three times the standard deviation of the intercept of the regression line. The corresponding concentration level is then calculated by interpolation through the equation of the regression line, excluding the intercept, provided it does not deviate significantly from naught.^{79,92,93}

The equation for the limit of detection, therefore, is:

$$c_{LOD} = \frac{3s_a}{b} \quad (30)$$

where s_a is the standard deviation of the y-intercept of the linear response model, and b is the slope of the linear regression line, calculated from the data. This equation assumes the intercept does not deviate significantly from naught.⁹²

It is likely that the experimental limit of detection will be higher than the theoretical limit since the theoretical limit does not account for the positive identification of the analyte. In such a case, the experimental limit of detection becomes the accepted limit.

7.4.3 Limit of analyte quantification (LoQ)

The aim of the limit of quantification is to minimise the interferences from the background in the quantification of the analyte. It is defined as the lowest concentration of analyte that can be determined with reasonable confidence and accuracy. Conventionally this limit is determined as the analyte concentration that produces a relative response y_{LOQ} , where y_{LOQ} is defined as:^{79,92}

$$y_{LOQ} = 10s_a \quad (31)$$

where s_a is the standard deviation of the y-intercept, calculated from the regression line. This calculated relative response is then interpolated through the regression model to obtain the corresponding concentration. If the y-intercept does not deviate significantly from naught, it is not included in the calculation.^{79,92,93}

This theoretical limit of quantification may be influenced by the limits of the linear range, where significant deviation from linearity will prevent the application of the regression model

to calculate the analyte concentration accurately.⁹³ It may be the case that the precision at these extreme values does not fall within confidence limits. In this project, a confidence level of 95.4% has been applied for quantitative analysis. In this project, samples were spiked at concentrations in the range of 1 ppm ($\mu\text{g}/\text{mL}$). In the Horwitz curve, this corresponds to an expected coefficient of variation of 0.16. At the limit of quantification (LoQ), the coefficient of variation (CV) must be less than 0.16 (%-Relative standard deviation < 16%) for multiple measurements of the sample with an analyte concentration equal to the LoQ.

From its definition, the theoretical limit of detection is less than the theoretical LoQ. However, it may be possible in extreme cases that the experimental limit of detection is greater than the LoQ. This will impose a further limit on the quantitative range of the regression model.

7.4.4 Linearity in the measured data

The limits of detection and quantification are closely related to the linearity and precision of the method being validated. The purpose of developing a quantitative analytical method is to obtain a precise and accurate *linear* response model that can be used to determine the quantity of analyte in a sample. Linearity has two components: qualitative linearity and quantitative linearity.

In qualitative linearity, the analyte must be positively identified (see Section 7.4.1) over the entire response model. In a homoscedastic model, the median analyte concentration is used to set up the confidence intervals for the characteristic corrected retention time and characteristic ion ratios of the analyte. At all the remaining analyte levels, the analyte must be positively identified with regard to these confidence intervals. The comparison for a significant difference in corrected retention time has been done with Student's t-test. In the comparisons of the characteristic ion ratios, Hotelling's T^2 -test was used.

Several aspects determine the quantitative component of linearity. For a linear model, the variance of the relative responses, around the centroid, must be greater than can be attributed to random error. The intercept of the line, determined from non-zero values, must contain the origin within its 95.4% confidence interval. This has been determined with Student's t-test with the appropriate degrees of freedom and confidence level.

The fitting of a linear equation to the data must be suitable. There must be a close correlation between the data points and the calculated trendline. On its own, the correlation coefficient (r^2) does not prove, nor disprove, a relationship between the data points. It only indicates how closely the data points correspond to the calculated response values in the trendline.^{79,86,94}

To determine the nature of the relationship between the data points, the y -residuals are plotted against the concentration range. If the residuals are randomly dispersed around the x -axis, the linear model applies to the data. If a pattern emerges where the residuals deviate from the x -axis in a clear trend, the linear model does not apply to the data, despite a possible close correlation between them.^{79,86,94}

7.4.5 Precision in measurements

The precision of a method describes how closely measured values, obtained under identical circumstances from the same samples, are spaced. Thus, “Do the results obtained from applying the method, multiple times over multiple days, change significantly?”⁹³ A method must first be repeatable in identifying the analyte over the entire concentration range before it can be considered repeatable in accurately quantifying the analyte over the entire concentration range. Ideally, inter- and intra-laboratory precision should be determined. In this project, only intra-laboratory precision has been determined by a single analyst.^{93,95}

Typically, precision is determined at the experimental limit of quantification, the median concentration level, and the highest concentration level of the response model. Each level is analysed multiple times (within-level precision and between-level variation) on multiple days (between-day variation). For identification, the corrected retention time of the analyte and the interdependent characteristic ion ratios must remain within their specified confidence ranges, set up during the pre-validation and linearity studies. The significance tests were carried out as in the linearity study.⁹³

Once the analyte was selectively identified in each case, the regression model set up in the linearity study could be used to quantify the analyte present in each sample. The concentrations calculated from the measured responses for the high, median, and low levels, were then compared to the expected values from the linearity and pre-validation studies for a significant difference at the 95.4% confidence level. As in the linearity study, a two-tailed version of Student’s t -test was used with the appropriate degrees of freedom and confidence level. Since only the repeatability was assessed in this project, the reproducibility standard deviation could not be determined.^{93,95}

If one of the calculated measurements (precedence to qualitative analysis) falls outside its confidence interval, the repeatability of the method is compromised. This test was also applied post-validation in quality control to determine whether a response model has remained valid or whether it should be re-calibrated.⁹⁶

7.4.6 Accuracy of quantification and analyte recovery

Determining the accuracy and bias of a method is paramount. Precision measures only the repeatability of the analytical method but refrains from determining the closeness of the measured value to the true value. This trueness is often interpreted in terms of the recovery of the analyte from samples spiked with known levels of analyte.⁹³

Poor sample recovery can lead to a negative additive bias in the measurement of analyte concentrations. A positive additive bias can be produced by a constant contribution by the sample matrix or background. With optimal selectivity, this should not occur at a significant level. If the recovery is related to the concentration of the analyte in the sample, a multiplicative bias is produced. The significance of bias can be assessed with a basic Student's t-test if the number of samples analysed is less than 30.⁹³

Significant bias can be corrected by a correction function generated from the regression analysis of a measured concentration vs. true concentration data plot. The data points should, ideally, follow a linear trend (no curvature should be present in the residual plot) with a tight correlation to the calculated trendline ($r^2 > 0.995$). This trendline's linear equation was of the form

$$y = \beta x + \alpha \quad (32)$$

It was then used as the correction function. The x -values correspond to the theoretical concentration and the y -values to the concentration calculated from the regression model.^{95,97}

In the ideal case of accuracy with maximal analyte recovery from the sample, the slope of the correction function (β) should not deviate significantly from one. The intercept of the correction function (α) should, similarly, not deviate significantly from the origin. For this project, the significance of these bias indicators was determined at the 95.4% confidence level.^{79,93,95}

If there exists significant bias, the %-bias at each concentration can be determined with the equation:⁹³

$$\%Bias = \frac{c(Analyte)_{Meas} - c(Analyte)_{True}}{c(Analyte)_{True}} \times 100 \% \quad (33)$$

7.4.7 Analytical range of a developed method

The range is the upper and lower limits of analyte concentration in a sample that can be measured with acceptable levels of measurement uncertainty. The analytical range is limited by the limits of detection and quantification. Accurate and precise quantitative measurement can only be achieved if the analyte can be accurately and precisely identified. Therefore, the quantitative analytical range is limited by the qualitative analytical range.⁹³

The qualitative range is established between the concentration levels where the uncertainty in the calculation of the identification variables exceed their confidence interval limits (a 99.7% confidence level has been applied for this evaluation). Within these limits, the quantitative range is defined by the concentration levels where the standard deviation of measurement is less than two standard deviations at the median concentration level. The analytical range is then limited by the highest lower limit and the lowest upper limit.⁹³

7.4.8 Robustness of a method

For a method to be robust, it must not be sensitive to small changes during sample preparation and analysis. In this project the focus will be on the pH of samples for extraction, the volume of extraction solvent (or elution solvent in the case of SPE), and the re-use of SPE-cartridges. To decrease the number of analyses required for the study, a Plackett-Burman (fractional factorial) experimental design was employed. This design allows monitoring the effect on analyte response following simultaneous changes in several variables.^{82,93,95}

7.4.9 Stability of sample solutions

Samples are often required to be stored, before preparation or afterward, due to uncontrollable factors. These factors include rolling blackouts or health-and-safety drills and assessments. If a sample cannot be accurately analysed after storage for a specific length of time, the application of the method is limited. The stability of samples under various storage conditions can be assessed in time studies where batches of samples at different stages of preparation, are stored and analysed at specific time intervals.

7.4.10 Carry-over of analyte between samples

A major risk in many analytical methods is the carry-over of the analyte or matrix components. This can affect the method sensitivity and the accuracy of identification and quantification. In routine laboratories, the risk also exists that different analytes from other samples can contaminate the samples being analysed, or that the analyte of interest causes contamination of other samples. These risks are assessed by preparing and analysing samples of high analyte

concentration with solvent blank samples between replicate analyses. A significant deviation of the measured concentration above the true concentration (95.4% confidence level, one-tailed) indicates possible analyte carry-over.

8. Limitations of the project

This project was limited in scope in assuming the parent toxin would be detectable in the urine of a poisoned individual. The metabolism of the toxins, covered by the project scope, was explored based on the known metabolism of similar analytes in literature. A full metabolomic study was not conducted due to logistical restrictions.

References

- (1) Wink, M. & Van Wyk, B.-E. 2008. Poisonous and mind-altering plants in human history - murder, magic and medicine. *In: Pearson, D. (ed.) Mind-altering & Poisonous Plants of the World*. First ed. Pretoria: Briza Publications, pp. 17-25.
- (2) Abdullahi, A. A. 2011. Trends and challenges of traditional medicine in Africa. *African journal of traditional, complementary, and alternative medicines : AJTCAM*, 8, 115-123.
- (3) Meel, B. L. 2007. Fatalities by poisoning in Mthatha area of South Africa. *South African Family Practice*.
- (4) Mcvann, A., Havlik, I., Joubert, P. & Monteagudo, F. 1992. Cardiac glycoside poisoning involved in deaths from traditional medicines. *South African Medical Journal*, 81, 139-141.
- (5) Van Wyk, B.-E., Van Heerden, F. & Van Oudtshoorn, B. 2014. *Urginea sanguinea*. *In: Ferreira, R. (ed.) Poisonous plants of South Africa*. 1st ed. ed. Pretoria: Briza Publications, pp. 214-215.
- (6) Van Wyk, B.-E., Van Oudtshoorn, B. & Gericke, N. 2017. *Catharanthus roseus*. *Medicinal Plants of South Africa*. Pretoria: Briza Publications, pp. 82-83.
- (7) Van Wyk, B.-E., Van Heerden, F. & Van Oudtshoorn, B. 2014. *Acokanthera oppositifolia*. *In: Ferreira, R. (ed.) Poisonous plants of South Africa*. 1st ed. ed. Pretoria: Briza Publications, pp. 34-35.
- (8) Neuwinger, H. D. 1996. *Acokanthera* spp. *African Ethnobotany - Poisons and Drugs*. Weinheim: Chapman & Hall GmbH, pp. 60-80.
- (9) Van Wyk, B.-E., Van Heerden, F. & Van Oudtshoorn, B. 2014. *Boophane disticha*. *In: Ferreira, R. (ed.) Poisonous plants of South Africa*. 1st ed. ed. Pretoria: Briza Publications, pp. 52-53.
- (10) Milne, S. T. & Meek, P. D. 1998. Fatal colchicine overdose: Report of a case and review of the literature. *The American journal of emergency medicine*, 16, 603-608.
- (11) Tamilselvan, N., Thirumalai, T., Shyamala, P. & David, E. 2014. A review on some poisonous plants and their medicinal values. *Journal of Acute Disease*, 3, 85-89.

- (12) De Ruijter, A. 2008. *Strophanthus speciosus* (N.B. Ward & Harv.) Reber. In: Schmelzer, G. H. & Gurib-Fakim, A. (eds.) *Medicinal plants*. Wageningen, Netherlands: PROTA Foundation, pp. 560.
- (13) Botha, C. & Penrith, M.-L. 2008. Poisonous plants of veterinary and human importance in southern Africa. *Journal of Ethnopharmacology*, 119, 549-558.
- (14) Foukaridis, G. N., Osuch, E., Mathibe, L. & Tsipa, P. 1995. The ethnopharmacology and toxicology of *Urginea sanguinea* in the Pretoria area. *Journal of Ethnopharmacology*, 49, 77-79.
- (15) Bradfield, J., Wadley, L., Lombard, M., Maharaj, V., Coote, D. & Wooding, M. 2015. Chemical weapons of the San Bushmen: identifying plant-based toxins on arrows from southern Africa. *SUPPLEMENTO*, 140, 185-187.
- (16) Wooding, M., Bradfield, J., Maharaj, V., Koot, D., Wadley, L., Prinsloo, L. & Lombard, M. 2017. Potential for identifying plant-based toxins on San hunter-gatherer arrowheads. *South African Journal of Science*, 113, 1-10.
- (17) Bradfield, J., Lombard, M. & Wadley, L. 2015. Southern African arrow poison recipes, their ingredients and implications for Stone Age archaeology. *Southern African Humanities*, 27, 29-64.
- (18) West, R. 1984. An excursion into pharmacology: curare in medicine. *Medical history*, 28, 391-405.
- (19) Chaboo, C. S., Biesele, M., Hitchcock, R. K. & Weeks, A. 2016. Beetle and plant arrow poisons of the Ju|'hoan and Hai|om San peoples of Namibia (Insecta, Coleoptera, Chrysomelidae; Plantae, Anacardiaceae, Apocynaceae, Burseraceae). *ZooKeys*, 9-54.
- (20) Du Plooy, W. J., Jobson, M. R., Osuch, E., Mathibe, L. & Tsipa, P. 2001. Mortality from traditional-medicine poisoning : a new perspective from analysing admissions and deaths at Ga-Rankuwa Hospital. *South African Journal of Science*, 97, 70.
- (21) Marks, C. J. & Van Hoving, D. 2016. A 3-year survey of acute poisoning exposures in infants reported in telephone calls made to the Tygerberg Poison Information Centre, South Africa. *South African Journal of Child Health*, 10, 43-46.
- (22) Tygerberg Poison Information Centre. 2015. *Annual Report 2014*. Cape Town: Centre, T. P. I. Available:
<http://www.sun.ac.za/english/faculty/healthsciences/Clinical%20Pharmacology/Poison%20Information%20Centre/Documents/Annual%20Report%20Jan%20-%20Dec%202014.pdf>
[Accessed 2019-01-06].
- (23) Veale, D. J. H., Wium, C. A. & Müller, G. J. 2013. Toxicovigilance I: A survey of acute poisonings in South Africa based on Tygerberg Poison Information Centre data. *South African Medical Journal*, 103, 293-297.
- (24) Veale, D. J. H., Wium, C. A. & Müller, G. J. 2013. Toxicovigilance II: A survey of the spectrum of acute poisoning and current practices in the initial management of poisoning cases admitted to South African hospitals. *SAMJ: South African Medical Journal*, 103, 298-303.
- (25) Neuwinger, H. D. 1974. Die Giftpflanzen und ihre Wirkstoffe. *Afrikanische Pfeilgifte*. Stuttgart: Wissenschaftliche Verlagsgesellschaft m.b.H., pp. 9-27.

- (26) Hutchings, A., Scott, A. H., Lewis, G. & Cunningham, A. B. 1996. *Acokanthera oppositifolia* (Lam.) Codd. *Zulu Medicinal Plants - An Inventory*. South Africa: University of Natal Press, pp. 243.
- (27) Adedapo, A. A., Jimoh, F. O., Afolayan, A. J. & Masika, P. J. 2008. Antioxidant activities and phenolic contents of the methanol extracts of the stems of *Acokanthera oppositifolia* and *Adenia gummifera*. *BMC Complementary and Alternative Medicine*, 8, 54.
- (28) De Villiers, J. 1962. The cardiac glycosides of *Acokanthera oblongifolia*. *South African Journal of Chemistry*, 15, 82-84.
- (29) Kellerman, T. S., Naudé, T. & Fourie, N. 1996. The distribution, diagnoses and estimated economic impact of plant poisonings and mycotoxicoses in South Africa.
- (30) Neuwinger, H. D. 1996. *Boöphone disticha* (Linne f.) Herbert. *African Ethnobotany - Poisons and Drugs*. Weinheim: Chapman & Hall GmbH, pp. 10-16.
- (31) Hutchings, A., Scott, A. H., Lewis, G. & Cunningham, A. B. 1996. *Boophane disticha* (L. f.) Herb. *Zulu Medicinal Plants - An Inventory*. South Africa: University of Natal Press, pp. 49-50.
- (32) Steenkamp, P. 2005. *Chemical analysis of medicinal and poisonous plants of forensic importance in South Africa*. PhD Thesis, University of Johannesburg, Johannesburg.
- (33) Scott, G. 2003. Acute toxicity associated with the use of South African traditional medicinal herbs. *Transactions of the Royal Society of South Africa*, 58, 83-92.
- (34) Du Plooy, W. J., Swart, L. & Van Huysteen, G. W. 2001. Poisoning with *Boophane disticha*: a forensic case. *Human & experimental toxicology*, 20, 277-278.
- (35) Gunasekaran, K., Mathew, D. E., Sudarsan, T. I. & Iyyadurai, R. 2019. Fatal colchicine intoxication by ingestion of *Gloriosa superba* tubers. *BMJ Case Reports*, 12, e228718.
- (36) Kande Vidanalage, C. J., Ekanayeka, R. & Wijewardane, D. K. 2016. Case report: a rare case of attempted homicide with *Gloriosa superba* seeds. *BMC pharmacology & toxicology*, 17, 26-26.
- (37) Toyin, Y. M., Olakunle, A. T. & Adewunmi, A. M. 2014. Toxicity and Beneficial Effects of Some African Plants on the Reproductive System. In: Kuete, V. (ed.) *Toxicological Survey of African Medicinal Plants*. Waltham: Elsevier Inc.
- (38) Neuwinger, H. D. 1996. *Gloriosa superba* Linné. *African Ethnobotany - Poisons and Drugs*. Weinheim: Chapman & Hall GmbH, pp. 554-561.
- (39) Ng, S. W., Ching, C. K., Chan, A. Y. W. & Mak, T. W. L. 2013. Simultaneous detection of 22 toxic plant alkaloids (aconitum alkaloids, solanaceous tropane alkaloids, sophora alkaloids, strychnos alkaloids and colchicine) in human urine and herbal samples using liquid chromatography–tandem mass spectrometry. *Journal of Chromatography B*, 942, 63-69.
- (40) Balkrishna, A., Das, S. K., Pokhrel, S., Joshi, A., Verma, S., Sharma, V. K., Sharma, V., Sharma, N. & Joshi, C. 2019. Colchicine: Isolation, LC–MS QToF Screening, and Anticancer Activity Study of *Gloriosa superba* Seeds. *Molecules*, 24, 2772.
- (41) Beyer, J., Peters, F. T., Kraemer, T. & Maurer, H. H. 2007. Detection and validated quantification of toxic alkaloids in human blood plasma—comparison of LC-APCI-MS with LC-ESI-MS/MS. *Journal of Mass Spectrometry*, 42, 621-633.

- (42) Jones, G. R., Singer, P. P. & Bannach, B. 2002. Application of LC-MS Analysis to a Colchicine Fatality. *Journal of analytical toxicology*, 26, 365-369.
- (43) Samanidou, V. F., Sarantis, G. A. & Papadoyannis, I. N. 2006. Development and Validation of a Rapid HPLC Method for the Direct Determination of Colchicine in Pharmaceuticals and Biological Fluids. *Journal of Liquid Chromatography & Related Technologies*, 29, 1-13.
- (44) Neuwinger, H. D. 1996. *Drimia sanguinea* (Schinz) Jessop. *African Ethnobotany - Poisons and Drugs*. Weinheim: Chapman & Hall GmbH, pp. 548-551.
- (45) Tamokou, J.-D.-D. & Kuete, V. 2014. Toxic Plants Used in African Traditional Medicine. In: Kuete, V. (ed.) *Toxicological Survey of African Medicinal Plants*. Elsevier, pp. 135-180.
- (46) Majinda, R. R., Waigh, R. D. & Waterman, P. G. 1997. Bufadienolides and other constituents of *Urginea sanguinea*. *Planta medica*, 63, 188-190.
- (47) Hutchings, A., Scott, A. H., Lewis, G. & Cunningham, A. B. 1996. *Gloriosa superba* L. *Zulu Medicinal Plants - An Inventory*. South Africa: University of Natal Press, pp. 26.
- (48) Williams, V. L., Raimondo, D., Crouch, N. R., Brueton, V. J., Cunningham, A. B., Scott-Shaw, C. R., Lötter, M. & Ngwenya, A. M. 2008. *Drimia sanguinea* (Schinz) Jessop. *National Assessment: Red List of South African Plants* [Online]. Pretoria: SANBI (South African National Biodiversity Institute). Available: <http://redlist.sanbi.org/species.php?species=3812-53> [Accessed 2019-10-14].
- (49) Thurman, E. M. & Mills, M. S. 1998. Overview of Solid-Phase Extraction. In: Winefordner, J. D. (ed.) *Solid-Phase Extraction - Principles and Practice*. New York: John Wiley & Sons, Inc., pp. 1-23.
- (50) Flanagan, R. J., Taylor, A., Watson, I. D. & Whelpton, R. 2007. Modes of Sample Preparation. *Fundamentals of Analytical Toxicology*. West Sussex: John Wiley & Sons, Ltd., pp. 51-79.
- (51) Merck. 2020. *Reversed-Phase SPE Methodology* [Online]. Darmstadt: Merck KGaA. Available: <https://www.sigmaaldrich.com/analytical-chromatography/sample-preparation/spe/reversedphase-methodology.html> [Accessed 2020-09-10].
- (52) Kotz, J. C., Treichel, P. M., Townsend, J. R. & Treichel, D. A. 2015. Properties of Liquids. In: Inc., G. (ed.) *Chemistry & Chemical Reactivity*. 9 ed. Stamford: Cengage Learning, pp. 421-435.
- (53) Knapp, D. R. 1979. Uses of Analytical Derivatisation. *Handbook of Analytical Derivatisation Reactions*. New York: John Wiley & Sons, Inc., pp. 2-6.
- (54) Knapp, D. R. 1979. Derivative Types and Reagents. *Handbook of Analytical Derivatisation Reactions*. New York: John Wiley & Sons, Inc., pp. 8.
- (55) Chemspider. 2020. *MSTFA* [Online]. London: Royal Society of Chemistry. Available: <http://www.chemspider.com/Chemical-Structure.30134.html> [Accessed 2020-08-28].
- (56) Chemspider. 2020. *TMSI* [Online]. London: Royal Society of Chemistry. Available: http://www.chemspider.com/Chemical-Structure.26905.html?rid=02ca4bf6-f86a-4f4c-9a54-f7329799ee6e&page_num=0 [Accessed 2020-08-28].
- (57) McNair, H. M. & Miller, J. M. 2009. Capillary Columns and Inlets. *Basic Gas Chromatography*. 5th ed. New Jersey: John Wiley & Sons, Inc., pp. 84-103.

- (58) McNair, H. M. & Miller, J. M. 2009. Instrument Overview. *Basic Gas Chromatography*. 2nd ed. New Jersey: John Wiley & Sons, Inc., pp. 14-28.
- (59) McNair, H. M. & Miller, J. M. 2009. Basic Concepts and Terms. *Basic Gas Chromatography*. 5th ed. New Jersey: John Wiley & Sons, Inc., pp. 29-52.
- (60) Laopongsit, W., Szrednicki, G. & Craske, J. 2014. Preliminary study of solid phase micro-extraction (SPME) as a method for detecting insect infestation in wheat grain. *Journal of Stored Products Research*, 59, 88-95.
- (61) McNair, H. M. & Miller, J. M. 2009. Programmed Temperature. *Basic Gas Chromatography*. 5th ed. New Jersey: John Wiley & Sons, Inc., pp. 145-155.
- (62) Smith, J. G. 2017. Other Types of Mass Spectrometry. In: Timp, T., Pellerito, A. & Murdzek, J. (eds.) *Organic Chemistry*. 5th ed. New York: The McGraw-Hill Companies Inc., pp. 504-506.
- (63) McNair, H. M. & Miller, J. M. 2009. Gas Chromatography-Mass Spectrometry (GC-MS). *Basic Gas Chromatography*. 2nd ed. New Jersey: John Wiley & Sons, Inc., pp. 156-169.
- (64) De Hoffmann, E. & Stroobant, V. 2007. Quadrupole Analysers. *Mass Spectrometry - Principles and Applications*. 3rd ed. West Sussex: John Wiley & Sons, Inc., pp. 88-100.
- (65) De Hoffmann, E. & Stroobant, V. 2007. Detectors. *Mass Spectrometry - Principles and Applications*. 3rd ed. West Sussex: John Wiley & Sons, Inc., pp. 175-182.
- (66) European Commission: Directorate General for Health and Food Safety. 2017. *SANTE/11945/2015: Guidance document on analytical quality control and method validation procedures for pesticides residues analysis in food and feed*. European Commission: Directorate General for Health and Food Safety. Available: https://ec.europa.eu/food/sites/food/files/plant/docs/pesticides_mrl_guidelines_wrkdoc_2017-11813.pdf [Accessed 2020-08-26].
- (67) Niessen, W. M. A. 2006. Liquid Chromatography and Sample Pretreatment. In: Cazes, J. (ed.) *Liquid Chromatography-Mass Spectrometry*. 3rd ed. Boca Raton: CRC Press, Taylor and Francis Group, LLC, pp. 3-22.
- (68) Skoog, D. A., Holler, F. J. & Crouch, S. R. 2007. Column Efficiency In LC. In: Kiselica, S. (ed.) *Principles of Instrumental Analysis*. 6th ed. Belmont: Brooks/Cole Cengage Learning, pp. 817-817.
- (69) Jandera, P. 2017. Separation Mechanism and Effects of the Adsorbed Water and Mobile Phase. In: Holcapek, M. & Byrdwell, W. C. (eds.) *Handbook of Advanced Chromatography/Mass Spectrometry Techniques*. San Diego: Elsevier Inc., pp. 56-68.
- (70) Skoog, D. A., Holler, F. J. & Crouch, S. R. 2007. Partition Chromatography. In: Short, M. A. (ed.) *Principles of Instrumental Analysis*. 6th ed. Belmont: Brooks/Cole Cengage Learning, pp. 828-837.
- (71) Fjeldsted, J. C. 2009. Accurate Mass Measurements with Orthogonal Axis Time-of-Flight Mass Spectrometry. In: Ferrer, I. & Thurman, E. M. (eds.) *Liquid Chromatography Time-of-Flight Mass Spectrometry - Principles, Tools, and Applications for Accurate Mass Analysis*. New Jersey: John Wiley & Sons, Inc., pp.
- (72) De Hoffmann, E. & Stroobant, V. 2007. Time-of-Flight Analysers. *Mass Spectrometry - Principles and Applications*. 3rd ed. West Sussex: John Wiley & Sons, Inc., pp. 126-143.

- (73) Niessen, W. M. A. 2006. Mass Spectrometry. *In: Cazes, J. (ed.) Liquid Chromatography-Mass Spectrometry*. 3rd ed. Boca Raton: CRC Press, Taylor and Francis Group, LLC, pp. 23-50.
- (74) De Hoffmann, E. & Stroobant, V. 2007. Chemical Ionisation. *Mass Spectrometry - Principles and Applications*. 3rd ed. West Sussex: John Wiley & Sons, Inc., pp. 17-28.
- (75) Rice, J. A. 2007. Survey sampling. *In: Crockett, C. (ed.) Mathematical Statistics and Data Analysis*. Belmont: Thomson Brooks/Cole, pp. 199-254.
- (76) Cooley, W. W. & Lohnes, P. R. 1971. The Basic Vectors and Matrices. *In: Jordan, J. F. & St. John, R. (eds.) Multivariate Data Analysis*. New York: John Wiley & Sons, Inc., pp. 29-46.
- (77) Härdle, W. K. & Simar, L. 2015. Moving to Higher Dimensions. *Applied Multivariate Statistical Analysis*. 4th ed. Berlin: Springer-Verlag Berlin Heidelberg, pp. 79-117.
- (78) Miller, J. N. & Miller, J. C. 2010. Statistics of repeated measurements. *Statistics and Chemometrics for Analytical Chemistry*. 6th ed. Essex: Pearson Education Limited, pp. 17-36.
- (79) Miller, J. N. & Miller, J. C. 2010. Calibration methods in instrumental analysis: regression and correlation. *Statistics and Chemometrics for Analytical Chemistry*. 6th ed. Essex: Pearson Education Limited, pp. 110-153.
- (80) Cooley, W. W. & Lohnes, P. R. 1971. Principal Components. *In: Jordan, J. F. & St. John, R. (eds.) Multivariate Data Analysis*. New York: John Wiley & Sons, Inc., pp. 96-128.
- (81) Rice, J. A. 2007. Testing Hypotheses and Assessing Goodness of Fit. *In: Crockett, C. (ed.) Mathematical Statistics and Data Analysis*. Belmont: Thomson Brooks/Cole, pp. 329-376.
- (82) Ellison, S. L. R., Barwick, V. J. & Farrant, T. J. D. 2009. Analysis of Variance. *Practical Statistics for the Analytical Scientist - A Bench Guide*. 2nd ed. Cambridge: The Royal Society of Chemistry, pp. 59-91.
- (83) Rice, J. A. 2007. The Analysis of Variance. *In: Crockett, C. (ed.) Mathematical Statistics and Data Analysis*. Belmont: Thomson Brooks/Cole, pp. 477-513.
- (84) 2020. *Lesson 8: Multivariate Analysis of Variance (MANOVA)* [Online]. Pennsylvania: The Pennsylvania State University. Available: <https://online.stat.psu.edu/stat505/book/export/html/762> [Accessed 2020-08-28].
- (85) Cooley, W. W. & Lohnes, P. R. 1971. Multivariate Analysis of Variance. *In: Jordan, J. F. & St. John, R. (eds.) Multivariate Data Analysis*. New York: John Wiley & Sons, Inc., pp. 223-242.
- (86) Rice, J. A. 2007. Linear Least Squares. *In: Crockett, C. (ed.) Mathematical Statistics and Data Analysis*. 3rd ed. Belmont: Thomson Brooks/Cole, pp. 542-603.
- (87) 2012. Step 2. Identifying Uncertainty Sources. *In: Ellison, S. L. R. & Williams, A. (eds.) EURACHEM/CITAC Guide CG 4 - Quantifying Uncertainty in Analytical Measurement* 3rd ed.: EURACHEM/CITAC, pp. 14-15.
- (88) Lee, J. H., Choi, J.-H., Youn, J. S., Cha, Y. J., Song, W. & Park, A. J. 2015. Comparison between bottom-up and top-down approaches in the estimation of measurement uncertainty. *Clinical Chemistry and Laboratory Medicine (CCLM)*, 53, 1025-1032.

- (89) 2012. Step 4. Calculating the Combined Uncertainty. *In: Ellison, S. L. R. & Williams, A. (eds.) EURACHEM/CITAC Guide CG 4 - Quantifying Uncertainty in Analytical Measurement* 3rd ed.: EURACHEM/CITAC, pp. 26-29.
- (90) Meinrath, G. & Lis, S. 2002. Application of cause-and-effect diagrams to the interpretation of UV-Vis spectroscopic data. *Analytical and bioanalytical chemistry*, 372, 333-340.
- (91) European Commission: Directorate General for Health and Food Safety. 2020. *SANTE/12682/2019: Guidance document on analytical quality control and method validation procedures for pesticide residues analysis in food and feed*. European Commission: Directorate General for Health and Food Safety. Available: https://ec.europa.eu/food/sites/food/files/plant/docs/pesticides_mrl_guidelines_wrkdoc_2017-11813.pdf [Accessed 2020-08-26].
- (92) Center for Drug Evaluation and Research. 1996. *Guidance for Industry - Q2B Validation of Analytical Procedures: Methodology*. Rockville: Center for Drug Evaluation and Research. Available: https://ec.europa.eu/food/sites/food/files/plant/docs/pesticides_mrl_guidelines_wrkdoc_2017-11813.pdf [Accessed 2020-08-26].
- (93) Ellison, S. L. R., Barwick, V. J. & Farrant, T. J. D. 2009. Validation and Method Performance. *Practical Statistics for the Analytical Scientist - A Bench Guide*. 2nd ed. Cambridge: The Royal Society of Chemistry, pp. 144-160.
- (94) Ellison, S. L. R., Barwick, V. J. & Farrant, T. J. D. 2009. Regression. *Practical Statistics for the Analytical Scientist - A Bench Guide*. 2nd ed. Cambridge: The Royal Society of Chemistry, pp. 92-113.
- (95) Miller, J. N. & Miller, J. C. 2010. The quality of analytical measurements. *Statistics and Chemometrics for Analytical Chemistry*. 6th ed. Essex: Pearson Education Limited, pp. 74-109.
- (96) European Commission: Directorate General for Health and Food Safety. 2020. *SANTE/12682/2019: Guidance document on analytical quality control and method validation procedures for pesticides residues analysis in food and feed*. European Commission: Directorate General for Health and Food Safety. Available: https://ec.europa.eu/food/sites/food/files/plant/docs/pesticides_mrl_guidelines_wrkdoc_2017-11813.pdf [Accessed 2020-08-26].
- (97) Bouveresse, E., Hartmann, C., Massart, D. L., Last, I. R. & Prebble, K. A. 1996. Standardization of Near-Infrared Spectrometric Instruments. *Analytical chemistry*, 68, 982-990.

Chapter II

Boophane disticha (L.f.) Herb.

1. Background and information

1.1 Ethnopharmacology of *Boophane disticha*

In ethnopharmacology, the primary component of *B. disticha* that is used, is its bulb, which contains potent neurotoxic alkaloids. Decoctions made from the scales of the bulb retain sufficient alkaloidal content to be lethal if not administered in the proper dose.¹⁻³ They are administered either orally or as enemas, with the latter significantly increasing the potency of the alkaloids as they are absorbed directly into the blood stream.^{2,4,5} Administration of large doses is known to cause hallucinations and is applied for ritualistic or recreational use.^{3,5,6}

The decoctions are prescribed for the treatment of headaches, hysteria, intense pain in the chest, and bladder pains.^{5,7} The decoctions are also administered to treat weakness, eye conditions⁸ and cramps in the lower extremities² as well as to calm down psychotic patients.⁴ Scales from the bulb are used as anti-microbial wound dressings and as a treatment for abscesses.⁸

Livestock in rural areas can be exposed to *B. disticha*'s alkaloids when decoctions made from the plant material are used as drenching agents to treat constipation in ruminants. This poses a serious risk to the lives of these animals.²

1.2 Alkaloids of *B. disticha*

The bulbs of *B. disticha* contain eleven principal alkaloids within the class Amaryllidaceae-alkaloids. These alkaloids are known to have neurotoxic effects, as expected of tropane alkaloid (scopolamine, hyoscyamine, cocaine) toxicosis¹ and are characteristic of plants in the family Amaryllidaceae.⁹ The general structure of Amaryllidaceae-alkaloids is illustrated in **Figure II-1**.

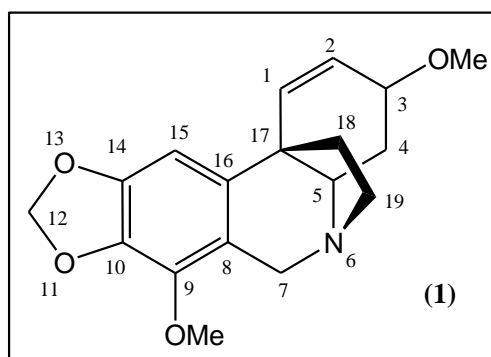


Figure II-1. Molecular structure of buphanidrine (I) as cited in literature.^{9,10}

Many of the alkaloids known to be present in *B. disticha*, including buphanidrine (**1**), its principal toxic constituent (**Figure II-2**), are present in other plants of the family.^{1,11} Three unique Amaryllidaceae-alkaloids found in *Boophane* spp. are distichamine (**2**) (**Figure II-2**), 3-O-acetylnerbowdine (**3**) (**Figure II-2**) and buphacetine.^{11,12} The latter three alkaloids are, however, not present in large quantities in the plant material of *B. disticha*, compared to the amount of buphanidrine (**1**) present.^{12,13} Based on research by Hauth and Stauffacher, distichamine (**2**) made up 5.4% of the alkaloid content in the extracts from *B. disticha* they analysed. 3-O-acetylnerbowdine (**3**) made up only 0.6%, and buphacetine only 0.3% of the total alkaloid content. In contrast, they determined buphanidrine (**1**) accounted for 19.4% of the alkaloid content.^{12,13}

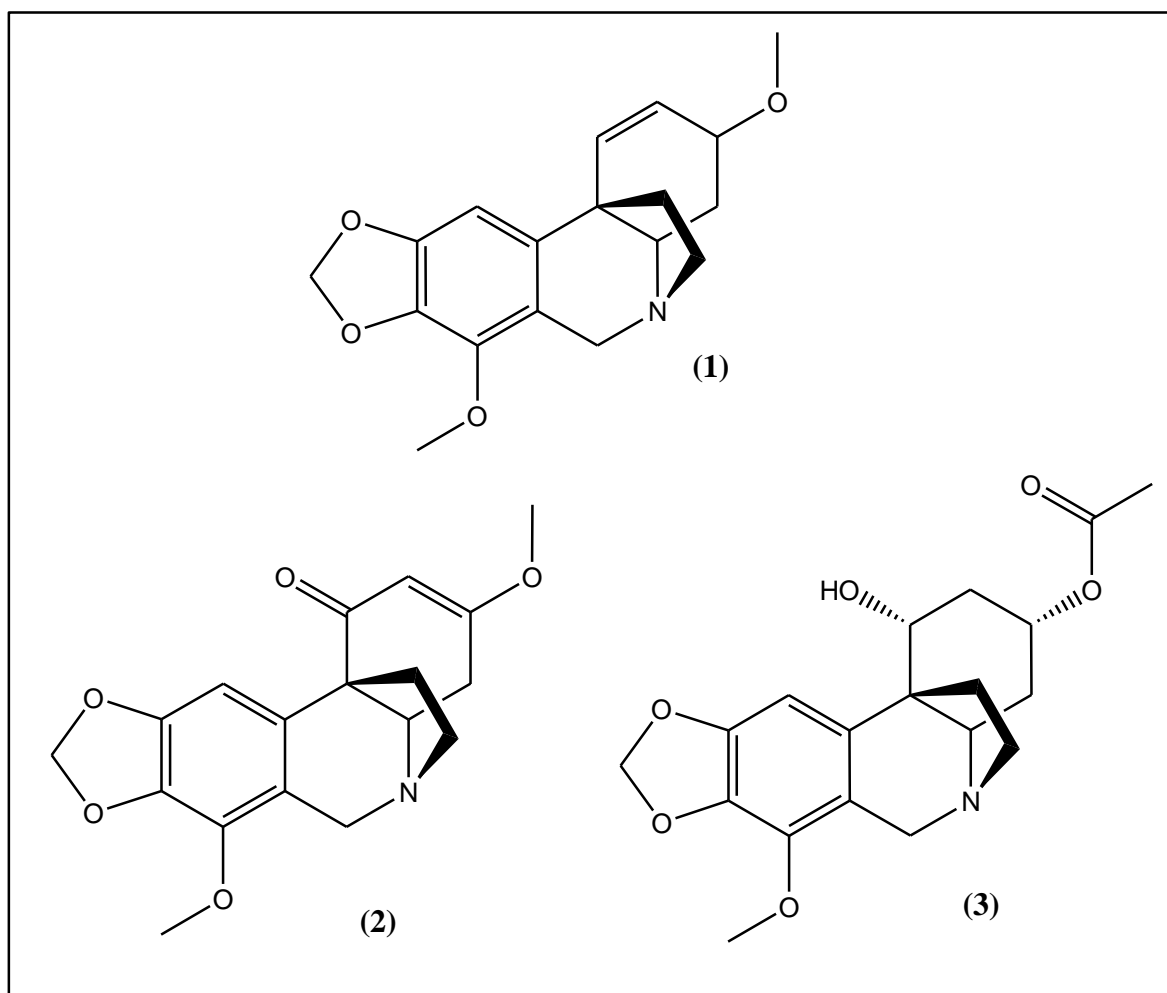


Figure II-2. Important alkaloids from *B. disticha*: buphanidrine (**1**) – its principal toxic constituent, distichamine (**2**) and 3-O-acetylnerbowdine (**3**) (the latter two alkaloids being unique to *B. disticha*).^{11,12}

1.3 Notable cases of poisoning with *B. disticha*

Alkaloids from plants in the family Amaryllidaceae are highly toxic and their potency makes them ideal for application in ethnic medicine, provided the correct dosage is administered. Acute poisoning, with fatal consequences, has been reported following the use of *B. disticha* for medicinal purposes. Neuwinger¹ describes a case where an extract of *B. disticha* was administered to a 10-year-old child as an enema. The child succumbed shortly after administration of the decoction. In a post-mortem investigation, *Boophane*-alkaloids were detected in the liver, kidneys, stomach and intestines of the child.¹

In 1979, Laing⁶ a medical officer of then Fort Victoria, reported three cases of poisoning by *B. disticha*. Although all three patients recovered, notable hallucinogenic symptoms were recorded as well as an elevated heart rate (tachycardia), hypertension and an elevated body temperature (37.4-37.6 °C). Difficulty breathing was recorded as well.⁶

A recent case of non-fatal intoxication with an extract from *B. disticha* was described by du Plooy et al.³ in 2001. The patient consumed 150 mL of a decoction made from *B. disticha*, given to him by a traditional healer. When the patient started to hallucinate, he reacted violently. Upon his arrest, a sample of the decoction was analysed by the South African Police Forensic Services and found to contain alkaloids from *B. disticha* (buphanidine (**1**), buphanine, crinamide and undulatine).³

In 2005 Steenkamp¹⁴ cited a case where a female patient requested the aid of a traditional healer to cleanse her system. The healer provided her with 750 mL of *muti*, prepared from *B. disticha*, and instructed her to administer half as an enema and drink the remainder of the *muti*. Upon doing so the patient developed severe nausea and continuously vomited. Shortly after falling ill, the patient succumbed to the toxic effects of the *muti*.¹⁴

1.4 Physiological symptoms observed in cases of Amaryllidaceae-alkaloid toxicosis

In cases of acute Amaryllidaceae-alkaloid toxicosis the observed symptoms often include neurological, cardiovascular, and gastro-intestinal symptoms.¹⁵ An experiment in dogs, recorded by Hutchings & Terblanche¹⁶, showed that tachycardia and difficulty breathing can develop from Amaryllidaceae-alkaloid toxicosis.¹⁶ These symptoms were observed in addition to violent hallucinations in the three cases of poisoning with *B. disticha* that was recorded by Laing⁶ in 1979 and a case of homicide described by du Plooy³ in 2001.

1.5 Detection of buphanidrine

The detection of buphanidrine, and alkaloids in general, in plant material and extracts thereof is well studied. Regarding the detection of Amaryllidaceae-alkaloids, specifically buphanidrine, in urine and other physiological fluids has not yet been extensively researched. Of major importance was the discovery of distichamine and its uniqueness to plants of the genus *Boophane*. Despite its low abundance in the material of *B. disticha*, it is an important chemical marker. In both humans and animals, it would indicate consumption of the plant material. In plants it serves to aid in the identification of the source plant.^{7,11}

Chromatography techniques, hyphenated with mass spectrometric detection, have been employed in the analysis of solutions known to contain Amaryllidaceae-alkaloids. In the case study described by du Plooy et al.,³ GC-MS was utilised to analyse a chloroform extract from *muti* prepared from *B. disticha*.³ GC-MS was also employed in the analysis of a crude plant extract, prepared from the bulb of *Amaryllis belladonna*.¹⁷

As an alternative to GC-MS, LC-MS has also been utilised for the analysis of samples suspected of containing Amaryllidaceae-alkaloids. For the analysis of a crude extract, prepared by the maceration of bulb material of *B. disticha* in a dichloromethane-methanol (1:1) extraction solvent, a UPLC-MS/MS system has been used by Wooding, et al.¹⁸ Qualitative analyses of a patient's viscera, following fatal overdosage with alkaloids from *B. disticha*, was performed by Steenkamp¹⁴ with the aid of an HPLC-MS system.

2. Experimental

2.1 List of reagents used in the methods of this chapter

Table II-1. List of reagents and chemicals utilised for experimental work in Chapter II.

Chemical	Quality	Company	City [†]
2,2,3,3,3-Pentafluoro-1-propanol (PFPOH)	>99.9% (GC)	Sigma-Aldrich Chemie GmbH	Schnelldorf, DEU
5- α -Cholestane	99.9% (HPLC)	Sigma Life Sciences	St. Louis, USA
Acetone	>99%	Radchem	Johannesburg, ZA
Acetonitrile	99.9% (GC)	Sigma-Aldrich Chemie GmbH	Schnelldorf, DEU
Acetonitrile	100.0%	Macron, via Radchem	Johannesburg, ZA
De-ionised water	$\rho = 20. \Omega.M^{\dagger}$	Merck (Pty.) Ltd.	Modderfontein, ZA

Deuterated chloroform	99.8%	Sigma-Aldrich Chemie GmbH	Schnelldorf, DEU
Dichloromethane	≥99.8%	Merck KGaA	Darmstadt, DEU
Dichloromethane	>99%	Radchem	Johannesburg, ZA
Disodium hydrogen orthophosphate dihydrate	≥99.5% (A)*	Merck (Pty.) Ltd.	Modderfontein, ZA
Ethyl acetate	99.9%	Radchem	Johannesburg, ZA
Formic acid	98.2%	Sigma-Aldrich Chemie GmbH	Schnelldorf, DEU
Hydrochloric acid	33.8%	Radchem	Johannesburg, ZA
Hydrochloric acid	32.7%	Sigma-Aldrich Chemie GmbH	Schnelldorf, DEU
Isopropanol	99.99% (GC)	Sigma-Aldrich Chemie GmbH	Schnelldorf, DEU
Methanol	99.98% (GC)	Sigma-Aldrich Chemie GmbH	Schnelldorf, DEU
Methanol	99.9%	Radchem	Johannesburg, ZA
Methanol	100.0%	Macron, via Radchem	Johannesburg, ZA
Methanol	>99.9%	ROMIL, via Microsep	Johannesburg, ZA
n-Hexane	≥98.0%	Radchem	Johannesburg, ZA
Pentafluoro-propionic anhydride (PFPA)	99.9% (GC)	Sigma-Aldrich Chemie GmbH	Schnelldorf, DEU
Silica gel 60	Particle diameter = 0.063-0.2 mm	Fluka	Steinheim, DEU
Sodium chloride	>99%	Radchem	Johannesburg, ZA
Sodium hydroxide	≥99.0% (A)	Merck (Pty.) Ltd.	Modderfontein, ZA
Sodium hydroxide	99.75% (A)	Promark Chemicals	Robertsham, ZA
Sodium sulphate	>99%	Radchem	Johannesburg, ZA
Triethylamine	99.99% (GC)	Sigma-Aldrich Chemie GmbH	Schnelldorf, DEU
Trifluoroacetic acid	99.96%	Radchem	Johannesburg, ZA
Water	>18 Ω.m	ROMIL, via Microsep	Johannesburg, ZA

*A: Acid-base titration

2.2 Isolation of buphanidrine from *B. disticha*

Several techniques and processes were utilised in the extraction and isolation of buphanidrine from the plant material and subsequent extracts. The experimental route to fractionation of the alkaloids via silica gel column chromatography, is summarised in **Figure II-3**. The figure only indicates the fractions suspected of containing buphanidrine. Each combined fraction was labelled according to the convention: “Analyst initials”-“Notebook page number”-“Capital letter index”. The sequence of combined fractions from the silica gel column follows an increase in polarity with an increase in index (A to Z).

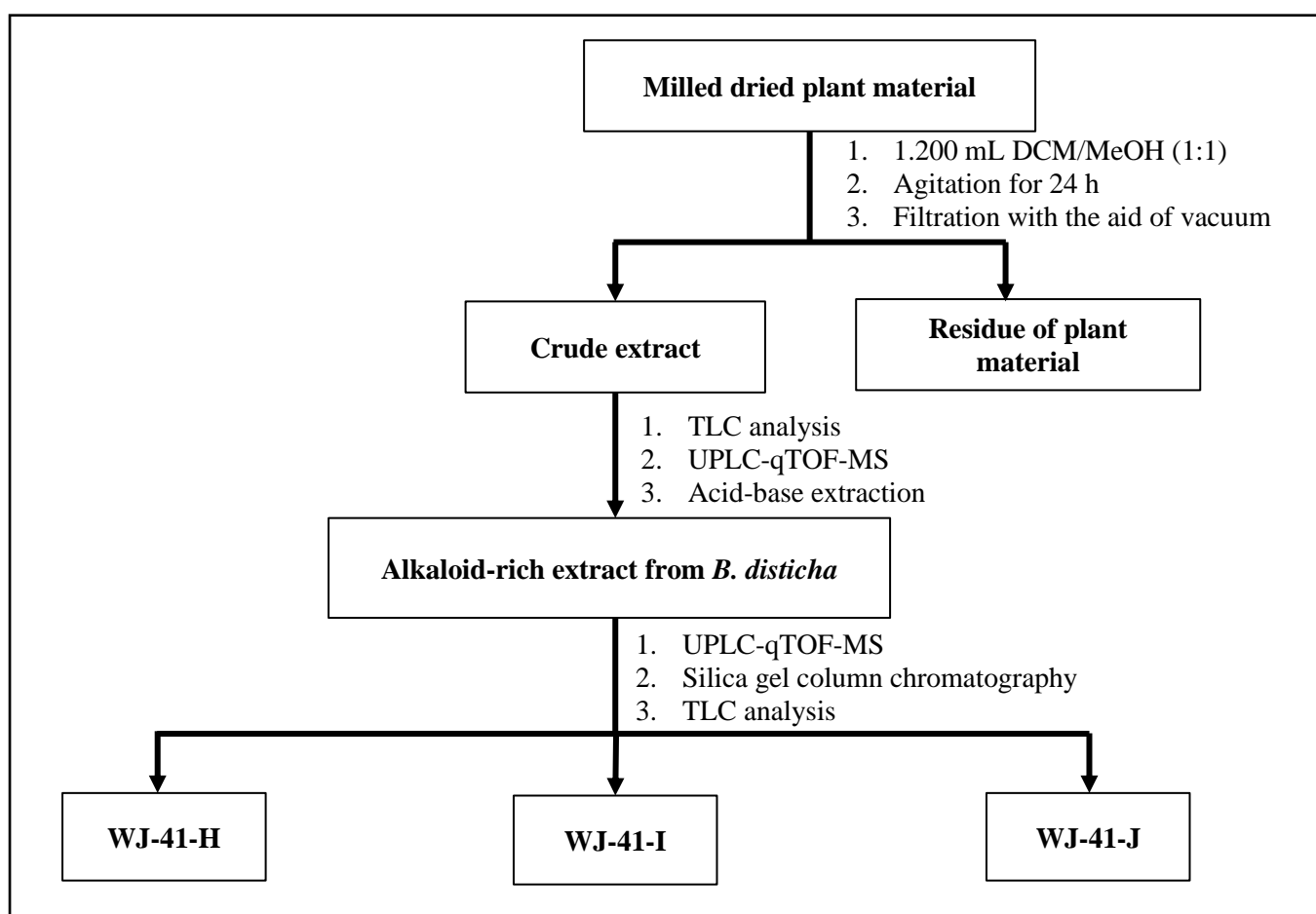


Figure II-3. Illustration of the extraction and fractionation of alkaloids from *B. disticha*.

2.2.1 Preparation and extraction of plant material

For the purposes of this study, two bulbs of *B. disticha* were sourced from a nursery and kept in the University of Pretoria’s greenhouses until used. One bulb (455.379 g – with leaves and roots removed) was removed from the soil and peeled. The scales of the bulb were cut into

small pieces and dried in a laboratory oven for six days at 35-40 °C. The dried scales were milled with a grinder to a fine powder.

As indicated in **Figure II-3**, compounds were extracted from the dried material (120.14 g) by maceration in a dichloromethane-methanol solvent system (Radchem[®], 1 200 mL, 1:1) for 24 h. The mixture was filtered the following day by vacuum filtration with a Büchner-funnel and Whatman[®] Grade 1 filter paper. Any remaining solvent was washed with the dichloromethane-methanol solvent system (Radchem[®], 200 mL, 1:1). The filtrate was again filtered by vacuum through fresh filter paper to capture any macroscopic particles that were not removed during the first filtration. Once clear, the extract was dried using a rotary evaporator.

To ensure maximum extraction of the alkaloids from the plant material, the process was repeated on the extracted plant material twice. The extracts were combined and dried via rotary evaporation. A sample of crude extract (259 mg) was stored as reference sample NS-2-A. The crude extract was analysed via UPLC-qTOF-MS under generic conditions.

2.2.2 Concentration of alkaloids from crude extract

For the isolation of alkaloids from the crude extract, a classic acid-base liquid-liquid extraction process was followed, as indicated in **Figure II-3**. The crude extract was solubilised in a dichloromethane-methanol solvent system (Radchem[®], ~350 mL, 1:1) and acidified with HCl_(aq) (Radchem[®], ~20 mL). The organic phase was then extracted with distilled water (~200 mL) three times.

For extraction of the alkaloids from the aqueous fraction, sodium hydroxide pellets (Promark Chemicals[®]) were added to the aqueous solution to obtain a pH ~ 11. Isolation of the alkaloids was achieved by liquid-liquid extraction of the alkaline aqueous phase with dichloromethane (Radchem[®], 1 000 mL), four times. The collected organic phases were combined, and the aqueous phase and emulsion were collected separately.

The collected organic layer was then sequentially washed with sodium chloride brine (300 mL, 26% m/v) and distilled water (300 mL). Residual water was removed from the organic extract by addition of sodium sulphate (Radchem[®]) to the organic phase. The drying agent was removed by filtration under vacuum through Whatman[®] Grade 1 filter paper. This filtrate was dried via rotary evaporation and reconstituted in dichloromethane (Radchem[®]) for up-concentration in a polytop-vial and evaporated in a Genevac[®] EZ-2 Plus evaporator.

2.2.3 UPLC-qTOF-MSqTOF-MS analysis of the crude extract from *B. disticha*

UPLC-qTOF-MSqTOF-MS analysis was performed on both the crude extract from the dried plant material and the concentrated alkaloid rich fraction, obtained via acid-base extraction from the crude extract, as per **Figure II-3**. The same process was followed for the preparation of both samples for analysis. Both UPLC-qTOF-MS analyses utilised the same gradient solvent system for separation in the same column.

A small amount of the dried extract (~1.00 mg) was weighed into an Eppendorf centrifuge vial (1.5 mL) and solubilised in ROMIL[®] Ultra-pure Solvent (UpS)[®] methanol (1.000 mL) by sonication for 30 min at 25 °C. Precipitates were removed by centrifugation at 7 000 rpm in a Baygene[®] Micro Centrifuge (BG-Qspin[™]). The supernatant was diluted ten-fold into a clear glass LC-vial (2 mL) with UpS[®] methanol. The sample was applied to the system as a 10 µL injection. A gradient solvent system was applied to the column to separate the sample components. For the mobile phase solvents, ROMIL[®] Ultra-pure Solvents[™], buffered with 0.1% (v/v) formic acid, were utilised (**Table II-1**). The composition of the solvent system is given in **Table II-2**.

Table II-2. Generic UPLC-qTOF-MS solvent system.

Time (min)	Flow rate (ml/min)	Percentage: dH₂O + 0.1% Formic acid	Percentage: MeOH + 0.1% Formic acid	Gradient type
Initial	0.300	97.0	3.0	Initial
0.10	0.300	97.0	3.0	Linear
14.00	0.300	0.0	100.0	Linear
16.00	0.300	0.0	100.0	Linear
16.50	0.300	97.0	3.0	Linear
20.00	0.300	97.0	3.0	Linear

For this project UPLC-analyses were performed with a Waters[®] Aquity[™] system, consisting of a binary solvent manager, a sample manager and an Aquity[®] UPLC-column (2.1 × 100 mm) with a BEH C18-type stationary phase (particle diameter = 1.7 µm). Accurate mass analysis of the eluting compounds was performed with a Synapt[™] G2 High-Definition Mass Spectrometry system with a set acquisition mass-charge ratio (m/z) range of 50-1200. Electrospray ionisation (capillary voltage of 2.6000 kV, source temperature = 120 °C) was used to generate positive analyte ions. Analyte ions were sampled from the source through the sampling cone (25.0000 V) and the extraction cone (4.0000 V). Sample desolvation during ionisation was

accomplished at 350 °C. The cone gas flow rate was set to 10.0 L/h and the desolvation gas flow rate to 650.0 L/h.

The detector was set to scan over the whole m/z-ratio range in 0.3 s. Between each scan there was a delay of 0.024 s. Mass calibration was achieved with a direct injection of a lock spray solution (Leucine Enkephalin) every 10.0 s at a rate of 3 µL/min. Positive ion mass correction was done relative to the lock spray mass 556.2771 Da. Negative ion mass correction was done relative to the lock spray mass 554.2615 Da. Mass correction was done manually post-run. The system had a mass resolution of 18 000 based on full width at half peak maximum (FWHM) of mass signals.

2.2.4 Isolation of buphanidrine from the alkaloid fraction

Fractionation of the alkaloid extract using column chromatography

To separate the alkaloids in the concentrated alkaloid rich fraction, silica gel (Fluka[®] Chemika, particle diameter = 0.063 – 0.2 mm) column chromatography was utilised as indicated in **Figure II-3**. The column had a diameter of 40 mm and was packed to a length of 550 mm. The column was packed with a suspension of silica gel 60 (395 g in ethyl acetate – Radchem[®]) modified with triethylamine (TEA, Sigma-Aldrich[®], 0.1% v/v). A suitable solvent system for fractionation (8:2 ethyl acetate/methanol – Radchem[®]) was developed on thin layer chromatography plates (Macherey-Nagel[®], Pre-coated TLC sheets ALUGRAM[®] Xtra SIL G/UV₂₅₄, Stationary phase: 0.20 mm thick layer silica gel 60 with UV₂₅₄ fluorescent indicator).

The alkaloid sample (677 mg) was loaded as a concentrated solution of the collected fraction in dichloromethane/ethyl acetate (Radchem[®], 1:9). Once adsorbed onto the top of the column, the column flow was initiated by addition of the mobile phase. The solvent system used is described in **Table II-3**.

Table II-3. Solvent system used for column chromatography of the alkaloid rich fraction.

% Ethyl acetate	% Methanol	% TEA	Volume used (mL)
100	0	0.1	1000
95	5	0.1	2500
90	10	0.1	1500
80	20*	0.1	~9000

*Since silica was used as the stationary phase, a maximum of 20% MeOH was employed with minimal risk of eluting dissolved silica from the column.

Fractions were collected in test tubes and concentrated in an SP Scientific Genevac EZ-2 Plus[®]-evaporator. Of the collected fractions, every second fraction was analysed by TLC. TLC-analysis was done with the aid of Dragendorff reagent³ to test for the presence of alkaloids.¹⁹ Based on the results of these analyses, fractions with similar TLC profiles were identified and combined. Quantitative transfer was achieved by rinsing the tubes into the vials with DCM (Radchem[®]).

Selection of collected fractions for further purification by preparative TLC

Combined column fractions that tested positive for the presence of amines were compared to results from a UPLC-qTOF-MS analysis of a fraction that tested positive for the presence of alkaloids (WJ-41-H, **Figure II-3**). Based on the elution profile of alkaloids in this combined fraction, those likely to contain buphanidrine (**1**) were determined. Further purification of buphanidrine (**1**) was achieved by utilising preparative thin layer chromatography (Merck[®] (Pty.) Ltd., stationary phase: silica gel 60 pre-treated with UV₂₅₄ fluorescent indicator, layer thickness: 1.5 mm) (**Figure II-4**).

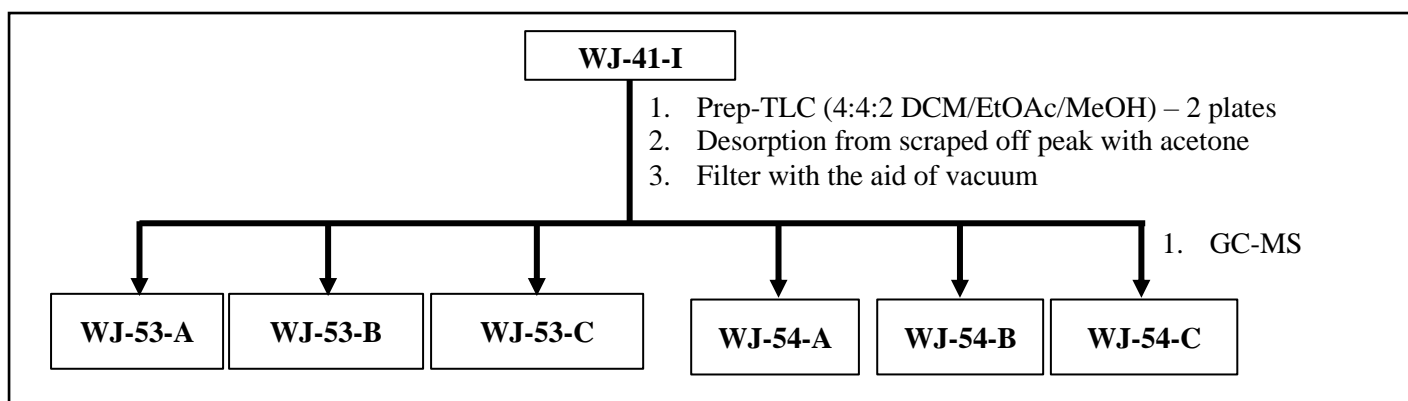


Figure II-4. Purification of silica gel column fraction WJ-41-I by prep-TLC analysis.

Based on literature from Boloko²⁰ and Steenkamp¹⁴, a prep-TLC solvent system (4:4:2 DCM-EtOAc-MeOH (Radchem[®]) with no triethylamine) was tested and developed on standard UV₂₅₄-fluorescent TLC-plates. For prep-TLC, the sample was split over two plates to mitigate the risk of over concentration of the sample alkaloids on the silica. Following development of the plates, the outlines of the eluted peaks were marked in pencil and etched for scraping off. Three peaks were scraped off each plate and soaked in analytical grade acetone (Radchem[®]). The silica was filtered out with the aid of a sintered disc funnel and negative pressure

³ For preparation of Dragendorff's reagent see Appendix II-D

differential (w.r.t. ambient pressure), and the filtrates were dried with the aid of Genevac[®] EZ-2 Plus[®]-evaporators.

The constituents of the most polar peak of each plate (WJ-53-C and WJ-54-C, **Figure II-4**) were selected for GC-MS analysis to investigate the identity of the alkaloids in the isolated peaks. Dried residue of WJ-54-C (2.14 mg) was reconstituted in methanol (Macron[®], 1.570 mL) and a small volume (10.00 mL) transferred to a conical glass insert in an amber glass GC-vial (2 mL).

GC-MS analysis was performed on an Agilent[®] Technologies 7890B GC System, coupled to a 7693 Autosampler and a Hewlett-Packard 5973 Mass Selective Detector were utilised. The system was equipped with a Phenomenex[®] Zebron[®] ZB-5 MSi GC-column (15 m in length, internal diameter = 0.25 mm, film thickness = 0.25 µm). For analysis, the sample (2 µL) was applied through an inlet heated to 280°C in a 20:1 split ratio. The analysis was initiated at a column temperature of 85°C, with a flow rate of 2 mL/min. The initial temperature was maintained for 0.35 minutes before increasing, at a gradient of 62°C per minute, to 115°C. After 0.8 minutes the temperature was increased to 320°C at a rate of 65°C per minute. The final temperature was maintained for 1.5 minutes.

The relative abundance of the major alkaloid component in the prep-TLC-fraction was estimated from the GC-MS chromatogram signal areas, utilising the NIST's Automated Mass Spectral Deconvolution and Identification System (AMDIS[®], version 2.73, April 2017).

Isolation of buphanidrine via semi-preparative HPLC (semi-prep HPLC)

As an alternative to prep-TLC, semi-preparative HPLC was utilised in the purification of alkaloids from column fraction WJ-41-J (**Figure II-5**). The dried fraction residue was reconstituted in methanol (Macron[®], 3.000 mL) and solubilised with the aid of vortex mixing and ultra-sonication. The sample was filtered through an Agilent[®] Technologies syringe filter (13 mm diameter, 0.2 µm pore size) before application to the HPLC-system.

The HPLC-setup consisted of a Waters[®] 2545 Binary Gradient Module, a Waters[®] System Fluidics Organizer, and a Waters[®] 2767 Sample Manager. Analytes were detected with a Waters[®] 2998 Photodiode Array Detector. The system was equipped with two HPLC-columns with the similar stationary phases. A 4.6 × 150 mm XBridge[®] C18 analytical HPLC-column (5 µm particle diameter) was utilised to develop a suitable solvent system for the separation of analytes in the sample. A 19 × 250 mm XBridge[®] Prep C18 OBD[™] column (5 µm particle

diameter) was utilised in sample fractionation. To operate the system, the MassLynx[®] version 4.1 software suite was utilised.

The semi-prep HPLC column (19 × 250 mm) was used to fractionate the silica gel column fraction (WJ-41-J, 39.55 mg) prepared at a concentration of 13.18 mg/mL in HPLC-grade methanol (Macron[®], 3.000 mL). In each analysis 100. µL, 150. µL, or 200. µL were applied to the system.

Optimal separation of the sample components was achieved by applying the gradient solvent system in **Table II-4**. HPLC-grade methanol (Macron[®]) and filtered de-ionised water, both modified with trifluoroacetic acid (Radchem[®]), were utilised in the fractionation of the collected column fractions. The de-ionised water was filtered through GH Polypropylene filters (Pall[®] Corporation) with a diameter of 47 mm and a pore size of 0.2 µm.

Table II-4. Solvent system employed in the isolation of buphanidrine from prep-TLC-fractions.

Time (min)	Flow rate (mL/min)	% De-ionised water (+ 0.05% TFA)*	% Methanol (+ 0.05% TFA)*	Curve
0.00	8.53	80.0	20.0	-
0.83	8.53	75.0	25.0	6
1.67	8.53	60.0	40.0	6
8.33	8.53	40.0	60.0	6
11.67	8.53	35.0	65.0	6
16.67	8.53	0.00	100.0	6
20.00	8.53	20.0	80.0	6
25.00	8.53	50.0	50.0	6
28.33	8.53	80.0	20.0	6
30.00	5.00	80.0	20.0	6

*TFA = Trifluoroacetic acid (Radchem[®])

The system was programmed to automatically collect the detected chromatographic peaks based on the rate of increase and intensity in detected UV-absorbance. The parameters for the collection of fractions are given in **Table II-5**.

Table II-5. Preparative HPLC parameters for fraction collection.

Parameter	Value
Minimum fraction width	15 s
Maximum fraction width	70 s
Minimum intensity threshold	2 500 absorbance units
Maximum intensity threshold	5 000 000 absorbance units
Peak starts at:	Leading edge gradient = 0.5%
Peak ends at:	Maximum fraction width

Once collected, the respective fractions were recombined, based on the relative retention times of the detected peaks, in separate vials and dried in a Genevac[®] EZ-2 Plus[®]-evaporator. The fraction that showed the greatest magnitude of absorbance, was suspected of containing buphanidrine (WJ-106-A – **Figure II-5**). The collected fraction was dried in a Genevac[®] EZ-2 Plus evaporator and stored at -26 °C. Subsequently, this combined fraction was further analysed via GC-MS, UPLC-qTOF-MS and NMR-spectrometry to confirm both the purity and identity of the compound in the isolated fraction.

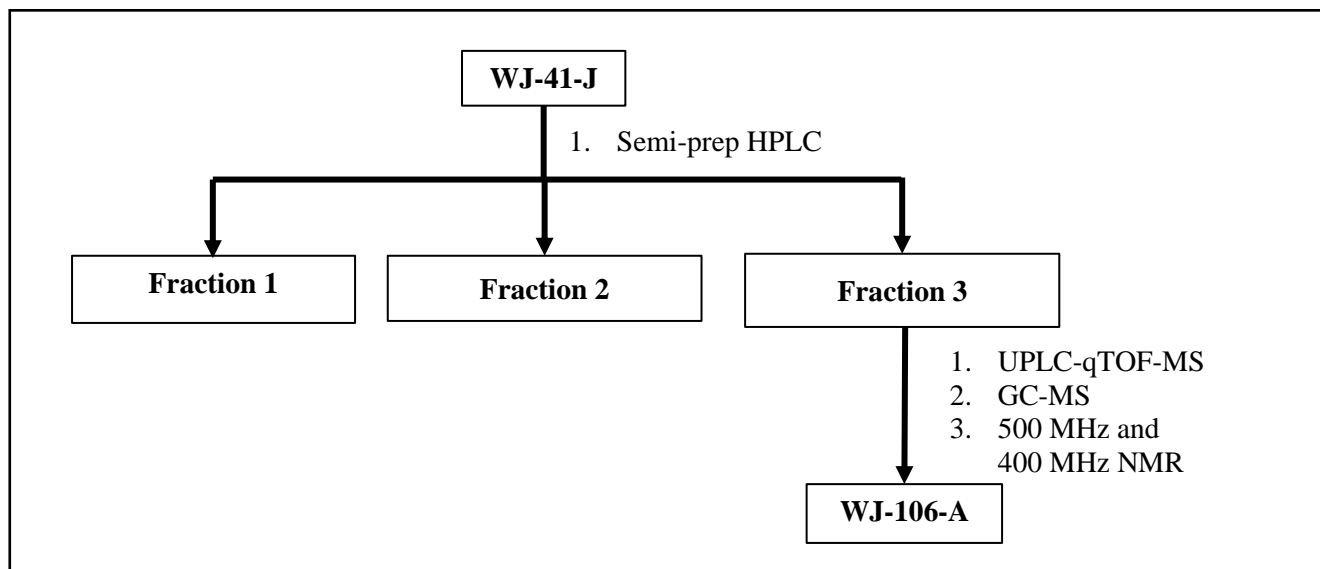


Figure II-5. Partitioning of column fraction WJ-41-J by semi-preparative HPLC.

UPLC-qTOF-MS analysis of the isolated HPLC-fraction

The residue was reconstituted in UpS[®]-grade methanol (ROMIL[®], 1.000 mL) and solubilised by sonication. A small volume of this solution (10.64 μ L) was transferred to a clear glass LC-vial (2 mL) and diluted to 500. μ L with UpS[®]-grade methanol (ROMIL[®], 1.000 mL) to produce an analyte concentration of 0.1 mg/mL. Of this sample 10 μ L was applied to the UPLC-qTOF-MS system for analysis. A gradient solvent system (**Table II-2**) was used as mobile phase.

Gas chromatography-mass spectrometry (GC-MS)

From the reconstituted HPLC-fraction (4.70 mg/mL in HPLC-grade methanol, Sigma-Aldrich[®]) a small volume (25.0 μ L) was transferred to an amber glass GC-vial (2 mL) and dried in a heating block (~40 °C), with the aid of a stream of dry compressed air. The sample was reconstituted in acetonitrile (40.0 μ L) and solubilised by vortex mixing. For GC-MS analysis, the sample was transferred to a conical glass insert in a GC-vial (2 mL). The same GC-MS system was utilised as in the case of the analysis of the prep-TLC fraction (WJ-54-C). The sample (4 μ L) was applied to the GC-MS system and the analysis initiated at a temperature of 180 °C. This temperature was maintained for 3 minutes, then increased to 310 °C along a gradient of 30 °C per minute. The final temperature was maintained for 8 minutes.

Nuclear magnetic resonance (NMR) analysis of the samples

To confirm the identity of the isolated compound as buphanidrine (**1**), the fraction was prepared and submitted for NMR-analysis. The sample was transferred to a 5 mm NMR-tube for 400 MHz $\delta^1\text{H}$ -NMR-analysis by a Bruker[®] UltraShieldTM 400-AVANCE III 400 spectrometer, equipped with a BBI probe optimised for proton NMR. The sample was loaded into the probe with a Bruker[®] B-ACS-60 autosampler.

Further NMR-analyses were performed on the 500 MHz Bruker AscendTM 500 spectrometer coupled with the AVANCE III HD data interface. Both $\delta^{13}\text{C}$ - and $\delta^1\text{H}$ -NMR analyses were performed. The correlation of the nuclei was examined by performing 2D-NMR HMBC experiment.

2.3 GC-MS analysis of samples spiked with buphanidrine

2.3.1 Preparation of a concentrated sodium hydroxide solution

A concentrated sodium hydroxide solution (100.00 mL, 10 M) was prepared by dissolving sodium hydroxide pellets (Merck[®], 39.944 g) in de-ionised water (Merck[®], 100.00 mL). The solution was prepared in a volumetric flask, calibrated to 100.00 ± 0.10 mL at 20 °C.

2.3.2 Preparation of an alkaline phosphate buffer

A 0.8 M (pH ~ 11) disodium hydrogen orthophosphate buffer was prepared by first weighing disodium hydrogen orthophosphate dihydrate (Merck[®], 35.6 g) into a glass vessel. The salt was dissolved in de-ionised water by continuous heating and stirring at 60-70 °C. The solution was transferred quantitatively to a 250.00 ± 0.23 mL volumetric flask and diluted to the volumetric mark with de-ionised water. To homogenise the solution, the flask was decanted five times and shaken by hand. The solution was transferred to a container and concentrated sodium hydroxide (1.0000 mL, 10 M) was added to adjust the pH to ca. 11. The buffer was kept heated to prevent the precipitation of di-sodium hydrogen orthophosphate crystals.

2.3.3 Preparation of stock standard solutions

Following confirmation on the identity of the isolated buphanidrine (**1**), the sample was dried under a stream of dry air in a drying block, set to a temperature of 40 °C. The dried residue was reconstituted in DCM (Merck[®], 1.0000 mL) and vortex mixed to ensure homogenisation of the residue in the solvent. The final concentration of this sample was, assuming 100% purity, 3.90 mg/mL. Stock solution (256.4 µL) was transferred to an amber glass GC-vial (2 mL). The solution was diluted with DCM (Merck[®], 743.6 µL) and homogenised by vortex mixing to give a solution with a final concentration of 1.00 mg/mL. The stock solutions were stored in the freezer at -26 °C.

To prepare a 1.00 mg/mL stock solution of the internal standard (5- α -cholestane), 5- α -cholestane crystals (10.04 mg) was weighed into a 10.00 ± 0.04 mL volumetric flask. The crystals were dissolved in a small volume of HPLC-grade ethyl acetate (Sigma-Aldrich[®]) before the flask was filled to the mark with the solvent. To homogenise the solution, the flask was stoppered and shaken with a vortex mixer. This gave a final concentration of 1.004 mg/mL. The solution was transferred to amber glass GC-vials (2 mL) and stored in the freezer at -26 °C.

2.3.4 Preparation method and parameters for GC-MS analysis of samples containing buphanidrine

A series of samples, containing different concentration levels of buphanidrine (**1**), was prepared by first aliquoting the relevant matrix (de-ionised water or urine, 5.00 mL) into the batch of empty test tubes. Into each tube, the appropriate volume of 1.00 mg/mL buphanidrine (**1**) stock solution was spiked into the sample, followed by 1.004 mg/mL 5- α -cholestane solution (30.0 μ L). The samples were vortex mixed and divided into two equal parts in separate test tubes. To each tube di-sodium hydrogen orthophosphate buffer (0.250 mL, 0.8 M, pH ~ 11.5) was added. The pH of each sample was adjusted to 11 with the addition of 10 M aqueous sodium hydroxide solution (12.5 μ L) to each tube. The samples were vortex mixed to ensure equal distribution of the buffer and alkaline solution.

For the extraction of the alkaloids, DCM (Merck[®])/isopropanol (Sigma-Aldrich[®]) (2.000 mL, 9:1) extraction solvent was added to each tube. To ensure interaction of the extraction solvent with the whole of the aqueous phase, the samples were vortex mixed. Phase separation was induced by centrifuging the samples at 3 500 rpm for 10 min. Since the samples were divided into two parts, the organic phase of the first part was collected in individual amber glass GC-vials (2 mL) and dried in the drying block (40 °C) under the stream of dried air. The organic phase of the second half of each sample was then added to the corresponding vial and, likewise, dried. The extraction process was repeated.

For GC-MS analysis of the samples, the same system was utilised as in the analysis of the prep-TLC-fraction in Section 2.2.4 of this chapter. The dried residues were reconstituted in acetonitrile (Sigma-Aldrich[®], 40.0 μ L), homogenised by vortex mixing and transferred to conical inserts, in vials, for GC-MS analysis. For the GC-MS analysis of a sample, 2 μ L of the sample were applied to the GC-column (Phenomenex[®] Zebron[®] ZB-5 MSi, length 15 m, internal diameter 0.25 mm, film thickness 0.25 μ m) and the chromatographic analysis was initiated with a flow of 2.000 mL/min and a temperature of 150 °C. The temperature ramp was immediately initiated at a gradient of 60 °C/min and allowed to reach 240 °C. The gradient was adjusted to 8 °C/min and applied without holdup. The system proceeded to reach 250 °C. After 2.5 min the gradient was adjusted back to 60 °C/min and allowed to reach 340 °C. This final temperature was maintained for 0.75 min.

Mass detection in the scan mode was performed over a range from $m/z = 50$ to $m/z = 800$. In the selected ion mode, eight ions were selected for detection of buphanidrine (**1**). The

quadrupole was set to focus each ion at the detector for a dwell time of 100 ms. The following ions were selected: $m/z = 115, 130, 215, 245, 260, 284, 300, 315$. For the detection of 5- α -cholestane, four ions were selected: $m/z = 149, 217, 357, 372$. The quadrupole dwell time was maintained at 100 ms per ion m/z -ratio.

2.3.5 Replicate analysis of samples for method validation

To determine method validation figures of merit, replicate analyses of spiked sample were performed. Three batches of samples were prepared in urine and de-ionised water, respectively. Within each batch, samples were spiked such that six different, equally spaced, theoretical concentration levels were produced. The samples were spiked at 0.600, 1.20, 1.80, 2.40, 3.00 and 3.60 ppm ($\mu\text{g/mL}$).

Each sample was prepared following the procedure in Section 2.3.4 and analysed in duplicate by GC-MS. Within each batch (except for batch 1 prepared in urine) a method blank was prepared in parallel. This blank was spiked only with the internal standard and was prepared identically to the samples of the batch. By performing replicate analyses, evaluation of precision and linearity figures of merit was possible. Replicate analyses also allow the evaluation of between-batch contribution to variance in the measured values via univariate and multivariate analysis of variance (ANOVA and MANOVA).

3. Results and discussion

3.1 Analysis of the extracts from *B. disticha*

3.1.1 Plant extraction

To provide a reference to the plant material processed for this component of the study, a voucher specimen (ref. no. PRU 127862) of the plant was submitted to the H.G.W.J. Schweickerdt Herbarium of the University of Pretoria. Extraction of the dry plant material (120.14 g) yielded 14.36 g of crude extract. Following the acid-base partitioning of the extract an alkaloid-rich fraction (849 mg) was obtained which accounted for approximately 0.7% of the dry plant mass. This is close to the alkaloid content, reported by Hauth & Stauffacher¹³, for a *B. disticha* bulb (0.2849%).

3.1.2 UPLC-qTOF-MS analysis of the crude extract and alkaloid fraction from *B. disticha* Tentative identification of buphanidrine in the crude extract from *B. disticha*

In the UPLC-qTOF-MS chromatogram of the crude extract from *B. disticha*, recorded in the positive ionisation mode and shown in **Figure II-6**, for which the Amaryllidaceae-alkaloids were predominantly abundant. These alkaloids were tentatively identified by accurate mass and elemental composition analysis with utilisation of the Dictionary of Natural Products, ChemSpider and PubChem.²¹⁻²³ These provided monoisotopic mass, structural and elemental composition data for comparison to detect accurate masses and calculated elemental compositions.

Based on accurate mass analysis of the detected chromatographic peaks, eleven alkaloids were detected, nine of which are known constituents of *B. disticha*. The tentative identities of the constituents of the crude extract are shown in **Table II-6**.¹³ The tentative identification of the alkaloid molecular formulae conformed to the required mass difference tolerance of 5 ppm for each chromatographic peak in both the crude extract and the alkaloid-rich fraction.

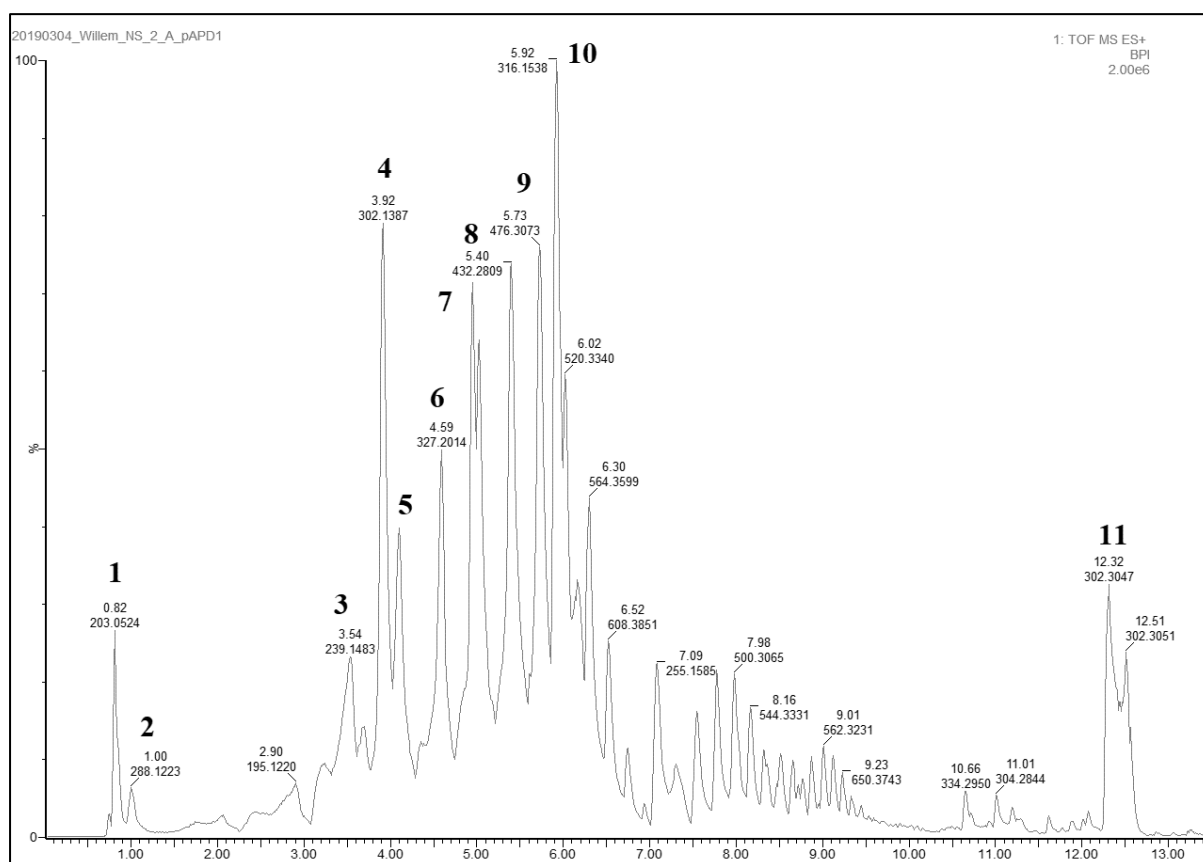


Figure II-6. A ESI (+) UPLC-chromatogram of the crude extract from *B. disticha*. The x-axis is retention time in minutes.

Table II-6. Analysis of the UPLC-qTOF-MS results for the crude extract (**Figure II-6**).

Peak no.	t _R (min)	m/z ([M+H] ⁺)	Calc. molecular mass (Da)	Formula	Theoretical mono-isotopic mass (Da)	Tentative identification
1	0.818	203.0524	180.0632	C ₆ H ₁₂ O ₆	180.0634	D-Glucose
2	1.000	288.1223	287.1148	C ₁₆ H ₁₇ NO ₄	287.1157	(-)-Lycorine
3	3.557	302.1388	301.1315	C ₁₇ H ₁₉ NO ₄	301.1314	(-)-Buphanamine
4	3.919	320.1491	319.1418	C ₁₇ H ₂₁ NO ₅	319.1420	Nerbowdine
5	4.111	320.1488	319.1415	C ₁₇ H ₂₁ NO ₅	319.1420	Deacetylbowdensine
6	4.578	358.2027	357.1954	C ₂₁ H ₂₇ NO ₄	357.1940	Laudanosine
7	4.854	286.1449	285.1376	C ₁₇ H ₁₉ NO ₃	285.1365	Buphanisine
8	5.311	330.1340	329.1267	C ₁₈ H ₁₉ NO ₅	329.1263	Distichamine (2)
9	5.567	332.1487	331.1414	C ₁₈ H ₂₁ NO ₅	331.1420	Undulatine
10	5.843	316.1551	315.1478	C ₁₈ H ₂₁ NO ₄	315.1471	Buphanidrine (1)
11	12.317	302.3051	301.2978	C ₁₈ H ₃₉ NO ₂	301.2981	+/- Sphinganine

In the initial crude extract of *B. disticha* two alkaloids were detected, at retention times of 4.111 min (Peak 5) and 4.578 min (Peak 6) respectively, and tentatively identified as deacetylbowdensine and laudanosine. Deacetylbowdensine was suspected as the most likely identity of Peak 5 since it is known to be present in the bulbs of some plants in the family of Amaryllidaceae.

Of particular interest was the identity of Peak 10 (5.843 min) in the chromatogram of the crude extract (**Figure II-6**). In the crude extract this peak showed the greatest intensity. The first order mass spectrum of Peak 10 contained, as base peak ion, the suspected quasi-molecular ion ([M+H]⁺) with an accurate mass of m/z = 316.1538. The accurate mass, detected in the crude extract, corresponded to the elemental composition for the quasi-molecular ion of buphanidrine (**1**) (C₁₈H₂₂NO₄⁺) with a 74.99% confidence (corresponding to an isotopic (i-FIT) ratio of 65.4).

The theoretical monoisotopic mass of the calculated quasi-molecular ion ([M+H]⁺) for buphanidrine (**1**) is m/z = 316.1544.¹⁴ Compared to the theoretical quasi-molecular ion accurate mass, the detected base peak ion in Peak 10 deviated with a mass difference of -1.9 ppm. Since the calculated elemental composition corresponds to within 5 ppm of the mono-isotopic mass of buphanidrine's (**1**) molecular formula, Peak 10 is tentatively identified as buphanidrine (**1**).²⁴

UPLC-qTOF-MS analysis of the alkaloid rich fraction

The analysis of the fraction collected from acid-base partitioning is showed in **Figure II-7** and the tentative identification of the labelled peaks in **Table II-7**. Tentative identification of the eight analysed peaks, was done similar as for the peaks in the chromatogram of the crude extract. Of primary interest in the UPLC-qTOF-MS chromatogram of the alkaloid-rich fraction, showed in **Figure II-7**, was the identity of Peak 7. This peak was also the most intense in the chromatogram and its retention time was close to that of Peak 10 in **Figure II-6**. The base peak ion of Peak 7 correlated closely with that of Peak 10 in **Figure II-6**.

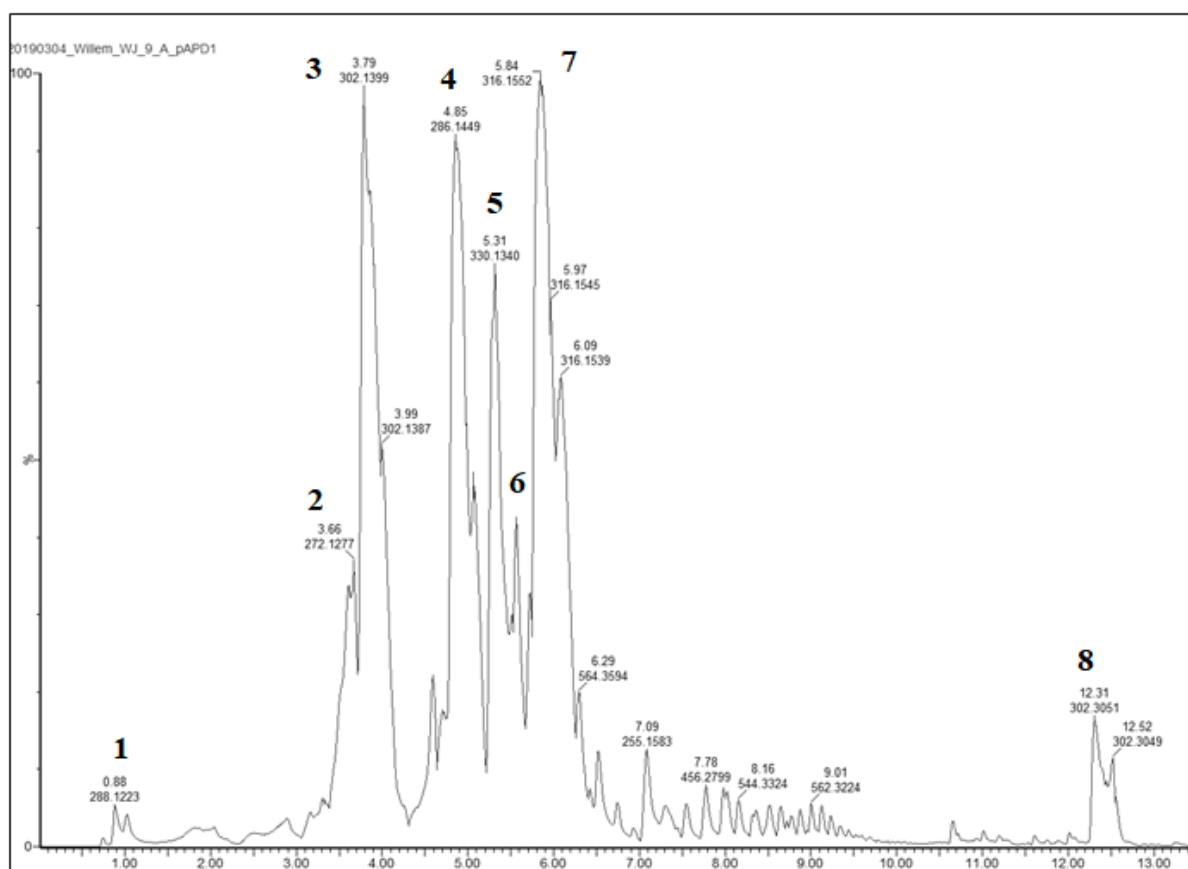


Figure II-7. A ESI (+) UPLC-analysis of the alkaloid rich fraction extracted from the crude extract. The x-axis is the retention time in minutes.

Table II-7. Alkaloids detected in the alkaloid rich fraction of *B. disticha* (**Figure II-7**).

Peak no.	t _R (min)	m/z ([M+H] ⁺)	Calc. molecular mass (Da)	Formula	Theoretical mono-isotopic mass (Da)	Tentative identification
1	0.890	288.1223	287.1148	C ₁₆ H ₁₇ NO ₄	287.1157	(-)-Lycorine
2	3.674	302.1380	301.1307	C ₁₇ H ₁₉ NO ₄	301.1314	(-)-Buphanamine
3	3.804	320.1492	319.1419	C ₁₇ H ₂₁ NO ₅	319.1420	Nerbowdine
4	4.854	286.1449	285.1376	C ₁₇ H ₁₉ NO ₃	285.1365	Buphanisine
5	5.311	330.1340	329.1267	C ₁₈ H ₁₉ NO ₅	329.1263	Distichamine (2)
6	5.567	332.1487	331.1414	C ₁₈ H ₂₁ NO ₅	331.1420	Undulatine
7	5.843	316.1551	315.1478	C ₁₈ H ₂₁ NO ₄	315.1471	Buphanidrine (1)
8	12.317	302.3051	301.2978	C ₁₈ H ₃₉ NO ₂	301.2981	+/- Sphinganine

Suitability of acid-base extraction in the simplification of the crude extract composition

Comparison of the chromatograms of the crude extract (**Figure II-6**) and the acid-base extract (**Figure II-7**). It was observed that there were fewer peaks in the chromatogram of the concentrated fraction, than in that of the original crude extract. For example, Peak 1 of the crude extract, tentatively identified as D-glucose, was absent from the acid-base partition. Both laudanosine and deacetylbowdensine (Peaks 5 and 6 of the crude extract) were also absent from the acid-base partition.

The base peak ions of the peaks in the acid-base partition, that correlate with those in the crude extract, all have even value accurate masses. This typically indicates the presence of an odd number of nitrogen atoms in the analytes under UPLC-MS/MS conditions. The principal constituents of the acid-base partition were, therefore, alkaloids.

The intensity of the detected alkaloids in the acid-base partition is greater than the corresponding peaks' intensities in the crude extract, when measured relative to the high frequency of peaks between 7.00 and 10.00 min. Comparing the retention time width of the peaks in the two samples showed the peaks in the acid-base partition were broader than the peaks to which they correspond in the crude extract. Therefore, estimation of the peak areas in both chromatograms indicated the constituents of the acid-base partition were more concentrated than those in the crude extract. This increase in concentration can be observed Peaks 3, 4, and 7 (nerbowdine, buphanisine and buphanidrine (1)).

These observations indicate the acid-base extraction process was successful in simplifying the composition of the crude extract for further purification processes. This simplified fraction, with improved separation, is more amenable to purification via silica column chromatographic separation.

3.1.3 TLC-analysis and comparison of crude extract and alkaloid fraction

A TLC-analysis was performed to investigate the complexity of the crude extract and the alkaloid rich fraction. A comparison of the detected bands under short wavelength ultraviolet light ($\lambda = 254$ nm) revealed a more intense UV-absorbance in the concentrated alkaloid-rich fraction, compared to the crude extract. For further comparison of the alkaloid content of the extracts the TLC-plate was sprayed with Dragendorff reagent (Appendix to Chapter II, Section D). This reagent stained the alkaloids orange (viz. the stained regions in **Figure II-8**). This comparison of alkaloid content showed the acid-base partitioning was effective in the extraction of alkaloids from the crude extract.

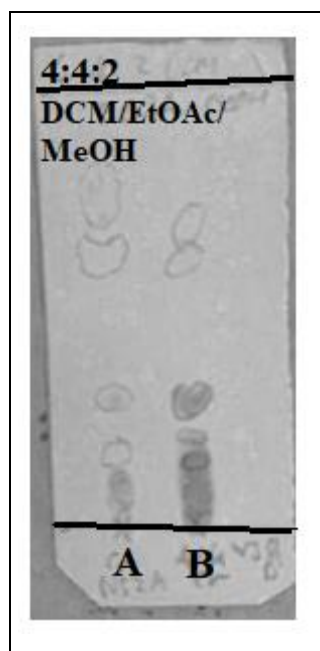


Figure II-8. Illustration of the TLC-analysis of the crude extract (A) and the alkaloid fraction obtained via liquid-liquid extraction (B). The stained regions were produced by alkaloids stained with Dragendorff's reagent.

3.2 Isolation of buphanidrine from the alkaloid fraction

3.2.1 Column chromatography of the alkaloid fraction

To separate the alkaloids via column chromatography, a solvent system was developed on TLC-plates with triethylamine (0.1% v/v) added to the total eluant volume. After testing multiple solvent systems, an ethyl acetate-methanol (8:2) system was found to provide optimal separation of the alkaloids. Since a maximum of 20% (v/v) methanol can be used in silica column chromatography eluants, the method was adjusted to an initial system of ethyl acetate-methanol (95:5) which was also expected to give excellent separation based on TLC analysis. It was also a smaller step in polarity from the 100% ethyl acetate packing eluant.

Throughout the fractionation by silica gel column chromatography, the eluted fractions were monitored by TLC-analysis. Based on the results of the Dragendorff-tests (Appendix II-D gives the protocol for preparing Dragendorff reagent) performed on the TLC-plates, the alkaloids started eluting at a higher rate when the solvent system polarity was changed from ethyl acetate-methanol (9:1) to ethyl acetate-methanol (8:2). By maintaining this solvent system, the alkaloids were systematically eluted, and the fractions combined based on similarity in R_f -values of alkaloids, as determined by TLC-analysis.

A total of 15 combined fractions, WJ-41-A to WJ-41-O, were collected. The fractions WJ-41-H to WJ-41-J are shown in **Figure II-3**. The combined fraction, WJ-41-A, was collected as the solvent front of the column. The following four combined fractions (WJ41-B to WJ-41-D) did not test positive for alkaloids and showed only low intensity UV-absorbance at $\lambda = 254$ nm. Fractions WJ-41-D and WJ-41-E showed strong UV-fluorescence at $\lambda = 365$ nm. Fractions WJ-41-H to WJ-41-O tested positive for alkaloids in the Dragendorff-test.

From the silica gel column, a total alkaloid yield of 41.2% (0.27925 g of 0.677 g alkaloid rich fraction) was collected. It was observed that the solvent system used, ethyl acetate-methanol (8:2) modified with triethylamine (0.1% v/v), could not elute all the alkaloids from the alkaloid rich fraction, partitioned out of the crude extract. Exposing the silica column to long wavelength UV-light ($\lambda = 365$ nm) produced strong fluorescence in the sample band on top of the column. The adsorption of eluting alkaloids to the silica gel, despite modification of the silica gel with triethylamine, could also contribute to analyte loss.

3.2.2 Preparative thin layer chromatography (prep-TLC)

From the combined fractions, suspected of containing buphanidrine (**1**), WJ-41-I was selected for purification via preparative thin layer chromatography (prep-TLC), as indicated in **Figure II-4**. In the isolation of alkaloids from fraction WJ-41-I, via prep-TLC (see **Figure II-9**), three bands were obtained on each of the two prep-TLC-plates at R_f -values of 0.3875 (**A**), 0.4615 (**B**), and 0.5059 (**C**) respectively. The most polar band (**A**), with an R_f -value of 0.3875, was scraped off both prep-TLC-plates.

Following desorption of the analytes with analytical grade acetone (Radchem[®]), the silica was filtered out and the filtrate dried in the Genevac[®] EZ-2 Plus[®] evaporator. From the most polar band on the first plate an analyte yield of 1.95 mg was obtained, and from the most polar band of the second plate, 2.14 mg. These bands are indicated in **Figure II-4** as WJ-53-C on plate 1, and WJ-54-C on plate 2. It was analysed by GC-MS to confirm whether buphanidrine (**1**) was present (**Figure II-10**).

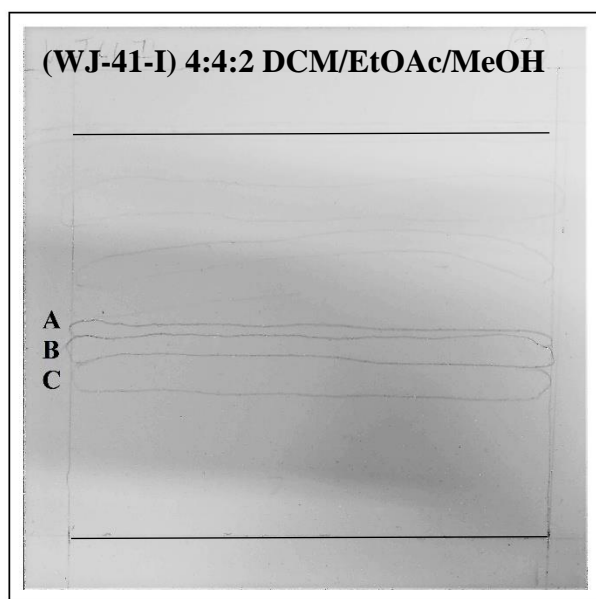


Figure II-9. Prep-TLC-plate developed in the purification of alkaloids from the combined fraction WJ-41-I. The bands were outlined in pencil. The bands are labeled **A** to **C** where **A** is the least polar and **C** the most polar band. The lines indicate the initial sample band and the solvent front.

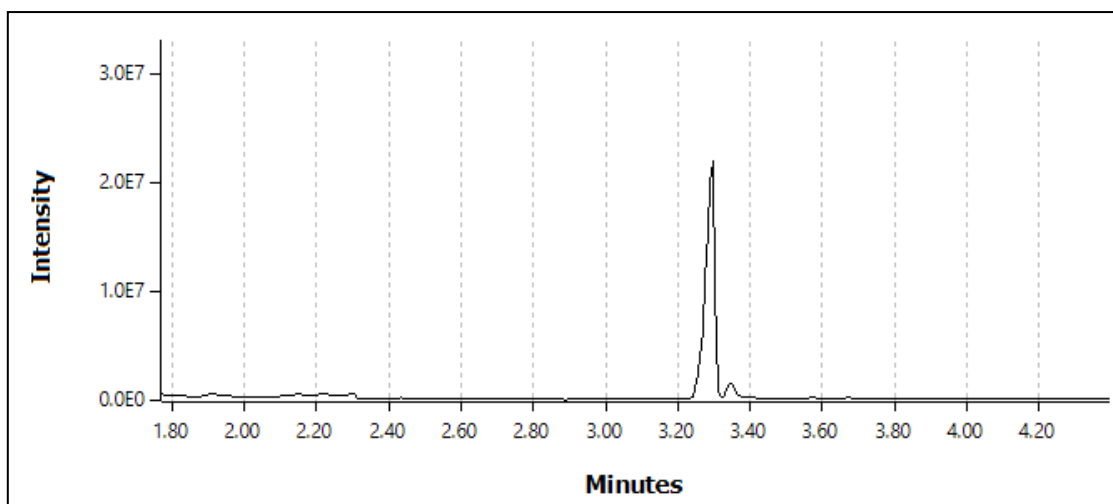


Figure II-10. Total ion chromatogram recorded for the GC-MS analysis of the prep-TLC-peak, WJ-54-C, suspected of containing buphanidrine.

Based on the results from the GC-MS analysis of the most polar prep-TLC-peak on plate 2, WJ-54-C, there were two compounds present in the fraction. One a major and the other a minor constituent. The primary constituent at 3.296 min (**Figure II-11**) was identified from the Wiley-NIST Mass Spectral Library as buphanidrine (**1**), with a 99% spectral correlation (see Appendix to Chapter II, **Figure A (II)-1**). The minor constituent at 3.344 min (**Figure II-12**) was identified, also with a 99% spectral correlation, as buphanamine (see Appendix to Chapter II, **Figure A (II)-2**), a known alkaloid from *B. disticha*.

The relative abundance of buphanidrine (**1**), measured with respect to buphanamine, was 94.6%, based on chromatographic peak area calculated with the AMDIS[®] (Automated Mass Spectral Deconvolution and Identification System, version 2.73, 2017) software suite.

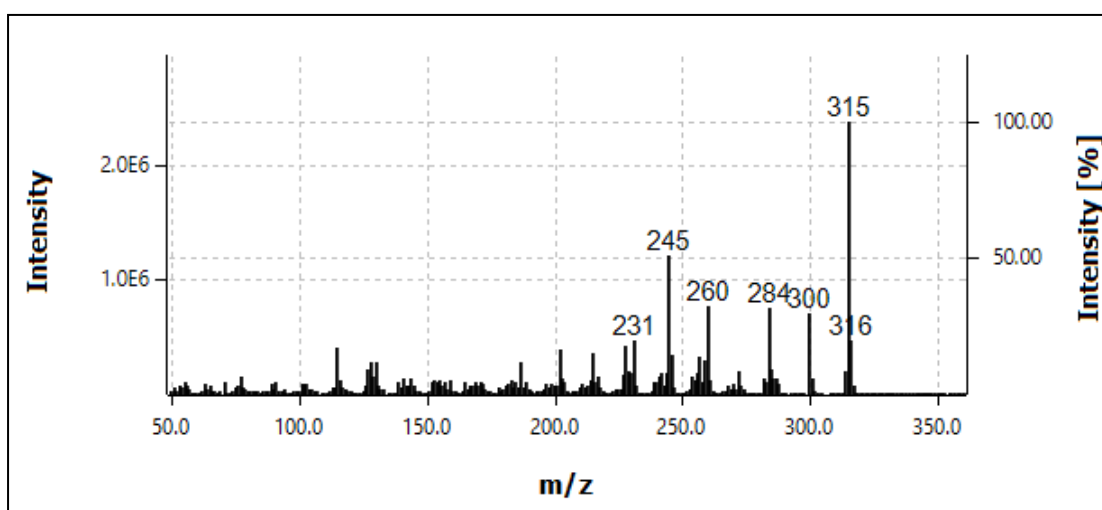


Figure II-11. EI-mass spectrum recorded for the chromatographic peak at 3.296 min.

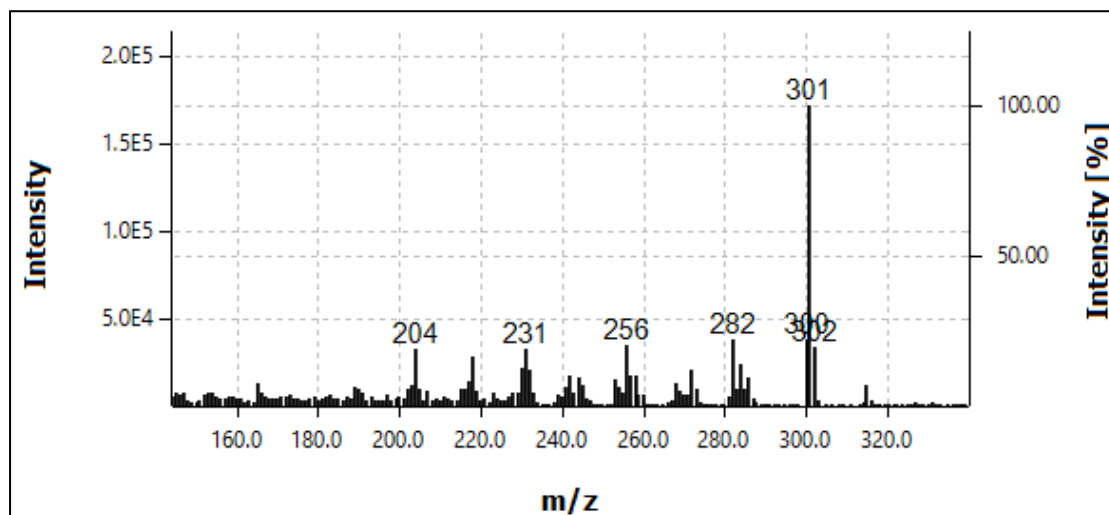


Figure II-12. EI-mass spectrum recorded for the chromatographic peak at 3.344 min.

3.2.3 Semi-preparative HPLC purification of buphanidrine

The prep-TLC-fractions (WJ-53-C and WJ-54-C) were utilised in determining the expected retention time range for buphanidrine (**1**) in the silica gel column fraction, WJ-41-J, and developing a suitable method for sample fractionation. Method development on the detection of buphanidrine (**1**) was performed, utilising the analytical HPLC-column (4.6 × 150 mm). This helped to mitigate the negative impact of method development on the yield.

The chromatogram in **Figure II-13** shows the resolution produced by applying the developed solvent system, shown in **Table II-4**, in the analysis of WJ-41-J on the semi-prep HPLC-column (19 × 250 mm). The shaded regions indicate the retention time ranges during which the column eluate was collected, based on the criteria for fraction collection, summarised in **Table II-5**.

It was expected that the peak between 12.00 and 14.00 min corresponded to buphanidrine (**1**). This assumption was based on a preliminary GC-MS and HPLC-PDA analyses of prep-TLC-fractions (Section 3.2.2), in which buphanidrine (**1**) was present in the greatest abundance. This combined fraction had a mass of 4.70 mg, resulting in an isolated alkaloid yield of 11.9% from the column fraction, WJ-41-J. With respect to the mass of dried plant material (120.14 g), a yield of 0.00391%.

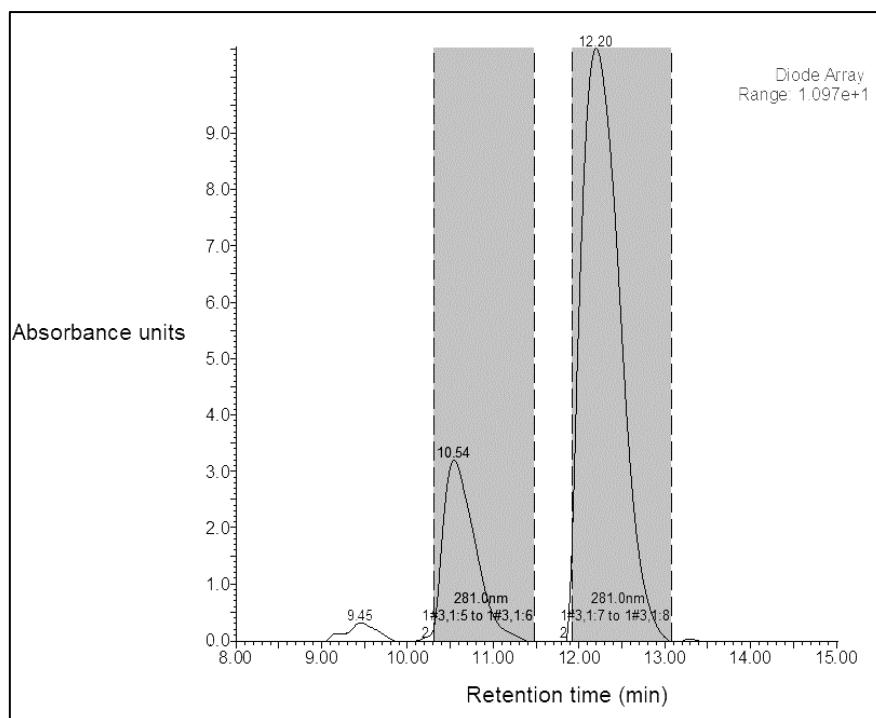


Figure II-13. Chromatograms of sample WJ-41-J using semi-preparatory HPLC.

3.2.4 Confirmation of the identity and purity of isolated buphanidrine

UPLC-qTOF-MS accurate mass analysis

A small sample of the isolated alkaloid (0.1 mg/mL, 0.5000 mL), expected to be buphanidrine (**1**), was submitted for UPLC-qTOF-MS analysis. The chromatogram was recorded in the positive ionisation mode since alkaloids are readily protonated in the column by the formic acid buffer to produce the corresponding quasi-molecular $[M+H]^+$ -ion. Following subtraction of the ESI (+)-mode chromatogram of the method blank, the chromatogram in **Figure II-14** was obtained.

In the resulting UPLC-chromatogram four peaks were detected, including one (peak 1 of **Figure II-14**) with a base peak ion of $m/z = 316.1528$, corrected relative to leucine-enkephalin. Elemental composition analysis of this m/z -ratio corresponded to the formula $[C_{18}H_{22}NO_4]^+$ with 16.51% confidence. This %-certainty is based on an isotopic fit-ratio of 16.9. The calculated elemental composition has a calculated monoisotopic mass of 316.1549 Da. This is less than 5 ppm from the detected accurate ion mass. Therefore, the peak 1 of **Figure II-14** can be tentatively identified as buphanidrine (**1**), in accordance with the guidelines on identification of analytes set out by the Director General of the European Commission for Health and Food Safety.²⁴

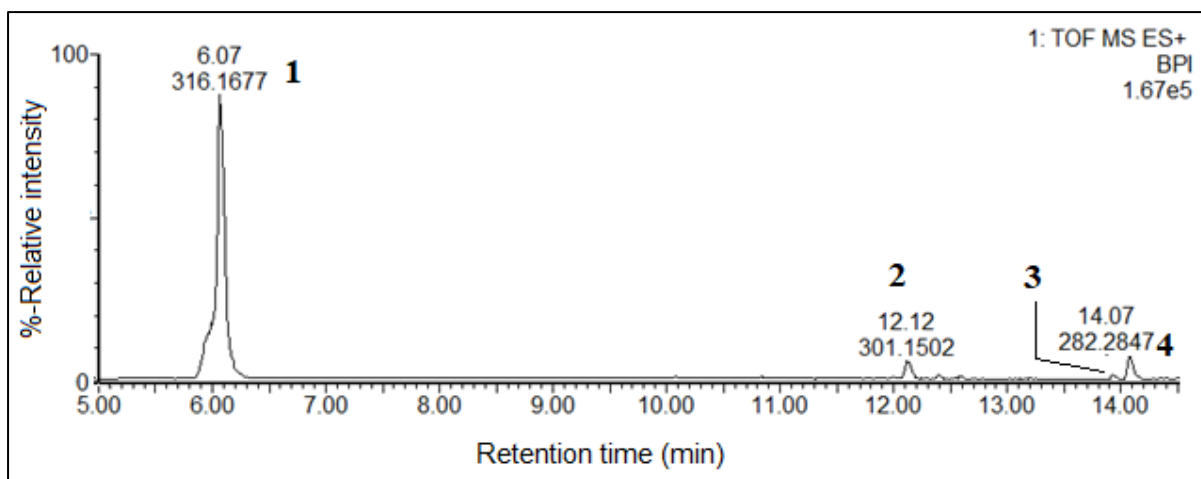


Figure II-14. Chromatogram recorded in the positive ion mode for buphanidrine, isolated from the silica gel column fraction, WJ-41-J, following subtraction of the blank chromatogram.

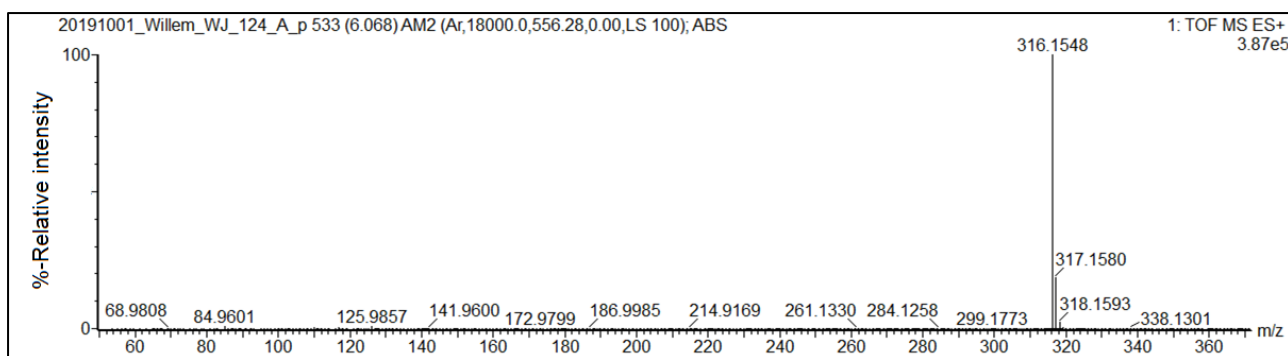


Figure II- 15. First order positive ionisation mode mass spectrum for peak 1 of **Figure II-14** at 6.062-6.068 minutes.

Once buphanidrine (**1**) was tentatively identified by accurate mass, the purity of the sample was estimated based on the area under the chromatographic peaks (recorded in TIC mode), after subtraction of the method blank chromatogram. Based on the fraction of area contributed by Peak 1 to the total area measured, the tentatively identified alkaloid was isolated with a 90.36% purity (See **Table II-8**).

Table II-8. Percent composition of the sample containing isolated buphanidrine.

Peak no.	Retention time (minutes)	Area measured	Percent of total area
1	6.062	13 043.29	90.36
2	12.13	591.44	4.10
3	13.93	73.52	0.509
4	14.08	726.93	5.04
Total	N/A	14 435.18	100.00

GC-MS analysis of isolated buphanidrine

Further confirmation on the identity of the isolated alkaloid as buphanidrine (**1**) was obtained via GC-MS analysis. The electron impact mass spectrum recorded for the detected chromatographic peak, correlated well (98% spectral match) with that of buphanidrine (**1**) in the Wiley-NIST library²⁵ (**Figure II-16 & Figure A (II)-1**).

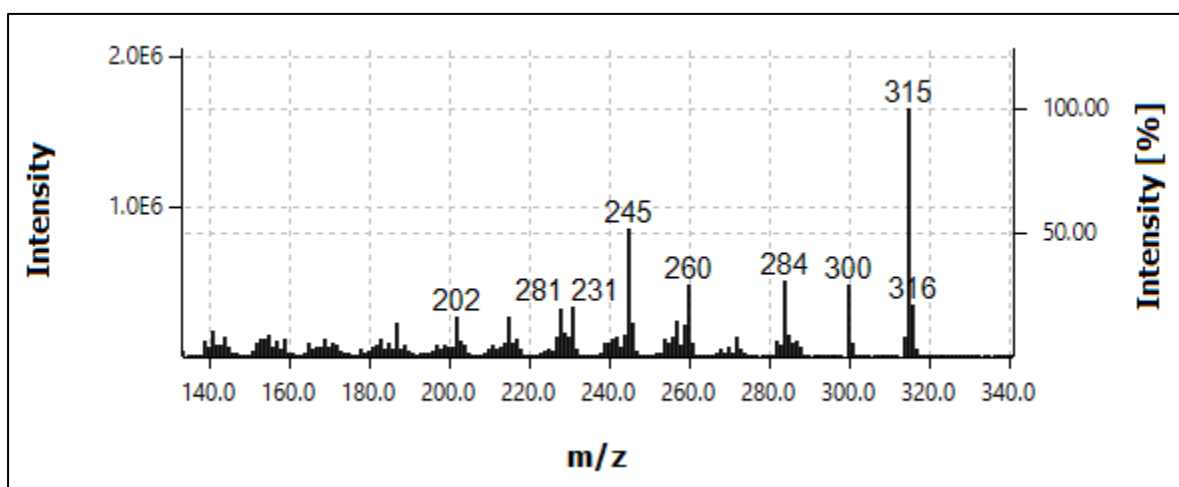


Figure II-16. GC-MS EI-mass spectrum recorded for the chromatographic peak at 3.269 minutes in Figure II-17, for the isolated sample.

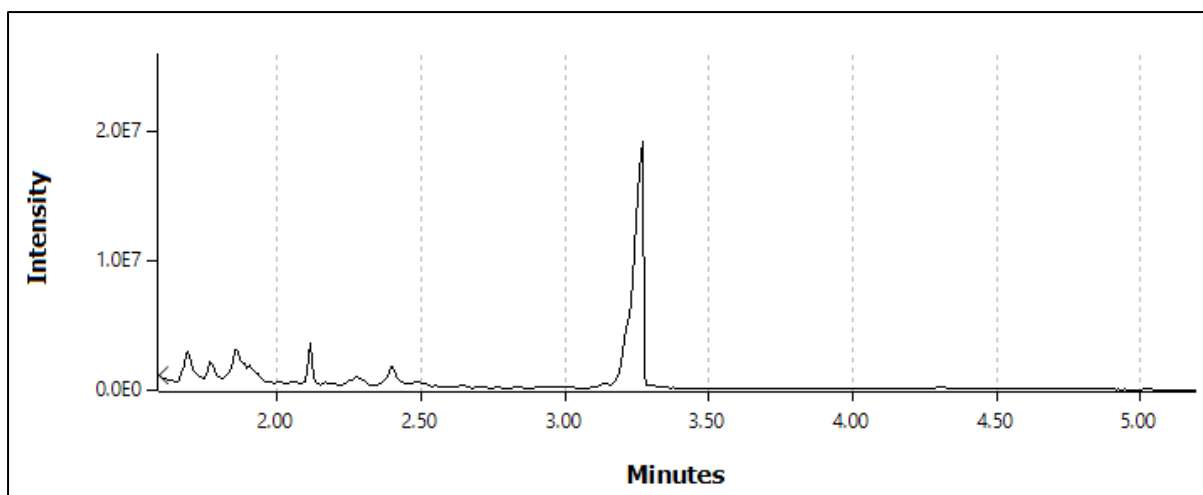


Figure II-17. GC-MS chromatogram of buphanidrine (**1**), isolated from the silica gel column-fraction, WJ-41-J.

From the recorded and library spectra for buphanidrine (**1**), the fragmentation pathway, under 70 eV electron impact conditions, can be deduced (**Figure II-18**). Starting from the molecular ion ($m/z = 315$), a loss of a methyl group (from either one of the methoxy substituents) produces the fragment ion of $m/z = 300$ (**4**). Either as a subsequent or as a single event, the loss of a methoxy group produces the $m/z = 284$ fragment ion. A fragment ion of mass 245 Da is produced when the 1,3-dioxole ring is lost from the molecular ion (**5**). The formation of the $m/z = 260$ fragment ion (**6**) follows from the loss of the tropane amine ($\text{C}_2\text{H}_4(\text{N}^{\bullet})\text{CH}^{\bullet} = 55$ Da).

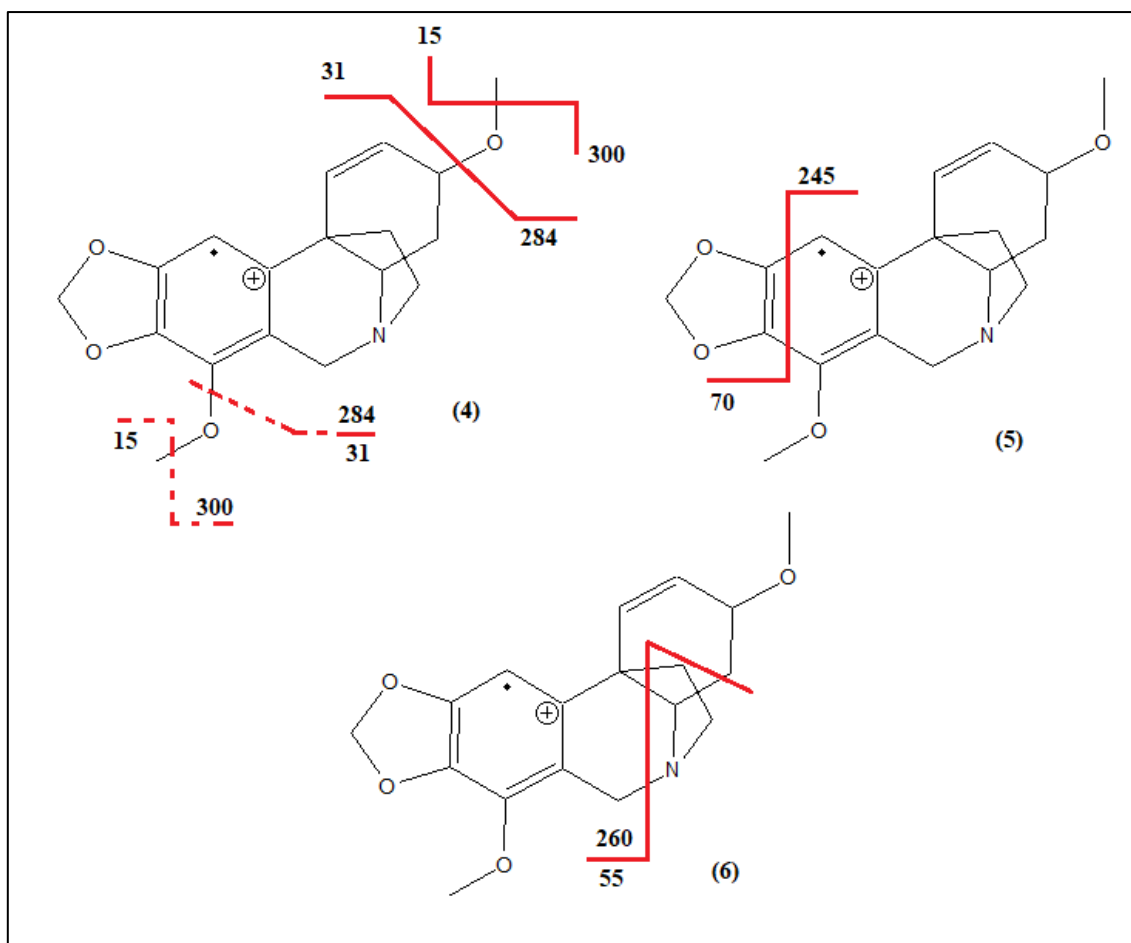


Figure II-18. Proposed fragmentation of buphanidrine to its most abundant fragment ions.

Nuclear magnetic resonance spectroscopy (NMR)

Buphanidrine (**1**) has previously been analysed by NMR-spectroscopy. Since the proton-NMR spectra of the analysed species are almost unique, previously recorded spectra can be used as reference with which the experimental spectra can be compared. For confirmation that the isolated compound is indeed buphanidrine (**1**), the measured $\delta^1\text{H}$ -NMR spectrum was compared, in **Table II-9**, to the literature $\delta^1\text{H}$ -NMR and $\delta^{13}\text{C}$ -NMR spectra for buphanidrine (**1**), measured by Cheesman¹¹ in methanol- D_4 .

The isolated compound (WJ-106-A) was analysed by NMR in chloroform- D_1 (500 MHz, CDCl_3) for both $\delta^{13}\text{C}$ - and $\delta^1\text{H}$ -resonance. The sample was rerun in chloroform- d_1 at 400 MHz. In the downfield region of the $\delta^1\text{H}$ -NMR two alkene protons were detected at δ 6.42 (1H, H, d, $J = 10.58$ Hz) and δ 6.07 (1H, , dd, $J = 5.42; 10.2$ Hz). Another signal at δ 6.57 (1H, s) corresponds to the aromatic proton on C-15.

Upfield from the aromatic region, the notable signal of the methylene protons, in the dioxole ring (C-12), was observed at δ 5.92 (2H, dd, $J = 1.44; 4.57$ Hz). The signals at δ 4.62 (1H, d, $J = 17.12$ Hz) and δ 4.24 (1H, d, $J = 17.12$ Hz) were attributed to the α and β protons of C-7, respectively. The chemical shift at δ 3.84 (1H, m) corresponds to the allylic proton on C-3, deshielded by the electronegativity of the adjacent oxygen atom. The signal at δ 4.02 (3H, s), was attributed to the C-9 methoxy protons. This downfield shift of the methyl group was caused by the deshielding nature of the oxygen atom's electronegativity.

The second signal at δ 3.84 (1H, dd, $J = 3.61; 13.84$ Hz) could likely be caused by the resonance of the proton on C-5, deshielded by the electronegativity of the neighbouring nitrogen atom. The signal at δ 3.36 (3H, s) was attributed to the second methoxy group on C-3. Its further upfield signal than that of the methoxy group at δ 4.02 could be caused by the shorter conjugated bond chain in the allylic system, than on the aromatic ring-system, that induces a weaker electron-withdrawing action than the aromatic system. Both chemical shifts, however, experience deshielding by electron withdrawal from the methyl group by the oxygen atom.²⁶

A set of complex signals between δ 2.20 and δ 4.13 were likely caused by the tropane ring, when compared to the observed signals in Neergaard, et al.¹⁰ The chemical shifts at δ 3.24 (1H, m) and δ 4.13 (1H, m) were attributed to the *endo*- and *exo*-protons protons on C-19, respectively. The two complex signals at δ 2.37 (1H, m) and δ 2.20 (1H, m) are assigned to the *endo*- and *exo*-protons on C-18. The signals with further downfield shifts were assigned to the protons of C-19 since this position experiences greater electron density withdrawal from the nitrogen atom than the C-18 position does. This is corroborated by the findings of Cheesman.¹¹

In the far upfield region of the $\delta^1\text{H}$ -NMR spectrum two complex chemical shifts were observed at δ 1.73 (1H, dt, $J = 3.61; 13.84$ Hz) and δ 2.67 (1H, broad d). These chemical shifts suitably describe the remaining two protons on C-4, where δ 1.73 was attributed to the β - ^1H and δ 2.67 to the α - ^1H on C-4, where H-4 α was spatially oriented closer to the methoxy group on the neighbouring carbon atom (C-3).

. An interesting observation in the measured $\delta^1\text{H}$ -NMR spectrum is the large deviation of δ 4.13 from the cited chemical shift of δ 3.30. The deviation of +0.83 ppm from the literature value, for the proton at C-19, was the largest deviation between the spectra. Large differences between the measured and cited spectra, in the order of 0.6 ppm, were also observed. In addition to the random variation in measurement, these differences may also be attributed to the use of different spectrometers and solvents in analysis.¹¹

The measured $\delta^{13}\text{C}$ -NMR spectrum correlated well with the recorded spectrum in Cheesman's thesis.¹¹ The close correlation between the measured spectra and literature confirms the identity of the isolated alkaloid as buphanidrine (**1**).

The full NMR-spectra for the isolated compound, confirmed to be buphanidrine (**1**), are given in Section B of Appendix II.

Table II-9. Comparison of recorded ^1H -NMR chemical shifts (left), with chemical shifts recorded by Cheesman¹¹ in literature.

Present study: CDCl_3 , 500 MHz (^{13}C), 400 MHz (^1H)					Cheesman: CDCl_3 , 500 MHz (^{13}C), 400 MHz (^1H)			
Position	$\delta^{13}\text{C}$ (ppm)	$\delta^1\text{H}$ (ppm)	Splitting, J (Hz)	Integral	$\delta^{13}\text{C}$ (ppm)	$\delta^1\text{H}$ (ppm)	Splitting, J (Hz)	Integral
1	128	6.42	<i>d</i> , 10.0	1H	135	6.62	<i>d</i> , 10.0	1H
2	127	6.07	<i>dd</i> , 10;4,65	1H	127	5.96	<i>dd</i> , 10;5,16	1H
3	70	3.84	<i>m</i>	1H	75	3.84	<i>m</i>	1H
4α	25	2.67	<i>brd d</i> , 14,74	1H	30	1.64	<i>brd d</i> , 13,6	1H
4β		1.73	<i>dt</i> , 3,61; 13,84	1H		2.03	<i>ddd</i> , 13,6;13,5;4,1	1H
5	64	3.84	<i>dd</i> , 11,24;4,82	1H	65	3.22	<i>dd</i> , 13,5;4,0	1H
7α	56	4.61	<i>d</i> , 17,12	1H	60	4.15	<i>d</i> , 17,2	1H
7β		4.24	<i>d</i> , 17,12	1H		3.79	<i>d</i> , 17,2	1H
8	110				118			
9	141				143			
10	135				135			
12	101	5.93	<i>dd</i> , 4,57;1,44	2H	102	5.84	<i>s</i>	2H
14	150				150			
15	97	6.57	<i>s</i>	1H	99	6.61	<i>s</i>	1H
16	136				141			
17	46				47			
18-endo	41	2.37	<i>m</i>	1H	46	2.13	<i>ddd</i> , 12,6;9,16;4,0	1H
18-exo		2.2	<i>m</i>	1H		1.94	<i>ddd</i> , 2,6;10,9;6,04	1H
19-endo	52	3.24	<i>m</i>	1H	55	2.87	<i>ddd</i> , 13,1;9,1;6,04	1H
19-exo	52	4.13	<i>m</i>	1H		3.30	<i>m</i>	1H
3-OMe	57	3.36	<i>s</i>	3H	58	3.34	<i>s</i>	3H
9-OMe	60	4.02	<i>s</i>	3H	61	3.96	<i>s</i>	3H

3.3 Quantification of buphanidrine in spiked samples -Validation figures of merit

3.3.1 Matrix matched samples – Urine

Linearity of response models

By accounting for the purity of the reference sample of buphanidrine (**1**) used to spike the samples, the true theoretical concentration of each sample can be calculated. Spiking the samples, as described in Section 2.3.5, the samples will, theoretically, have the concentrations 0.542, 1.08, 1.63, 2.17, 2.71 and 3.25 ppm ($\mu\text{g/mL}$).

A summary of the linearity figures of merit calculated for each of the three batches, and the mean response model, is given in **Table II-10**. These response models were calculated for the relative response of the base peak (and molecular) ion relative to the response of the base peak ion in the internal standard ($m/z = 217$). The models calculated for the individual batches were the average relative responses of the base peak ion per batch. The response models are shown in **Figure II-19**.

The linear response models produced from the analysis of the spiked urine samples, show good correlation to the calculated linear best-fit trendlines. This is also observed in the response model generated by the overall average relative responses measured for buphanidrine (**1**). For each response model, the correlation was confirmed as significant at the 95.4% confidence level ($\alpha = 0.046$) by performing a t-test with $n-2$ degrees of freedom. Upon analysis of the y-residual plots, no curvature was observed for either the individual batches, or for the mean response model.

Table II-10. Linearity figures of merit calculated for the response models, generated by spiked urine samples.

	r^2	Slope (b)	s_b	Intercept (a)	S_a	$S_{y/x}$
Batch 1	0.950	0.116	0.013	-0.039	0.028	0.0301
Batch 2	0.835	0.125	0.028	0.123	0.059	0.0632
Batch 3	0.964	0.115	0.011	0.218	0.024	0.0253
Average	0.977	0.1186	0.0092	0.101	0.019	0.0191

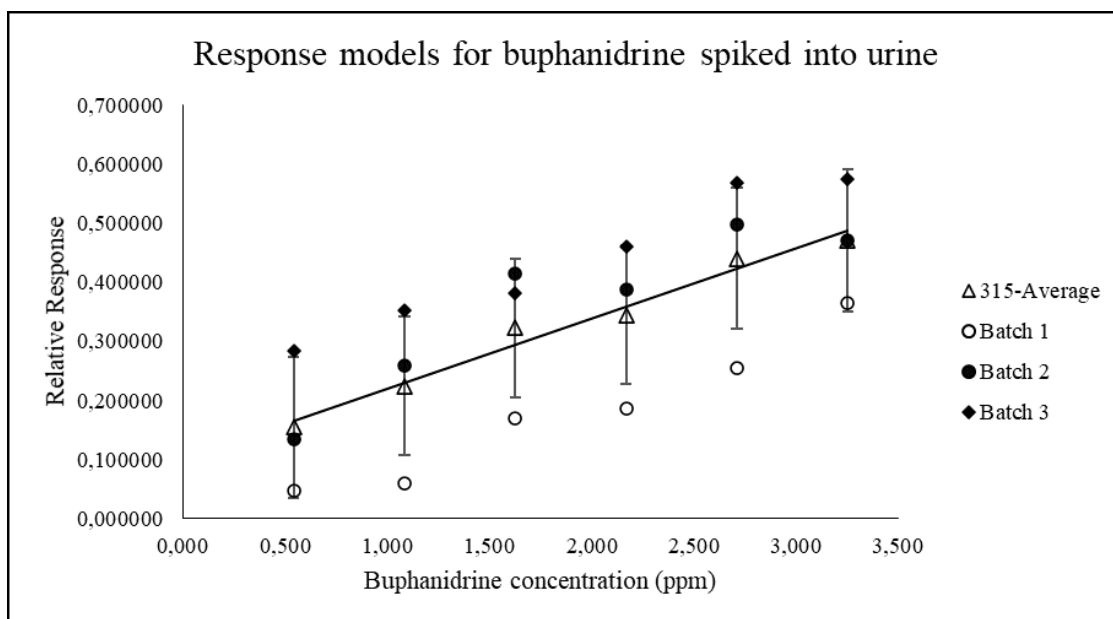


Figure II-19. An illustration of the response models generated by the individual batches of urine samples and the average relative response produced. The x-axis is in units of ppm ($\mu\text{g}/\text{mL}$).

The theoretical limits of detection and quantification were determined based on the mean of the relative responses of the blank samples prepared according to the sample preparation procedure as described by the U.S. Department of Health and Human Services.²⁷ Since the intercept of the mean response model is significantly greater than naught, the contribution of the background to the measured response must be considered when calculating the limits. Therefore, the y-value of the theoretical detection limit is given by $y_B + 3s_B$, where y_B is the average y-relative response of the blank signal and s_B is the standard deviation of the average blank relative response.

Applying this reasoning to the calculation, the limit of detection was calculated to be 0.0647 ppm with a standard deviation of 0.2068 ppm. Similarly, for ten standard deviations of the y-residuals, the limit of quantification was calculated to be 0.2158 ppm with a standard deviation of 0.2012 ppm.

The slopes of the regression models did not differ significantly from each other at the 95.4% confidence level. This implies that between Batches 1 and 2, there exists no significant difference in the relationship between the measured relative responses and the expected concentration of buphanidrine (1). Despite its intercept, which is significantly greater than naught for $\alpha = 0.046$, the response model from Batch 3 does not differ significantly from that

of Batch 2. This follows from the overlap of the significance intervals around the intercepts of the two response models.

There is, however, a significant difference between the response models for Batches 1 and 3. This significant difference would imply that the method is not fully repeatable between batches. A more detailed investigation by analysis of variance at each concentration level across the batches (One-way ANOVA) provided further insight. The F-tests are summarised for each concentration in **Table II-11**.

Based on the ANOVA results, the variation produced between the individual batches is only significant at low concentrations of buphanidrine (**1**). This significant contribution of variance implies that at low levels of buphanidrine, the method is less repeatable between batches than at higher concentrations. This observation correlates well with the significant difference between the intercepts of Batches 1 and 3.

Table II-11. Calculated F-values (F-stat) for the ratio of Between-batch and Within-batch variances at the different concentration levels.

Conc. (ppm)	F-stat	F (2,3)
0.542	15.0	10.2
1.08	13.6	10.2
1.63	5.06	10.2
2.17	6.35	10.2
2.71	8.49	10.2
3.25	2.20	10.2

Repeatability of measurement

The significant contribution of variance due to different batches at low levels of buphanidrine (**1**) may contribute to a skewed distribution of variance over the average linear response model. This is illustrated by the %-relative standard deviation at the individual concentration levels of the mean response model. The error in the y-direction produced by the error at each spiked concentration value is illustrated by the error bars in **Figure II-19**. At first glance they show an equal distribution of variance. The corresponding %-RSD values in the x-direction are, however, more insightful as they relate to the concentrations that will be calculated via interpolation.

Table II-12. %-RSD values for variance in the x-direction, calculated at each individual concentration.

Concentration (ppm)	%-RSD
0.542	30.3
1.08	13.3
1.63	8.51
2.17	6.50
2.71	6.16
3.25	5.50

The %-RSD values show that relative to the concentration at which the variance is calculated, the variance in the response model is distributed heteroscedastically. As the concentration increases, the variance decreases. This trend was observed in the contribution of variance from the between-batch variation relative to the within-batch variation. At low concentrations of buphanidrine (**1**), this contribution became significant and may explain some of the increase in %-RSD values at the lowest concentration level.

Based on the Horwitz-equation, the %-RSD for a batch of samples in the range of 0.1-1 ppm should be close to 16%.²⁸ At a %-RSD value of 30.3%, the repeatability of a quantitative measurement is no longer suitable for application. Therefore, an experimental limit of quantification was reached between 0.542 and 1.08 ppm.

Following from this, a more repeatable linear range can be suggested for quantitative analyses. Since five concentration levels remain if the lowest level is deemed unfit for purpose, a new mean response model can be calculated (**Table II-13**):

Table II-13. Comparison of linearity figures of merit for 6-point and 5-point response models.

	r^2	Slope (b)	s_b	Intercept (a)	s_a	$s_{y/x}$
Average	0.977	0.1186	0.0092	0.101	0.019	0.0191
New	0.961	0.113	0.013	0.116	0.030	0.0223

Excluding the lowest concentration level from the model does not significantly impact the relationship between the measured relative responses and the corresponding spiked concentrations of buphanidrine (**1**).

Accuracy and recovery of analyte from the sample

Table II-14. Accuracy and recovery data for the mean response model of urine samples.

Theoretical conc.(ppm)	Experimental conc. (ppm)	%-Bias*
0.542	0.472	-13.0
1.08	1.08	-0.623
1.63	1.94	19.4
2.17	2.13	-1.55
2.71	2.98	9.82
3.25	3.24	-0.360

$$*\% \text{-Bias} = [(\text{Experimental conc.} - \text{Theoretical conc.}) \div \text{Theoretical conc.}] \times 100\%$$

A comparison of the theoretical and experimental concentrations present in the analysed samples should ideally be a linear model of gradient +1 and an intercept of naught. The slope is interpreted as the fraction of theoretically present analyte recovered, or detected, in the samples. The intercept indicates whether a constant amount of analyte is gained or lost in the method, for example due to pipetting action or analyte loss during preparation.

In the calculated accuracy data for the analysis of urine samples for buphanidrine (**1**), there does not seem to be a consistent bias in one direction from the theoretical concentration values. There is also no fixed trend in the %-bias calculated for each concentration (**Table II-14**). This correlates well with the linearity figures of merit calculated for the regression of the experimental concentration values on the theoretical concentration values (**Table II-15**).

Table II-15. Linearity figures of merit for the accuracy analysis.

r²	Slope (b)	s_b	Intercept (a)	S_a	S_{y/x}
0.977	1.000	0.077	0.00	0.16	0.175

The close correlation between the experimental and theoretical concentrations is visible when plotted as the regression of experimental concentration on theoretical concentration (**Figure II-20**). The correlation was confirmed to be significant via a t-test. In the plot of the residuals, no curvature or fixed trend is observed across the concentration range (**Figure II-21**). This implies the relationship between the experimental and theoretical concentrations is linear with significant correlation.

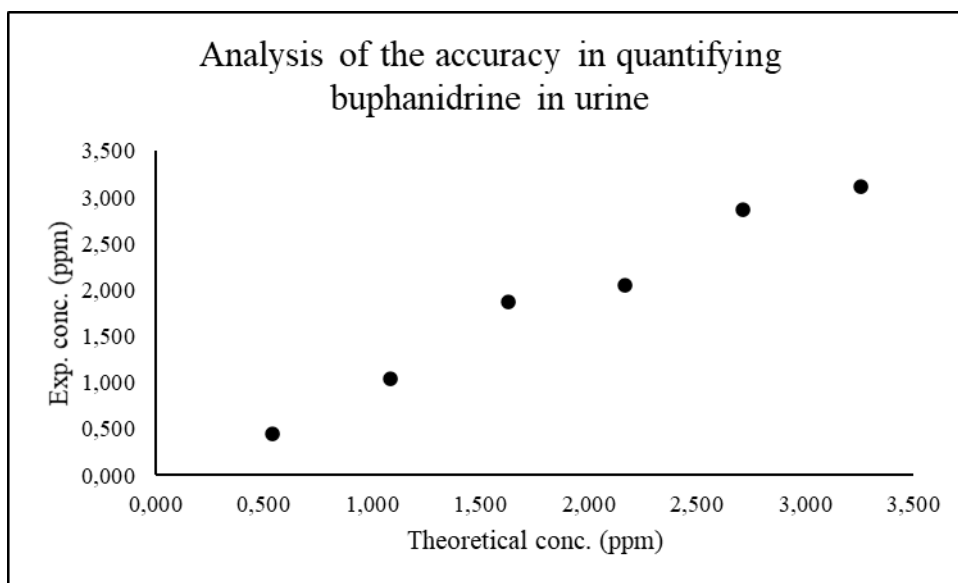


Figure II-20. A plot showing the regression of the experimental concentration on the theoretical concentration.

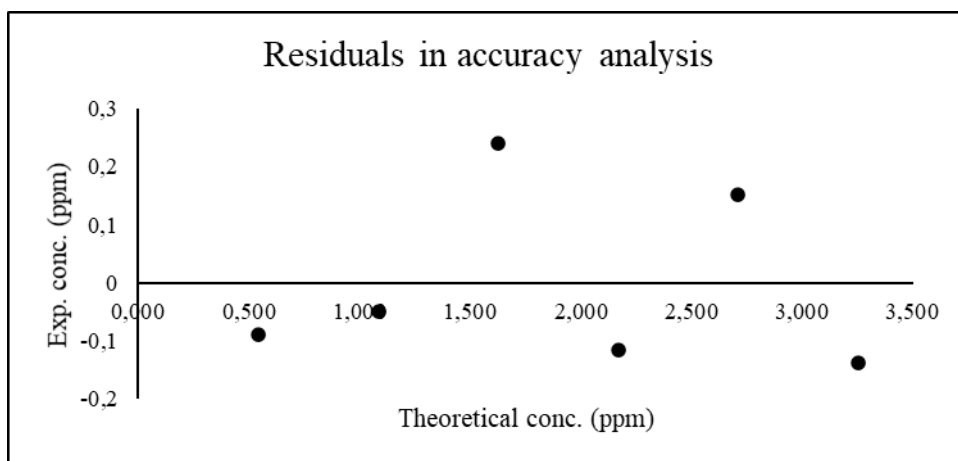


Figure II-21. Residuals in the y-direction, calculated for the regression of experimental concentration on the theoretical concentration.

Based on the calculated figures of merit, the slope of the regression line does not differ significantly from 1.000 at the 95.4% confidence level. This implies there is no significant deviation in the experimentally detected concentration from the theoretical concentration. Similarly, the intercept of the regression line does not differ significantly from naught, therefore additive bias is negligible at the 95.4% confidence level (**Table II-15**).

3.3.2 Analysis of spiked de-ionised aqueous samples

Linearity of the trend in the measured data

For a suitable linear fit, the data must closely correlate with the calculated linear trend line and must show no curvature. Curvature in the response model is best observed through the plot of the y-residuals over the analysed concentration range. Since there are less matrix components in aqueous samples, a linear fit of ideal quality is expected for the samples prepared in de-ionised water. The response models obtained for each batch of samples and for the average batch are illustrated in **Figure II-22**, and the corresponding figures of merit summarised in **Table II-16**.

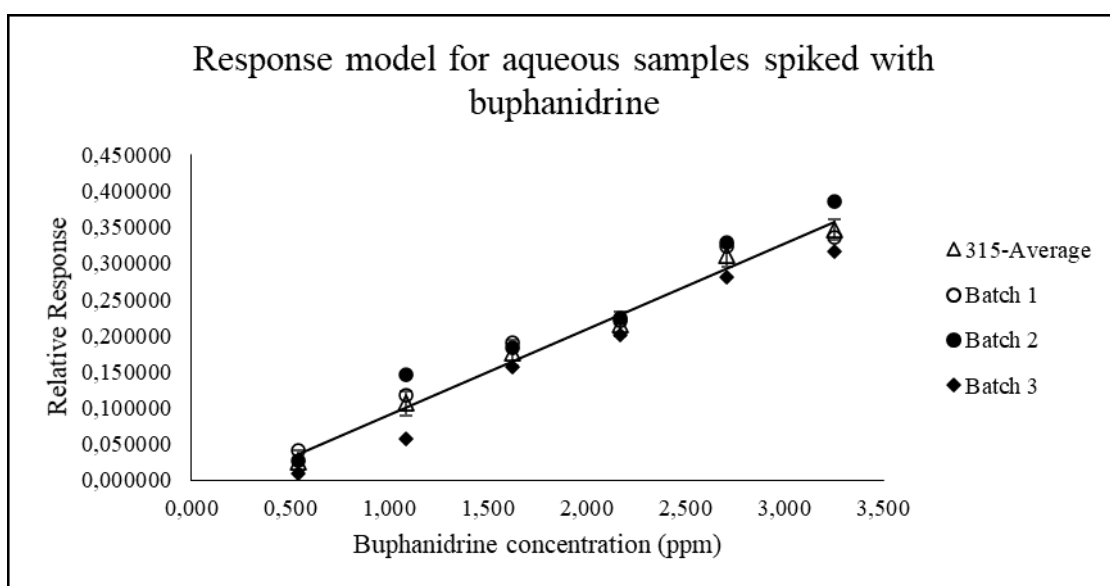


Figure II-22. The mean response model for aqueous samples of buphanidrine. The regression data points for the individual batches are also shown. The x-axis is in units of ppm ($\mu\text{g/mL}$).

Table II-16. Linearity figures of merit calculated for aqueous samples spiked with buphanidrine.

	r^2	Slope (b)	s_b	Intercept (a)	S_a	$S_{y/x}$
Batch 1	0.972	0.1122	0.0095	-0.008	0.020	0.0215
Batch 2	0.974	0.126	0.010	-0.022	0.022	0.0232
Batch 3	0.986	0.1189	0.0070	-0.056	0.015	0.0160
Average	0.988	0.1189	0.0067	-0.029	0.014	0.0138

In the response models generated from aqueous samples, close correlation is observed between the relative responses and the corresponding concentration levels within each individual batch and for the mean response model. The significance of the correlations was confirmed as such by performing a t-test on the product-moment correlation coefficient (r^2) for each individual batch and for the mean response model. The suitability of the linear model, in describing the trend in regression, is further supported by the random distribution of the y-residuals about the x-axis, as seen in **Figure II-23**.

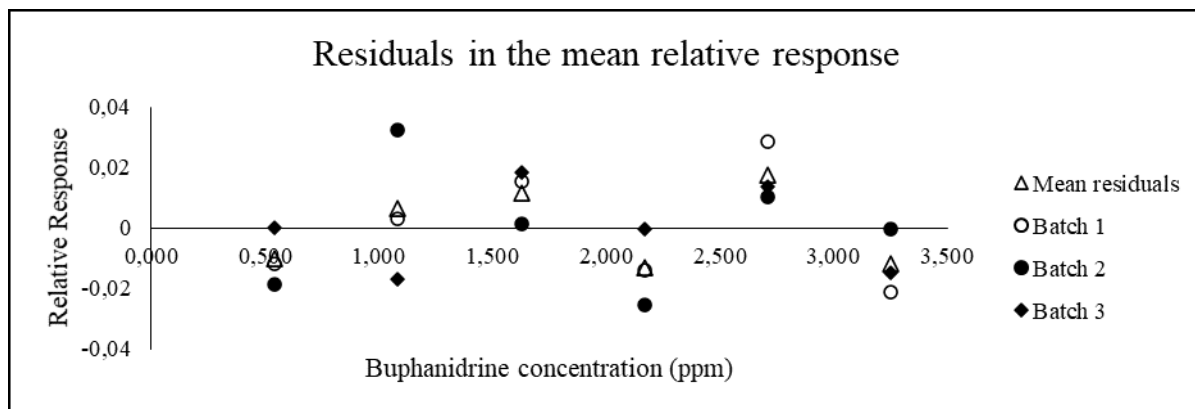


Figure II-23. An illustration of the y-residuals calculated at each concentration for the mean and individual batches' response models.

The calculated figures of merit, regarding the intercepts of the models, show that batches 1 and 2 have y-intercepts that do not differ significantly from naught for $\alpha = 0.046$. The intercept calculated for batch 3, however, is significantly different from naught at the confidence level. This implies there is a different relationship between the measured relative response values and the spiked concentrations for Batch 3 than those in Batches 1 and 2. In contrast to the mean response model for urine samples, the intercept of the mean response model for de-ionised aqueous samples does not differ significantly from naught.

Even though there is no significant difference between the slopes of the regression models for the individual batches, the difference between the intercept of Batch 3 and those of Batches 1 and 2 implies a different relationship between the variables in Batch 3. This difference, however, is not significant at the 95.4 % confidence level since the confidence intervals for the intercepts of the response models overlap. This implies the models do not significantly differ from each other at the 95.4% confidence level.

A comparison of the figures of merit for the mean response model to those obtained for the individual batches show that there is no significant difference in the slope, of the mean response model and the slopes of any of the three individual batches' response models. In the residuals plot a large variation between the residuals of data points is observed at the second lowest concentration level (**Figure II-23**). This spike in variation is also observed for the linear response models (**Figure II-22**). By performing single factor ANOVA, it was shown that at this concentration of buphanidrine (**1**), the between-batch variation contributes significantly to the observed variance.

The limits of quantification and detection were calculated for the mean response model, following the same reasoning as for the matrix matched samples. The limit of detection was determined to be 0.0159 ppm, with a standard deviation of 0.1504 ppm, and the limit of quantification was 0.0531 ppm, with a standard deviation of 0.1494 ppm.

Repeatability of measurement

As was observed in the case of urine samples, a significant contribution of between-batch variation to variance in measurement may cause a sharp increase in the %-RSD value in the x -direction at the corresponding concentration. To determine the distribution of variance over the analytical range, the %-RSD values along the x -axis were calculated for each theoretical concentration of buphanidrine (**1**) in the samples.

Table II-17. %-RSD values calculated for aqueous buphanidrine samples at each respective concentration level.

Concentration (ppm)	%-RSD
0.542	20.7
1.08	9.06
1.63	5.85
2.17	4.50
2.71	4.21
3.25	3.78

In contrary to the expected spike in %-RSD at the second lowest concentration level, the %-RSD values followed a steady heteroscedastic trend, decreasing with an increase in concentration. Like the urine samples, the error bars in the y -direction (**Figure II-22**), as well as the corresponding standard deviations in the x -direction from which they were calculated,

do not show notable trends. When these x -deviations are, however, measured relative to the theoretical concentration to which they correspond, a skewed trend is observed (**Table II-17**).

At the lowest concentration level (0.542 ppm), the %-RSD, again, is not suitable for repeatable quantitative analysis when compared to the suggested %-RSD from Horwitz's equation for analyte concentrations in the order of 0.1-1.0 ppm ($\text{\%-RSD}_{\text{exp}} = 20\% > \text{\%-RSD}_{\text{Horwitz}} = 16\%$).²⁸ This fixes an experimentally observed limit of quantification on the analytical method, which lies between 0.542 and 1.08 ppm. The quantitative range of the response model can then be adjusted to only include the upper five concentration levels.

Accuracy and analyte recovery from samples

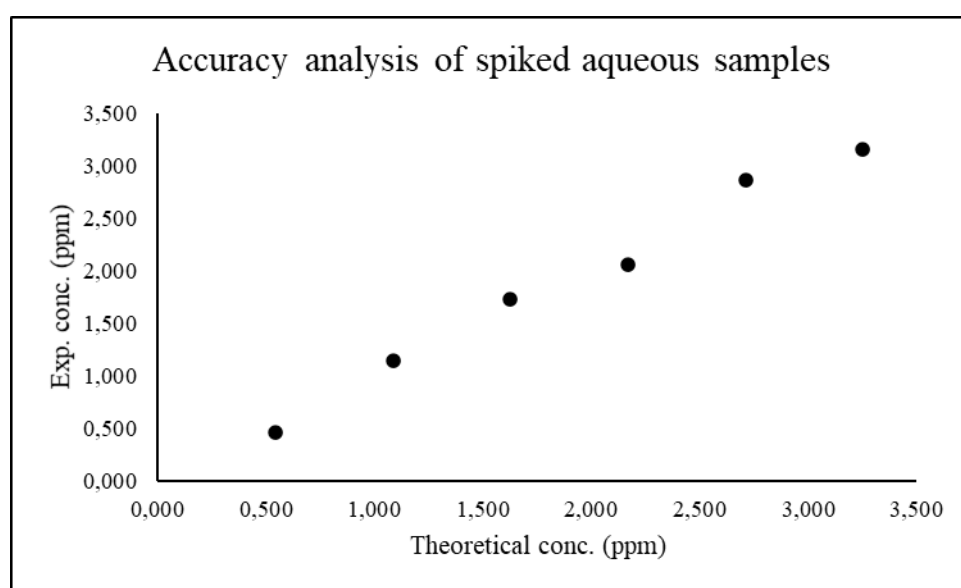


Figure II-24. A plot with linear trendline illustrating the regression of the experimental concentration on the theoretical concentration.

By performing regression analysis to determine the relationship between the experimentally observed buphanidrine (**1**) concentration and the theoretical concentration at which the samples were spiked, the extent of bias in the analytical method was estimated. The linearity figures of merit for this analysis are summarised in **Table II-18**. In the analysis of aqueous samples, the linear regression model obtained in the accuracy analysis closely correlated with the measured concentration levels (**Figure II-24** & **Table II-18**). The correlation was confirmed to be significant based on a t-test performed on the product-moment correlation coefficient.

Table II-18. Figures of merit for the evaluation of linearity in the accuracy analysis.

	r^2	Slope (b)	s_b	Intercept (a)	s_a	$s_{y/x}$
Accuracy	0.988	1.000	0.056	0.00	0.12	0.127

Curvature in the data relative to the calculated linear model was assessed by visual inspection of the plot of the y -residuals. This plot showed a random distribution of the residuals around the x -axis. Since the data did not follow a curved trend and closely correlated to the calculated trendline, a linear function is suitable in describing the trend in the data.

In the figures of merit, summarised in **Table II-18**, the slope of the trend in the data was calculated to be 1.000 with a standard deviation (s_b) of 0.112, and an intercept of 0.00 ppm, with a standard deviation (s_a) of 0.12 ppm. The linear model does not, therefore, significantly differ from the function $y = x$. Since there is no significant deviation from this trend in a fixed direction, it can be assumed that there is no significant systematic error produced by this analytical method.

3.3.3 A comparison of response models generated for samples prepared in urine and de-ionised water

Comparing the figures of merit calculated for the mean response models in de-ionised water and urine, the slopes of the calculated trendlines do not differ significantly from each other (**Table II-19 & Figure II-25**). A notable observation is the significant intercept of the response model for the urine samples. This indicates a different relationship between the variables in urine samples from those in de-ionised aqueous samples. By comparing the confidence intervals of the intercepts at the 95.4% confidence level, the difference between the intercepts was determined to be significant.

Since the response model generated for the spiked urine samples is significantly different from that obtained for spiked, de-ionised, aqueous samples, they cannot be used interchangeably. This also indicates that the presence of a physiological matrix (urine) in the sample significantly contributes to the measured relative response values.

Table II-19. Comparison of the linearity figures of merit for the mean response models in the respective matrices.

Matrix	r ²	Slope (b)	s _b	Intercept (a)	S _a	S _{y/x}
Urine	0.977	0.1186	0.0092	0.101	0.019	0.0191
De-ionised water	0.988	0.1189	0.0067	-0.029	0.014	0.0138

For a comparison of the limits of detection between the matrices, a 99.7% confidence interval was used. At this level of confidence, there is no significant difference between the calculated limits. In the comparison of the limits of quantification, a 95.4% confidence level was applied. The limits of quantification did not differ significantly at this level.

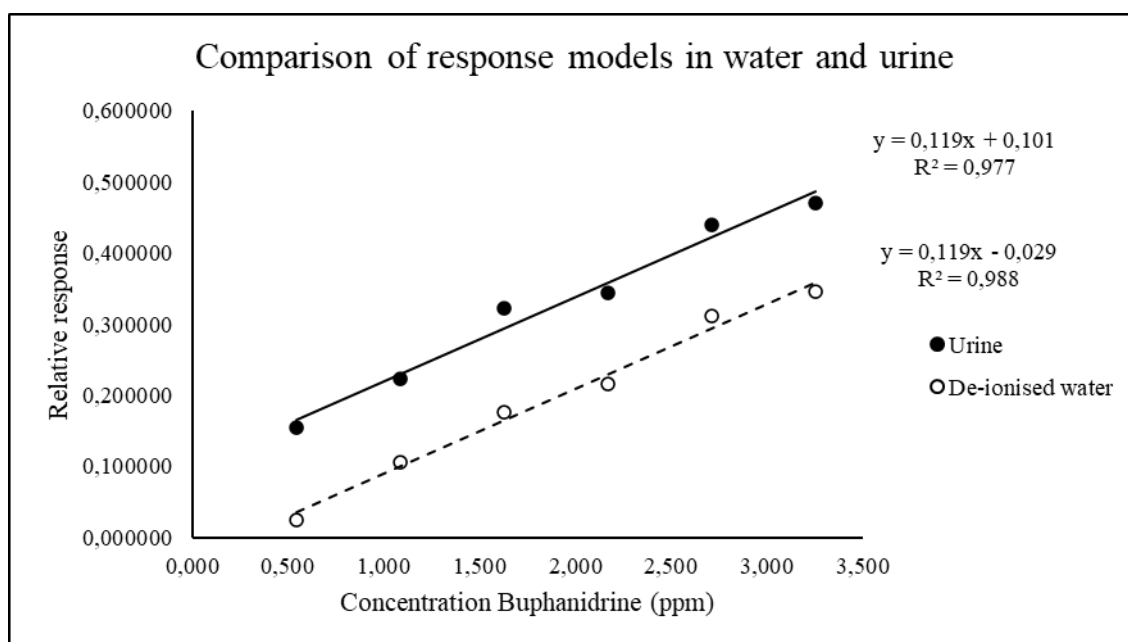


Figure II-25. A comparison of the response models generated for urine and de-ionised aqueous samples.

3.4 Qualitative analysis of buphanidrine in spiked matrices

3.4.1 Matrix matched samples

Trends in ion ratios with a change in concentration

Quantification relies on first identifying the target analyte with high confidence (99.7%). This 99.7% confidence is reflected in the theoretical calculation of the limit of detection. This calculation does not account for the phenomena that influence the mass spectrometry of analytes at various concentrations. Ideally, the observed mass spectrum, or at least the ratios of the most abundant ions therein, must remain within confidence limits over the entire analytical

range. Ion ratios are more robust than individual ion abundances, since the ion abundance has a strong relationship with the analyte concentration in the spiked sample. Ion ratios, however, are more closely related to the analyte molecular structure than to the concentration of the analyte. The ion ratios that were monitored for the analysis of buphanidrine (**1**) are given in **Table II-20**.

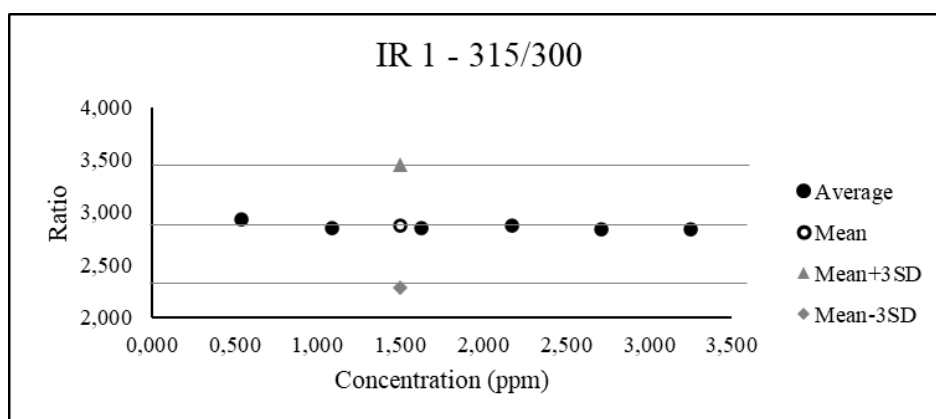
Table II-20. Definition of ion ratios for buphanidrine.

Identifier	Ion ratio
IR 1	Area m/z = 315/Area m/z = 300
IR 2	Area m/z = 315/Area m/z = 284
IR 3	Area m/z = 260/Area m/z = 284
IR 4	Area m/z = 260/Area m/z = 245
IR 5	Area m/z = 315/Area m/z = 260

Central values for the confidence limits of the ion ratios can be calculated from the recorded responses of individual ions at the middle concentration level of the response model (2.17 ppm). The resulting centroid and 99.7% confidence interval were defined by the vectors \bar{m} (centroid) and \bar{s} (standard deviation vector):

$$\bar{m} = \begin{bmatrix} 2.8683 \\ 2.5465 \\ 1.1285 \\ 0.59884 \\ 2.2602 \end{bmatrix} \text{ with } \bar{s} = \begin{bmatrix} 0.1942 \\ 0.1048 \\ 0.0756 \\ 0.07020 \\ 0.0725 \end{bmatrix}$$

If variation in the spiked concentration, and therefore analyte activity in the ion source, is varied to either side of this concentration, a corresponding change in ionisation and fragmentation can be observed from the central control value for the ion ratios.



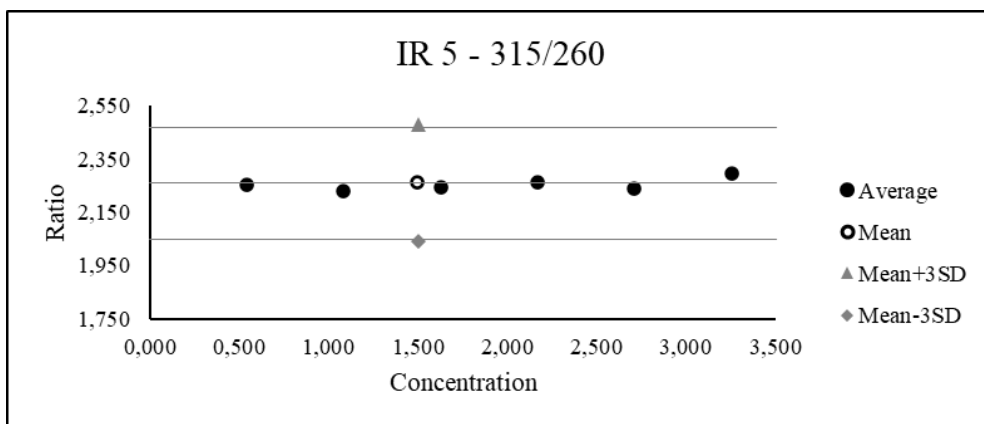
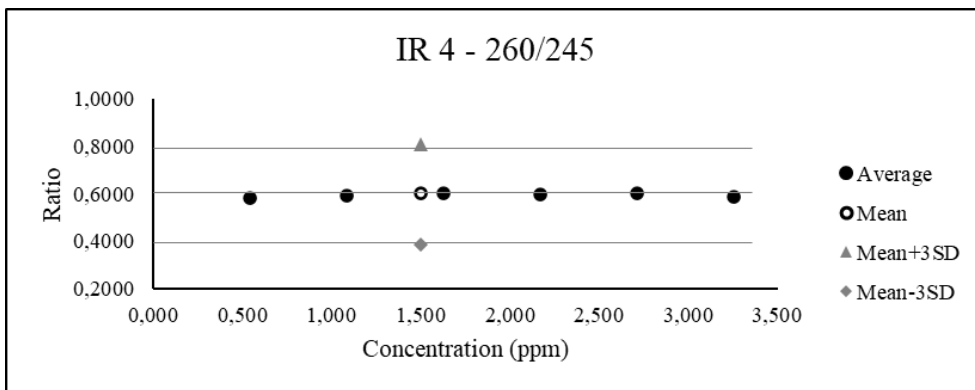
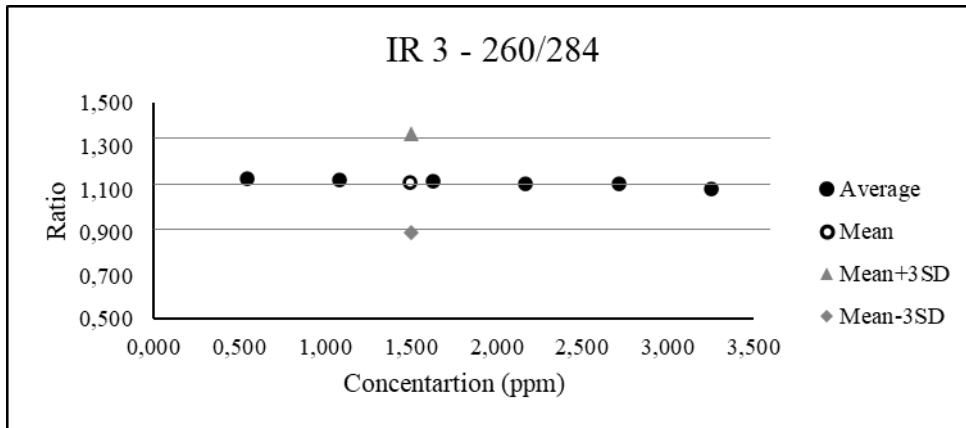
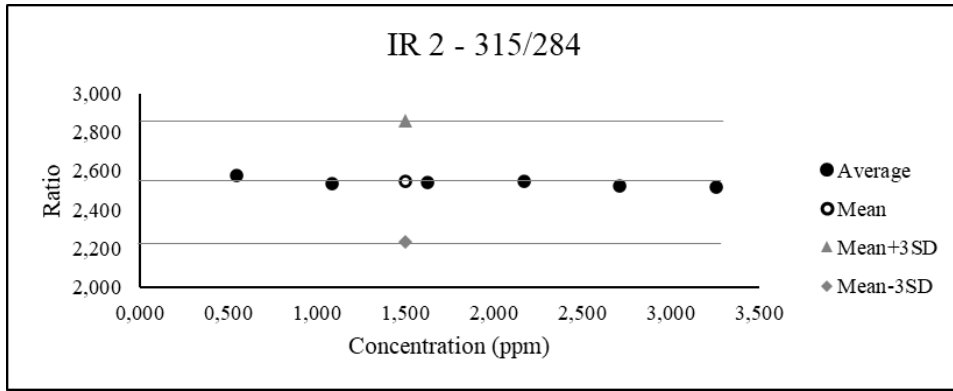


Figure II-26. The distribution of ion ratios (IR 1 to 5) over the concentration range of the analytical model. The mean was calculated for the ion ratios at 2.17 ppm.

In each plot of the ion ratios over concentration, the measured ratios are randomly distributed around the mean ratio, calculated at 2.17 ppm. Based on the visual inspection of the data there is no significant difference between the ratios measured for the respective ion ratio definitions and the mean of each ion ratio at 2.17 ppm with $\alpha = 0.003$. The ion ratios, therefore, do not deviate significantly from the control value within the analytical range.

Further inspection to determine a possible point where the deviation becomes significant was done through the analysis of the lower concentrations of buphanidrine (**1**) (0.0181, 0.0904 and 0.181 ppm). To determine whether the vector of measured ion ratios for these concentrations, differ significantly from the mean vector at 2.17 ppm, Hotelling's T^2 -test was performed for each significance test.

In Hotelling's T^2 -test, the number of measurements to determine the control value at 2.17 ppm was six – three batches each measured in duplicate. The number of variables was counted as five. The critical F-value was then calculated for five degrees of freedom in the numerator and one degree of freedom in the denominator at $\alpha = 0.003$. H_0 was defined as: $x_0 = \bar{m}$, and H_1 as: $x_0 \neq \bar{m}$. The results are summarised in **Table II-21**.

Table II-21. Results from performing Hotelling's T^2 -test on ion ratios measured for low concentrations of buphanidrine (**1**) in urine.

ppm	T^2	F-stat	F(5, 1, $\alpha = 0.003$)	Accept or reject H_0
0.0181	44025	1761.0	0.035	Reject
0.0904	277.69	11.108	0.035	Reject
0.181	1252.8	50.111	0.035	Reject

The results from Hotelling's T^2 -test show that, at the 99.7% confidence level, concentrations of buphanidrine (**1**) less than or equal to 0.181 ppm, produce mass spectra with ion ratios that differ significantly from the control at 2.17 ppm. This fixed an experimentally determined limit of detection between 0.542 and 0.181 ppm, which is significantly different from the calculated limit of detection in urine, which was 0.0647 ppm with a standard deviation of 0.2068 ppm.

Repeatability of ion ratios between batches

Ideally the ion ratios measured from the mass spectra at a concentration of 2.17 ppm buphanidrine, should not differ significantly between batches of samples. Therefore, the variation in the ratios between the batches should not be significantly greater than that produced

by random variation. To evaluate the contribution of between-batch variation in the ion ratios, multivariate analysis of variance (MANOVA) was performed at the 2.17 ppm level. Replication was included in the analysis since each batch was analysed in duplicate.

The MANOVA-analysis was performed on the ion ratios using IBM®'s SPSS® Statistics package (Version 26). The analysis calculated a Wilks' lambda (Λ) value of 0.000011 corresponding to an F-value of 99.72, which is less than the critical F-value (F(6,2)) of 332.67, determined at the 99.7% confidence level. The hypothesis, that the between-batch variation is accounted for by random variation, is accepted.

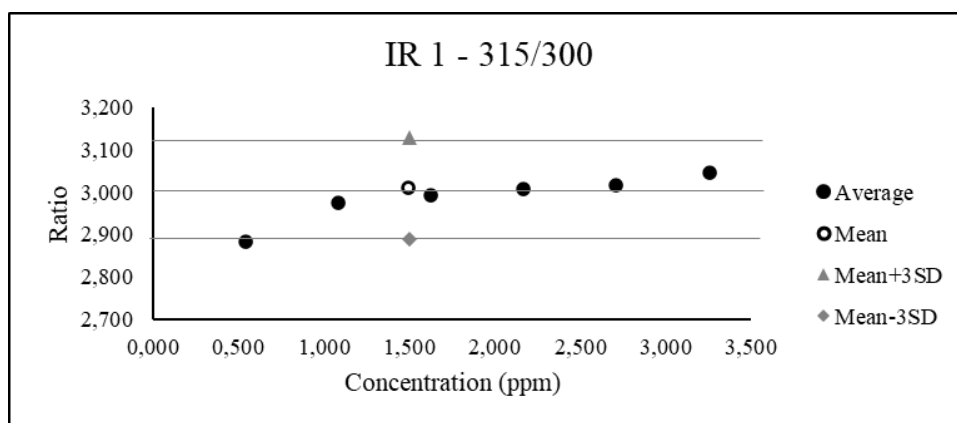
3.4.2 De-ionised aqueous samples

Trends in ion ratios with a change in concentration

To determine the effect of the concentration of buphanidrine (**1**) spiked into de-ionised aqueous samples on the individual ion ratios (**Table II-20**), the mean measured ion ratios from the individual batches were determined for each concentration. These measured ratios were compared to the mean ratios calculated from the three batches, each analysed in duplicate, at the 2.17 ppm concentration level. A deviation from this mean by the measured ratios was deemed significant if it fell outside the 99.7% confidence interval around the mean value. The mean and its 99.7% confidence interval are given by:

$$\bar{m} = \begin{bmatrix} 3.009 \\ 2.5786 \\ 1.1854 \\ 0.52679 \\ 2.1753 \end{bmatrix} \text{ with } \bar{s} = \begin{bmatrix} 0.0402 \\ 0.0415 \\ 0.0075 \\ 0.00541 \\ 0.0317 \end{bmatrix}$$

By plotting the measured ratios against concentration (**Figure II-27**), the deviations from the mean values can be visually inspected.



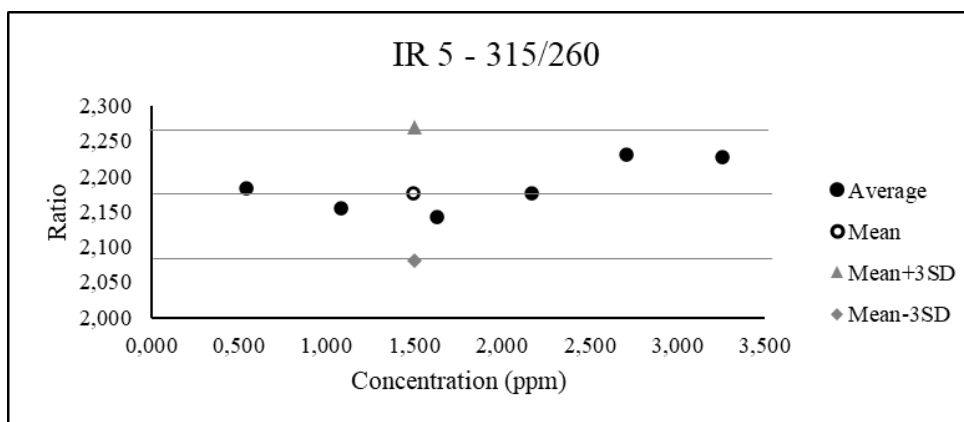
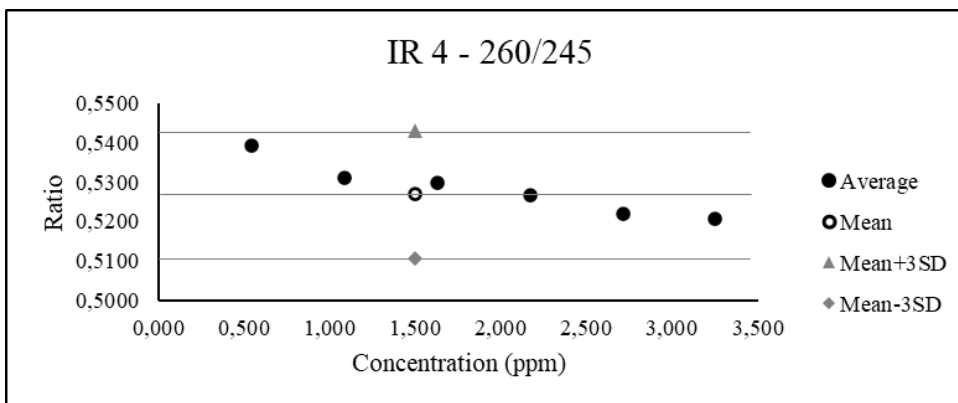
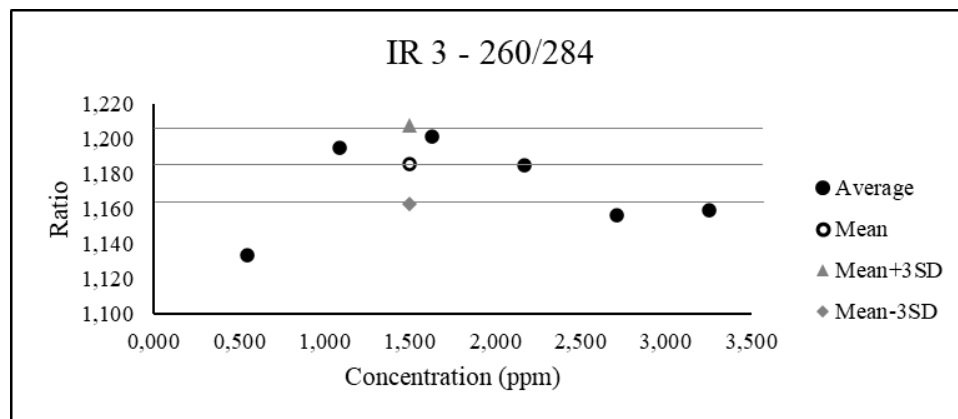
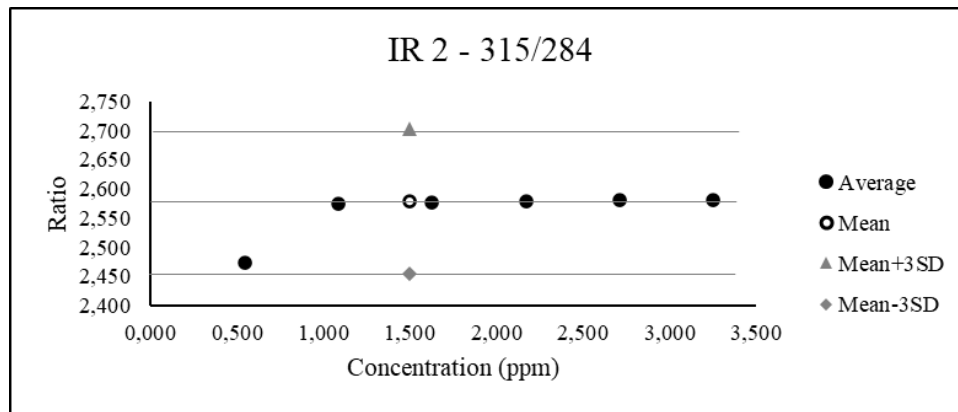


Figure II-27. Distribution of ion ratios about the corresponding control values, calculated at 2.17 ppm.

In the IR 1 graph, the ratios follow a shallow positive gradient with increasing concentration, however, the trend contains a plateau region between 1.08 and 2.71 ppm. The ratios mostly lie within the 99.7% confidence interval about the mean ($y = 3.009 \pm 0.040$). In the IR 2 graph a similar trend to that in IR 1 is observed, except that the plateau region does not have an upper limit within the analytical range. The recorded ratios all lie within the 99.7% confidence interval of the calculated control value ($y = 2.579 \pm 0.042$). These plateau regions are of great importance in the identification, of the target analyte, since it provides a range of higher precision in identification, with less risk of a false positive or a false negative identification.

The distribution of measured ratios for IR 3 falls outside the 99.7% confidence interval ($y = 1.185 \pm 0.023$). At 0.542, 2.71 and 3.25 ppm the measured ion ratios lie below the lower confidence limit. These significant deviations place upper and lower limits on the range where buphanidrine (**1**) can be positively identified by its ion ratios. Based on the distribution for IR 3, the analytical range is effectively limited between 1.08 ppm and 2.17 ppm. The lower detection limit of 1.08 ppm is significantly greater than the calculated limit of 0.0647 ppm.

The recorded ratios for IR 4 all lie within the 99.7% confidence interval around the calculated control value ($y = 0.527 \pm 0.016$). The ratios follow a negative gradient with an increase in concentration. The clear trend in the measured ratios could be utilised in determining a limit of detection based on IR 4. This limit could be compared to the limit experimentally observed in IR 3. For IR 5 the recorded ratios are more randomly distributed around the calculated control and are encompassed by the 99.7% confidence interval limits ($y = 2.175 \pm 0.095$).

Between-batch repeatability of the ion ratios

As was done for the spiked urine samples, the ion ratios were analysed by MANOVA to determine the significance of the between-batch variation in the total variance between the ratios at a 2.17 ppm concentration of buphanidrine (**1**). The analysis was performed using the IBM® SPSS® Statistical analysis software suite. Wilks' lambda (Λ) was calculated to be 0.028, corresponding to an F-value of 1.667. This F-value is less than the critical F-value ($F(6,2) = 332.666$) for $\alpha = 0.003$. This implies the variation between the batches can be explained by random variation, therefore the ratios are not expected to differ significantly between the batches.

3.4.3 Calculation of a limit of detection from the ion ratios

A theoretical limit of detection, for the urine samples, is proposed based on the relationship between the individual ion ratios and the concentration. By analysing the regression of the measured ratios on the concentrations in the analytical range, a relationship between the individual ratios and the concentrations was determined. The figures of merit for each response model, assuming a linear trend, is summarised in **Table II-22**.

Table II-22. Figures of merit for the evaluation of linearity in the ion ratios regressed on the concentration of buphanidrine in urine.

	r^2	Slope (b)	s_b	Intercept (a)	s_a	$S_{y/x}$
IR1	0.575	-0.0267	0.0115	2.9154	0.0243	0.0261
IR2	0.697	-0.0180	0.00594	2.5734	0.0125	0.0135
IR3	0.861	-0.0153	0.00308	1.15982	0.00651	0.00700
IR4	0.0904	0.00217	0.00343	0.59092	0.00725	0.00779
IR5	0.368	0.0137	0.00896	2.2264	0.0189	0.0203

The figures of merit, calculated in **Table II-22**, show that most of the ion ratios *do not* correlate closely with the calculated linear best fit lines associated with them. Ion ratio 3 was the closest to a significant correlation at the 99.7% confidence level. At the 95.4% confidence level, both ion ratios 2 and 3 significantly correlate to the associated linear best fit lines.

An example of the proposed calculated limit of detection in the bivariate case, for $\alpha = 0.046$

For positive identification of detected buphanidrine, *all* five the ion ratios must lie within the 99.7% confidence limits around the mean ratios calculated at the central concentration in the analytical range, 2.17 ppm. An estimation of the concentration where one of the measured ion ratios reaches either the upper or the lower limit, can be obtained by extrapolation of the linear models to the ratio limits. The highest limit should be used as theoretical lower limit of detection. For the upper limit of detection, the lowest concentration level should be reported.

The results for the upper and lower limits of detection are given in **Table II-23** and **Table II-24**.

Table II-23. Calculated upper limits of detection for buphanidrine, in urine samples, based on ion ratios 2 and 3.

Ion ratio	LOD _y	LOD _x (ppm)	s _{x₀} (ppm)
IR 2	2.4736069	5.5428	1.4487
IR 3	1.0803890	5.1771	0.8230

Table II- 24. Lower limits of detection for buphanidrine in urine samples, calculated from ion ratios 2 and 3.

Ion ratio	LOD _y	LOD _x (ppm)	s _{x₀} (ppm)
IR 2	2.60482224	-1.7478	1.4487
IR 3	1.18102534	-1.3820	1.1242

The shallow gradients of the response models for ion ratios 2 and 3 prevent the linear trend from passing through the upper confidence limits of the ion ratios before intercepting the y-axis. However, it was observed earlier that at 0.0181 ppm, there existed a significant difference between the measured ion ratios and the control value at the 99.7% confidence level. Closer examination showed both ion ratios 2 and 4 were significantly different from the control values at $\alpha = 0.003$. This sudden deviation from the linear trend in ion ratio 2 suggests a more instantaneous change in the ion ratios, rather than a steady change along a linear trend.

Regarding the upper limit of detection (**Table II-23**), the regression line intercepts the lower confidence limits of the centroid outside the calibration range. The lowest concentration at which the intercept with the limit is expected, is 5.1771 ppm with a standard deviation of 0.8230 ppm.

4. Conclusion to Chapter II

In the absence of reference material from commercial suppliers, buphanidrine (**1**) was isolated from plant material in sufficient quantities to develop and partially validate a quantitative method for its detection in urine samples. Buphanidrine was isolated with a 90.37657% purity from the plant material of *B. disticha*. Its identity was confirmed by 1D- and 2D-NMR-spectroscopy, UPLC-qTOF-MS accurate mass analysis in the positive ionisation mode (with a 1.3 ppm mass difference) and by GC-MS where its 70 eV EI-mass spectrum was compared to the reference spectrum in the Wiley-NIST Registry.²⁵

The isolated buphanidrine (**1**) sample was then employed in the development of a quantitative method for its detection in human urine. A response model was calculated from the average relative responses, measured at each concentration in the calibration range. This response model had a heteroscedastic distribution of variance over the concentration range, wherein the variance decreased with an increase in concentration.

To identify buphanidrine in the selected ion mode in the GC-MS analysis, the ion ratios in its SIM-mass spectrum were evaluated. In urine, the centroid vector for buphanidrine's (**1**) ion ratios was determined at the 99.7% confidence level as:

$$\bar{m} = \begin{bmatrix} 2.8683 \\ 2.5465 \\ 1.1285 \\ 0.59884 \\ 2.2602 \end{bmatrix} \text{ with } 3 \times \bar{s} = \begin{bmatrix} 0.1206 \\ 0.1246 \\ 0.0226 \\ 0.01624 \\ 0.0951 \end{bmatrix}$$

By comparing the ion ratios at the different concentration levels to this confidence interval, an experimentally determined limit of detection was obtained. When calculated conventionally from the standard deviation of the blank signal, the detection limit was 0.0647 ppm with a standard deviation of 0.2068 ppm. Based on the evaluation of the ion ratios for spiked urine samples, the limit observed was between 0.542 and 0.181 ppm. In this case there was no significant difference between the observed limit of detection and the theoretical limit of detection at the 99.7% confidence level.

References

- (1) Neuwinger, H. D. 1996. Boöphone disticha (Linne f.) Herbert. *African Ethnobotany - Poisons and Drugs*. Weinheim: Chapman & Hall GmbH, pp. 10-16.
- (2) Hutchings, A., Scott, A. H., Lewis, G. & Cunningham, A. B. 1996. Boophane disticha (L. f.) Herb. *Zulu Medicinal Plants - An Inventory*. South Africa: University of Natal Press, pp. 49-50.
- (3) Du Plooy, W. J., Swart, L. & Van Huysteen, G. W. 2001. Poisoning with Boophane disticha: a forensic case. *Human & experimental toxicology*, 20, 277-278.
- (4) Van Wyk, B.-E. & Gericke, N. 2018. Mind & Mood Plants. *People's Plants - A guide to useful plants of southern Africa*. 2nd ed. Pretoria: Briza Publications, pp. 185-213.
- (5) Gadaga, L. L., Tagwireyi, D., Dzangare, J. & Nhachi, C. F. 2011. Acute oral toxicity and neurobehavioural toxicological effects of hydroethanolic extract of Boophane disticha in rats. *Human & experimental toxicology*, 30, 972-980.
- (6) Laing, R. 1979. Three cases of poisoning by Boophane disticha. *Central African Journal of Medicine*, 25, 265-266.

- (7) Nair, J. J. & Van Staden, J. 2014. Traditional usage, phytochemistry and pharmacology of the South African medicinal plant *Boophone disticha* (Lf) Herb.(Amaryllidaceae). *Journal of Ethnopharmacology*, 151, 12-26.
- (8) Van Wyk, B.-E., Van Oudtshoorn, B. & Gericke, N. 2017. *Boophone disticha*. *Medicinal Plants of South Africa*. Pretoria: Briza Publications, pp. 66-67.
- (9) Bastida, J., Berkov, S., Torras Claveria, L., Pigni, N. B., Andrade, J. P. D., Martínez, V., Codina Mahrer, C. & Viladomat Meya, F. 2011. Chemical and biological aspects of Amaryllidaceae alkaloids. *Recent Advances in Pharmaceutical Sciences, 2011, Chapter 3, p. 65-100*. Editor: Diego Muñoz-Torrero.
- (10) Neergaard, J. S., Andersen, J., Pedersen, M. E., Stafford, G. I., Van Staden, J. & Jäger, A. K. 2009. Alkaloids from *Boophone disticha* with affinity to the serotonin transporter. *South African journal of botany*, 75, 371-374.
- (11) Cheesman, L. 2013. *Micropropagation and pharmacological evaluation of Boophone disticha*. PhD, University of KwaZulu-Natal,
- (12) Nair, J., Manning, J. & Van Staden, J. 2012. Distichamine, a chemotaxonomic marker for the genus *Boophone* Herb.(Amaryllidaceae). *South African journal of botany*, 83, 89-91.
- (13) Hauth, H. & Stauffacher, D. 1961. Die Alkaloide von *Buphane disticha* (L. f.) Herb. 2. Mitteilung über Amaryllidaceen-Alkaloide. *Helvetica Chimica Acta*, 44, 491-502.
- (14) Steenkamp, P. 2005. *Chemical analysis of medicinal and poisonous plants of forensic importance in South Africa*. PhD Thesis, University of Johannesburg, Johannesburg.
- (15) Botha, C. & Penrith, M.-L. 2008. Poisonous plants of veterinary and human importance in southern Africa. *Journal of Ethnopharmacology*, 119, 549-558.
- (16) Hutchings, A. & Terblanche, S. 1989. Observations on the use of some known and suspected toxic Liliiflorae in Zulu and Xhosa medicine. *South African Medical Journal*, 75, 62-69.
- (17) Tallini, L., Andrade, J., Kaiser, M., Viladomat, F., Nair, J., Zuanazzi, J. & Bastida, J. 2017. Alkaloid constituents of the Amaryllidaceae plant *Amaryllis belladonna* L. *Molecules*, 22, 1437.
- (18) Wooding, M., Bradfield, J., Maharaj, V., Koot, D., Wadley, L., Prinsloo, L. & Lombard, M. 2017. Potential for identifying plant-based toxins on San hunter-gatherer arrowheads. *South African Journal of Science*, 113, 1-10.
- (19) Munier, R. 1953. Separation of alkaloids from their N-oxides by paper chromatography. *Bulletin de la Societe de chimie biologique*, 35, 1225-1231.
- (20) Boloko, T. M. 2007. *The use of high performance liquid chromatography for the analysis of medicinal plants*. MSc Dissertation, University of Pretoria, Pretoria.
- (21) 2007. Dictionary of Natural Products. Boca Raton: Chapman and Hall/CRC.
- (22) 2020. ChemSpider. Raleigh: Royal Society of Science.
- (23) 2020. PubChem. Bethesda: National Center for Biotechnology Information.
- (24) European Commission: Directorate General for Health and Food Safety. 2017. *SANTE/11945/2015: Guidance document on analytical quality control and method validation*

procedures for pesticides residues analysis in food and feed. European Commission: Directorate General for Health and Food Safety. Available: https://ec.europa.eu/food/sites/food/files/plant/docs/pesticides_mrl_guidelines_wrkdoc_2017-11813.pdf [Accessed 2020-08-26].

- (25) 2017. Wiley Registry/NIST Mass Spectral Library. *In*: Wiley-Nist (ed.) 11 ed.: John Wiley & Sons, Inc.
- (26) Smith, J. G. 2017. Nuclear Magnetic Resonance Spectroscopy. *In*: Timp, T., Pellerito, A. & Murdzek, J. (eds.) *Organic Chemistry*. 5th ed. New York: The McGraw-Hill Companies Inc., pp. 527-569.
- (27) Center for Drug Evaluation and Research. 1996. *Guidance for Industry - Q2B Validation of Analytical Procedures: Methodology*. Rockville: Center for Drug Evaluation and Research. Available: https://ec.europa.eu/food/sites/food/files/plant/docs/pesticides_mrl_guidelines_wrkdoc_2017-11813.pdf [Accessed 2020-08-26].
- (28) Rivera, C. & Rodríguez, R. 2014. Horwitz equation as quality benchmark in ISO/IEC 17025 testing laboratory. *Private communication*.

Chapter III

Gloriosa superba L.

1. Background and information

1.1 Medicinal applications of *Gloriosa superba*

As one of only a few natural sources of the antigout medication colchicine (**Figure III-1 (7)**), *G. superba* is well known and cultivated for the sourcing of colchicine (**7**).^{1,2} Its potent anti-inflammatory qualities attracted the attention of researchers in the search for treatments for the Novel Coronavirus Disease 2019 (COVID-19) and Zika-flavivirus.³⁻⁵ In South African ethnic pharmacology, however, it is better known for its applications in the treatment of fertility and reproductive problems.^{1,2,6-9} Outside South Africa, *G. superba* is also used by other African ethnic groups as far north as the Ivory Coast for treating various other ailments including malaria and leprosy.⁸⁻¹⁰ *G. superba* is also used in ethnic medicine in the Indian subcontinent.⁸

The consumption of plant material from *G. superba* with food, or as a decoction, carries great risk since colchicine (**7**) is a major chemical component of the plant material.¹¹ It is a potent neurotoxin with a narrow therapeutic range. Chronic exposure can also cause severe axonopathy.¹² Many cases of suicides and attempted suicides have been reported where the individual either consumed pharmaceutical drugs containing colchicine (**7**)¹³⁻¹⁶ or plant material from *G. superba*^{17,18} or *Colchicum autumnale*.¹⁹

G. superba has been used to treat animals for snakebites. When bitten, the animal is forced to inhale vapours produced from a stew of *G. superba* rhizomes.⁹

1.2 Known chemical constituents of *G. superba*

Primarily material from *G. superba* contains alkaloids, specifically colchicine (**7**) and other tropane alkaloids, such as gloriosine (**8**), deacetylcolchicine derivatives (**8**) and demethylcolchicines (**9**), (**10**) (see **Figure III-1**).^{9,20,21} A study performed by Ntahomvukiye et al.²² indicated that the juvenile leaves of *G. superba* are expected to contain the highest levels of colchicine (**7**) (2.36 %) as a percentage of dry mass, followed by the flowers (1.05-1.18%) and the rhizomes (0.66-0.92%).

The relative alkaloidal content of *G. superba* plant material differs based on the geographical location. Colchicine (**7**) remained the dominant tropane alkaloid in the *G. superba* rhizomes, followed by gloriosine (**8**) and 2- (**9**) or 3-demethylcolchicine (**10**).⁹ In one case, however, Merchant & Joshi²³ detected only β - (**12**) and γ -lumicolchicine (**13**) in rhizomes sourced from India.

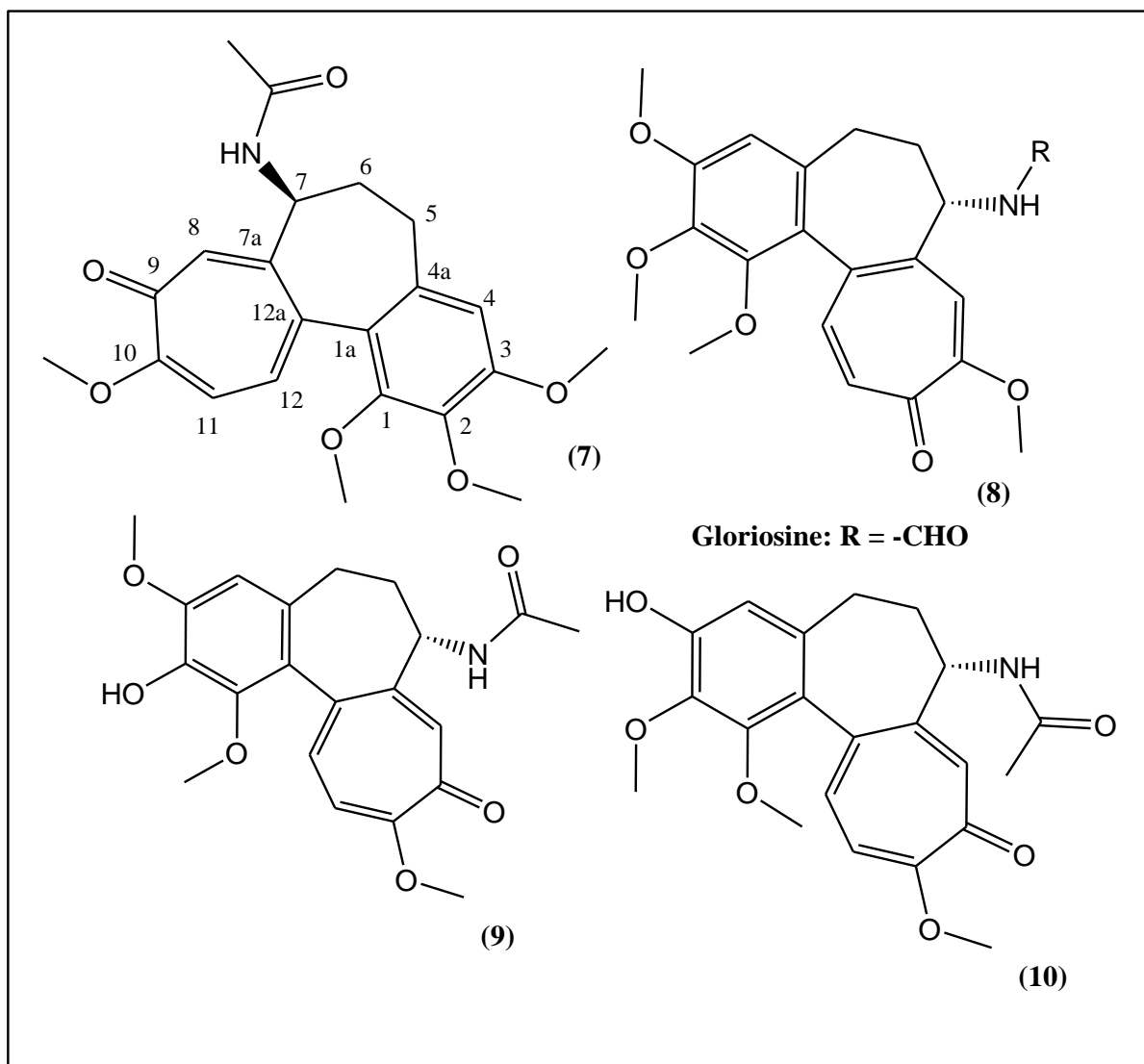


Figure III-1. Dominant chemical constituents of *G. superba* L. colchicine (7) (with indexed carbon skeleton), general structure for deacetylcolchicine (8), 2-demethylcolchicine (9), 3-demethylcolchicine (10).^{9,20,21,24}

Exposure of plant material to ultraviolet light induces almost complete photo-isomerisation of colchicine to a mixture of α -, β - and γ -lumicolchicines. Based on the results from Dvoráčková et al.,²⁵ β - and γ -lumicolchicines and various related derivatives are more abundant than α -lumicolchicine in *G. superba*. The photo-isomerisation proceeds via the intramolecular rearrangement of the tropone group to a four-membered ring fused to a five-membered ring. In addition to structural rearrangement, α -lumicolchicine is formed by dimerization of lumicolchicine via the newly formed five-membered rings.²⁶

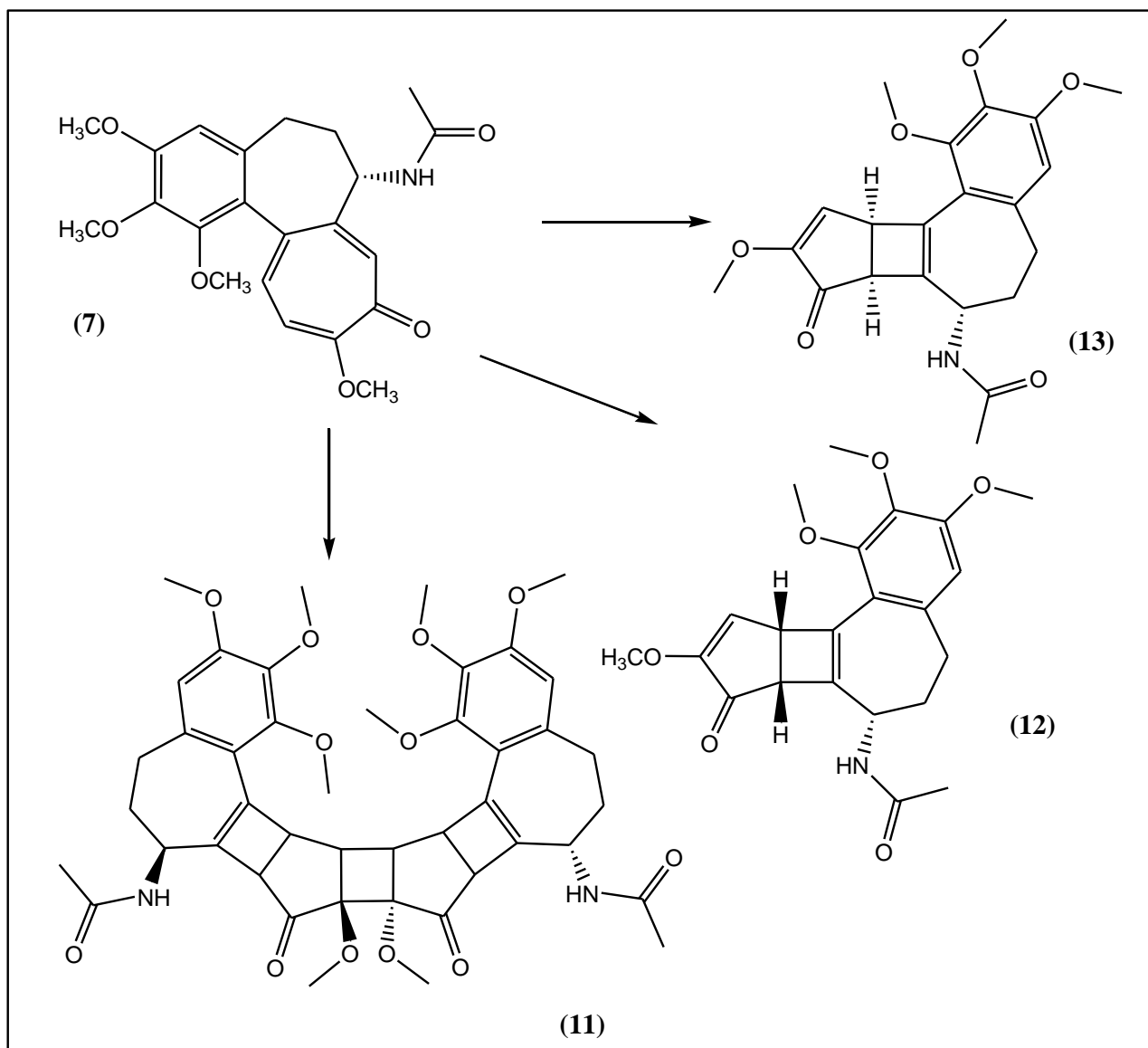


Figure III-2. Photo-isomerisation of colchicine (7) to lumicolchicines: α -lumicolchicine (11), β -lumicolchicine (12), γ -lumicolchicine (13).^{9,26-28}

1.3 Recorded cases of poisoning with colchicine and *G. superba*

In 2019, Gunasekaran et al.¹⁷ described a case of fatal overdose with colchicine (7) in a female patient who consumed rhizomes from *G. superba*. The symptoms the patient presented were typical of colchicine (7) poisoning – abdominal pains, nausea, and diarrhoea. After 12 h in hospital she developed respiratory distress. The patient succumbed to the effects of the toxin after eight days.¹⁷ According to Fernando & Fernando²⁹, the plant most often associated with poisoning cases in Sri Lanka is *G. superba*. They reported that 44% of plant poisoning cases were attributed to *G. superba*.²⁹

Milne & Meek¹⁵ studied a case of suicidal overdose with medicinal colchicine (**7**) tablets by a 21-year-old female patient in 1997. The patient presented with the typical symptoms of colchicine (**7**) poisoning. After eight days, the patient succumbed to asystolic cardiac arrest, not unlike the case of *G. superba* poisoning described by Gunasekaran et al.^{15,17}

A case of fatal poisoning with *G. superba* was described by Peranantham et al.¹⁸ in 2014, where a patient ingested between three and five rhizomes of *G. superba* to treat her abdominal pains. The patient presented with the following symptoms: nausea and vomiting, a burning sensation in the throat and numbness in the mouth. After two hours at hospital, she developed bloody diarrhoea and subsequent dehydration. After 30 h of hospitalisation, she succumbed to multiple organ failure and acute respiratory distress.¹⁸

1.4 Physiological effect

1.4.1 Relief of gout inflammation

The primary action of colchicine (**7**) is the halting of microtubule growth through depolymerisation of microtubules at high concentrations by binding to both α - and β -tubulin.^{12,30,31} By inhibiting the formation of microtubules, various cellular functions can be negatively impacted including mitosis and active organelle transport.^{32,33} In its treatment of gout, colchicine does not prevent the formation of the gout-inducing monosodium urate (MSU) crystals but inhibits the inflammatory response to its formation.³⁴ Formation of the MSU-crystals triggers the formation of the NLRP3-inflammasome complex, stimulating the release of pro-inflammation cytokines such as interleukin-1 (IL-1 β).^{30,33,34}

In the assembly of NLRP3-inflammasome, all the components must be in close vicinity of the endoplasmic reticulum where protein synthesis for exocytosis is performed by the ribosomes.³⁵ A component of the NLRP3-inflammasome complex is localised in the cell mitochondria, which must be transported in the retrograde along microtubules to the endoplasmic reticulum.³² colchicine (**7**) inhibits this transport by depolymerising microtubules and preventing its assembly. Therefore, the assembly and subsequent activation of NLRP3-inflammasome cannot take place.³⁰

Colchicine (**7**) also has prophylactic actions such as suppressing the expression of L-selectin on leukocytes activated in response to the detection of MSU-crystals. By inhibiting the binding of these leukocytes to the proximal endothelial cells, the storage of primed leukocytes that can respond to MSU-crystal precipitation, is inhibited. In this manner, chronic gout-inflammation

is suppressed. The same holds for the arrangement of E-selectin on the surface of the proximal endothelial cell membranes.^{30,33,34}

1.4.2 Neurotoxicity

Negative side-effects of colchicine (**7**) use can be observed in the nervous system. Its primary action of disrupting the structure of microtubules³³ has dire consequences in the structural and functional stability of axons. In patients with impaired kidney function, it primarily causes axonopathy in the peripheral nervous system (PNS) which is often accompanied by severe myopathy in the lower extremities.¹² Since the axons rely on microtubules for fast transport (400 mm/day) of organelles (such as mitochondria) and vesicles (containing neurotransmitters or chemical information from the synaptic cleft) in both the anterograde and the retrograde, they are hypersensitive to disturbances in these microtubule structures.³¹ The axon structure relies on the slow transport of the cytoskeleton and structural components, such as actin and clathrin, in the retrograde at a rate of 2-4 mm/day.¹²

When colchicine (**7**) enters the axons of neurons, they depolymerise these microtubules,^{30,34} leading to a loss in communication between the neuron cell body and the synaptic cleft at the axon terminal. The effect is felt once the final communication on the remaining microtubule components reaches their destinations. The effect, despite being a chemical cleavage, resembles that of a physical cleft of the axon. The terminal of the axon degenerates first, followed by the remainder of the disconnected axon.

If the axon is not regenerated, the neural function will not be restored. The axons most likely to be affected first by a colchicine (**7**) overdose are those with the greatest surface area, that is the longest peripheral axons. These are typically the axons associated with the motor neurons of the hands and feet. Initial symptoms of colchicine (**7**) toxicosis may precipitate as abnormal sensations (e.g. 'pins and needles') in the fingers, clumsiness and muscle weakness. It may be the case that some distal sensory loss may be permanent if the axonal damage is too severe, or if axonopathy of CNS-associated axons occurred.

1.4.3 Systemic toxicosis

As mentioned, the inhibition of microtubule synthesis can have various implications in various cells. Axonopathy can also have indirect effects on other organs connected to the PNS and CNS. A case study described by Clevenger et al.³⁶ lists hypotension, nervousness, delirium and drowsiness as symptoms observed in a 36-year-old female patient who ingested 30 mg

colchicine amongst other prescription medicines (Prolixin, Ativan and Cogentin). These prescription medicines could also have been the cause of the observed symptoms.³⁶

Colchicine (**7**) severely impacts the immune system when administered in exceedingly high doses. The systemic effect of its ability to depolymerise microtubules and inhibit the expression of L- and E-selectins to combat inflammation can result in an overall decrease in the levels of leukocytes.³³ The production of bone marrow is also suppressed by the action of colchicine (**7**).³⁰ These effects can leave an individual vulnerable to pathogens for several days, despite acting as a prophylaxis agent for inflammation.

Primary symptoms of colchicine (**7**) toxicosis is gastro-intestinal (GI) in character.³¹ The gastro-intestinal injury resulting from the inhibition of cell-division required by the rapid-turnover cells in the walls of the GI-tract stimulates sensory neurons in the abdominal region, producing nausea, diarrhoea and abdominal pain.^{33,37} Hypotension follows from the rapid onset of dehydration due to watery diarrhoea.³⁸

Cell-division is inhibited in the metaphase of mitosis, since the spindles of microtubules required for chromosomal division and cell cleavage cannot form effectively.³⁰ The injuries to the GI-tract could include vascular injuries of proximal capillaries which introduces blood into the digestive system.³³ This could contribute to the presence of blood in an intoxicated individual's urine and stool.

Mitotic inhibition also causes damage to liver tissue and tubules in the kidneys. The damaged kidneys not only introduce blood into the urine and stool of an intoxicated individual, but also leads to acute renal failure.³⁷ The inability of the kidneys to effectively remove toxins from the blood leads to a build-up of uremic toxins that can cause severe damage to the nervous system.³⁹

Colchicine (**7**) activates thrombocytes to cause disseminated intravascular coagulation and subsequent activation of fibrinolysis, to break down the newly formed blood clots.³⁰ This decreases the level of thrombocytes in the blood, inhibiting clotting of blood at sites of vascular injury, such as in the kidneys and GI-tract.³³

The axonopathy associated with colchicine (**7**) overdose is typically mild and slow regeneration of the axons may occur. Ascending paralysis has been observed in both central and peripheral NS and may lead to respiratory distress and hyperventilation.³¹ The acute dehydration, resulting from diarrhoea, combined with the systemic development of myoneuropathy, muscle weakness

and intravascular coagulation decreasing cardiac output can cause the body to enter a state of shock, comatose, or even cardiac arrest.³¹

1.5 The metabolic pathway of colchicine

Colchicine (**7**) typically undergoes hepatic metabolism catalysed by the cytochrome-P450 (3A4) complex, which is responsible for most of the hepatic metabolism of xenobiotics. Colchicine and its metabolites readily undergo enterohepatic circulation, which re-introduces unmetabolized colchicine to the blood stream and allows for multiple metabolic steps to be performed.^{40,41}

In an extensive study, Xu et al.⁴² determined the primary metabolites of colchicine (**7**) for both phase I and phase II pathways *in vivo* in rat bile.⁴² Hepatic metabolism of colchicine involves deacetylation to a small extent, likely followed by glucuronidation to give the *N*-glucuronide derivative of deacetylcolchicine (**18**) (**Figure III-3**).⁴³

However, this is not the main pathway of metabolic transformation.⁴³ The study performed by Xu, et al. shows colchicine is readily demethylated to produce 2-, 3- and 10-*O*-demethylcolchicine ((**9**), (**10**), (**14**)), followed by sulphation (**17**) and glucuronidation (**16**).^{42,44} Xu et al.⁴² found that 2- (**9**) and 3-demethylcolchicine (**10**) both undergo these conjugation reactions. However, 2-demethylcolchicine (**9**) prefers the pathway of glucuronidation (**16**) and 3-demethylcolchicine (**10**) prefers the metabolic pathway of sulphation (**17**).⁴² The major metabolic pathways of colchicine (**7**) are illustrated in **Figure III-3**.

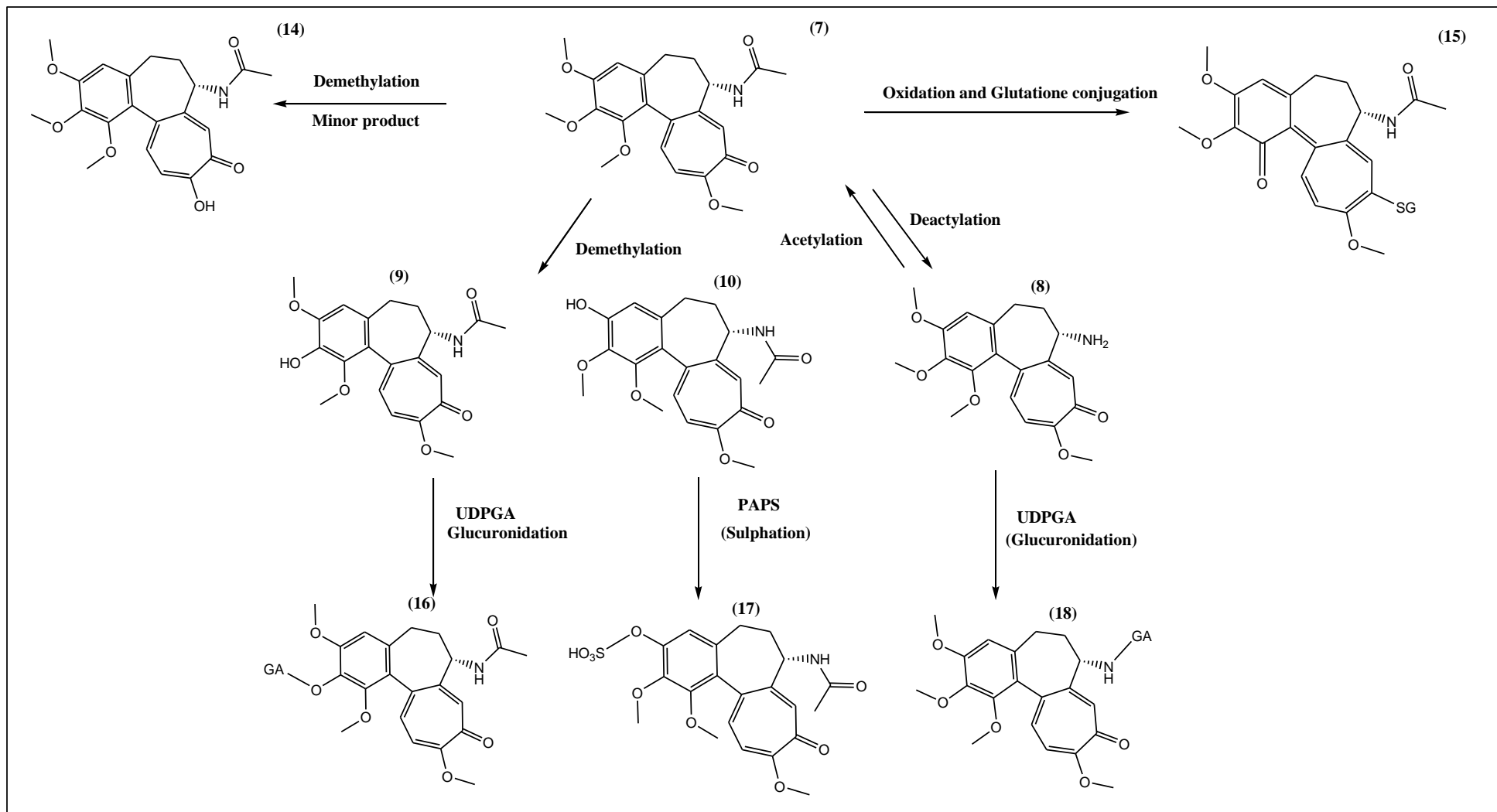


Figure III-3. Major hepatic metabolic pathways of colchicine.^{42,44}

1.6 Methods cited in literature for the detection of colchicine

The analysis of physiological samples in screening for the presence and amount of colchicine (7), is an important part of monitoring its application in chronic gout therapy. Most of the analytical methods in literature utilise LC-MS methods for the analysis of colchicine in physiological samples.^{13,45-48}

In 2019 Theofel et al.⁴⁷ performed a study where the performance of LC-qTOF and GC-MS, in the quantification of colchicine (7) in urine were compared. The LC-qTOF method used was capable of detecting colchicine (7) at the 0.56 µg/mL level. However, GC-MS was unable to positively identify colchicine (7) through comparison of the detected mass spectrum with those in a spectral library at this concentration level.⁴⁷

Schreiber et al.'s 2019 study⁴⁸ produced similar results to that of Theofel et al.⁴⁷, of the same year. In Schreiber et al.'s study⁴⁸ it was observed that for colchicine concentration levels less than 1 µg/mL, UPLC-qTOF MS analytical methods outperform the conventional GC-MS and HPLC-PDA methods for the qualitative analysis of blood samples.⁴⁸

Prior to these studies, in 2005 Miller et al.¹⁴ utilised GC-MS to quantify colchicine (7) in human plasma to a level of 6.1 ng/mL.¹⁴ Clevenger et al.³⁶ also utilised GC-MS for the identification of colchicine (7) in the physiological fluids of an individual who attempted to commit suicide by ingesting colchicine tablets.³⁶

2. Experimental

2.1 List of chemicals used for experimental work in this chapter

Chemical	% Purity	Company	City [†]
5- α -Cholestane	99.9 (HPLC)	Sigma Life Sciences	St. Louis, USA
Acetonitrile	99.9 (GC)	Sigma-Aldrich Chemie GmbH	Schnelldorf, DEU
Colchicine	99 (HPLC)	Sigma-Aldrich Chemie GmbH	Schnelldorf, DEU
De-ionised water	20. Ω .m [†]	Merck (Pty.) Ltd.	Modderfontein, ZA
Dichloromethane	\geq 99.8 (GC)	Merck KGaA	Darmstadt, DEU
Disodium hydrogen orthophosphate dihydrate	\geq 99.5 (A)*	Merck (Pty.) Ltd.	Modderfontein, ZA

Ethyl acetate	99.98 (GC)	Sigma-Aldrich Chemie GmbH	Schnelldorf, DEU
Hydrochloric acid	32.7	Sigma-Aldrich Chemie GmbH	Schnelldorf, DEU
Isopropanol	99.99 (GC)	Sigma-Aldrich Chemie GmbH	Schnelldorf, DEU
Methanol	99.98 (GC)	Sigma-Aldrich Chemie GmbH	Schnelldorf, DEU
Methanol	99.9	Radchem	Johannesburg, ZA
Methanol	>99.9	ROMIL via Microsep	Johannesburg, ZA
Sodium hydrogen carbonate	>99	Merck KGaA	Darmstadt, DEU
Sodium hydroxide	>99	Merck KGaA	Darmstadt, DEU

*Acidimetric assay via acid-base titration.

†Resistivity assay: A resistivity of ~18.5 Ω .m in water indicates the %-ionic content is near naught

Since colchicine (**7**) is readily available in high purity (HPLC-grade, $\geq 95\%$) from Sigma-Aldrich[®] and time was limited, it was deemed unnecessary to attempt to isolate colchicine (**7**) from the rhizomes of *G. superba* with high purity and in acceptable quantity. The use of plant material was limited to the development of a crude extract that was analysed via UPLC-qTOF MS and used for method development in the quantitative analysis of physiological fluid via GC-MS.

2.2 Preparation of a crude extract

Fresh rhizomes of *G. superba* was given by a community member in Brakpan, Gauteng. A whole plant was submitted as voucher specimen to the H.G.W.J. Schweickerdt Herbarium at the University of Pretoria for identification. The rhizomes were cut into small segments and dried in a laboratory oven for one week at 35 °C. The dried rhizomes were ground to a homogeneous powder (38.830 g) with a Labotec[®]-grinder. Extraction was accomplished by soaking the plant material in a de-ionised water-methanol (Radchem[®]) extraction solvent (400 mL, 1:1) for 24 hours with agitation.

Three repeat extractions were performed where the material was soaked in the extraction solvent for 24 h with vigorous stirring. Crude extracts were filtered through coarse filter paper and combined. The extract was subsequently dried in polytop-vials using Genevac-evaporators

(SP Scientific EZ-2 Plus[®]). Since a methanol-water solvent system was used, the extracts were dried using the pre-programmed HPLC-solvent method on the Genevac[®] instrument.

2.3 UPLC-qTOF MS analysis of the crude extract

For UPLC-analysis, dried crude extract (ca. 1 mg) was weighed into an Eppendorf-vial and dissolved in methanol (ROMIL[®] UpS[®] ultra lc-grade, 1.000 mL) with the aid of an ultrasonic cleaner. The sample was then centrifuged with a Baygene[®] Micro Centrifuge (BG-Qspin[™]), and the supernatant filtered into a GC-vial (2 mL). Filtration was done with Agilent Technologies' 13 mm Econofilters, containing a nylon membrane with a pore diameter of 0.2 µm.

For liquid chromatography, ROMIL[®] Ultra-pure Solvents[™], were modified with formic acid (Sigma-Aldrich[®], 0.1% v/v). Chromatography was performed with the same gradient solvent system employed for the analysis of extracts from *B. disticha* (Chapter II, Section 2.2.2, **Table III-1**).

Table III-1. Solvent gradient used for UPLC-qTOF MS analysis.

Time (min)	Flow rate (ml/min)	Percentage: dH₂O + 0.1% Formic acid	Percentage: MeOH + 0.1% Formic acid	Gradient type
Initial	0.300	97.0	3.0	Initial
0.10	0.300	97.0	3.0	Linear
14.00	0.300	0.0	100.0	Linear
16.00	0.300	0.0	100.0	Linear
16.50	0.300	97.0	3.0	Linear
20.00	0.300	97.0	3.0	Linear

Instrument settings for positive ion formation were the same as those used in the positive ion mode analysis of the crude extracts from *B. disticha* and those for buphanidrine (**5**) (Chapter II, Section 2.2.2). For positive ion mode detection, the LockSpray[®] standard (leucine-enkephalin) was applied directly to the ion source every ten seconds. Measured high resolution ion masses were corrected with respect to the [M+H]⁺-quasi-molecular ion mass of leucine-enkephalin (556.2771 Da).

The system and data analysis were managed by MassLynx[™] v4.1 software developed by the Waters Corporation[®].

2.4 GC-MS method and parameters for quantitative analysis of samples containing colchicine

2.4.1 Preparation of stock solutions

The colchicine stock solution was prepared by weighing colchicine crystals (**7**) (Sigma-Aldrich[®], 10.03 mg) into a 10.00 ± 0.04 mL volumetric flask and filling the flask to the calibrated mark with methanol (Sigma-Aldrich[®]). The resulting stock solution (1.003 mg/mL) was transferred to amber vials (2 mL) for storage at -26 °C. Before spiking into matrices, the standard was left on the bench to reach room temperature (~ 25 °C). Once in thermal equilibrium, the standard was diluted to half its concentration (0.5002 mg/mL) with methanol (Sigma-Aldrich[®]) and spiked into the sample matrices.

A stock solution of 5- α -cholestane was prepared with a similar process. 5- α -cholestane crystals (10.04 mg) were weighed into a 10.00 ± 0.04 mL volumetric flask. The flask was filled to the calibrated mark with ethyl acetate (Sigma-Aldrich[®]). After homogenisation of the solution by shaking, the stock solution was transferred into amber vials (2 mL) for storage.

2.4.2 Preparation of the bicarbonate buffer

For this method, an aqueous sodium bicarbonate buffer (0.1 M, pH ~ 8) was prepared by weighing NaHCO₃ (840.07 mg) into a beaker and dissolving it in de-ionised water (40 mL). The solution was quantitatively transferred to a 100.00 ± 0.10 mL volumetric flask. De-ionised water was added to the flask to the calibrated mark and homogenised by shaking.

2.4.3 Analysis of samples spiked with colchicine

Samples containing colchicine (**7**) were simulated by spiking a blank matrix (10.00 mL of de-ionised water or urine) with the appropriate volume of diluted colchicine (**7**) stock solution (0.5002 mg/L). For the evaluation of linearity, the samples were spiked to theoretical concentrations of 1.00, 1.500, 2.000, 2.500, 3.000 and 3.500 ppm (ppm = $\mu\text{g/mL}$), assuming 100% purity in the reference material and an original stock solution with a concentration of 1.000 mg/mL. Each sample was then spiked with an internal standard stock solution (1.004 mg/mL, 30.0 μL). The simulated samples were buffered to pH ~ 8 by addition of the sodium bicarbonate buffer (2.000 mL, 0.1 M, pH ~ 8) and aqueous sodium hydroxide (10.00 μL , 10 M). The samples were applied to prepared C18 BondElut SPE-cartridges (6 cc, 500 mg sorbent mass, 40 μm particle diameter).

2.4.4 Preparation of SPE-cartridges and analyte elution

Each SPE cartridge was prepared by first conditioning it with HPLC-grade methanol (Sigma-Aldrich[®], 4.00 mL), and then equilibrating it with de-ionised water (Merck[®], 8.00 mL). To equilibrate the cartridges to the sample pH, each cartridge was rinsed with sodium bicarbonate buffer (3.00 mL, 0.1 M, pH ~ 8). Solvent rinsing for conditioning and equilibrating was done with the aid of a vacuum to generate a negative pressure differential (5 "Hg = 17 kPa). The samples were then loaded on to their respective cartridges with the aid of a small vacuum (< 1 "Hg = 3.4 kPa). The cartridges were not allowed to run dry.

Once the samples were loaded, the cartridges were rinsed with the sodium bicarbonate buffer (4.00 mL, 0.1 M, pH ~ 8) and de-ionised water (Merck[®], 4.00 mL) with the aid of a negative pressure differential across the cartridge (5 "Hg). The cartridges were dried by aspirating air through the sorbent beds. The analytes were eluted with HPLC-grade ethyl acetate (Sigma-Aldrich[®], 4.00 mL), followed by HPLC-grade methanol (Sigma-Aldrich[®], 4.00 mL). The cartridges were left to run dry for circa three minutes. The combined eluate was dried in a heating block set to 40 °C under a stream of dried, compressed air.

2.4.5 Liquid-liquid extraction of colchicine and 5- α -cholestane

For the liquid-liquid extraction of the analytes, the volumes of the eluates were reduced to ~500 μ L. Each sample was then spiked with the sodium bicarbonate buffer (0.500 mL, 0.1 M, pH ~ 8), de-ionised water (Merck[®], 1.000 mL) and dichloromethane (Merck[®], 2.00 mL). The samples were vortex mixed and centrifuged at 3 500 rpm for 10 min. From these samples, the respective organic phases were extracted and transferred to the corresponding amber glass GC-vials (2 mL) and dried in a heating block at 40 °C under a stream of compressed, dry air. The extraction was repeated, and the organic extract added to the respective dried residues. These samples were again dried in the heating block.

2.4.6 GC-MS analysis of the prepared samples

To analyse the samples, each dried residue was reconstituted in HPLC-grade acetonitrile (Sigma-Aldrich[®], 40.0 μ L) and agitated with a vortex mixer. The samples were transferred to conical inserts, placed in vials, and analysed by GC-MS.

Samples were applied to the GC-MS system as 2 μ L injections of the reconstituted sample. Gas chromatographic separation of the analytes was achieved with a temperature program initiated at 180 °C and maintained for three minutes. The column temperature was ramped at 30 °C/min to 310 °C and maintained for three minutes.

Eluting analytes were analysed in the selected ion mode. For 5- α -cholestane (t_R = 2.50-7.00 min), the following ions were selected with 100 ms dwell times: m/z = 149.00, 217.00, 357.00, 372.00. The ions selected for colchicine (t_R = 7.00-10.33 min) were: m/z = 254.00, 281.00, 297.00, 340.00, 356.00, 371.00, 399.00.

3. Results and discussion

Prior to the extraction of the dried plant material, a voucher specimen was submitted to the H.G.W.J. Schweickerdt Herbarium of the University of Pretoria for identification. It was catalogued with the reference number PRU 126646.

3.1 UPLC-qTOF MS analysis of the crude extract

As can be seen from the UPLC-data in **Figure III-4** and **Table III-2**, the crude extract consists predominantly out of very polar to medium polar compounds. This can be attributed to the selectively high polarity of the extraction solvent system used. The constituents of the polar extract were tentatively identified by elemental composition and accurate mass analysis. As reference point the data in the Dictionary of Natural products was utilised.⁴⁹

The base peak ions, also the quasi-molecular ions, for Peaks 2 and 3 are nearly identical in measured accurate mass and calculated elemental composition. These are likely isomers of slightly different polarities that co-exist in the plant extract. Some of the possible tentative identities are given in **Table III-2**.

For tentative identification to hold, the recommended threshold of 5 ppm in mass difference, between the measured ion mass and the calculated mono-isotopic mass of the expected elemental composition, must not be exceeded. This threshold is recommended by the European Commission for Health and Food Safety⁵⁰ in their guidelines for the identification of analytes by accurate mass analysis. For each of the 5 identified peaks this threshold was not exceeded, however, it was matched in Peak 1.

According to the chromatogram recorded in the positive ionisation mode, at least six different compounds were extracted from the plant. The principal constituent of the crude extract was detected at 7.568 minutes (Peak 4 in **Figure III-4**). In this peak the base peak ion (also the quasi-molecular ion $[M+H]^+$) had an accurate m/z -ratio of 4.1773, with a calculated elemental composition of $C_{22}H_{26}NO_6^+$. The mono-isotopic mass of the calculated molecular formula was 400.1760 Da. This mono-isotopic mass differs from the measured mass by 3.2 ppm, producing a close match (55.54%, isotopic fit ratio = 421.4) between the calculated and measured accurate

masses and the calculated elemental composition. Therefore, the neutral analyte species of Peak 4 in **Figure III-4** is tentatively identified by the molecular formula of colchicine (**7**).

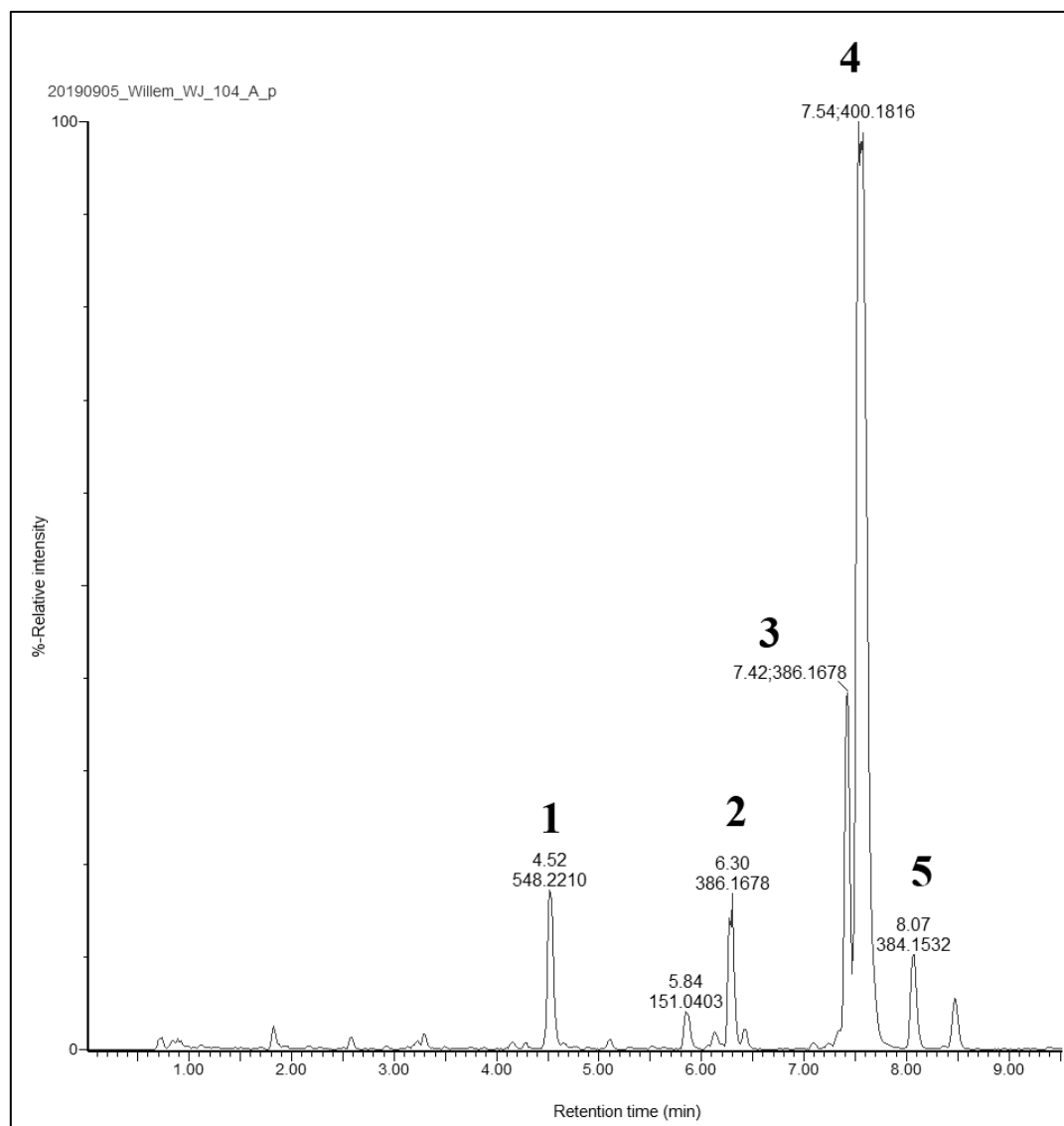


Figure III-4. ESI (+)-chromatogram detected for the crude extract (water-MeOH) of *G. superba* via UPLC-qTOF MS.

A notable observation is the predominant presence of colchicine-type alkaloids in this polar extract from *G. superba*. As expected, Peak 4, tentatively identified as colchicine (**7**), is present in the greatest abundance. Most of the other alkaloids in the extract are closely related to colchicine (**7**) in terms of structure. The alkaloid cornigerine (Peak 5) is a known compound present in *Colchicum autumnale*, the original source of colchicine in Europe. Its suspected presence in *G. superba* shows the similarity between the plants in the production of secondary metabolites.

Table III-2. Compounds detected in the crude extract of *G. superba*.

Peak no.	t _R (min)	m/z ([M+H] ⁺)	Calculated accurate mass (Da)	Formula	Theoretical monoisotopic mass (Da)	Tentative identification(s)
1	4.526	548.2144	547.2071	C ₂₇ H ₃₃ NO ₁₁	547.2054	1'-Epicolchicoside Colchicoside
2	6.290	386.1607	385.1534	C ₂₁ H ₂₃ NO ₆	385.1525	2-Demethylcolchicine
3	7.398	386.1607	385.1534	C ₂₁ H ₂₃ NO ₆	385.1525	3-Demethylcolchicine N-Deacetyl-N-formylcolchicine N-Deacetyl-N-formyl-β-lumicolchicine 2-O-Demethyl-β-lumicolchicine 3-O-Demethyl-β-lumicolchicine N-Deacetyl-N-formyl-γ-lumicolchicine 2-O-Demethyl-γ-lumicolchicine
4	7.568	400.1773	399.1700	C ₂₂ H ₂₅ NO ₆	399.1682	(-)-Colchicine
5	8.067	384.1446	383.1373	C ₂₁ H ₂₁ NO ₆	383.1369	Cornigerine

To confirm the identity of Peak 4 as colchicine (**7**), the detected accurate mass and relative retention time of Peak 4 was compared to the characteristics of the chromatographic peak produced by a certified reference standard of colchicine (**7**). The samples were both analysed in the positive ESI-mode.

To determine the relative retention time, a peak, present in the background of both samples, at a retention time of 15 min was used as reference point. In the crude extract the relative retention time was -7.5 min (w.r.t. m/z = 338.3469 at 15.04 min). The relative retention time of colchicine (**7**) in the chromatogram (PIM), of the reference standard, was -7.1 min. The closely spaced relative retention times of the tentatively identified peak in the crude extract, and the chromatographic peak of the certified reference material, supports the tentative identification of peak 4, in **Figure III-4**, as colchicine (**7**).

The detected quasi-molecular ion, [M+H]⁺, in the chromatographic peak of the reference standard had an accurate mass of 400.1758 Da. Comparing this accurate mass to the mass measured for the tentatively identified quasi-molecular ion in Peak 4 of **Figure III-4**, as shown in **Figure III-5**, the resulting mass difference is 3.7 ppm. This differs from the detected mass in the crude by 3.7 ppm.

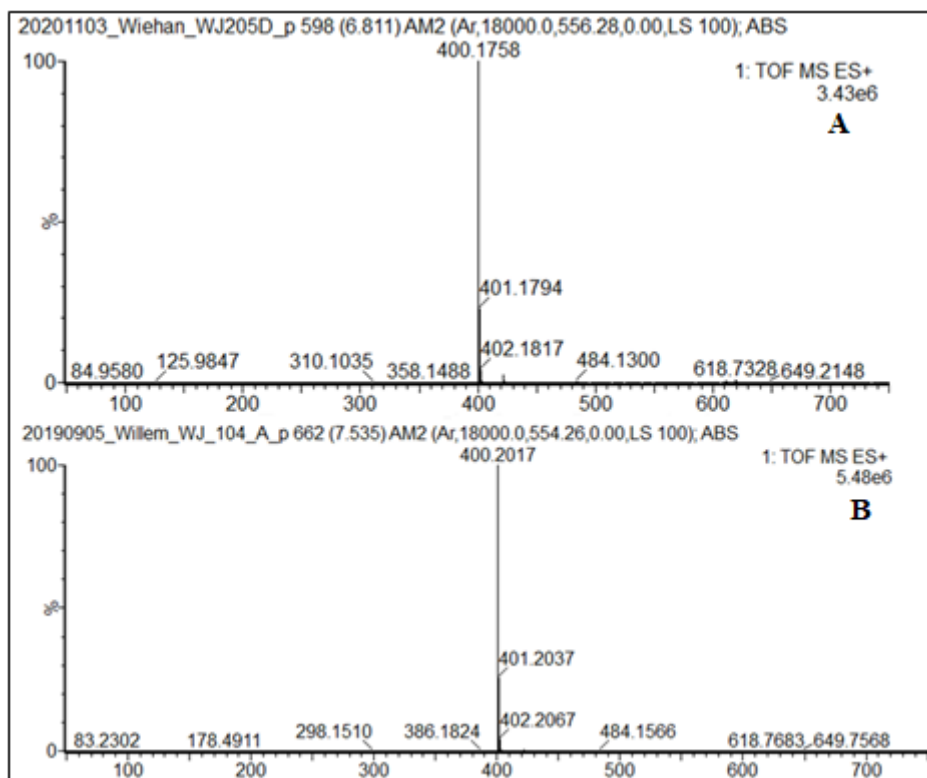


Figure III-5. A comparison of the first order ESI-mass spectra (positive ion mode) for colchicine (**7**) in the reference standard of colchicine (**7**) (A), and tentatively identified in the crude extract (B).

Following the recommendations for identification of analytes by accurate mass and elemental composition analysis, stipulated by the European Commission for Health and Food Safety⁵⁰, the second order mass spectrum of colchicine (**7**), in the certified reference standard, is compared to the second order mass spectrum of Peak 4 in **Figure III-4**, tentatively identified as colchicine (**7**). This comparison, in **Figure III-6**, shows the presence of the same fragments in both the reference standard (A) and Peak 4 of the crude extract (B).

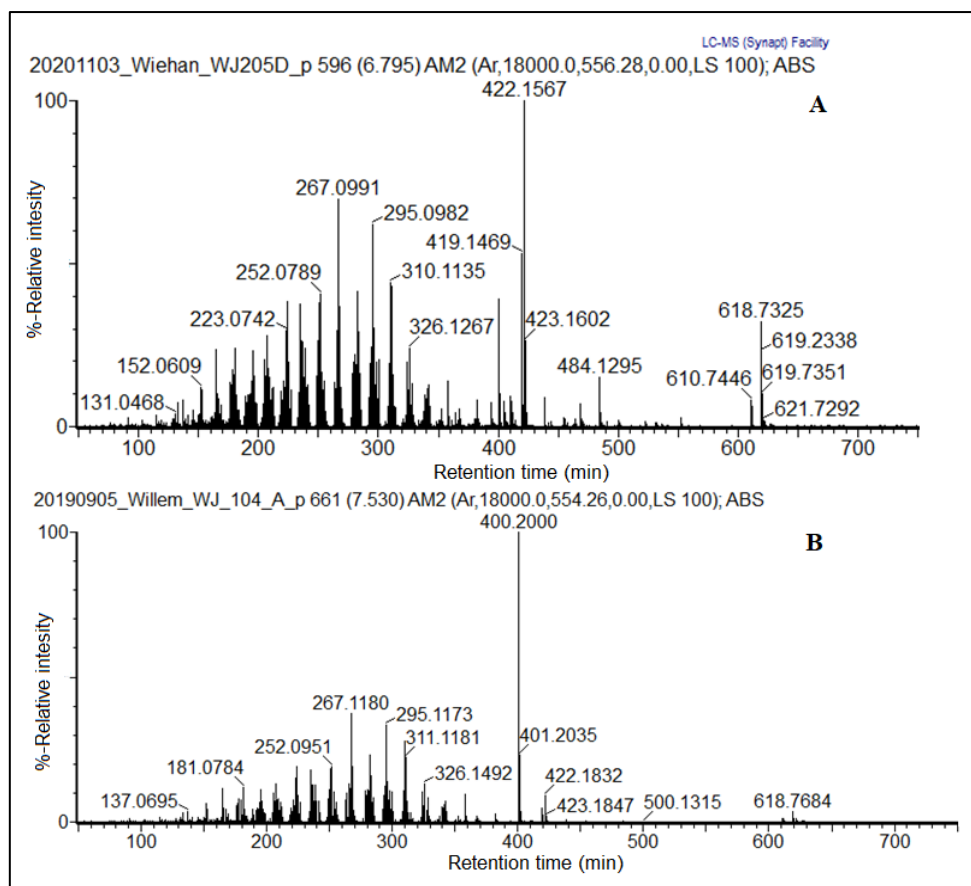


Figure III-6. Second order mass spectra of colchicine (**7**) in the certified reference standard (A), and tentatively identified in the crude extract (B).

3.2 Mass spectral analysis of colchicine

3.2.1 Electron impact-Mass spectrum

Under GC-MS conditions, colchicine (**7**) was detected as an underivatized analyte and positively identified by a comparison of its 70 eV-electron impact mass-spectrum (**Figure III-7**) to the NIST spectral library. From this mass-spectrum, the possible fragmentation events for colchicine (**7**) could be elucidated (**Figure III-8**). The signal for $m/z = 399$ corresponds to the nominal mass of underivatized colchicine (**7**). The fragment ion $m/z = 371$ (**19**) is produced when a neutral loss of 28 Da occurs. This could be caused by the loss of carbon monoxide or ethene (**21**).

To generate the base peak ion, $m/z = 312$, a simultaneous loss of the carbonyl group (in the tropone ring) and the NH_2COCH_3 -group occurs (**19**).⁵¹ With further loss of a methoxy group from the six-membered ring, the fragment with $m/z = 281$ is generated (**19**).⁵¹ Following the

loss of a methyl radical from the fragment $m/z = 312$, the fragment $m/z = 297$ (**20**) could be produced.

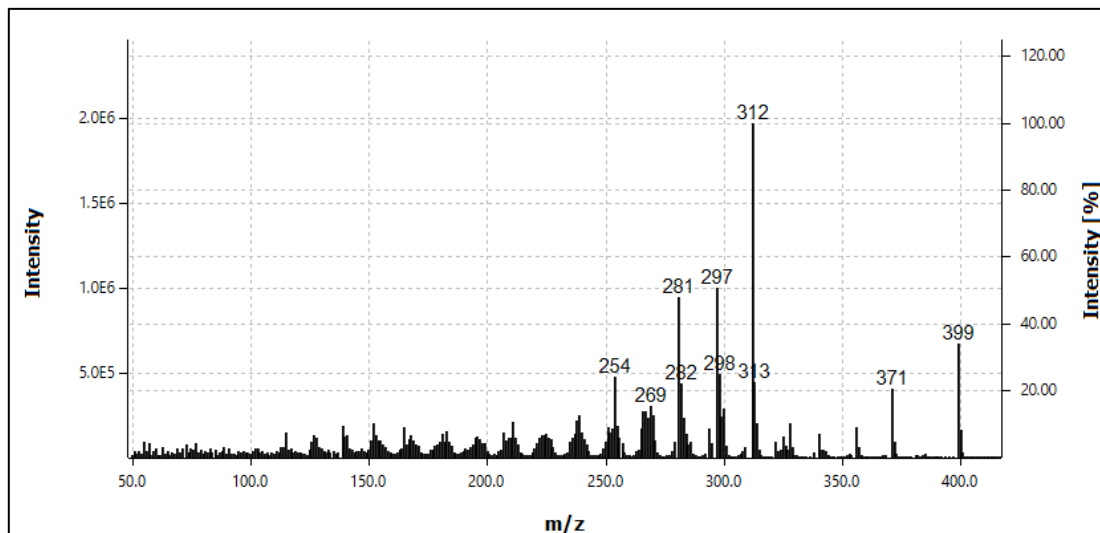


Figure III-7. Mass spectrum of colchicine (**7**) generated by 70 eV electron impact ionisation, following separation by gas chromatography.

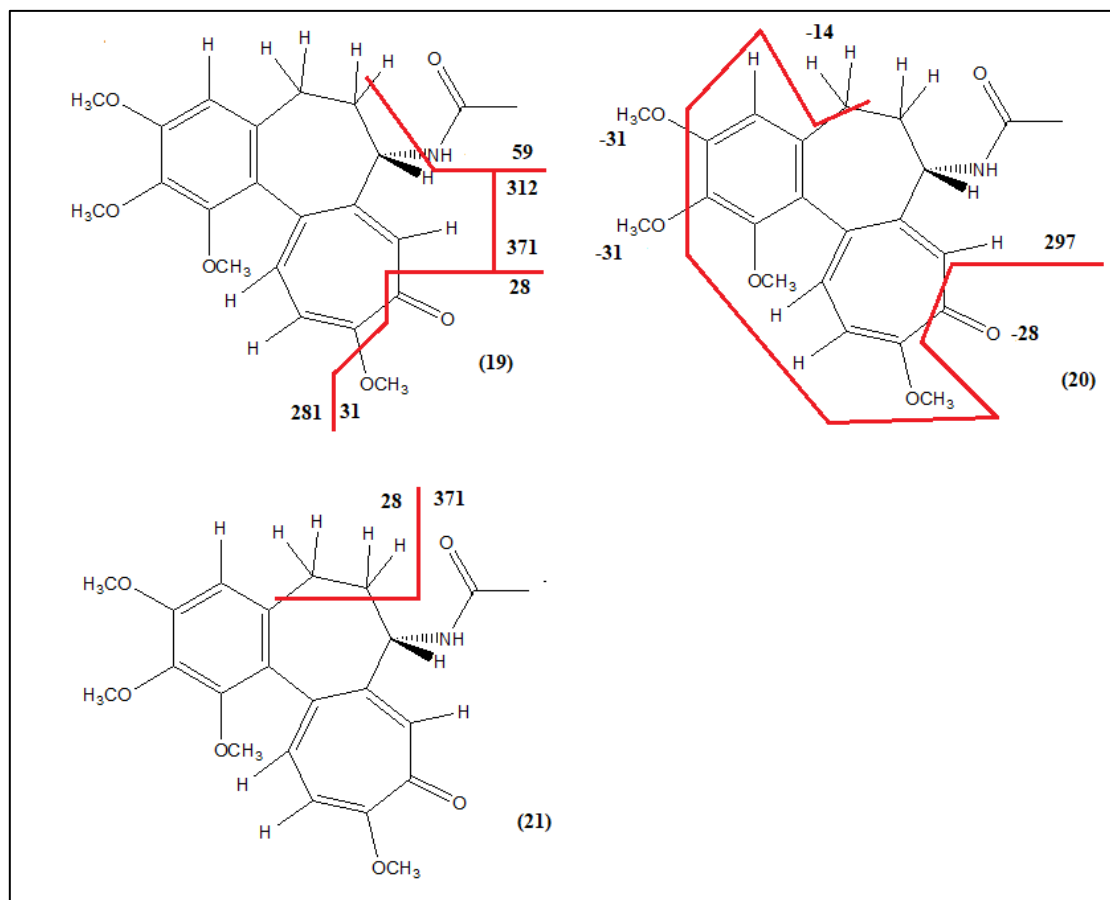


Figure III-8. Proposed fragmentation for colchicine under 70 eV electron impact conditions.

The interaction between ion abundances can be determined by inspecting the ratios between ions in the mass spectrum at a fixed concentration level across three batches. For colchicine (7), five ratios were selected and defined as:

Ratio 1: Area 399 ÷ Area 371

Ratio 2: Area 399 ÷ Area 312

Ratio 3: Area 281 ÷ Area 312

Ratio 4: Area 297 ÷ Area 312

Ratio 5: Area 281 ÷ Area 297

The average ratios for three sets of duplicate analyses were calculated at a colchicine (7) concentration of 2.382 ppm. The analyses were performed for samples prepared in de-ionised water and samples prepared in urine. To determine the inter-ion ratio relationships, multivariate Gaussian analysis was performed and the correlation matrices calculated (**Table III-3** & **Table III-4**).

Table III-3. Correlation matrix for colchicine ion ratios, detected in de-ionised water.

	IR 1	IR 2	IR 3	IR 4	IR 5
IR 1	1.000	-0.387	0.866	-0.965	0.935
IR 2	-0.387	1.000	0.126	0.616	-0.034
IR 3	0.866	0.126	1.000	-0.704	0.987
IR 4	-0.965	0.616	-0.704	1.000	-0.808
IR 5	0.935	-0.034	0.987	-0.808	1.000

Table III-4. Correlation matrix for colchicine ion ratios, detected in urine.

	IR 1	IR 2	IR 3	IR 4	IR 5
IR 1	1.000	-0.535	-0.977	-0.993	-0.978
IR 2	-0.535	1.000	0.703	0.633	0.698
IR 3	-0.977	0.703	1.000	0.996	1.000
IR 4	-0.993	0.633	0.996	1.000	0.996
IR 5	-0.978	0.698	1.000	0.996	1.000

In both correlation matrices, ratio 1 has strong correlations with ratios 3, 4 and 5. Based on the correlation coefficients in column 1 (r_{13} , r_{14} and r_{15}), of the correlation matrix for urine samples, an increase in ratio 1 would cause a decrease in ratios 3, 4 and 5. The interaction stems from a decrease in the abundance of the molecular ion when fragmentation occurs.

Ratios 3 and 4 also show strong correlation with ratio 5. This correlation exists since ratio 5 is the ratio of ratio 3 to ratio 4. Both matrices also indicate a strong correlation between ratios 3 and 4. Since both ratio 3 and 4 have the area of ion $m/z = 312$ as numerator, their relationship stems from the interaction between $m/z = 281$ and $m/z = 297$.

In de-ionised water, the correlation coefficient, $r_{34} = -0.704$, implies that as either one of these ions increase in abundance, the other will decrease. This implies there exists competition between these ions for formation. In urine, the interaction is described by a positive correlation coefficient, $r_{34} = 0.996$, which implies the ions do not compete for formation.

3.2.2 Electrospray ionisation-Mass spectrum

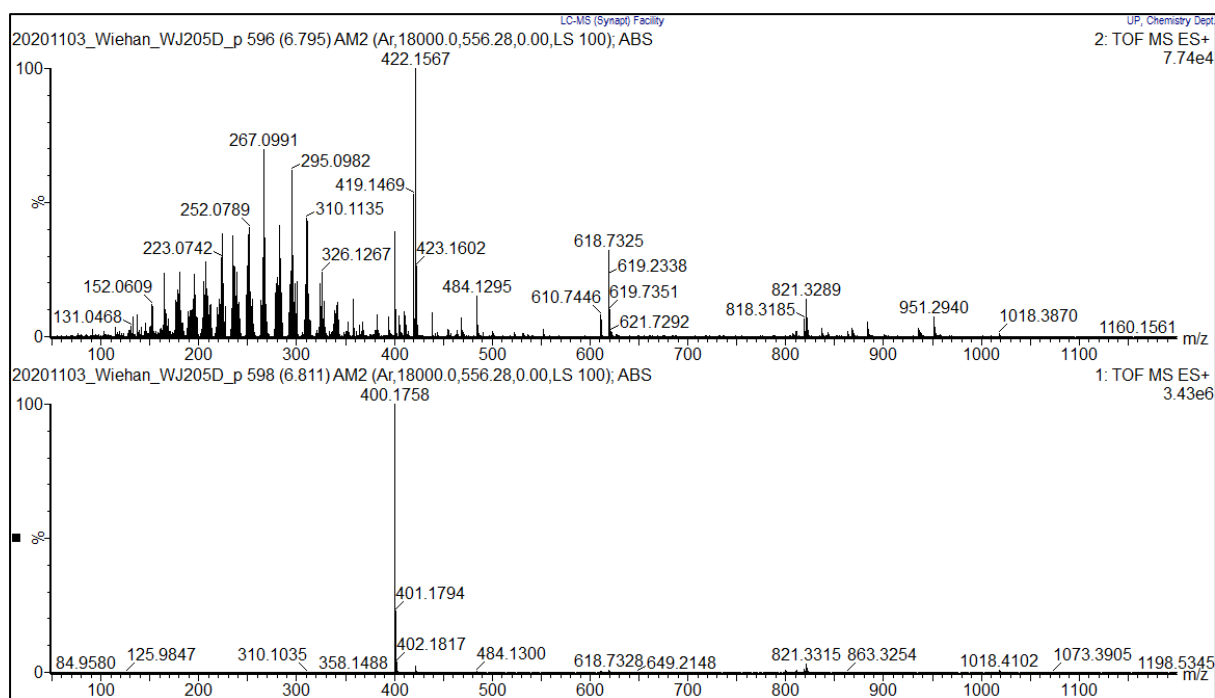


Figure III-9. Positive ion mode ESI-high resolution mass spectra of colchicine. Top: High energy ionisation mass spectrum. Bottom: Low energy ionisation mass spectrum. Masses corrected with regard to leu-enkephalin.

From both the electron impact (EI) and electrospray ionisation (ESI) mass spectra, the presence of an odd number of nitrogen atoms in the molecule is clear, since the suspected molecular ion has an odd nominal mass under EI conditions and an even nominal mass under ESI conditions due to protonation.

Under standard EI conditions (electron kinetic energy = 70 eV), colchicine undergoes various fragmentation processes. The base peak m/z -ratio of 312 is likely the result of the neutral loss of ethyl amide combined with the neutral loss of carbon monoxide. The initial neutral loss of carbon monoxide produces the fragment of $m/z = 371$ (**19**). Neutral loss was expected since the molecular ion at $m/z = 399$ fragmented to $m/z = 371$, both odd mass numbers. When the amide was simultaneously lost as a neutral molecule, an odd mass number was lost from an odd m/z -ratio to give the even m/z -ratio 312 (**19**). A further simultaneous loss of a methoxy group ($M^* = 31$), likely neighbouring the site of CO-loss, could produce the fragment with $m/z = 281$ (**19**) (**Figure III-8**).

The fragment ion of m/z -ratio 297 (**20**) was likely formed by simultaneous radical loss of a methylene group (CH_2^\bullet), two methoxy groups ($\text{CH}_3\text{O}^\bullet$) and neutral loss of CO (**Figure III-8**). The two methoxy groups lost are likely those on the six-membered ring. The loss of two methoxy radicals is somewhat stabilised by the formation of a benzyne-type functionality in the six-membered ring. This makes the loss from the six-membered ring more likely than methoxy loss at the seven-membered ring and six-membered ring simultaneously since this would not be stabilised.

The neutral loss of a mass number equal to 28 could also be explained by the loss of ethene from the central ring. This could also be a possible mechanism for the formation of the $m/z = 371$ fragment ion (**21**). The loss of the neutral amide could then be possible by geminal loss instead of 1,2-loss of the amide radical and a hydrogen radical.

Fragmentation around the conjugated rings occur easily since the highly delocalised electron cloud covers a large surface area and is easily struck by the high kinetic energy electrons. One of these delocalised electrons can then easily be knocked out of the molecule and result in ionisation of the compound. The conjugated nature of the rings allows charge migration that can cause fragmentation of the molecular ion on multiple fronts due to chemical stabilisation and destabilisation. Loss of radical groups is not always predictable, since the kinetic energy transferred from the electron is distributed throughout the whole molecule, not just locally at point of impact.

3.3 Assessment of quantitative figures of merit in the generated response model

3.3.1 Linearity in the response models generated from measured data

Based on the mass spectra generated by electron impact ionisation of colchicine and 5- α -cholestane, the ions selected for quantitative analysis are $m/z = 312$ (**19**) (colchicine base peak ion) relative to $m/z = 217$ (5- α -cholestane base peak ion). The relative response was measured as the ratio of the areas of the chromatographic peaks produced by these ions at their characteristic retention times. The selectivity of identification is discussed later in this chapter.

Linear response models were prepared, in triplicate, in both urine and de-ionised aqueous solutions. For each batch, analysed by duplicate application to a GC-MS system, the average response was calculated, and regression analysis performed to fit a linear equation to the data. For the samples prepared in de-ionised water, the calculated descriptive statistics are given in **Table III-5** and those for the samples prepared in urine are given in **Table III-7**.

Samples prepared in de-ionised water

Table III-5. Descriptive statistics regarding response model linearity in de-ionised aqueous samples.

Batch	r^2	Slope (b)	s_b	y-intercept (a)	s_a	$S_{y/x}$
1	0.952	2.96	0.38	-2.11	0.95	0.5779
2	0.256	2.71	2.67	0.055	6.602	4.018
3	0.882	3.62	4.73	-4.39	1.90	1.154
Average	0.735	3.10	1.07	-2.15	2.66	1.616

Linear regression analysis suggested a best fit linear trend line, with the equation $y = 3.10x - 2.15$ and a product-moment correlation coefficient of 0.735 for the mean response model. The slope had a standard deviation of 1.07 ppm^{-1} and the intercept had a standard deviation of 2.66. Therefore, the y-intercept does not differ significantly from naught at the 95.4% confidence level. Assuming a linear trend in the data, this would imply that the background noise in the measured data, does not significantly contribute to the analyte relative response.

By integrating the regions in the extracted ion chromatograms that correspond to the retention time of colchicine (**7**) of the method blanks in each batch, an average contribution to the analyte signal from the matrix was calculated. Following the recommendations by the U.S. Department for Health and Human Services⁵², the standard deviation of this mean contribution from the

matrix background was employed to estimate the limit of detection.⁵² Their guidance document defines the limit of detection, based on the matrix blank, as the concentration corresponding to a response equal to three times the blank standard deviation, divided by the slope of the regression model. If the intercept of the response model is significantly greater than naught, it is added to the calculated response. Thus, $y_{LOD} = (3 \times s_b)$.

Applying this convention to the mean response model, the theoretical limit of detection was calculated as 0.709 ppm with a standard deviation of 0.814 ppm. The limit of quantification, interpolated from the relative response at standard deviations of the mean blank signal, was 0.747 ppm, with a standard deviation of 0.805 ppm. Both these limits do not significantly differ from the lowest concentration level of colchicine (**7**) in the calibration range.

Viewing the mean response model and the individual batches of analyses as overlaid plots, notable deviations from a linear trend become visible (**Figure III-10**). The deviation from the expected linear trend was confirmed by analysis of the product-moment correlation coefficient and the y-residuals. By performing a t-test on the correlation coefficient, it was found that at a 95.4% confidence interval ($\alpha = 0.046$), there was no significant correlation. When visually inspecting the y-residual plot, severe curvature was also observed (**Figure III-11**). These factors indicate that a linear fit is not a suitable representation of the average trend in the data.

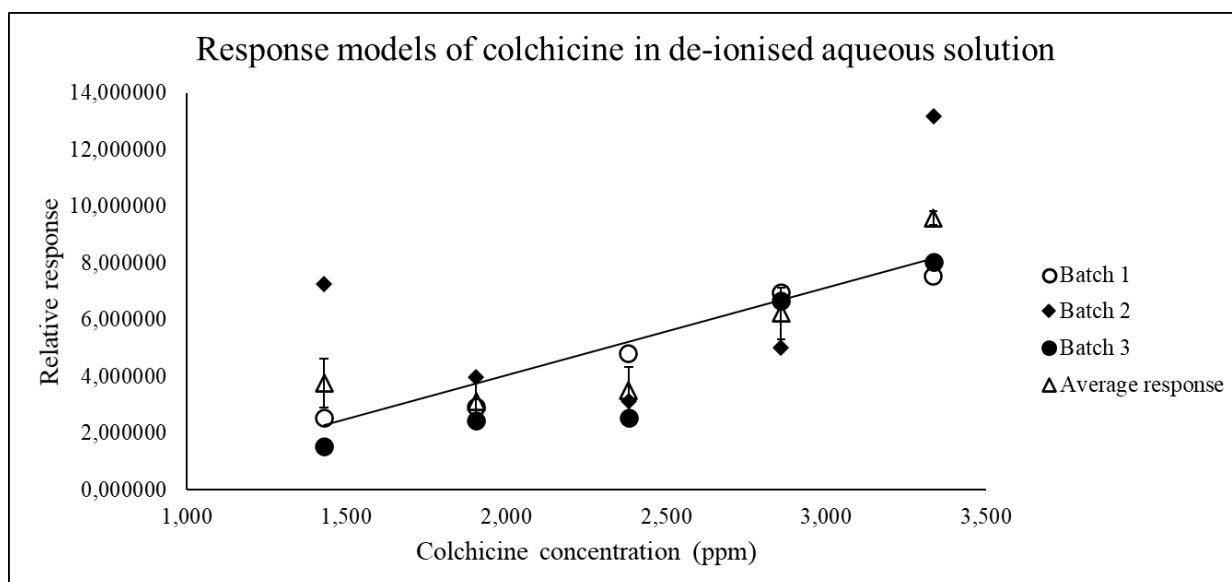


Figure III-10. Overlaid plots of the mean response model and the individual batches of analyses.

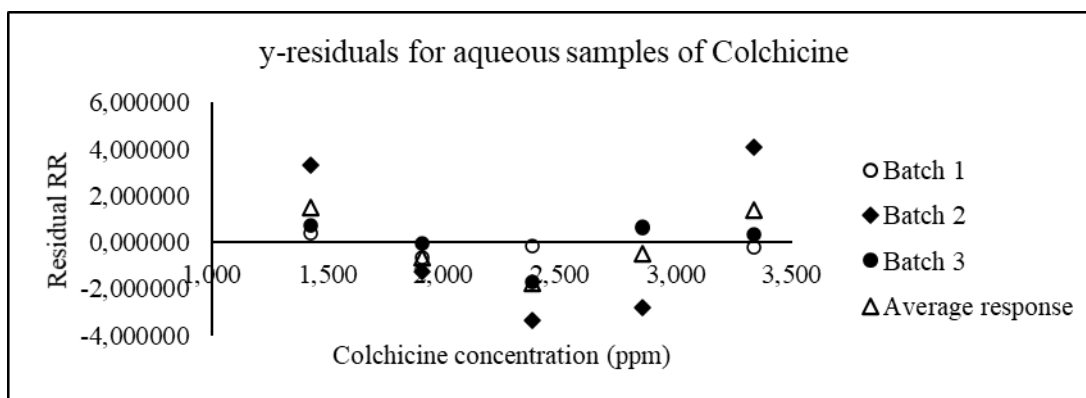


Figure III-11. *y*-residuals for the individual batches and the mean response model of samples prepared in de-ionised water. *RR: Relative Response.

To determine the distribution of variance over the calculated linear model, the standard deviation associated with each theoretical colchicine concentration (s_{x_0}) was calculated. From these standard deviations, the %-relative standard deviation (%-RSD) was calculated for each theoretical concentration level (**Table III-6**). The trend in relative variance, within each batch, was observed to be heteroscedastic with a decrease in variance as the concentration of colchicine increases. In the mean response model generated from the batches, the calculated %-RSD values indicate a homoscedastic trend with a centroid at 2.86 ppm colchicine (7).

Table III-6. %-relative standard deviations (%-RSDs) calculated from the average response of each respective batch of aqueous samples.

Concentration (ppm)	%-RSD (Batch 1)	%-RSD (Batch 2)	%-RSD (Batch 3)	%-RSD (Average)
1.43	13.7	88.8	21.7	29.0
1.91	9.78	81.1	15.0	23.6
2.38	6.87	73.2	11.9	18.0
2.86	6.51	47.3	10.5	13.9
3.33	5.97	81.5	10.4	18.5

Comparing the calculated limit of quantification (0.747 ppm, $s_{LOQ} = 0.805$ ppm) with the observed %-RSD values shows the absence of suitable precision across the calibration range significantly increases the limit of quantification in the average response model. Within batch 1 the precision is suitable for quantification across the whole calibration range. However, in batch 3 the 1.43 ppm level exceeds the expected %-RSD value from the Horwitz equation

(16%).^{53,54} In contrast to batches 1 and 3, batch 2 is not suitable for the quantification of colchicine in aqueous samples.

Second order polynomial and exponential models were also evaluated and compared to the linear (first order polynomial) trend for closeness of fit to the trend in the data. Ideally a linear model or a function transformed to a linear form is evaluated in regression analysis. These were obtained by applying the inverse operation of the trend under study, to the measured relative responses (i.e. the square root of the relative response vs. concentration, and the natural logarithm of the relative response vs. concentration) (**Figure III-12**).

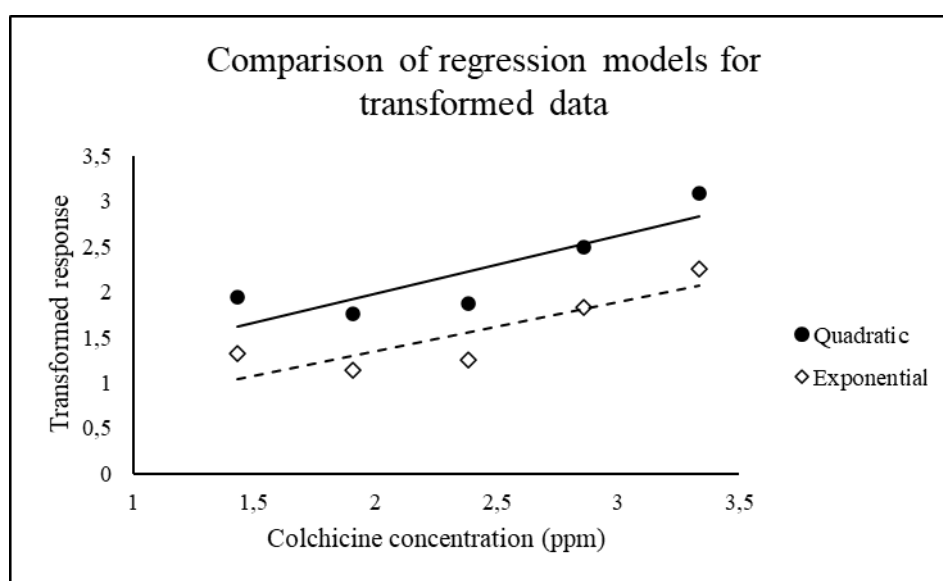


Figure III-12. A graphical comparison of the linear regression models for quadratic and exponential trends, following mathematical transformation.

The quadratic response was transformed to the linear equation $g(y) = \hat{b}x + \hat{a}$, where $g = \sqrt{y}$. The exponential response was transformed to $h(y) = \tilde{b}x + \tilde{a}$, where $h(y) = \ln(y)$. Neither of these transformations produced linear trends in the data with significant correlation (at the 95.4% confidence interval) and without curvature in their y-residuals.

Samples prepared in urine

Response model data for urine samples prepared in triplicate, and analysed in duplicate, was evaluated following the same process as those applied for the aqueous samples. A linear best-fit line was calculated for the mean of each batch's duplicate analyses. The quality of the linear fit was evaluated by analysing the figures of merit, summarised in **Table III-7**, calculated from the regression statistics for the response models.

Table III-7. Descriptive statistics regarding response model linearity in urine samples.

Batch	r²	Slope	s_b	y-intercept	s_a	S_{y/x}
1	0.992	0.0956	0.0050	-0.086	0.012	0.007497
2	0.814	0.330	0.091	-0.181	0.226	0.13727
3	0.916	0.409	0.071	-0.243	0.177	0.1075
Average	0.915	0.278	0.049	-0.170	0.122	0.0740

For the quantitative analysis of urine samples spiked with colchicine (**7**), a response model was calculated as the average relative response of the three analysed batches. The linear equation describing the fitted trendline for this model was $y = 0.278x - 0.170$, with a standard deviation in the slope of 0.049 ppm^{-1} and 0.122 in the intercept. The y-intercept, therefore, does not differ significantly from naught at the 95.4% confidence level.

Applying the same conventions for the limits of detection and quantification as were used for the aqueous samples, the theoretical limit of detection was calculated to be 0.623 ppm with a standard deviation of 0.426 ppm and the limit of quantification 0.653 ppm, with a standard deviation of 0.422 ppm. These calculated limits are not significantly different ($\alpha = 0.046$) from the lowest concentration level in the calibration range.

Comparing the calculated limit of detection for colchicine in urine to the levels at which colchicine (**7**) was detected via GC-MS as reported in literature, showed a difference of two orders of magnitude. Miller et al.¹⁴ were capable of detecting colchicine (**7**) in plasma at a level of 6.1 ng/mL utilising a GC-MS method. Samanidou et al.'s HPLC-PDA method⁴⁶ enabled them to detect colchicine in physiological fluids to a level of 0.005 $\mu\text{g/mL}$. The calculated limit of detection, however, does *not* significantly differ from those observed by Schreiber et al.⁴⁸ and Theofel et al.⁴⁷ at a significance level of $\alpha = 0.046$.

Regression analysis showed that the data points correlated significantly with the linear best-fit trendline with a product-moment correlation coefficient of 0.915 (see **Figure III-13**). The y-residuals show definite curvature in Batches 2 and 3. However, Batch 1 shows a more random distribution of data points about the x-axis (**Figure III-14**). The observed curvature in the mean response model indicates that, despite the close correlation, a linear equation might not be the best description of the trend in the data.

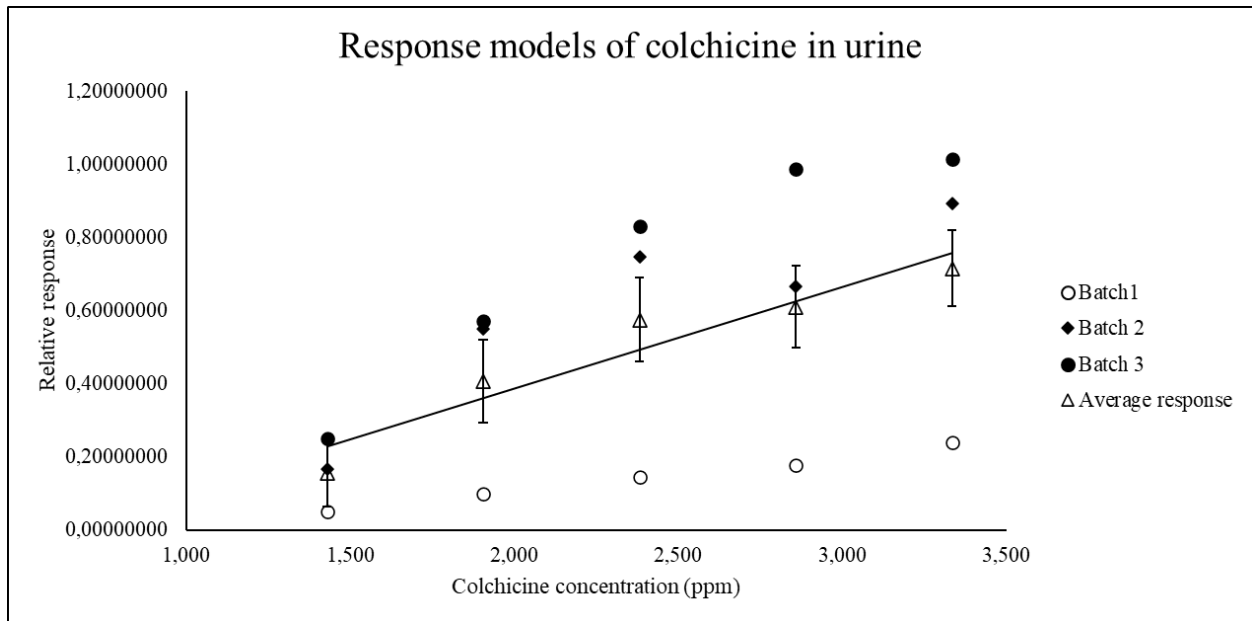


Figure III-13. Response models generated for colchicine spiked into blank urine samples. The mean response model is illustrated by the open triangles. A fitted trendline is illustrated for the mean response model.

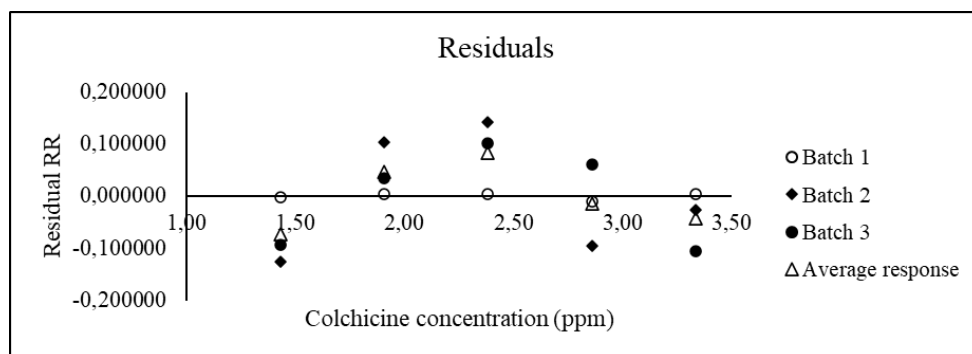


Figure III-14. Plot of the y-residuals for the individual batches and the mean response model, generated from spiked urine samples. RR*: Relative response.

For the average response in each batch, the standard deviation associated with a calculated x -value (s_{x_0}) was determined for each theoretical concentration at which the samples were spiked. From these standard deviations, the %-RSD at each concentration level was calculated (**Table III-8**).

The distribution of the relative variance over the linear models of Batches 2 and 3 show a heteroscedastic trend with a decrease in variance as the concentration of colchicine increases. In Batch 1 there is a slight increase in the relative variance near the upper concentration level. The overwhelming trend, however, remains heteroscedastic as seen in Batches 2 and 3. The %-RSD values calculated for Batch 1 does not exceed the 16% benchmark recommended by the Horwitz equation. In Batch 2 the value is exceeded at the 1.43 and 1.91 ppm levels. The %-RSD values calculated for the linear model in Batch 3 only exceeds the recommended benchmark, from the Horwitz equation (16%) at the 1.43 ppm level.^{53,55}

The %-RSD values calculated for the average model follows the same trend and exceeds the benchmark value between 1.43 and 1.91 ppm. Therefore, the experimental limit of quantification of colchicine (**7**) in urine is 1.91 ppm. This experimental limit is significantly greater than the calculated quantification limit (0.653 ppm, $s_{LOQ} = 0.422$ ppm) at the $\alpha = 0.046$ significance level.

Table III-8. %-Relative standard deviation (%-RSD) values calculated for each concentration of colchicine in each batch.

Concentration (ppm)	%RSD (Batch 1)	%RSD (Batch 2)	%RSD (Batch 3)	%RSD (Average)
1.43	5.79	35.5	21.1	20.3
1.91	3.65	18.4	12.1	10.6
2.38	2.76	15.5	9.41	8.44
2.86	2.39	12.3	8.59	7.28
3.33	2.52	12.7	7.54	7.21

Comparison of mean response models

Comparing the figures of merit in **Table III-5** with those in **Table III-7**, the significant difference between the response models is clearly visible. In contrast to the samples prepared in de-ionised water, the matrix matched samples show significant correlation (at a 95.4% confidence level – $\alpha = 0.04$) in all three of the measured batches. The trend followed by the y -

residuals for the aqueous samples, indicates curvature in the response models in the opposite direction to those calculated for the spiked urine samples (**Figure III-11 & Figure III-14**).

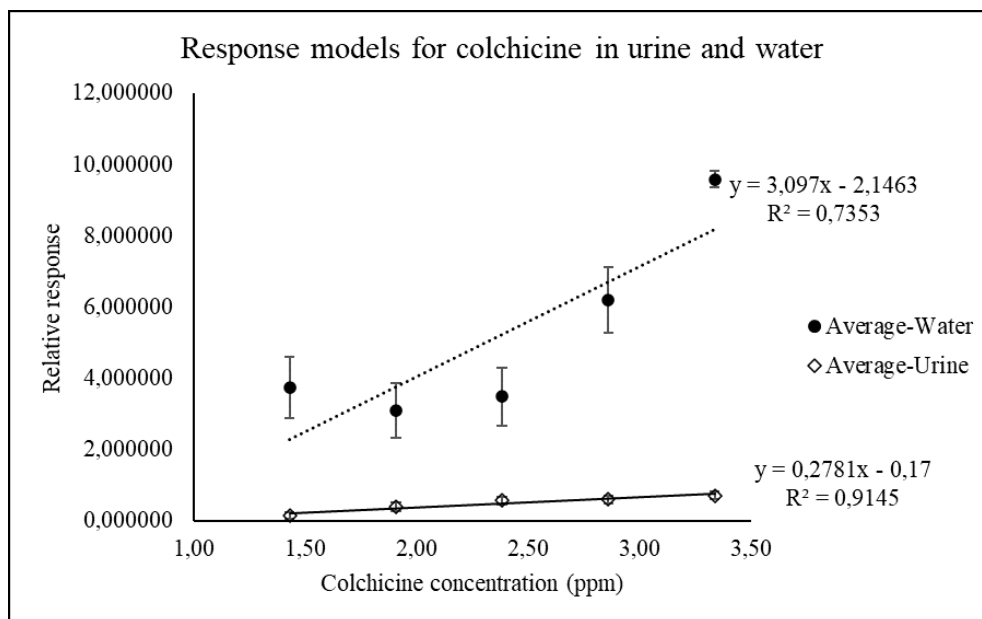


Figure III-15. A comparison of the mean response models calculated for colchicine spiked into de-ionised water and urine. Error bars show the y-standard deviation calculated from s_{x_0} via the linear models.

Both response models showed similar theoretical limits of detection and quantification. The limits of detection for aqueous samples were, however, greater than those in the case of the matrix matched (urine) samples. This was an unexpected result since the contribution of the urine to the background signal in the chromatogram was expected to increase the level of noise and, thereby, increase the limit of detection.

By simultaneously plotting the mean response models for aqueous and urine samples (**Figure III-15**), a marked difference in the slopes of the response models were observed. The large variance in the relative response of the response model for aqueous samples produced a large variance in the slope of its calculated regression line. At the 95.4% confidence level, the slope did not differ significantly from naught, nor from the 95.4% confidence level distribution around the slope of the response model for spiked urine samples.

Since the intercepts of both response models did not differ significantly from naught and the gradients of the response models did not differ significantly from each other, they can, theoretically, be applied interchangeably in the quantitative analysis of colchicine (7) in physiological samples. However, since the average response model, calculated for spiked

aqueous samples, did not show significant correlation between the linear model and the data points, it would not be applicable in the quantitative analyses of samples.

A comparison of the magnitude and distribution of variance between the two mean response models, showed the response models calculated for the urine samples were better suited for application in a testing laboratory than the aqueous samples' response models. In the former case the error in the y -direction, calculated from the standard deviation in the x -direction at each theoretical concentration, were minute compared to the errors in the y -direction of the latter case (**Figure III-15**). **Figure III-13** shows a magnified illustration of the errors in the y -direction calculated for the spiked urine samples.

3.3.2 *Repeatability of the analytical method and response models*

Samples prepared in de-ionised water

Based on the Horwitz equation, the expected %-RSD for the concentrations in the analytical range of the response model, at a concentration equal to 1 ppm, was 16%.^{53,54} At greater %-RSD values, the method repeatability (precision) was not suitable for application in the quantitative analysis of aqueous samples with similar colchicine concentration levels to the spiked level. The %-RSD values, calculated for each concentration level of the average response model, were all greater than this expected value (**Table III-6**), except at the 2.86 ppm concentration level. This suggests the analytical method is not suitable for application in quantifying colchicine (**7**) in de-ionised aqueous samples.

The contribution of the between-batch variation to the total variance in the measured relative responses at each respective concentration level of colchicine (**7**), was evaluated for significance at the $\alpha = 0.046$ significance level. At the 1.43 ppm concentration level of colchicine, the between-batch variation contributed significantly to the total variance between the measured relative responses. At higher concentration levels of colchicine, there is no significant contribution to the total variance in relative response by the between-batch variation. Therefore, at concentrations of colchicine greater than 1.43 ppm, the level of precision can be attributed to problematic repeatability of replicate sample analyses.

Upon closer examination of the variance within each batch, and the %-RSD's calculated for the concentrations of the analytical range in each batch, the large within-batch variation, especially in Batch 2, showed poor repeatability between the duplicate analyses performed for each respective batch of samples. This implies that the method may be sensitive to the sample storage conditions, to which samples are exposed during and between the analysis of individual

batches. During method development it was observed that if the GC-column was not baked out between batches, there was a severe decrease in method sensitivity. Therefore, between each batch of samples, the GC-oven was set to a high temperature (280 °C) for one hour.

Samples of colchicine spiked into urine

The same calibration range was evaluated for the urine samples. Therefore, the Horwitz equation indicated an expected %-RSD value of 16% at each concentration in the calibrated analytical range.^{53,54} In the average response model calculated for the spiked urine samples, the %-RSD values did not exceed the 16% level, with the exception of the %-RSD value at the 1.43 ppm concentration level (**Table III-8**). The method repeatability was, therefore, suitable for quantitative analysis of samples for colchicine at concentrations above 1.43 ppm.

Between batch repeatability was evaluated by estimating the significance of the between-batch variation to the total variation in the relative response at each concentration level. This evaluation was carried out by performing a single factor analysis of variance (ANOVA) F-test, with replication at each concentration level for the duplicate analyses across the three batches. At the $\alpha = 0.046$ significance level, the F-tests showed that the between-batch variation does not contribute significantly to the total variance at each respective concentration level of colchicine. This suggests the method can be effectively repeated without producing a significant contribution to variance in measured relative responses.

Comparison of repeatability between the different sample matrices

Since de-ionised water is not expected to significantly contribute background noise and variation to the measured relative responses, the response models developed from samples prepared therein was expected to show better repeatability than those developed in urine. In contrast to this expectation, the average response model as well as the response models calculated for the individual batches developed for urine samples, showed better repeatability than those for the de-ionised aqueous samples (compare **Table III-6** & **Table III-8**).

The more consistent precision in the response models of the urine samples was carried through to the corresponding average response model. From the second batch of de-ionised aqueous samples the absence of precision in the response model contributed to the inadequate precision of the average response model.

In terms of the between-batch repeatability, the variation in measured relative responses for the urine samples, was not significantly greater than the inherent random variation at each concentration level of colchicine (7) ion over the analytical range. In de-ionised aqueous samples, the between-batch variation was significantly greater than the inherent random variation for the samples with a colchicine (7) concentration of 1.43 ppm.

3.3.3 Accuracy in the measurement of the concentration of colchicine in a sample

Accuracy of measurement for de-ionised water samples

In the regression of the experimentally calculated concentration of colchicine (7) on the corresponding theoretical concentration in the spiked samples, a clear non-linear trend was observed (**Figure III-16**). This trend is reflected in the plot of the y-residuals over the analysed concentration range (**Figure III- 17**). Linear regression analysis of the trend, however, produced a regression line with a slope equal to 1.000 (standard deviation = 0.346), and an intercept that does not significantly differ from naught. The calculated trendline, therefore, does not significantly differ from the $y = x$ line if $\alpha = 0.046$.

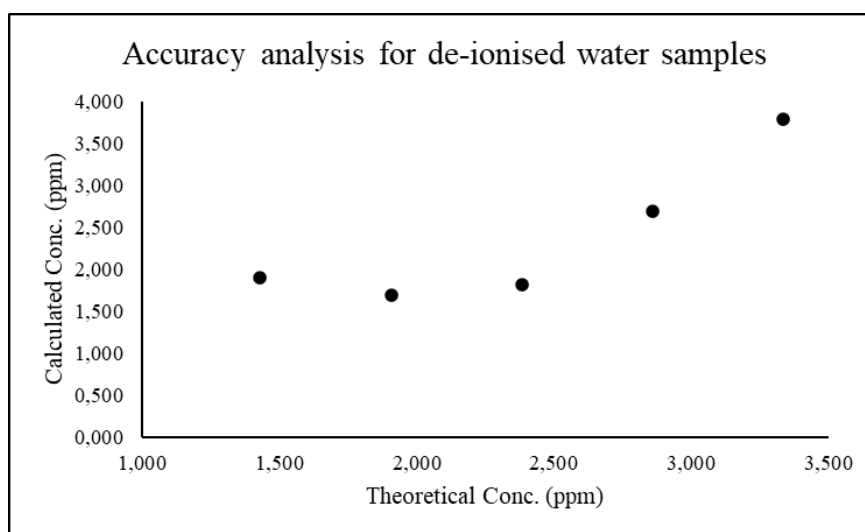


Figure III-16. A plot showing the regression of the experimentally calculated concentration for the measured responses on the theoretical concentration of colchicine in the samples.

The similarity of the regression line to the $y = x$ line indicates, theoretically, there is no significant additive or multiplicative bias in the calculation of the concentration of colchicine (7) from the response model data. However, the pronounced curvature in the data, relative to the calculated linear model, causes the data points to not significantly correlate with the calculated trendline, as confirmed by a t-test for significant correlation. This significant departure from correlation and the pronounced curvature in the data trend confirm a linear

model is not suitable in describing the relationship between the calculated concentration of colchicine (7) and the theoretical concentration in the spiked sample.

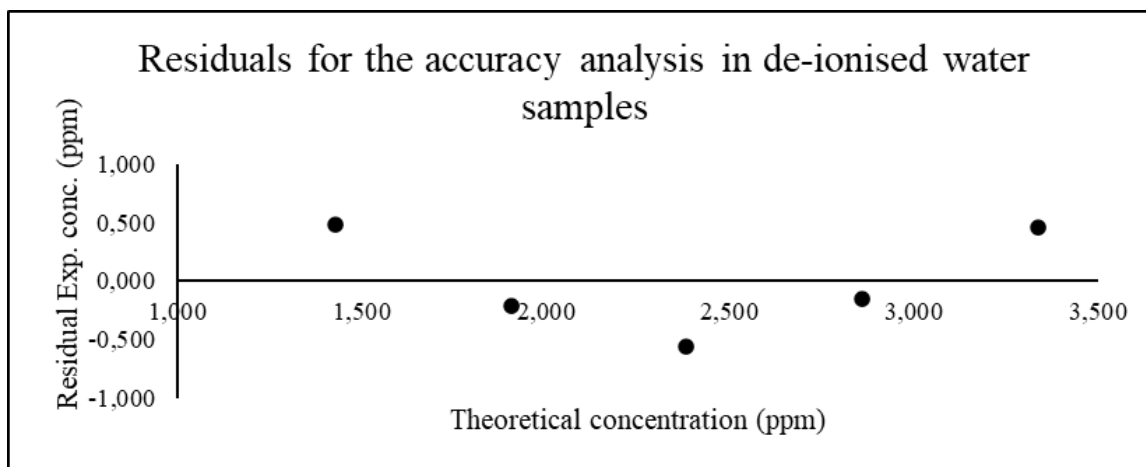


Figure III- 17. *y*-residuals in the regression of calculated colchicine concentration on theoretical concentration.

The pronounced curvature in the data also affects the %-bias calculated for each theoretical concentration level. A greater departure from the trendline produces a greater %-bias for that measured concentration. Thus, despite the linear trendline's similarity to the $y = x$ line, the bias at a specific concentration may be significant.

Accuracy in the calculation of the concentration colchicine in a urine sample

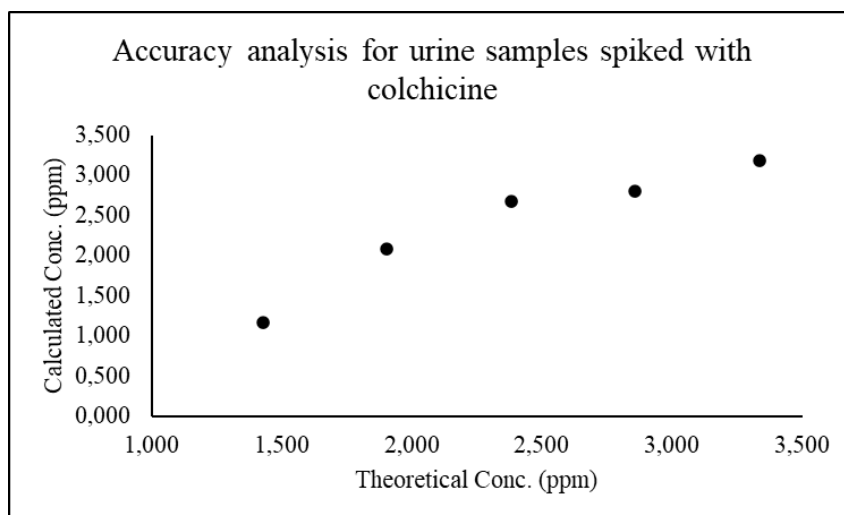


Figure III-18. A plot showing the regression of the calculated colchicine concentration on the theoretical concentration spiked into the urine matrix.

To determine the relationship between the observed concentration of colchicine (7) and the concentration theoretically present in the spiked samples, the two sets were graphically compared (**Figure III-18**). The trend in the plotted accuracy data closely correlates with the calculated linear trend estimated in regression analysis of the accuracy data with a product-moment correlation coefficient (r^2) of 0.926. The correlation is significant based on a t-test for significant correlation.

From the linear regression analysis results, the equation of the calculated trendline was calculated to be $y = 1.000 \times x + 0.000$, where the standard deviation of the slope is $s_b = 0.177$ and that of the intercept is 0.437 ppm. The calculated trendline, therefore, does not differ significantly from the $y = x$ line. This implies there is no significant additive or multiplicative bias in the calculation of the concentration of colchicine (7) in urine samples from the response model.

In the plot of the data points, some curvature in the data is observed relative to the calculated trendline. The deviation from linearity was also observed in the plot of the y-residuals over the range of analysed concentration levels (**Figure III-19**). The pronounced curvature in the data suggests the relationship between the calculated and the theoretical colchicine (7) concentrations might not follow a linear trend, despite the close correlation between the data and the $y = x$ line.

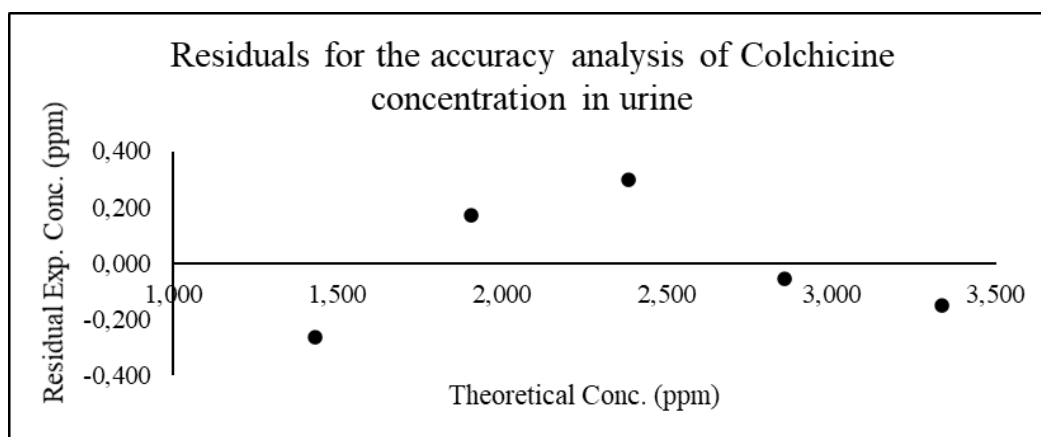


Figure III-19. Residuals calculated for the deviation of the experimental concentration from the theoretical colchicine concentration in the spiked samples.

Comparison of method accuracy in de-ionised and urine samples

Comparing the accuracy of the same method applied to samples in different matrices, is best done by comparing the %-bias at each concentration level in the analysed concentration range. In both matrices the calculated trendline did not differ significantly from the $y = x$ line. However, there is a marked difference in the %-bias at the respective concentrations (**Table III- 9**).

Table III- 9. Comparison of the %-bias in the average response model for each matrix.

Concentration (ppm)	%-Bias H₂O	%-Bias Urine
1.43	33.4	-18.4
1.91	-11.0	8.95
2.38	-23.6	12.5
2.86	-5.55	-1.87
3.33	13.6	-4.53

For each respective sample matrix, the calculated %-bias follows a non-linear trend over concentration. The curvature in these trends correspond to that of the respective calibration models. In the urine samples the calculated %-bias was markedly less than for the de-ionised aqueous samples, indicating better accuracy in the calculated colchicine (**7**) concentration for urine samples than for the aqueous samples.

3.4 Assessment of qualitative figures of merit in the analysis of samples for colchicine

Under selected ion conditions identification of colchicine with the aid of the spectral registry, may be problematic since this detection mode decreases the number of points for comparison to the spectra in the registry. Therefore, characteristic ion ratios are used to positively identify colchicine (**7**) in the chromatogram. Since an analyte must be positively identified before it can be quantified, the significance level associated with qualitative measurements is set to $\alpha = 0.003$. The ratios were calculated as the quotient of areas under the chromatographic peaks extracted for the relevant ions that elute at the same relative retention time as colchicine (**7**). Those selected for the analysis of colchicine (**7**) are given in **Table III- 10**:

Table III-10. Designation of ion ratios that were used in the qualitative analysis of colchicine (7) for detection in the selected ion mode (SIM).

Ratio designation	Description
IR 1	Area m/z = 399 ÷ Area m/z = 371
IR 2	Area m/z = 399 ÷ Area m/z = 312
IR 3	Area m/z = 281 ÷ Area m/z = 312
IR 4	Area m/z = 297 ÷ Area m/z = 312
IR 5	Area m/z = 281 ÷ Area m/z = 297

The control levels, relative to which the ion ratios had been measured, were determined from the ion ratios calculated as the centroid of the respective ratios over all three batches at the specific concentration of 2.38 ppm. For each mean value, the 99.7% confidence interval was calculated.

The centroid for urine samples, with its standard deviation, is then given by:

$$\bar{m}_{Urine} = \begin{bmatrix} 1.7361 \\ 0.35769 \\ 0.505756 \\ 0.55217 \\ 0.91448 \end{bmatrix} \text{ with } \bar{s}_{Urine} = \begin{bmatrix} 0.1304 \\ 0.07965 \\ 0.05506 \\ 0.03331 \\ 0.06435 \end{bmatrix}$$

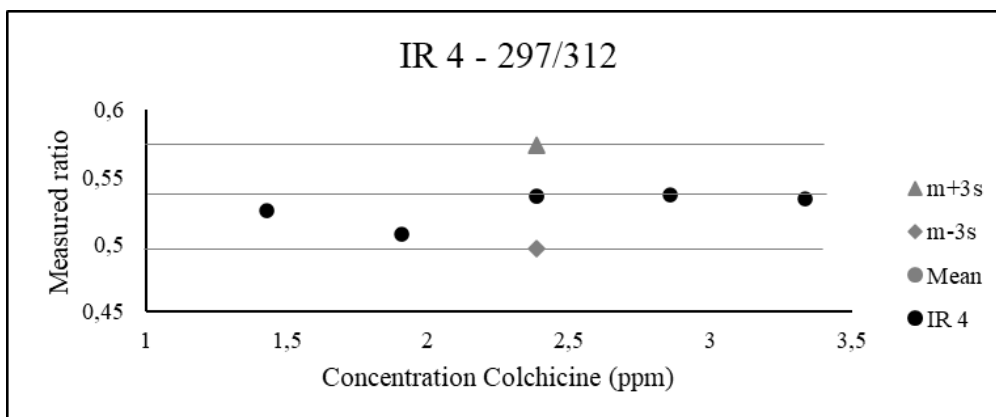
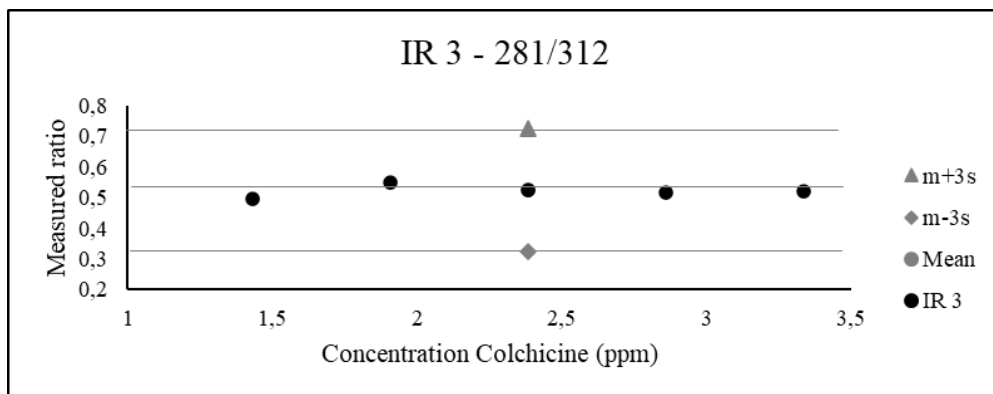
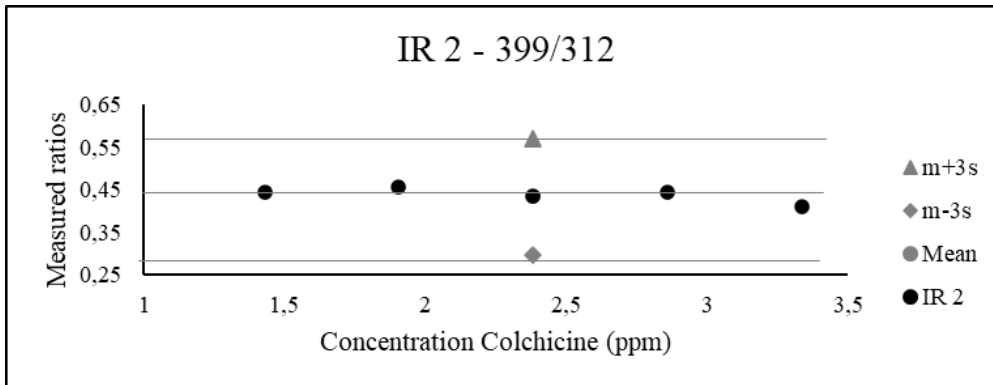
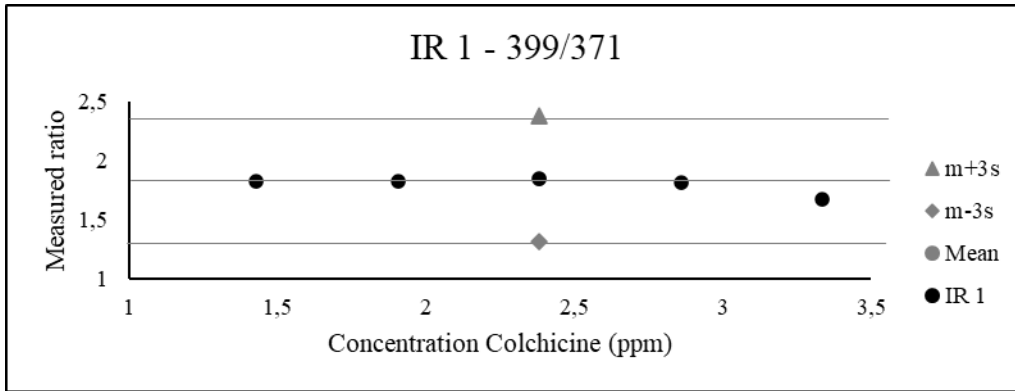
In the case of de-ionised aqueous samples, the centroid at the 99.7 % confidence level, is:

$$\bar{m}_{H_2O} = \begin{bmatrix} 1.8446 \\ 0.43420 \\ 0.52497 \\ 0.53568 \\ 0.98059 \end{bmatrix} \text{ with } \bar{s}_{H_2O} = \begin{bmatrix} 0.1773 \\ 0.04567 \\ 0.06696 \\ 0.01284 \\ 0.12713 \end{bmatrix}$$

3.4.1 The relationship between measured ion ratios and analyte concentration

Samples in de-ionised aqueous matrix

To evaluate the trend in the respective ion ratios measured at each theoretical concentration in the response model, the regression of the ion ratios on the concentration levels was illustrated as a plot of the measured ratio versus the concentration of colchicine (7). For each ratio, the measured values were compared to the relevant centroid to determine whether there exists a significant deviation from the control value with $\alpha = 0.003$.



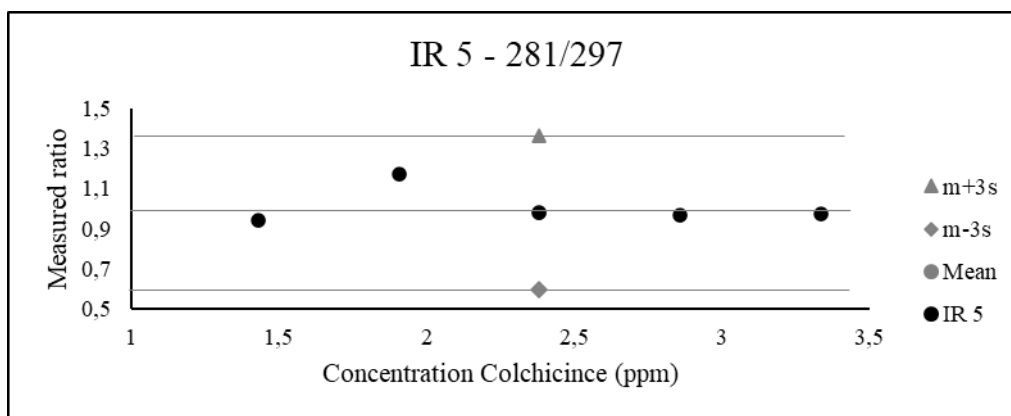


Figure III-20. Average ion ratios recorded at each theoretical concentration level. The confidence interval for each respective ion ratio is illustrated in the corresponding plot by the horizontal lines.

The illustrated distributions of the ion ratios around the corresponding control values in **Figure III-20**, showed that all the measured ion ratios for spiked concentrations of colchicine (7) in the response model, lie within the 99.7 % confidence interval. Therefore, colchicine (7) is positively identified at each concentration in the linear response mode, and the quantitative analyses remains valid at each level of colchicine (7).

To estimate a limit of detection, an additional spiked sample was analysed in each batch. The sample, spiked at 0.953 ppm colchicine (7), was observed in the pre-validation study to have different ion ratios from those in the samples spiked at higher concentrations. The significance of the difference was evaluated by Hotelling's T^2 -test for each of these samples.

Table III-11. Results from the Hotelling's T^2 -tests performed on the averages of three duplicate analyses of spiked colchicine samples of concentration 0.953 ppm.

	T^2	F-stat ($N = 6; p = 5$)	F (5, 1, $\alpha = 0.003$)
Batch 1	475.0	19.00	0.035
Batch 2	172.3	6.89	0.035
Batch 3	131889	5276	0.035

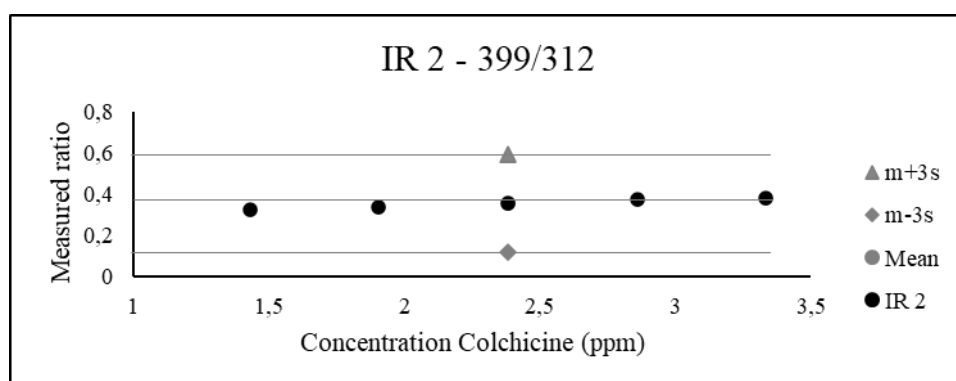
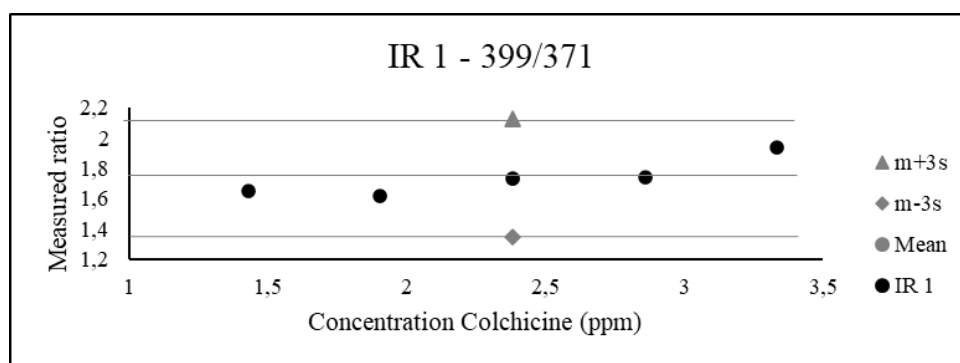
In each of the three samples' ion ratio vectors there existed a significant deviation from the centroid vector, at the $\alpha = 0.003$ significance level. Comparing the measured ion ratios to the calculated confidence interval of the centroid showed that the samples of Batch 2 did not differ significantly. This difference in result could be attributed to Hotelling's T^2 -test that accounts for the co-variances of the distribution matrix, which are neglected in the empirical comparison.

For the comparison of the average of three batches of duplicate ion ratio measurements to the control range (for $N = 6$), a T^2 value of 14231.44 was calculated. This corresponded to an F-value of 569.26 (with $p = 5$ variables), which was greater than the critical F-value, $F_1^5(\alpha = 0.003) = 0.04$). Since the calculated F-value was greater than the critical value, there exists a significant difference between the average vector of ion ratios for a colchicine (7) concentration less than 1.43 ppm and the 99.7 % confidence interval around the centroid of ion ratios.

This significant deviation from the centroid confidence interval limits the range of the analytical method for positive identification and quantification of colchicine (7) in an aqueous sample. The limit of detection was calculated from the calibration model as 0.709 ppm, with 0.814 ppm as standard deviation. This confidence interval is *not* significantly less than the observed limit of detection at 1.43 ppm.

Samples in matrix matched (urine) solutions

The same reasoning as for the de-ionised aqueous samples applies to the ion ratios recorded, for colchicine (7), in the spiked urine samples. Monitoring the variation in the measured ion ratios over concentration, the lowest concentration of colchicine (7) at which it can be positively identified by its ion ratios can be estimated. The experiment is also performed for matrix matched samples, since contribution from the background signal may alter the measured ratios relative to those recorded for the de-ionised aqueous samples.



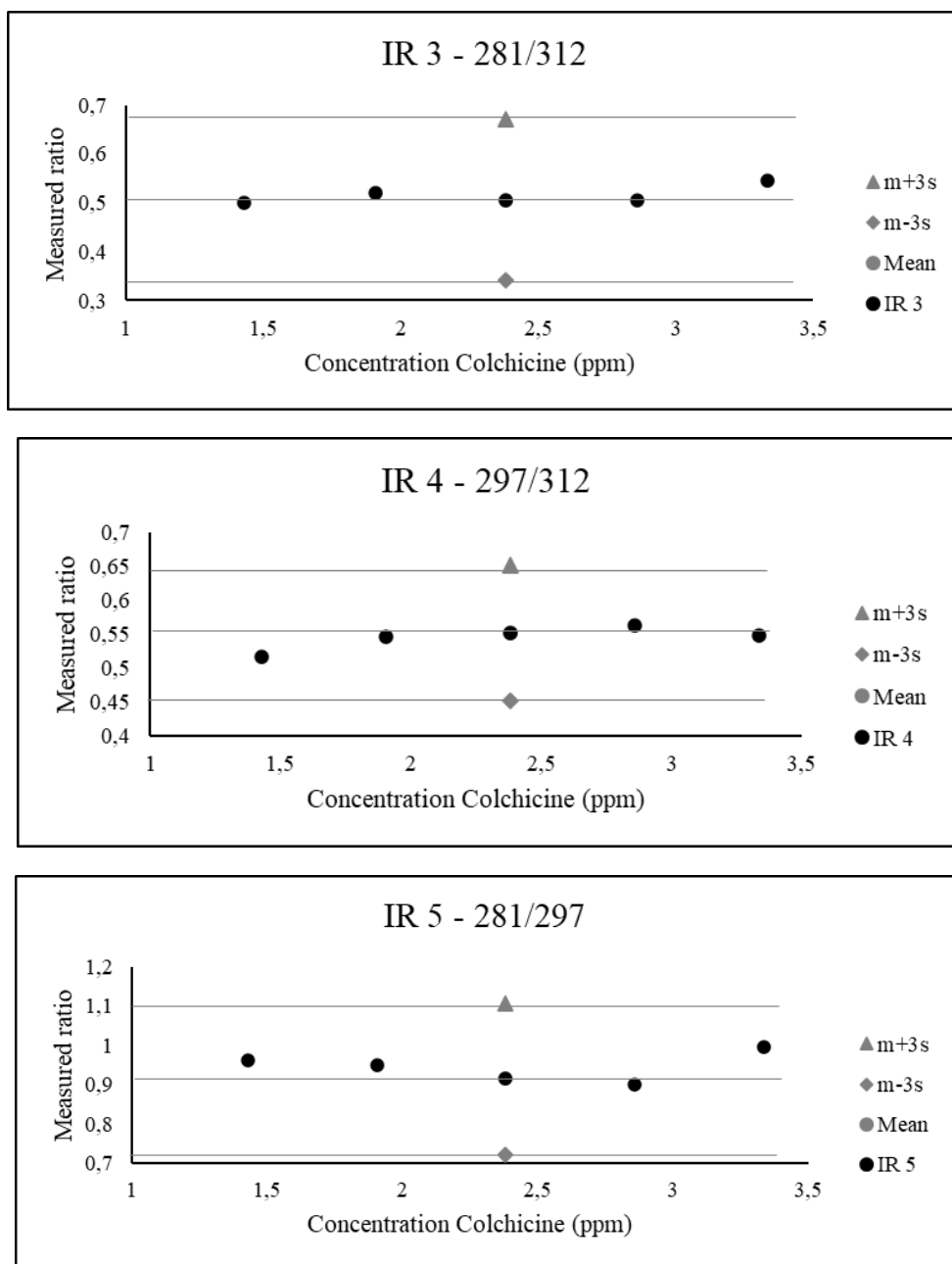


Figure III-21. The variation of the measured ion ratios with the theoretical colchicine concentrations in the samples.

For the positive identification of colchicine (7), the criterium holds that all five the ion ratios must lie within the 99.7% confidence interval around the centroid vector. **Figure III-21** shows the variation of each of the measured ratios with concentration. Based on these distributions, colchicine (7) can be positively identified by its ion ratios with 99.7% confidence at each concentration level.

Following the same experimental procedure as for the de-ionised aqueous samples, three urine samples were prepared at the 0.953 ppm concentration level and analysed in duplicate. The average ion ratios measured for each duplicate analysis were compared to the confidence region around the centroid vector for significant deviation from the centroid at the $\alpha = 0.003$ significance level. To determine the significance of the deviation from the centroid, Hotelling's T^2 -test was used.

Table III-12. Results from the Hotelling's T^2 -tests performed on the averages of the three urine samples prepared at 0.953 ppm.

	T^2	F-stat ($N = 6; p = 5$)	F ($5, 1, \alpha = 0.003$)
Batch 1	369,9	14,80	0.035
Batch 2	90620	3625	0.035
Batch 3	204,7	8,188	0.035

The results from the Hotelling's T^2 -tests are summarised in **Table III-12** and show that each of the three replicates, at the same concentration of colchicine (**7**), deviate significantly from the centroid at the $\alpha = 0.003$ significance level. In contrast, an empirical comparison of the measured ratios with the centroid confidence interval showed a significant deviation in only the second sample prepared in parallel with the second batch of samples analysed to generate the response model.

Two conclusions can be drawn from these results. Firstly, the contribution of co-variances to the significance testing, of vector sample deviations from the centroid vector should not be underestimated. These co-variances are accounted for by Hotelling's T^2 -test, but not by empirical comparison.

The second conclusion relates to the limit of detection associated with the analytical method. From the calibration model the detection limit for colchicine (**7**) in urine was estimated at 0.703 ppm (with a standard deviation of 0.384 ppm). Experimentally it was shown the ion ratios deviate significantly from the centroid vector at concentration levels less than 1.43 ppm. Despite not being significantly greater than the calculated limit, this observed detection limit as well as the limit for de-ionised aqueous samples, prompts awareness on the importance of ion ratios in determining the limit of detection.

In both sample matrices the limit of detection was experimentally estimated to be between 0.953 ppm and 1.43 ppm. This correlates well with the observations of Schreiber et al. and Theofel et al.⁴⁷ in their respective studies that show the identification of colchicine (**7**) in physiological samples via GC-MS becomes problematic at concentration levels below 1 ppm. In their studies, Schreiber et al.⁴⁸ and Theofel et al.⁴⁷ utilised mass spectral libraries to identify colchicine in samples, analysed by GC-MS.^{47,48}

3.4.2 Repeatability of ion ratios between individual batches

Between-batch repeatability of ion ratios measured for spiked samples

Theoretically, the ion ratios measured from the extracted ion chromatograms of an analyte should not change between respective samples prepared at the same concentration level of analyte. Such a significant change in measured values would also be reflected in the contribution of between-batch variation to the total variance between the measured ratios. A significant contribution of between-batch variation to the total variance would indicate the ion ratios, measured for the respective samples are not comparable.

To determine the significance of the contribution to the total variance by the between-batch variation, the multivariate analogue of ANOVA (i.e. MANOVA) was utilised. The analysis was done on the ion ratios measured for a fixed concentration of colchicine corresponding to the concentration at the centroid of the calibration model (2.38 ppm). For the MANOVA F-test, a significance level of $\alpha = 0.003$ was used. The MANOVA-analysis was performed via the IBM® SPSS® Statistics (version 26) software suite.

In the generated output results for urine samples, a Wilk's lambda (Λ) value of 0.073 was calculated for the ion ratios measured at the centroid concentration of colchicine. This Wilks' lambda value corresponded to a calculated F-value of 0.897. At a significance level of $\alpha = 0.003$, the critical F-value was 332.67, which is larger than the calculated F-value for Wilks' lambda. Thus, there is no significant contribution of variance from the between-batch variation to the total variance that cannot be accounted for by inherent random error.

The ion ratios, recorded for 2.38 ppm colchicine in de-ionised aqueous solution, were similarly evaluated and the Wilks' lambda calculated to be 0.173, with an associated F-value of 0.47. At the same significance level of $\alpha = 0.003$ the critical F-value, $F_2^6(\alpha = 0.003) = 332.67$, was greater than the calculated value, thus, the between-batch variation does not significantly contribute to the total variance between the ion ratios at this fixed concentration.

From these MANOVA results it followed that in either matrix the ion ratios can be obtained repeatably between samples spiked to the centroid concentration of colchicine. A more in-depth inspection of the ion ratios was also done by evaluating the %-RSD values associated with the variance of the measured vectors of ratios about the mean vector over all concentration levels.

Comparing the %-RSD's for the two matrices provided information on the precision in the ion ratios across concentration levels. The comparison showed the relative variation in the respective ion ratios over the range of theoretical concentrations at which the samples were spiked. From these %-RSD values it was observed that there was better precision in the measured ion ratios for the samples in de-ionised aqueous solutions than for the urine samples in ion ratios IR1 to IR3. In IR4 and IR5 the precision of qualitative analysis was greater in the case of urine samples, than in the case of the de-ionised aqueous samples. The greater precision in the analysis of the de-ionised aqueous samples is expected since the loss of precision in the measurement of the ratios for urine samples could be attributed to the signal contribution of the matrix components in urine at the same relative retention time as colchicine.

Table III-13. %-RSD values computed for the variation of the respective ion ratios of colchicine over the concentration range.

Ratio	%-RSD (H₂O)	%-RSD (Urine)
IR 1	10.30	14.65
IR 2	14.01	20.03
IR 3	10.85	11.37
IR 4	10.50	7.987
IR 5	24.12	8.565

4. Conclusion to Chapter III

In the study of colchicine (**7**) and its biological source, *Gloriosa superba*, a method was developed for the quantitative analysis of colchicine (**7**) in urine and, as for reference, de-ionised aqueous samples. The developed method was validated in both de-ionised water and urine to determine its applicability for routine sample analysis by GC-MS.

The calibration model for the urine samples was described by a calculated trendline with the equation $y = 0.278 \times x - 0.170$, with $s_b = 0.049 \text{ ppm}^{-1}$ and $s_a = 0.122$. Regression analysis indicated a significant product-moment correlation coefficient of 0.915. This calibration

model's detection limit was calculated from the standard deviation of the blank signal as 0.624 ppm with a standard deviation of 0.426 ppm.

Analysis of the y-residuals indicated that even though the data was closely correlated to the calculated trendline, a non-linear trend exists in the data. This observed curvature may have contributed to the increase in variance at low concentrations of colchicine (**7**). The %-RSD values calculated for the response model did, however, remained below the expected benchmark based on Horwitz's equation.

Validation of the ion ratios and their relationship to concentration showed that the positive identification of colchicine (**7**) from its ion ratios is valid at every concentration level of the calibration model. It was shown that these ion ratios can be reproduced across multiple batches of urine samples. The ion ratios were, further, successfully employed in estimating a detection limit based on positive identification, which is more robust than the theoretical estimation from the response model. This limit was estimated to be between 0.953 ppm and 1.43 ppm.

Drawbacks of the analytical method lie in the preparation of the samples for analysis by GC-MS. During the solid phase extraction of colchicine (**7**) and 5- α -cholestane from the urine samples, two separate elution steps, with different elution solvents, were used. This produced two different extraction efficiencies which might disrupt the ability of the internal standard (5- α -cholestane) to correct for analyte loss during extraction in the calculated relative responses. This negatively impacts the linearity, precision, and accuracy of the analytical method.

Further development of the method for the extraction of colchicine (**7**) from urine should be done. The application of liquid-liquid extraction with DCM from larger sample volumes and, as an alternative, the application of DCM as elution solvent for both colchicine (**7**) and 5- α -cholestane from the SPE-cartridges should be considered.

References

- (1) Van Wyk, B.-E., Van Heerden, F. & Van Oudtshoorn, B. 2014. *Gloriosa superba*. In: Ferreira, R. (ed.) *Poisonous plants of South Africa*. 1st ed. ed. Pretoria: Briza Publications, pp. 118-119.
- (2) Wink, M. & Van Wyk, B.-E. 2008. *Gloriosa superba*. In: Pearson, D. (ed.) *Mind-altering & Poisonous Plants of the World*. First ed. Pretoria: Briza Publications, pp. 133.

- (3) Rabbani, A. B., Parikh, R. V. & Rafique, A. M. 2020. Colchicine for the Treatment of Myocardial Injury in Patients With Coronavirus Disease 2019 (COVID-19)—An Old Drug With New Life? *JAMA Network Open*, 3, e2013556-e2013556.
- (4) Schlesinger, N., Firestein, B. L. & Brunetti, L. 2020. Colchicine in COVID-19: an Old Drug, New Use. *Current Pharmacology Reports*, 6, 137-145.
- (5) Corral, P., Corral, G. & Diaz, R. 2020. Colchicine and COVID-19. *Journal of clinical pharmacology*.
- (6) Hutchings, A., Scott, A. H., Lewis, G. & Cunningham, A. B. 1996. *Gloriosa superba L. Zulu Medicinal Plants - An Inventory*. South Africa: University of Natal Press, pp. 26.
- (7) Bayer, F. & Lebzelter, V. 1927. Treatment of Barrennes and Venereal Diseases Amongst the Zulus. *Anthropos*, 287-289.
- (8) Ashokkumar, K. 2015. *Gloriosa superba (L.): a brief review of its phytochemical properties and pharmacology*. *International Journal of Pharmacognosy and Phytochemical Research*, 7, 1190-1193.
- (9) Neuwinger, H. D. 1996. *Gloriosa superba Linné. African Ethnobotany - Poisons and Drugs*. Weinheim: Chapman & Hall GmbH, pp. 554-561.
- (10) Haerdi, F. 1964. The Indigenous Medicinal Plants of Ulanga District, Tanzania, East Africa. *Acta Tropica*, 1-278.
- (11) Mendis, S. 1989. Colchicine cardiotoxicity following ingestion of *Gloriosa superba* tubers. *Postgraduate medical journal*, 65, 752-755.
- (12) Moser, V., Aschner, M., Richardson, R. & Philbert, M. 2008. Toxic Responses of the Nervous System. In: Klaassen, C. D. (ed.) *Casarett and Doull's Toxicology - The Basic Science of Poisons*. 7 ed. New York: The McGraw-Hill Companies Inc., pp. 631-664.
- (13) Jones, G. R., Singer, P. P. & Bannach, B. 2002. Application of LC-MS Analysis to a Colchicine Fatality. *Journal of analytical toxicology*, 26, 365-369.
- (14) Miller, M. A., Hung, Y.-M., Haller, C., Galbo, M. & Levsky, M. E. 2005. Colchicine-related death presenting as an unknown case of multiple organ failure. *The Journal of emergency medicine*, 28, 445-448.
- (15) Milne, S. T. & Meek, P. D. 1998. Fatal colchicine overdose: Report of a case and review of the literature. *The American journal of emergency medicine*, 16, 603-608.
- (16) Folpini, A. & Furfori, P. 1995. Colchicine Toxicity Clinical Features and Treatment. Massive Overdose Case Report. *Journal of Toxicology: Clinical Toxicology*, 33, 71-77.
- (17) Gunasekaran, K., Mathew, D. E., Sudarsan, T. I. & Iyyadurai, R. 2019. Fatal colchicine intoxication by ingestion of *Gloriosa superba* tubers. *BMJ Case Reports*, 12, e228718.
- (18) Peranatham, S., Manigandan, G. & Shanmugam, K. 2014. Fatal *Gloriosa superba* poisoning—a case report. *Int J Med Pharm Sci*, 4.
- (19) Brvar, M., Koželj, G., Možina, M. & Bunc, M. 2004. Acute poisoning with autumn crocus (*Colchicum autumnale L.*). *Wiener Klinische Wochenschrift*, 116, 205-208.

- (20) Ndhkala, A. R., Ncube, B., Okem, A., Mulaudzi, R. B. & Van Staden, J. 2013. Toxicology of some important medicinal plants in southern Africa. *Food and Chemical Toxicology*, 62, 609-621.
- (21) Joshi, C. S., Priya, E. S. & Mathela, C. S. 2010. Isolation and anti-inflammatory activity of colchicinoids from *Gloriosa superba* seeds. *Pharmaceutical biology*, 48, 206-209.
- (22) Ntahomvukiye, D., Hakizimana, A. & Nkiliza, J. 1984. Dosage de la colchicine dans le *Gloriosa simplex* L. (liliacées) du Rwanda (Afrique Centrale). *Plantes medicinales et phytotherapie*, 18, 24-27.
- (23) Merchant, J. & Joshi, V. 1976. Chemical constituents of *Gloriosa superba* Linn.(Liliaceae). *Indian Journal of Chemistry B*, 14, 908.
- (24) Pubchem. 2020. *Colchicine* [Online]. Bethesda: National Center for Biotechnology Information. Available: <https://pubchem.ncbi.nlm.nih.gov/compound/6167> [Accessed 2020-08-28].
- (25) Dvoráčková, S., Sedmera, P., Potěšilová, H., Šantavý, F. & Šimánek, V. 1984. Alkaloids of *Gloriosa superba* L. *Collection of Czechoslovak chemical communications*, 49, 1536-1542.
- (26) Chapman, O., Smith, H. & King, R. 1963. The structure of α -lumicolchicine: Some examples of diamagnetic shielding by the carbon-oxygen double bond. *Journal of the American Chemical Society*, 85, 806-812.
- (27) Chapman, O. L., Smith, H. G. & King, R. W. 1963. The Structure of β -Lumicolchicine. *Journal of the American Chemical Society*, 85, 803-806.
- (28) Gardner, P. D., Brandon, R. L. & Haynes, G. R. 1957. The Structures of β - and γ -Lumicolchicine. Ring-D Elaboration Products. *Journal of the American Chemical Society*, 79, 6334-6337.
- (29) Fernando, R. & Fernando, D. 1990. Poisoning with plants and mushrooms in Sri Lanka: a retrospective hospital based study. *Veterinary and human toxicology*, 32, 579-581.
- (30) Leung, Y. Y., Hui, L. L. Y. & Kraus, V. B. Colchicine—Update on mechanisms of action and therapeutic uses. *Seminars in arthritis and rheumatism*, 2015. Elsevier, 341-350.
- (31) Wink, M. & Van Wyk, B.-E. 2008. Main classes of toxins and psychoactive compounds. In: Pearson, D. (ed.) *Mind-altering & Poisonous Plants of the World*. First ed. Pretoria: Briza Publications, pp. 252-337.
- (32) Raven, P., Johnson, G., Mason, K., Losos, J. & Singer, S. 2014. The Cytoskeleton. *Biology*. 10th ed. New York: The McGraw-Hill Companies Inc., pp. 75-79.
- (33) Grosser, T., Smyth, E. & Fitzgerald, G. A. 2011. Pharmacotherapy of Gout. In: Brunton, L. L., Chabner, B. A. & Knollmann, B. C. (eds.) *Goodman & Gilman's The Pharmacological Basis of Therapeutics*. 12 ed. New York: The McGraw-Hill Companies Inc., pp. 994-1004.
- (34) Dalbeth, N., Lauterio, T. J. & Wolfe, H. R. 2014. Mechanism of Action of Colchicine in the Treatment of Gout. *Clinical Therapeutics*, 36, 1465-1479.
- (35) Raven, P., Johnson, G., Mason, K., Losos, J. & Singer, S. 2014. The Endomembrane System. *Biology*. 10th ed. New York: The McGraw-Hill Companies Inc., pp. 69-73.
- (36) Clevenger, C. V., August, T. F. & Shaw, L. M. 1991. Colchicine Poisoning: Report of a Fatal Case with Body Fluid Analysis by GC/MS and Histopathologic Examination of Postmortem Tissues. *Journal of analytical toxicology*, 15, 151-154.

- (37) Lewis Sr., R. J. 2004. Colchicine. *Sax's Dangerous Properties of Industrial Materials*. 11 ed. New Jersey: John Wiley & Sons, Inc., pp. 982-983.
- (38) Jaeger, A., Flesch, F., Sauder, P. & Kopferschmitt, J. 1989. *Colchicine* [Online]. Strasbourg: International Programme on Chemical Safety. Available: <http://www.inchem.org/documents/pims/pharm/colchic.htm#SubSectionTitle:7.1.1%20%20Toxicodynamics> [Accessed 2020-04-14].
- (39) Hall, J. E. & Guyton, A. C. 2011. Diuretics, Kidney Diseases. In: Gruliow, R. (ed.) *Guyton and Hall Textbook of Medical Physiology*. 12 ed. Philadelphia: Saunders, Elsevier Inc., pp. 397-410.
- (40) Walaszek, E., Kocsis, J., Leroy, G. & Geiling, E. 1960. Studies on the excretion of radioactive colchicine. *Archives internationales de Pharmacodynamie et de Therapie*, 125, 371-382.
- (41) Finkelstein, Y., Aks, S. E., Hutson, J. R., Juurlink, D. N., Nguyen, P., Dubnov-Raz, G., Pollak, U., Koren, G. & Bentur, Y. 2010. Colchicine poisoning: the dark side of an ancient drug. *Clinical Toxicology*, 48, 407-414.
- (42) Xu, L., Adams, B., Jeliaskova-Mecheva, V. V., Trimble, L., Kwei, G. & Harsch, A. 2008. Identification of novel metabolites of colchicine in rat bile facilitated by enhanced online radiometric detection. *Drug metabolism and disposition*, 36, 731-739.
- (43) Naidus, R. M., Rodvien, R. & Mielke, C. H. 1977. Colchicine toxicity: a multisystem disease. *Archives of internal medicine*, 137, 394-396.
- (44) Niel, E. & Scherrmann, J.-M. 2006. Colchicine today. *Joint Bone Spine*, 73, 672-678.
- (45) Abe, E., Lemaire-Hurtel, A.-S., Duverneuil, C., Etting, I., Guillot, E., De Mazancourt, P. & Alvarez, J.-C. 2006. A Novel LC-ESI-MS-MS Method for Sensitive Quantification of Colchicine in Human Plasma: Application to Two Case Reports. *Journal of analytical toxicology*, 30, 210-215.
- (46) Samanidou, V. F., Sarantis, G. A. & Papadoyannis, I. N. 2006. Development and Validation of a Rapid HPLC Method for the Direct Determination of Colchicine in Pharmaceuticals and Biological Fluids. *Journal of Liquid Chromatography & Related Technologies*, 29, 1-13.
- (47) Theofel, N., Vejmelka, E., Tsokos, M. & Scholtis, S. What are the benefits of screening urine by means of LC-QTOF-MS/MS? A case report on colchicine.
- (48) Schreiber, L., Morovič, M., Špacayová, K. & Halko, R. 2019. Colchicine Extract Suicidal Lethal Poisoning Confirmation Using High-Resolution Accurate Mass Spectrometry: A Case Study. *Journal of forensic sciences*, 64, 1274-1280.
- (49) 2007. Dictionary of Natural Products. Boca Raton: Chapman and Hall/CRC.
- (50) European Commission: Directorate General for Health and Food Safety. 2020. *SANTE/12682/2019: Guidance document on analytical quality control and method validation procedures for pesticide residues analysis in food and feed*. European Commission: Directorate General for Health and Food Safety. Available: https://ec.europa.eu/food/sites/food/files/plant/docs/pesticides_mrl_guidelines_wrkdoc_2017-11813.pdf [Accessed 2020-08-26].
- (51) Kurek, J., Bartkowiak, G. & Nowakowska, Z. 2015. Mass spectrometric study of colchicine and its synthetic derivatives 10-alkylthiocolchicines. *Acta Chimica Slovenica*, 62, 605-616.

- (52) Center for Drug Evaluation and Research. 1996. *Guidance for Industry - Q2B Validation of Analytical Procedures: Methodology*. Rockville: Center for Drug Evaluation and Research. Available:
https://ec.europa.eu/food/sites/food/files/plant/docs/pesticides_mrl_guidelines_wrkdoc_2017-11813.pdf [Accessed 2020-08-26].
- (53) Rivera, C. & Rodríguez, R. 2014. Horwitz equation as quality benchmark in ISO/IEC 17025 testing laboratory. *Private communication*.
- (54) Massart, D. L., Smeyers-Verbeke, J. & Heyden, Y. 2005. Benchmarking for analytical Methods: The Horwitz curve. *LC GC Europe*, 18, 528-531.
- (55) Miller, J. N. & Miller, J. C. 2010. The quality of analytical measurements. *Statistics and Chemometrics for Analytical Chemistry*. 6th ed. Essex: Pearson Education Limited, pp. 74-109.

Chapter IV

Acokanthera oppositifolia (Lamarck)
Codd

1. Introduction to *Acokanthera oppositifolia* and acovenoside A

1.1 Ethnobotanical applications of *Acokanthera oppositifolia*

The ethnopharmacological application of, *A. oppositifolia* is in two main forms: as a decoction (or tea) made from the leaves and wood, or as dried wood, leaves and roots that are milled to a powder.¹⁻³ The decoctions are administered orally and produce a strong emetic effect. It is used for treating snakebites⁴, anthrax infections, intestinal worms,¹ excessive menstruation,^{5,6} abdominal pain,⁷ and septicaemia¹. The second is the milled plant material is applied topically to treat toothache⁸ or used as snuff to relieve headaches.⁹

A. oppositifolia is well known as the source of potent poisons applied to arrows used in hunting. It has been implicated in cases of homicide where prickly seeds are coated with the hunting poison and sowed on the paths where the victims walk.^{1,9-11}

1.2 Applications of acovenoside A in modern medicine

The application of *A. oppositifolia* as a hunting poison led Saeed et al.¹² to consider its primary constituent, acovenoside A (**22**) in their study of South African phytochemicals with anti-cancer activity. Their work indicated that acovenoside A (**22**) showed cytotoxic activity against various human cancer cell lines and inhibited the growth of both drug sensitive and multi drug resistant (MDR) tumours to a considerable extent, *in vitro*.¹²

In a study by El Gaafary et al.¹³, acovenoside A (**22**) was shown to be effective in inhibiting the growth of non-small-cell lung cancer (NSCLC) *in vitro*. NSCLC accounts for ~85% of lung cancer cases and is notoriously drug resistant. In this study, they found acovenoside A to be more selective in targeting cancer cells than targeting the surrounding tissue and mononuclear blood cells.¹³ The exceptional selectivity of acovenoside A (**22**) towards targeting NSCLC tumours and inhibiting tumor growth more effectively *in vitro*, than doxorubicin, a known anti-neoplastic agent, makes acovenoside A (**22**) an attractive option for further investigation as anti-cancer drug.^{13,14}

1.3 Occurrence of *A. oppositifolia* poisoning

Overdosage with the traditional remedies prepared from *Acokanthera* spp. can easily occur¹⁵ and have been mentioned by both Neuwinger¹ and Bethwell¹⁶ as causing death of patients in East Africa. They also mentioned intentional overdosing with *A. oppositifolia* extracts to commit suicide and homicide.^{1,16,17} Accidental poisoning and death has followed after the use of wood from *A. oppositifolia* as meat-skewers or firewood for cooking, as seen in cases of

accidental *Nerium oleander* poisoning.^{9,16} Accidental poisoning has occurred in children eating unripe fruit from the trees.^{4,16} Sometimes the ripe fruit also retain enough toxicity to be harmful.⁹

Even though deaths amongst cattle related to *A. oppositifolia* is thought to be uncommon, it does occur.¹⁸ As in the case of many poisonous plants of sub-Saharan Africa, *A. oppositifolia*'s evergreen and frost-resistant nature may draw the attention of livestock during winter and early spring.¹⁹ Livestock are more prone to eat the poisonous leaves during this period since there is little to no green feed during this period. During times of drought, the animals may also be drawn to eating these plants if no other feed is immediately available.²⁰

1.4 Toxic chemical constituents of *A. oppositifolia*

A. oppositifolia's potent toxicity originates from its multiple cardenolide glycoside constituents. The most abundant of which is acovenoside A (**22**), followed by acolongifloroside K (**23**) (see **Figure IV-3**).^{14,16,21} Other cardenolides known to be present in *A. oppositifolia* are acobioside A, acospectoside A, acovenoside C, acofrioside L, opposide and ouabain. The relative abundances of these cardenolides have been observed to differ based on differences of geographical location in habitat.^{11,16}

Cardenolide aglycones are recognised by the five-membered lactone ring and steroid hydrocarbon skeletons. At C-3 (**Figure IV-1**), β -oriented glycosidic bonds are formed with mono- or oligosaccharides. In the glycosidic form, cardenolides have both lipophilic and hydrophilic character, allowing distribution of the glycosides across lipid membranes and throughout the bloodstream.²²

Cardenolide toxicity is highly dependent on molecular conformation and the saturation of the lactone functionality. For the glycoside to show significant cardiotoxicity, the lactone must be unsaturated in the C-20/C-22 bond (**Figure IV-1** and **Figure IV-2**) and have a U-shaped conformation of the steroid skeleton.

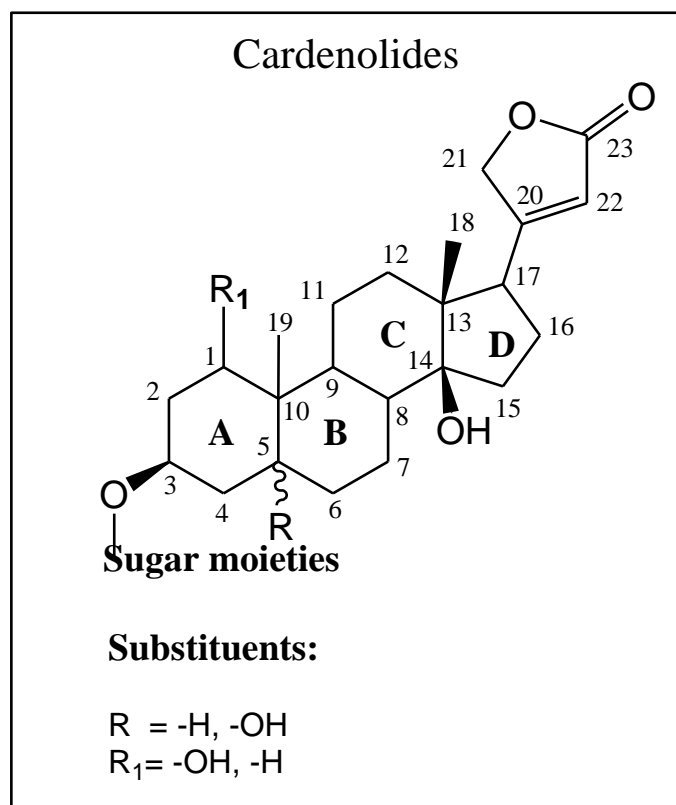


Figure IV-1. General structural definition of cardenolides.^{14,23-25}

The U-shaped conformation is obtained when the carbon-carbon bonds in ring B, that originate on ring A, are *cis* with respect to each other, and likewise in the case of the bonds from ring C to D ((II) in **Figure IV-2**). The flat conformation obtained when the bonds from ring A and B *trans* with respect to each other, remains cardioactive. However it has a lower bioavailability and is not often seen amongst the cardenolides ((I) in **Figure IV-2**). If the bonds, of ring C and ring D are *trans* with respect to each other, the cardenolide is expected to show no cardiotoxicity.²⁵⁻²⁹

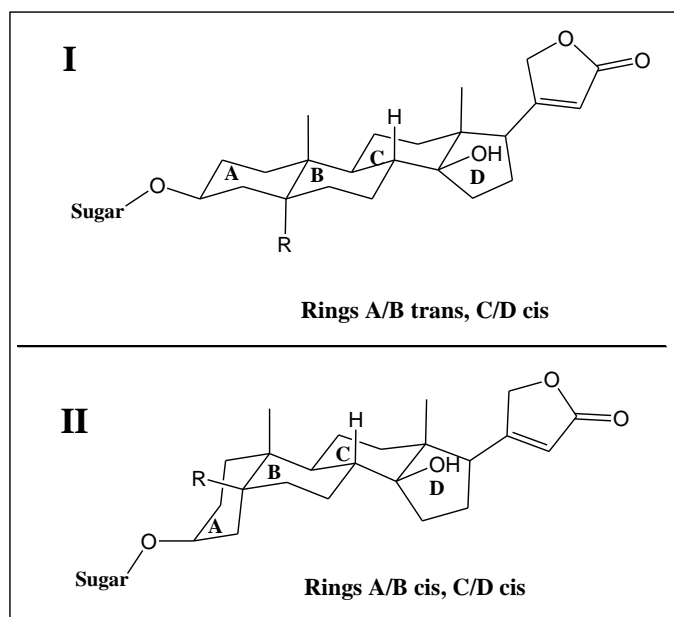


Figure IV-2. General chair conformational structures of cardiotoxic cardenolides. For acovenoside A, $R = H$.²⁵⁻²⁸

A further requirement for the cardiotoxicity of steroid glycosides is the presence of a β -oriented hydroxyl functional group on both C-3 (in the aglycone) and C-14.³⁰ Dehydration at the C-14 position is very probable under strong acidic conditions combined with a source of heating, due to the tertiary nature of the hydroxyl group at this position.³¹

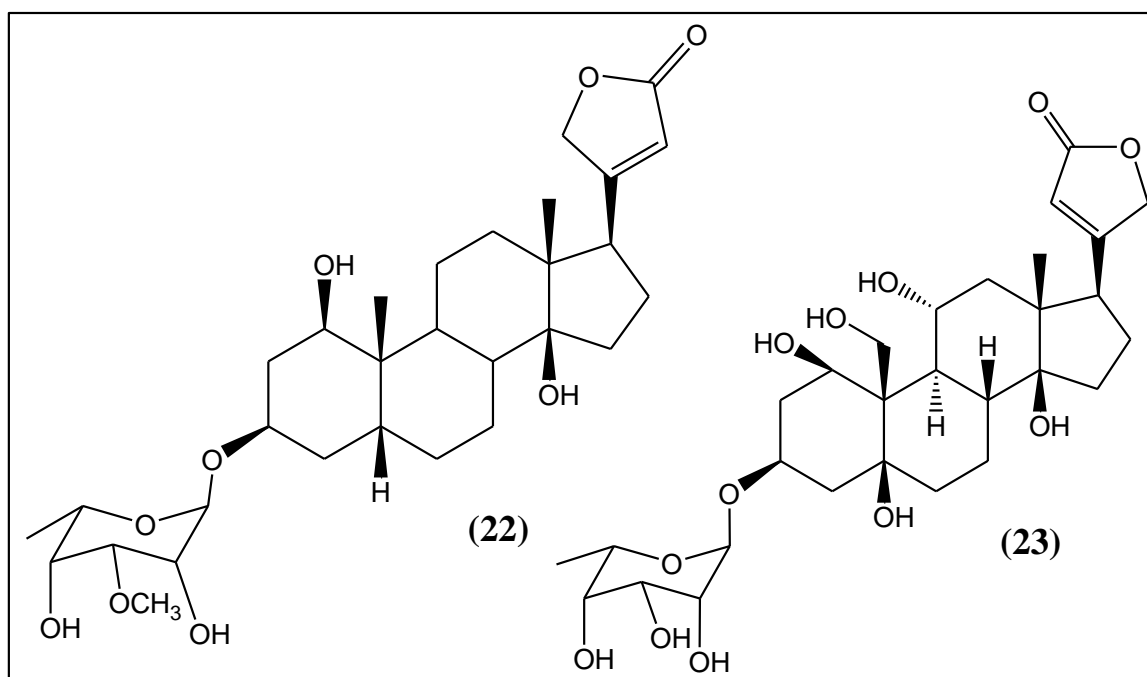


Figure IV-3. Two prominent chemical constituents of *A. oppositifolia*: acovenoside A (22), acolongifloriside K (23).^{1,21}

1.5 The physiological actions of cardiac glycosides

Cardiac glycosides primarily affect the heart muscle cells by inducing a positive inotropic effect. The effect is produced by the inhibition of the cells' Na^+/K^+ -ATPase pumps, thereby interfering with the ability of a cell to regulate its membrane potential.³²⁻³⁴ Inhibition of Na^+/K^+ -ATPase increases both the intracellular sodium ion concentration and the extracellular potassium ion concentration. Increasing the intracellular sodium ion level, induces the release of calcium ions from the sarcoplasmic reticulum and T-tubules and stimulates the atrial and ventricular contractions of the heart muscle.^{33,35-37} Due to the initial build-up of intracellular sodium ions, the re-uptake of calcium ions via the $\text{Na}^+/\text{Ca}^{2+}$ -exchange channel cannot be accomplished, producing an elongated spastic contraction of the heart muscle.^{34,36,38,39}

Following this spasmic elongated contraction of the atria, a premature contraction of the ventricles may occur, thereby decreasing the flow of oxygen rich blood to the body's extremities, causing muscle weakness.³³ Administration of toxic levels of cardiac glycosides induces an increased rate of contraction in the ventricles, which may develop to ventricular fibrillation and subsequent cardiac arrest.^{36,40}

Oral consumption of cardiac glycosides may produce an emetic effect. This effect is likely the result of a positive inotropic effect on the gastrointestinal tract, produced by the cardiac glycosides.⁴⁰ Cardiac glycosides are often administered in ethnic medicine for this purpose. Administration of toxic doses may cause severe emesis and dehydration. At these levels, direct action of the cardiac glycosides on the sodium ion levels in the cone cells of the eye, influence the signalling of colour vision to the brain. As a result, individuals poisoned with a cardiac glycoside often report yellow tinted vision.^{39,41}

The primary component, of a cardiac glycoside molecule, that is responsible for binding at a receptor site on Na^+/K^+ -ATPase, is the steroid skeleton.⁴² Its stringent conformational requirements were described in Section 1.4 of this chapter. The lactone functionality is not the active pharmacophore, however, its saturation, and relative orientation to the steroid skeleton, significantly impacts the ability of the steroid skeleton to bind into the receptor site on Na^+/K^+ -ATPase.^{42,43}

1.6 Proposed metabolic pathways for acovenoside A

To date very little information exists on the metabolism of acovenoside A (**22**). Based on the known metabolic pathways observed for digoxin and digitoxin, both cardenolide glycosides similar in mode of action to acovenoside A (**22**), possible pathways for acovenoside A (**22**) can

be considered. The metabolism of acovenoside A (**22**) is relevant since it can provide guidance to the identification of biomarkers linked with the use of acovenoside A (**22**) for various purposes. To confirm the presence of expected metabolites, case studies would be required wherein the physiological material (blood, stomach contents, bile, etc.) of the participants are chemically analysed.

Digoxin, when administered *per os* as a tablet or solution, is first incubated in the stomach at 36-37 °C (normal body temperature).⁴⁴ Stomach acid, being an aqueous solution of salts and hydrochloric acid, can easily cause hydrolysis of the glycosidic bond, thereby producing the aglycone of the cardiac glycoside.^{45,46} Since the hydroxyl groups present on the steroid backbone are secondary hydroxyl groups, they can be eliminated in concentrated acidic solutions, such as stomach acid.³¹ The presence of multiple hydroxyl groups implies the possibility of multiple dehydration products forming. The dehydration of the aglycone also plays an important role in sample preparation methods (Section 2 of this chapter).

Once absorbed into the vascular system, either as glycoside or aglycone, the cardiotoxin is transported to multiple metabolic centres, most importantly, the liver. Digoxin was found to undergo two main routes of metabolism: (1) hydrogenation to dihydrodigoxin and (2) sequential loss of the sugar moieties in its polysaccharide chain attached to C-3 (**Figure IV-1**).^{34,46}

Following on from the above metabolic processes, hepatic metabolism occurs rapidly via the enzymes UDP-glucuronyltransferase and sulfotransferase to produce the *O*-glucuronide and sulphate conjugates.^{34,47} In the event of enterohepatic recirculation, the *O*-glucuronide can be deconjugated with β -glucuronidase in the gut following excretion into the bile. The aglycone can be catabolised to a ketone via alcohol dehydrogenase in the liver to form the corresponding C3-ketone.⁴⁷ This metabolic action was recorded to decrease the cardiac activity of the aglycones by 90%. Conversion of this C3-ketone to an α -hydroxyl group completely inhibits cardiac activity.^{30,47}

A hypothetical metabolic profile can be suggested for acovenoside A (**22**) based on the known metabolic pathways of digoxin and digitoxin (see **Figure IV-4**). Confirmation of this requires *in vivo* case studies where physiological fluid and hepatic tissue from poisoned humans or animals are analysed.

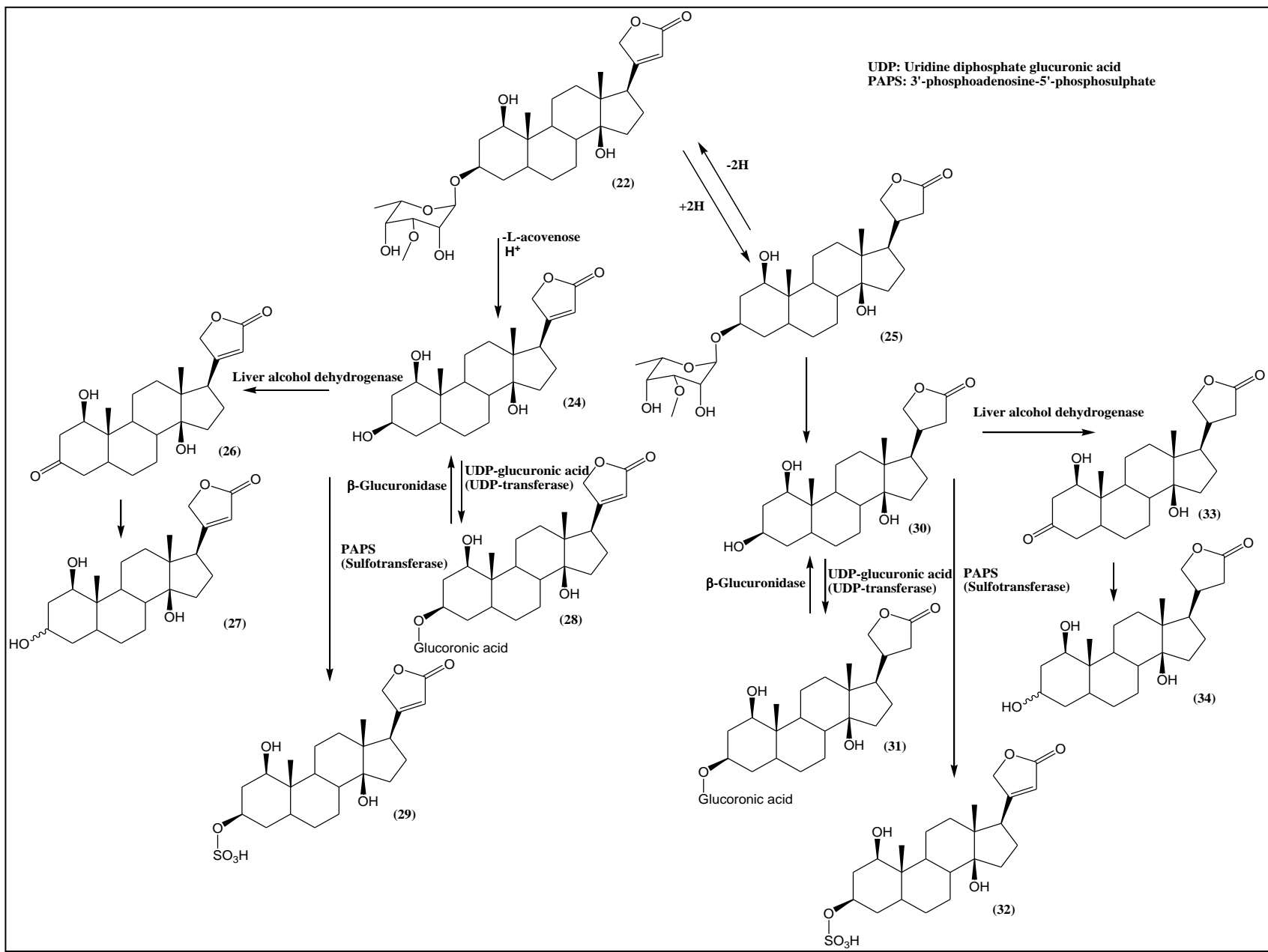


Figure IV-4. Proposed metabolic pathways for Acovenoside A.

1.7 Detection of cardenolides

Very little information specific to the detection of cardiac glycosides from *A. oppositifolia* in physiological fluids, is available. Most research on the detection of cardenolides is aimed at quantifying digoxin, digitoxin (*Digitalis purpurea*), oleandrin (*Nerium oleander*) and thevetin A and B (*Thevetia peruviana*).⁴⁸⁻⁵¹

1.7.1 Radioimmuno assay

In most cases of quantitative analysis for cardenolides in physiological fluids or aqueous solutions, radioimmuno assays are employed. According to Guan et al.⁵² the RIA-technique is the most sensitive in detecting cardiac glycosides in physiological samples. RIA has been shown to be capable of detecting cardiac glycosides at concentrations as low as 0.8 ng/mL in blood, 10 ng/mL in urine and 2.1 ng/mL in serum.⁵³⁻⁵⁵

RIA-techniques are not, however, selective to a specific cardenolide.^{52,56} In the process of analysing blood samples, glycoside concentrations may increase due to the haemolytic effect of the assay.⁵⁷ This drawback facilitates research in LC-MS and GC-MS analysis of physiological samples for cardiac glycosides.

1.7.2 Liquid chromatography – Mass spectrometry

As an alternative to RIA-techniques, liquid chromatography-mass spectrometry (LC-MS) techniques are employed in the analysis of physiological fluids for the quantification of cardiac glycosides. Most of these methods use solid phase extraction (SPE) to decrease the abundance of matrix components in the samples.⁵⁸ The lipophilic steroid skeleton of cardiac glycosides make the use of non-polar and lipophilic-hydrophilic balanced SPE-sorbent modifiers popular for sample preparation.^{48,52,58}

Multiple methods have been developed for the quantitative analysis of cardiac glycosides in physiological fluids by LC-MS. In most of the methods, tandem mass spectrometry is used to detect the eluted analytes. LC-MS methods, for the analysis of urine samples, were observed to have very low limits of detection and quantification. An HPLC-MS method developed by Frommhertz et al.⁵⁹ for the analysis of cardiac glycosides in urine samples, had a limit of detection equal to 0.1 ng/mL and a limit of quantification equal to 0.2 ng/mL.⁵⁹ Guan et al.'s HPLC-MS/MS method⁵² for detecting cardiac glycosides in urine samples, had a higher limit of detection equal to 1 ng/mL.

Methods for the detection and quantification of cardiac glycosides in whole blood, serum and plasma have also been developed. These methods, using of LC-MS/MS systems for analysis, have limits of detection ranging from 0.09 mg/mL to 2 ng/mL.^{58,60} In contrast to the more frequently used SPE-systems in sample preparation, Øiestad et al.⁶¹ used liquid-liquid extraction for sample preparation in the quantitative analysis of cardiac glycosides in whole blood.⁶¹

1.7.3 Gas chromatography – Mass Spectrometry

Gas chromatography-mass spectrometry analysis of cardiac glycosides has not drawn as much attention as the use of LC-MS for this purpose. For this reason, few methods have been developed for the quantitative analysis of cardiac glycosides in physiological fluids. The methods that have been developed are not unlike those employed for the GC-MS analysis of steroids. There are, however, a few differences between the sample preparation methods. Notably, the process, by which the glycosides are deconjugated from the attached sugar groups, uses acidic hydrolysis and not enzyme catalysed hydrolysis, as in the case of steroid analysis.

Chemical hydrolysis of the glycosidic bonds

In chemical hydrolysis the glycosidic bonds are broken by hydrolysis reactions with strong acids. There are benefits to this approach in that the acid is not selective to a specific sugar group and it cleaves all glycosidic bonds in oligosaccharides.⁶² A disadvantage of hydrolysing the glycosidic bonds under strong acidic conditions is the possible dehydration of the aglycone. This can negatively impact selectivity when multiple cardiac glycosides with similar aglycones need to be analysed simultaneously.⁵⁰

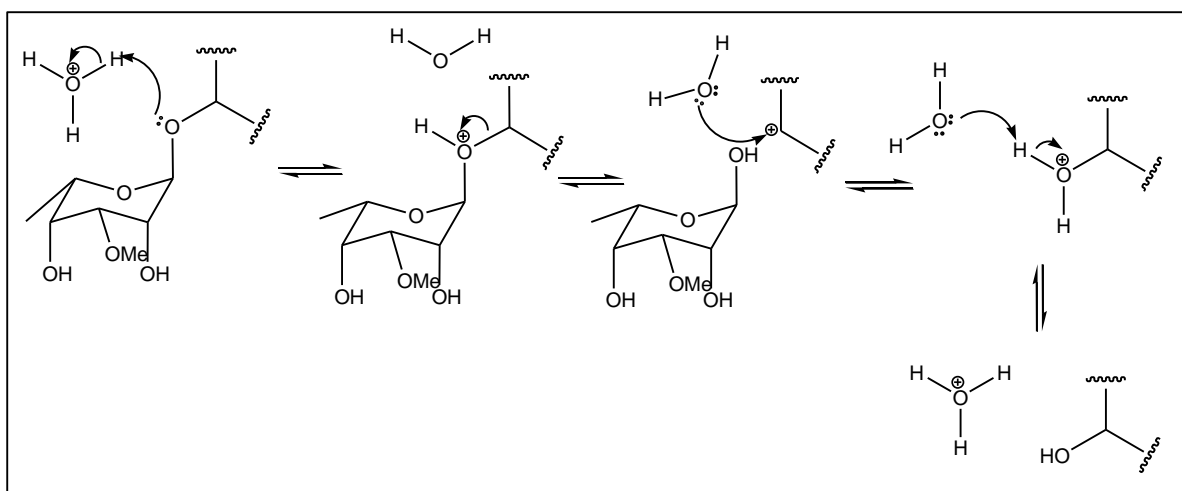


Figure IV-5. Mechanism proposed for the acidic hydrolysis of a glycosidic bond.

Methods for the derivatisation of aglycones

Similarities between the methods include the use of SPE to extract the conjugated analytes from the physiological fluid and silylation to derivatise the hydrolysis products for GC-MS analysis. Different reagents and processes were reported in literature for the silylation of steroids and cardiac glycosides. A frequently used reagent for the silylation of steroids and cardiac glycosides is *N*-methyl-*N*-(trimethylsilyl)trifluoroacetamide (MSTFA).^{50,63} Other silylation reagents used include trimethylsilyl imidazole (TMSI) and *N,O*-bistrifluoroacetamide (BSTFA).^{64,65}

In addition to silylation, acetylation and fluorination are also viable options. Knapp⁶⁶ describes the fluorination of digoxin with heptafluorobutyric anhydride (HFBA)/benzene in a 1:10 (v/v) ratio or alternatively with trifluoroacetic anhydride (TFAA)/lithium aluminium hydride (LiAlH₄)/hydrochloric acid (1 M).

1.7.4 Liquid chromatography-Diode array detection

The hyphenation of HPLC with a photodiode array detector is a frequently encountered analytical system in a chemical laboratory. The conjugated lactone groups of cardiac glycosides make the application of online-PDA detection in HPLC suitable in the quantification of these glycosides in samples. To enhance the sensitivity of HPLC-DAD detection of cardiac glycoside, derivatisation with strong chromophore-containing groups can be performed. Following derivatisation with a chromophore, levels as low as 5 ng/mL of digoxin was detected in urine.⁶⁷ A drawback of diode array detection is that without suitable reference standards, identification of a specific cardiac glycoside is not possible.¹⁸

2. Experimental methods

2.1 Reagents and chemicals utilised in this chapter

Table IV- 1. List of reagents and chemicals utilised in the experimental work of this chapter.

Chemical	% Purity	Company	City [†]
5- α -Cholestane	99.9 (HPLC)	Sigma Life Sciences	St. Louis, USA
Acetic Acid	99.9 (GC)	Sigma-Aldrich Chemie GmbH	Schnelldorf, DEU
Acovenoside A	N/A*	Aldrich	St. Louis, USA
β -Glucuronidase from <i>Helix pomatia</i> (112173 units) [†]	99.2	Sigma-Aldrich Chemie GmbH	Schnelldorf, DEU

De-ionised water	20. Ω .m [‡]	Merck (Pty) Ltd	Modderfontein, ZA
Dichloromethane	≥ 99.8 (GC)	Merck KGaA	Darmstadt, DEU
Dichloromethane	>99	Radchem	Johannesburg, ZA
Disodium hydrogen orthophosphate dihydrate	≥ 99.5 (A)**	Merck (Pty) Ltd	Modderfontein, ZA
Ethyl acetate	99.9	Radchem	Johannesburg, ZA
Ethyl acetate	99.98 (GC)	Sigma-Aldrich Chemie GmbH	Schnelldorf, DEU
Formic acid	98.2	Sigma-Aldrich Chemie GmbH	Schnelldorf, DEU
Hydrochloric acid	32.7 (A)	Aldrich	St.Louis, USA
Isopropanol	99.99 (GC)	Sigma-Aldrich Chemie GmbH	Schnelldorf, DEU
Methanol	99.98 (GC)	Sigma-Aldrich Chemie GmbH	Schnelldorf, DEU
Methanol	99.9	Radchem	Johannesburg, ZA
Methanol	>99.9	ROMIL via Microsep	Johannesburg, ZA
MSTFA	99.2 (GC)	Sigma-Aldrich Chemie GmbH	Schnelldorf, DEU
n-Hexane	>98.0 (GC)	Merck KGaA	Darmstadt, DEU
n-Hexane	>99	Radchem	Johannesburg, ZA
Pyridine	99.99 (GC)	Sigma-Aldrich Chemie GmbH	Schnelldorf, DEU
Sodium Acetate	< 99 (A)	Merck (Pty) Ltd	Modderfontein, ZA
Sodium hydroxide	≥ 99.0 (A)	Merck (Pty) Ltd	Modderfontein, ZA
Sodium sulphate	≥ 99.0 (A)	Merck (Pty) Ltd	Modderfontein, ZA
Water	18 Ω .m	ROMIL via Microsep	Johannesburg, ZA

*The purity of acovenoside A was determined experimentally.

†The number β -glucuronidase enzymatic units per millilitre solution.

‡Resistivity assay: A resistivity of $\sim 18.5 \Omega$.m in water indicates the %-ionic content is near naught

**Acidimetric assay via acid/base titration

2.2 Preparation of crude extract from *A. oppositifolia*

Plant material (leaves) was sourced from the *A. oppositifolia* tree on the Hatfield Campus of the University of Pretoria and from the Faraday Muti Market (Johannesburg). The leaves were rinsed with tap water, dabbed dry with paper towels, and placed in the laboratory oven (40°C) until it was brittle enough for milling. A flowering specimen of the *A. oppositifolia* tree on campus was submitted to the H.G.W.J. Schweikerdt Herbarium on campus (UP) for identification.

The initial crude extract was developed by soaking the milled leaves (50. g of 69.869 g dry mass) in a DCM/methanol (1:1, 500 mL, Radchem[®]) extraction solvent for 24 h. The extract was filtered through Whatman Grade 1 filter paper in a Büchner-funnel under vacuum and transferred to a round-bottomed flask for rotary evaporation of the solvent. This process was repeated twice.

The extract was stored at ca. 8 °C in a cold room after complete drying until it was later de-fatted by liquid-liquid partitioning. The extract was solubilised in methanol (500 mL, Radchem[®]) and 150 mL distilled water. This solution was extracted three times with n-hexane (Radchem[®], 500 mL).

2.3 UPLC-qTOF MS analysis of extracts

For the UPLC-qTOF MS analysis, a sample of the extract (2.94 mg) was weighed into an Eppendorff[®] microcentrifuge tube (2.0 mL) and solubilised in methanol (ROMIL[®] Ultra I-grade Ultra-pure Solvent (UpS)[®], 1.5 mL). To aid in dissolving the crude sample, it was sonicated for ca. 30 min. The sample was then centrifuged in a Baygene[®] Micro Centrifuge (BG-Qspin[™]) for 5 min. The supernatant was transferred to a clear glass LC-vial (2.0 mL) and applied to the UPLC-qTOF MS system. This process was repeated for the analysis of the de-fatted extract (1.50 mg).

UPLC-qTOF MS analysis was performed via a Waters[®] Aquity[™] UPLC system, consisting of a binary solvent manager and a sample manager. The system was equipped with an Aquity[®] UPLC-column (2.1 × 100 mm) containing a BEH C18-type stationary phase (particle diameter = 1.7 µm). Detection and accurate mass analysis of the eluting analytes was performed with a Synapt[™] G2 High Definition Mass Spectrometry system, over a mass acquisition range of 50 to 1 200 Da. Ionisation and mass correction parameters were set as used in Chapter II. For chromatographic separation of the sample constituents, a binary solvent

system was utilised as mobile phase and the composition altered along a gradient (**Table IV-2**).

Table IV-2. Gradient solvent system applied as mobile phase in the UPLC-qTOF MS analysis of samples.

Time (min)	Flow rate (ml/min)	Percentage: dH₂O + 0.1% Formic acid	Percentage: MeOH + 0.1% Formic acid	Gradient type
Initial	0.300	97.0	3.0	Initial
0.10	0.300	97.0	3.0	Linear
14.00	0.300	0.0	100.0	Linear
16.00	0.300	0.0	100.0	Linear
16.50	0.300	97.0	3.0	Linear
20.00	0.300	97.0	3.0	Linear

2.4 UPLC-qTOF MS analysis of hydrolysed acovenoside A

Hydrolysis of the glycosidic bond in acovenoside A (**22**) was paramount in preparing the samples for analysis. The aglycone of acovenoside A, acovenosigenin (**24**), has a lower molecular weight and fewer active hydrogen atoms, making it more ideal for GC-MS analysis than the glycoside. During method development, three approaches to hydrolysis were considered: (1) enzymatic hydrolysis, (2) concentrated acid hydrolysis and, (3) diluted acidic hydrolysis. The effectiveness of the reactions was measured by UPLC-qTOF MS analysis of the underivatized products.

A blank sample was prepared identically to the sample prepared for enzymatic hydrolysis. Each sample, excluding the blank, was spiked with a few crystals of acovenoside A (**22**) (Aldrich[®]) and a pipette tip size sample of a mixture of cardiac glycosides from *Urginea sanguinea*, known *not* to contain cardiac glycosides present in *A. oppositifolia*.

Enzymatic hydrolysis was performed by suspending the cardiac glycosides in de-ionised water (Merck (Pty) Ltd, 500. µL), β-Glucuronidase (Sigma-Aldrich[®], 50.0 µL) and an acetate buffer (160.0 µL, 0.2 M, pH ~ 4.5). The suspension was vortex mixed and allowed to incubate at ~70 °C for three hours. The acetate buffer (0.2 M, pH ~ 4.5) was prepared by first dissolving sodium acetate (Merck (Pty) Ltd, 1.64091 g) in de-ionised water (100.00 mL). An aqueous solution of acetic acid (Sigma-Aldrich[®], 1.150 ml) was prepared in a volumetric flask

(100.00 ± 0.10 mL), and combined with the sodium acetate solution in a ratio of 1.2:1.3 (sodium acetate-acetic acid).⁶⁸

For the extraction of glycosides, SPE was used as described by Bekker.⁶⁸ The C₁₈-SPE cartridge (Agilent® BondElut® 6 mL, 500 mg sorbent with 40 µm particle diameter) was conditioned with HPLC-grade methanol (Sigma-Aldrich®, 6.00 mL) and then with 8.00 mL de-ionised water (Merck (Pty) Ltd). To facilitate the flow of the solvents through the cartridges, a small pressure differential (5" Hg) was applied. After conditioning, the sample was loaded onto the cartridge without the aid of a pressure differential. Once the sample was loaded, the cartridge was rinsed with de-ionised water (6.00 mL), aspirated through the cartridge with the aid of a pressure differential equal to 5" Hg. The vacuum was maintained until all the moisture was removed from the sorbent bed.⁶⁸

The C₁₈-cartridge was eluted with HPLC-grade ethyl acetate (Sigma-Aldrich®, 6.00 mL) through an aminopropyl cartridge (Agilent® BondElut®, 3 cc, 200 mg sorbent mass with 40 µm particle diameter) containing anhydrous sodium sulphate (Merck, (Pty.) Ltd., 0.5 g). The eluted solvent was dried at 40 °C under dry air in a drying block.⁶⁸ The sample was prepared for UPLC-qTOF MS analysis by reconstituting it in methanol (ROMIL UsP®, 1.000 mL) and sonicating it for 15 min. Any remaining precipitates were removed by centrifugation at 7 000 rpm with a Baygene® BG-Qspin™ Micro Centrifuge. The supernatant was filtered through an Agilent Technologies Nylon Econofilter (Diameter: 13 mm, Pore size: 0.2 µm) into a clear glass LC-vial (2 mL) for UPLC-qTOF MS analysis.

Under concentrated acidic conditions, the sample was incubated for 30 min in hydrochloric acid (250 µL, 6 M) at ~60 °C, as described by Kiouisi et al.⁵⁰ The glycosides were extracted from the hydrolysis solution via liquid-liquid extraction with n-hexane (Merck® KGaA, 4.000 mL). The organic phase was dried at 40 °C with the aid of dry compressed air, in a heating block.⁵⁰ The residue was prepared for UPLC-qTOF MS analysis in the same manner as the blank and enzymatic hydrolysis samples.

Hydrolysis, under diluted acidic conditions, was attempted by following Deber et al.'s method⁶⁴ for hydrolysing digoxin. The cardiac glycosides were incubated at 25 °C for 3 h in hydrochloric acid diluted with methanol (2.00 µL, 6 M HCl and 198.0 µL MeOH).⁶⁴ After incubation, the reaction was quenched with sodium hydroxide (200.0 µL, 0.006 M) and the sample diluted with de-ionised water (5.000 mL). To extract the products of the hydrolysis reaction, the diluted sample was loaded on an Agilent® BondElut® C₁₈-SPE cartridge, prepared

identically to those used for the blank and enzymatic hydrolysis samples. The analytes were eluted with two sequential additions of HPLC-grade methanol (Sigma-Aldrich[®], 1.000 mL), and dried in the heating block (40 °C) under a stream of dry air.⁶⁴ The residues were prepared for UPLC-qTOF MS analysis identically to the sample for enzymatic hydrolysis.

2.5 Analytical method for the analysis of urine samples for acovenoside A

2.5.1 Preparation of acovenoside A stock solution

A stock solution was prepared by weighing acovenoside A (**22**) (Aldrich[®], 19.98 mg) into a volumetric flask (10.00 ± 0.04 mL) and filling it to the mark with HPLC-grade methanol (Sigma-Aldrich[®]). The solution, of concentration 1.998 mg/mL, was homogenised by decanting and stored at -20 °C.

2.5.2 Preparation of internal standard stock solution

In this project, 5- α -cholestane (Sigma[®] Life Sciences) was used as internal standard. A stock solution was prepared in a volumetric flask (10.00 ± 0.04 mL) as follows: 5- α -cholestane (10.04 mg) was weighed into the volumetric flask and dissolved in HPLC-grade ethyl acetate (Sigma-Aldrich[®]). After dissolving the 5- α -cholestane, the flask was filled to the volumetric mark with ethyl acetate and homogenised by decanting and vortex mixing. The stock solution, with concentration 1.004 mg/mL, was transferred into 2 mL amber glass vials and stored at -20 °C.

2.5.3 Preparation of acetate buffer

For the preparation of 200.00 mL of a sodium acetate-acetic acid buffer (0.1 M, pH ~ 4.5), anhydrous sodium acetate (Merck[®] (Pty) Ltd, 8.2034 g) was weighed out, dissolved in de-ionised water (Merck[®] (Pty) Ltd) and quantitatively transferred to a volumetric flask (100.00 ± 0.10 mL). The flask was filled to the volumetric mark with de-ionised water, stoppered and decanted to homogenise the solution. Into a separate flask, acetic acid (Sigma-Aldrich[®], 5.742 mL) was measured, and the flask filled to the volumetric mark with de-ionised water (Merck[®] (Pty) Ltd). Following homogenisation by decanting, the contents of the flask were combined and homogenised, by shaking, to produce the buffer.

2.5.4 Preparation of the alkaline phosphate buffer

For the preparation of samples containing cardiac glycosides, the same phosphate buffer was utilised as described in Chapter II. Disodium hydrogen orthophosphate dihydrate (35.6 g) was weighed into a beaker and solubilised in de-ionised water (Merck[®] (Pty) Ltd, 80 mL) at 60 °C

with stirring. The solution was quantitatively transferred to a volumetric flask (250.00 ± 0.23 mL) and diluted to the calibration mark of the flask, with de-ionised water. After homogenisation, by shaking and decanting, the solution was transferred to a glass container and the pH adjusted to ~ 11.8 with aqueous sodium hydroxide (1.000 mL, 10 M).

2.5.5 *Initial sample preparation and extraction via SPE*

Each spiked sample was prepared by first aliquoting blank urine (24.00 mL) into the respective polypropylene urine collection cups. The volume of each sample was adjusted with blank urine, so that the total volume of the sample would be 25.00 mL following spiking with the of acovenoside A (**22**) stock solution (1.998 mg/mL). Each sample was also spiked with of 1.004 mg/mL internal standard stock solution (30.0 μ L, 1.004 mg/mL). In preparation for SPE, each sample was buffered to pH ~ 5 with acetate buffer (5.00 mL, 0.1 M, pH ~ 4.5).⁵⁰

For SPE, Agilent[®] C18 Bond-Elut (500 mg sorbent bed, 6 mL volume) cartridges were used. They were conditioned with methanol (Sigma-Aldrich[®], 4.00 mL) and equilibrated with de-ionised water (Merck[®], (Pty) Ltd, 8.00 mL) followed by the acetate buffer (3.00 mL, 0.1 M, pH ~ 4.5). During conditioning and equilibration, the solvents and buffer were directed through the cartridges with the aid of a Phenomenex[®] vacuum manifold set to a pressure differential of 5" Hg.^{50,69}

The samples were loaded onto the sorbent beds with the aid of a weak vacuum (≤ 1 " Hg) to maintain a flow rate of two to three drops per second. If necessary, the pressure differential was increased to maintain the flowrate.⁶⁹ Once the samples were loaded, the cartridges were rinsed with acetate buffer (4.00 mL, 0.1 M, pH ~ 4.5) with the aid of a 5" Hg pressure difference applied across the cartridge.⁵⁰ The vacuum was maintained to remove any buffer and solvent from the cartridge.⁶⁹ Elution of the acovenoside A (**22**) and 5- α -Cholestane was accomplished with a dichloromethane (Merck[®])-isopropanol (Merck[®]) extraction solvent (5.00 mL, 9:1 DCM-IP). During elution only a weak vacuum (≤ 1 " Hg) was applied to the manifold.

2.5.6 *Microwave assisted hydrolysis of eluted samples*

During elution, some of the water that remained behind on the sorbent eluted with the DCM-IP (9:1) extraction solvent. This water was removed by centrifuging the eluted samples for 10 min at 3 500 rpm and transferring the organic phase to a set of test tubes. After removing the water, the samples were dried at ~ 40.0 °C under a stream of dry compressed air, reconstituted in aqueous hydrochloric acid (500. μ L, 6 M) and homogenised via vortex mixing.⁵⁰ To hydrolyse the glycosidic bond in acovenoside A (**22**), the reconstituted samples were irradiated in a

microwave oven for three minutes at a 50% power setting (equivalent to 500 W). The irradiation process was followed by aliquoting hydrochloric acid (250. μL , 6 M) to each sample.

2.5.7 *Liquid-liquid extraction of analytes from the hydrolysis solution*

To extract 5- α -Cholestane and the hydrolysis products of acovenoside A (**22**) from the hydrolysis solution, the pH was adjusted to and maintained at ca. 11.⁵⁰ This was achieved by first adding the phosphate buffer (1.500 mL, 0.8 M, pH \sim 11.5) followed by aqueous sodium hydroxide (330. μL , 10 M). The samples were then vortex mixed for homogenisation before the final pH adjustment with an aqueous sodium hydroxide solution (10 M). The samples were vortex mixed again before extraction of the analytes.

The extraction of the analytes was accomplished by three repetitions of liquid-liquid extraction with an ethyl acetate/n-hexane solvent system (2.000 mL, 1:1). The ethyl acetate (Sigma-Aldrich[®]) and n-hexane (Merck[®]) were kept dry with 4 Å molecular sieve beads (Sigma-Aldrich[®], 8-12 mesh). After each addition of extraction solvent, the samples were vortex mixed and centrifuged at 3 500 rpm for 10 min. The organic phase of each sample was collected in its corresponding vial and dried at \sim 40.0 $^{\circ}\text{C}$ under a stream of dry air. Three replicates of this process were performed and the organic phases collected cumulatively.

2.5.8 *Microwave assisted silylation of analytes*

The derivatisation of the hydrolysis products of acovenoside A was accomplished by reconstituting the dried samples in pyridine (Sigma-Aldrich[®], 20.0 μL) and *N*-Methyl-*N*-(trimethylsilyl)-trifluoroacetamide (MSTFA, Sigma-Aldrich[®], 20.0 μL). The samples were vortex mixed and irradiated in a microwave oven for six minutes at a 50% power setting (equivalent to 500 W). Following derivatisation, the samples were vortex mixed and transferred to conical inserts in amber glass vials (2 mL) for GC-MS analysis.

2.5.9 *GC-MS analysis of derivatised samples*

Analysis by GC-MS was accomplished on an Agilent[®] Technologies 7890B GC System, coupled to a 7693 Autosampler and a 5973 Mass Selective Detector. For gas chromatographic separation of the analytes from the matrix components, a Phenomenex[®] ZB-5 MSi column, of length 15 m, internal diameter 0.25 mm, and a film thickness of 0.25 μm was utilised. The system temperature program was initiated at 180 $^{\circ}\text{C}$ (held for 3 min) followed by three temperature ramp stages: (1) 30 $^{\circ}\text{C}/\text{min}$ to 230 $^{\circ}\text{C}$ (held for 2 min), (2) 15 $^{\circ}\text{C}/\text{min}$ to 290 $^{\circ}\text{C}$

(held for 2 min), (3) 30 °C/min to 310 °C (held for 1.5 min). This program required a total run time of 14.33 min.

The sample was introduced into the system via a deactivated glass inlet liner heated to, and maintained at, 280 °C. To maintain the vapour phase of the sample components outside the GC-oven, the column was passed through a heated transfer line maintained at a temperature of 230 °C, into the ion source inlet. For electron impact (EI) ionisation, the primary beam of electrons was accelerated toward the stream eluting vapor from the GC-column, across a 70 V potential difference. The ions generated by the impact of high energy electrons with the eluting molecules in the source (heated to 230 °C), were accelerated toward the quadrupole mass analyser (heated to 150 °C) and selectively directed onto the detector.

In the scan mode the quadrupole mass analyser was set to scan across the range of $m/z = 50-800$ throughout the chromatographic analysis. Under selected ion mode conditions, the mass analyser was programmed to select only ions with $m/z = 149, 217, 357, \text{ and } 372$ from the start of the analysis, after the 2.5 min solvent front, to 6.50 min. After 6.50 min, the analyser switches to selecting the ions for the derivatised hydrolysis products of acovenoside A: $m/z = 147, 170, 183, 356, 573, \text{ and } 588$. At 9.60 min the selected ions were changed to $m/z = 169, 197, 211, 226, \text{ and } 348$, for the detection of the derivatised hydrolysis products of scillaren A. In each detection zone the analyser was set to dwell on a single m/z -ratio for 100 ms.

2.5.10 Approach in analysis of detected chromatograms

Data analysis was performed via an Agilent[®] MSD ChemStation[®] software package (version E.02.02.1431). The retention time of the detected chromatographic peaks were estimated as the local maximum, the apex, of the selected chromatographic peak and was calculated by the software. Chromatographic peaks were manually defined with the 'Manual intergration' tool of the software package. The peaks detected for silylated acovenoside A and 5- α -Cholestane were defined between the local minima adjacent to either side of the peak.⁷⁰

By manually defining a chromatographic signal, the software was instructed to disregard its built-in definitions of peak shape and properties within the defined regions. It, however, retains the threshold on a minimum signal area detected following integration of the defined regions. The retention time of the signal apex was determined based on the changes in signal slope and curvature. Where the slope passed through naught, following the inflection point of negative

curvature, and preceding the inflection point of positive curvature, the apex was defined and the retention time indicated.⁷⁰

2.6 Validation of the analytical method

The method was validated for the analysis of both aqueous (de-ionised) and urine samples by analysing three batches of samples for each matrix. Samples within a batch were spiked to sequentially higher concentrations of acovenoside A (**22**) (1.00, 1.20, 1.40, 1.60, 1.80 ppm ($\mu\text{g/mL}$)). Each sample was analysed in duplicate on the same GC-MS system to evaluate the variation in results produced by the instrumentation. The theoretical concentrations at which the samples were spiked assumed 100% purity in the sourced reference material.

To provide a reference point for comparison, the ideal case of a de-ionised aqueous matrix was also evaluated in the same manner on the same GC-MS system. For both sample matrices the linearity of the generated calibration models, and the method precision and accuracy were evaluated. As part of evaluating the calibration model linearity, the limits of detection and quantification were also calculated.

To validate the quality of measurement, the ion ratios in the electron impact mass spectrum of acovenoside A were also evaluated for precision and significant deviation from the centroid of the respective ratios, calculated at the centroid concentration in the calibration model. Ion ratios were evaluated by employing unbiased multivariate Gaussian statistical methods. The significance of deviation was determined via Hotelling's T^2 -test. From the concentration levels at which the measured ion ratios deviate significantly from the centroid, at the $\alpha = 0.003$ significance level, the limit of detection was estimated.

3. Results and discussion

For confirmation of the identity of the plant from which the material was collected, a flowering branch of the *A. oppositifolia* tree (indicated *A. venenata* on campus) was submitted as voucher specimen to the University of Pretoria's H.G.W.J Schweickerdt Herbarium. The voucher specimen was assigned the reference number PRU 126152.

3.1 UPLC-qTOF MS analysis of crude extracts from plant material

In the extract from the leaves of *A. oppositifolia*, six cardiac glycosides were detected in the negative ionisation mode with UPLC-MS/MS. The chromatogram and tentatively identified ions are shown in **Figure IV-6** and **Table IV-3**, respectively. Tentative identification of the analytes in the chromatogram was done based on accurate mass and elemental composition analyses.

To determine which peak likely corresponds to the formic acid adduct of acovenoside A (**22**), based on accurate mass, a chromatogram was extracted from chromatogram B for the selected mass 595.312 Da. This specific mass corresponds to the theoretical mass of the formic acid adduct ($[M-H+FA]^-$) of acovenoside A. The extracted ion chromatogram (A in **Figure IV-6**) indicated Peak 3 in chromatogram B was likely produced by acovenoside A (**22**), based on the similarity in retention time and the absence of other significant peaks in the extracted ion chromatogram.

First order mass spectral analysis, in **Figure IV-7**, of Peak 3 showed the presence of four ions, with the base peak ion at $m/z = 755.3519$. The elemental composition of this ion was calculated to be $[C_{37}H_{55}O_{16}]^-$, with 33.02% confidence (isotopic fit ratio = 49.5), and a mono-isotopic mass of 755.3490 Da. This theoretical mass differed from the measured accurate mass by 3.8 ppm, which was within the limits, for tentative identification, stipulated by the European Commission for Health and Food Safety.⁷¹ From the accurate mass and calculated elemental composition, this ion is tentatively identified as the formic acid adduct of K-strophanthin- β , a cardenolide known to be present in *Strophanthus* spp. according to the Dictionary of Natural Products.⁷²

In the same chromatographic peak (Peak 3 in **Figure IV-6**), an ion of accurate mass $m/z = 595.3101$ was detected. Elemental composition analysis of this ion produced the formula $[C_{31}H_{47}O_{11}]^-$, with 98.95% confidence (isotopic fit ratio = 39.9), which corresponds to the composition of the formic acid adduct of acovenoside A. The calculated molecular formula of the ion had an accurate mass of 595.3118 Da. This theoretical mass differs from the measured mass by -2.9 ppm, which lies below the threshold mass difference for tentative identification.⁷¹ Therefore, Peak 4 was produced by the co-elution of at least two cardenolides, tentatively identified as acovenoside A and K-strophanthin- β , respectively.

The remaining constituents in **Table IV-3** were tentatively identified in a similar manner, from the Dictionary of Natural Products⁷², with mass differences, between the measured and calculated accurate ion masses, below 5 ppm.

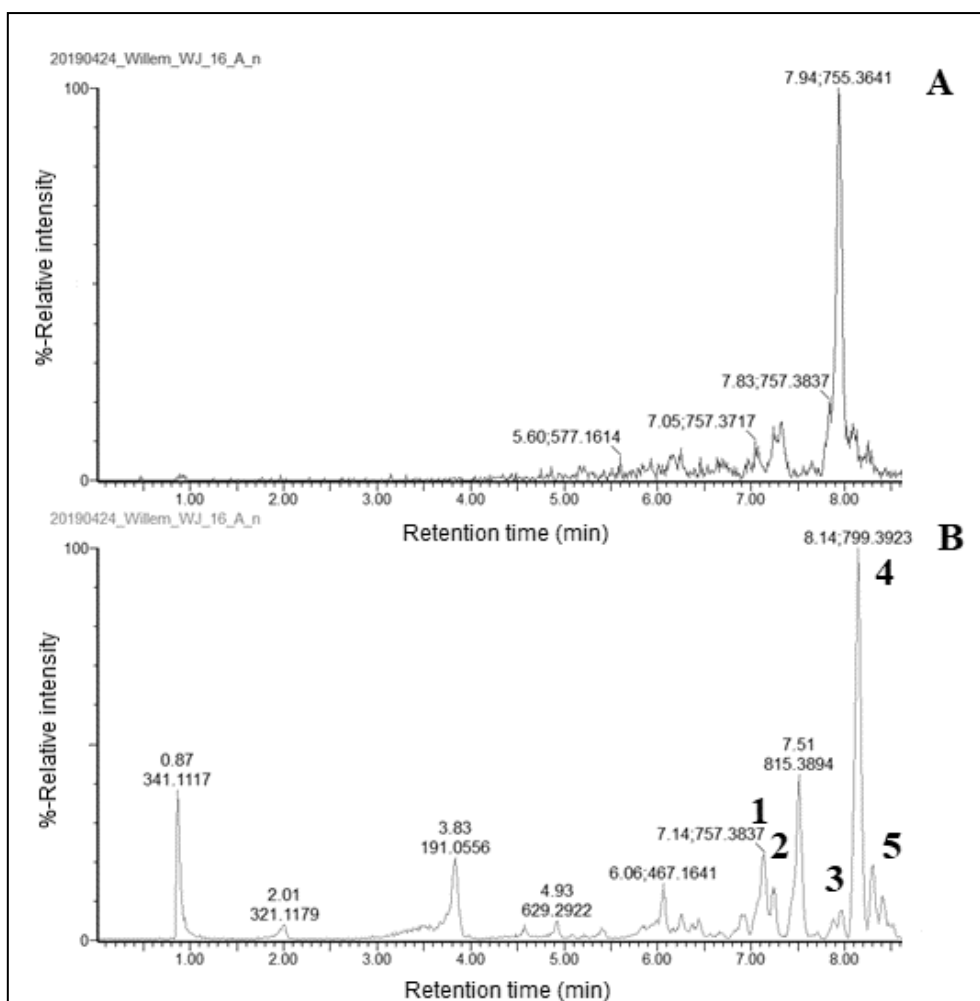


Figure IV-6. (A): ESI (-)-mode extracted ion chromatogram for $m/z = 595.312$, the theoretical $[M-H+FA]$ - mass for acovenoside A (**22**). (B): ESI (-)-mode total ion current (TIC) chromatogram of the *A. oppositifolia* crude extract.

Table IV-3. Compounds detected in ESI (-)-mode UPLC-qTOF MS analysis of *A. oppositifolia* crude extract (peaks described from TIC).

Peak no.	t _R (min)	m/z ([M+FA-H] ⁺)	Calc. accurate mass (Da)	Formula	Theoretical mono-isotopic mass (Da)	Tentative identification
1	7.140	757.3652	712.3670	C ₃₆ H ₅₆ O ₁₄	712.3670	Acobioside A
2	7.237	639.3024	594.3042	C ₃₁ H ₄₆ O ₁₁	594.3040	Oleandrogenin β-D-glucoside
3	7.940	595.3101	550.3170	C ₃₀ H ₄₆ O ₉	550.3142	Acovenoside A
		755.3519	710.3530	C ₃₆ H ₅₄ O ₁₄	710.3514	K-Strophanthin-β
4	8.140	799.3781	754.3799	C ₃₈ H ₅₈ O ₁₅	754.3776	Acospectoside A
5	8.310	783.3455	738.3473	C ₃₇ H ₅₄ O ₁₅	738.3463	Antibiotic F 10748A ₁

The presence of acovenoside A (**22**) was confirmed in for the ESI (-) mode by comparing the relative retention time and ion accurate mass, of the tentatively identified formic acid adduct in the crude extract, with those of acovenoside A (**22**) in a reference sample. The relative retention times were measured with respect to a background signal present in both samples at a retention time of ca. 13 minutes.

In the first order mass spectrum of the reference sample, acovenoside A (**22**) was detected as a formic acid adduct, with accurate mass $m/z = 595.3118$ observed in **Figure IV-8**, at a relative retention time of -5.1 minutes. Compared to the detected accurate mass of the reference sample, the mass of the tentatively identified ion in the crude extract ($m/z = 595.3101$) is within the tolerance range for identification by accurate mass ($\Delta m < 5.0$ ppm).⁷¹ The relative retention time of the identified tentatively identified ion in the crude extract was -5.58 minutes, supporting the tentative identification of the sample ion ($m/z = 595.3101$) as acovenoside A (**22**).

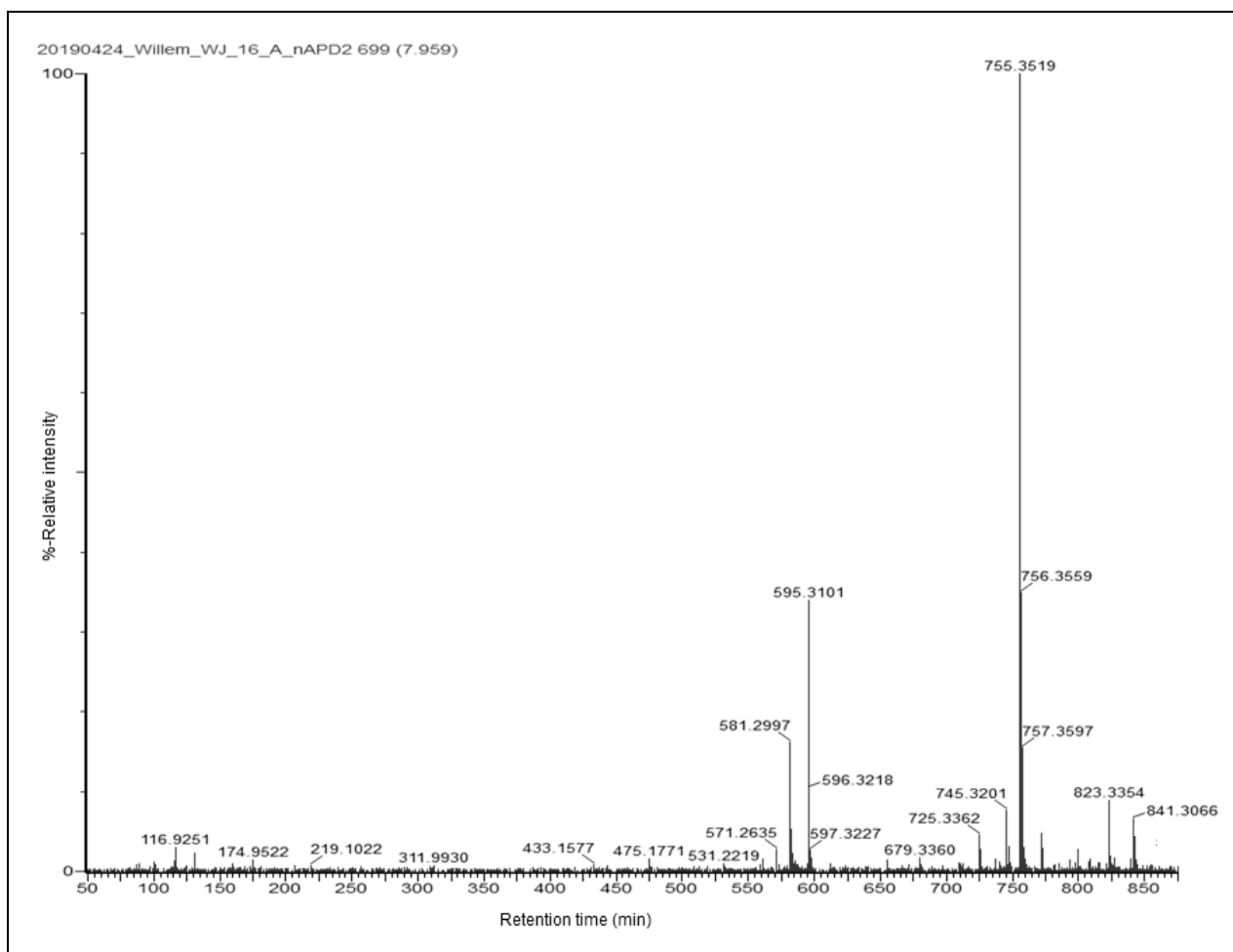


Figure IV-7. First order mass spectrum of acovenoside A (22) in crude extract. Detection was done in the negative ionisation mode (NIM).

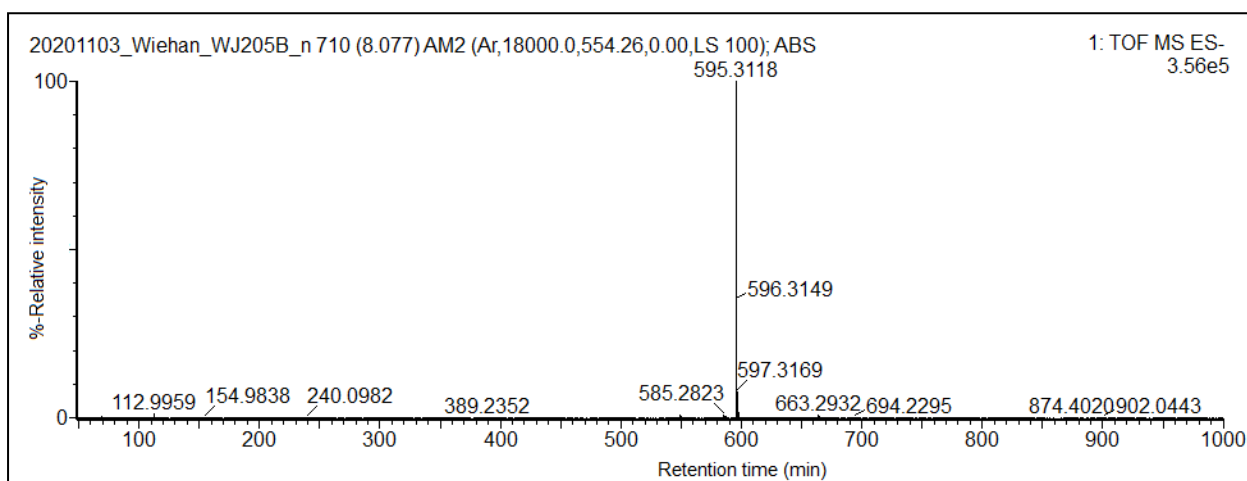


Figure IV-8. First order ESI (-) mass spectrum for the reference sample of acovenoside A (22).

Compared to the abundances of acospectoside A and acobioside A, acovenoside A (**22**) was detected at an unexpectedly low level, since literature sources cite it as being the most abundant cardiac glycoside in *A. oppositifolia*.^{11,14,16,21} Similarly, the absence of acolongifloroside K (**23**) from the extract was unexpected. A study by Hauschild-Rogat et al.¹¹ indicated that acolongifloroside K (**23**) is expected to be the second-most abundant cardiac glycoside in *A. oppositifolia*.

It is notable that, based on the toxicological data of the other cardiac glycosides present, acovenoside A (**22**) is the toxic compound which has the lowest LD₅₀-values in multiple organisms. This supports the validation of a quantitative method for its presence. acovenoside A (**22**) is also more selective toward *A. oppositifolia*, unlike acospectoside A (**3**), which can be found in most plants of the genus *Acokanthera*. K-strophanthin- β , acospectoside A (**3**) and acobioside A could be used as biomarkers for determining the source of the acovenoside A (**22**) poisoning.

Two compounds of particular interest are oleandrogenin β -D-glucoside and a compound tentatively identified as an antibiotic. Regarding the oleander glycoside, it is possible that the glycoside is common to plants of the family Apocynaceae, of which the genus *Acokanthera*, *Nerium* and *Thevitia* are members. The antibiotic could possibly be a cardiac glycoside based on its retention time and calculated molecular formula that has not yet been well documented. This presents a possible topic for further research in natural products.

3.2 Determining the purity of commercially sourced acovenoside A

The acovenoside A (**22**) reference material, sourced commercially, was not certified to conform to a specific level of purity. The material was assessed by UPLC-qTOF MS analysis, in both the positive and negative ionisation mode to determine the level of purity. The recorded chromatograms were compared to the chromatograms of a method blank to determine which peaks in the analyte chromatograms could be attributed to contamination from the sample preparation method. Those peaks not produced by the background in the matrix were selected and integrated. In determining analyte purity, the area under the total ion current chromatograms were calculated.

In the positive ion mode, 94.44 % of the area under the chromatogram (not produced by the blank) was contributed by acovenoside A (**22**) In the negative ion mode, 92.24% of this area was attributed to the signal produced by acovenoside A (**22**). Taking the average of these two percent area measurements, a purity of 93.34% was estimated.

3.3 Analysis of hydrolysed acovenoside A

3.3.1 UPLC-qTOF MS analysis of the hydrolysis products of acovenoside A

During method development, two routes were considered to hydrolyse acovenoside A (**22**): (1) Enzymatic hydrolysis via β -glucuronidase (sample WJ-170-B), (2) incubation in hydrochloric acid (sample WJ-170-D). The tertiary and secondary hydroxyl groups in the genins of cardiac glycosides are highly susceptible to elimination reactions under acidic conditions, due to the improved stability of the carbocation intermediates.

In GC-MS analysis the products of the hydrolysis process would require derivatisation by silylation to improve the analyte chromatography on the GC-column. By first determining which hydrolysis products are likely to be formed in each process, the target masses of the products, after silylation, could be determined.

In the positive ionisation mode analysis of WJ-170-B, the $[M+H]^+$ quasi molecular ion of acovenoside A (**22**) was detected with an accurate mass of $m/z = 551.3239$ at a retention time of 8.907 min. This corresponds to a parent molecule with mono-isotopic mass 550.3166 Da. The calculated molecular formula for this parent molecule is $C_{30}H_{46}O_9$, with a theoretical mono-isotopic mass of 550.3141 Da. Comparison of the sample chromatogram with the chromatogram measured for the method blank (WJ-170-A), in the positive ion mode, showed that no hydrolysis products were formed in detectable quantities.

In the negative ionisation mode, acovenoside A (**22**) was observed at the same retention time as its formic acid adduct. The comparison of the sample chromatogram with the chromatogram recorded for the blank sample, again showed that no significant hydrolysis occurred. Therefore, incubation in a suspension of β -glucuronidase was not effective in deconjugating L-acovenose from acovenoside A (**22**).

When incubated in concentrated (6 M) hydrochloric acid, no unhydrolyzed acovenoside A (**22**) was detectable in the positive ionisation mode. When the detected chromatogram was compared to those for enzymatic hydrolysis conditions and the blank sample, an additional peak was observed at a retention time of 10.63 min. The absence of this peak from the chromatograms of WJ-170-B and the blank sample, indicates that it is likely a hydrolysis product derived from acovenoside A (**22**). In the negative ionisation mode, an additional peak was observed at the same retention time. The detected masses for these peaks are summarised in **Table IV-4**. The mass differences measured in the elemental composition analysis of each

ion was within the 5.0 ppm tolerance range recommended by the European Commission for Health and Food Safety.⁷¹

Of these detected ions in **Table IV-4**, three ions are molecular ion adducts that correspond to the parent molecular formula, C₂₃H₃₂O₄, within a mass difference of 5 ppm. The cation of mass 355.2273 Da, corresponds to the protonated fragment of the analyte molecule, following the loss of water during fragmentation, with a mass difference less than 5. Applying the guidelines set out in the European Commission Directorate General for Health and Food Safety⁷³ on positive identification of pesticides via accurate mass analysis, the chromatographic peak was positively identified as an analyte with molecular formula C₂₃H₃₂O₄.

This confirmed molecular formula, when compared to that of acovenoside A (**22**), is produced by the loss of seven carbon atoms, 14 hydrogen atoms and five oxygen atoms. The hydrolysis of the glycosidic bond would account for the loss of C₇H₁₃O₄ (L-acovenose) and the addition of a proton to the oxygen on C-3. The further loss of two hydrogen atoms and an oxygen atom is accounted for by a dehydration reaction, whereby one of the hydroxyl functional groups are eliminated to give a Dehydro-acovenosigenin. An investigation into the analysis of cardiac glycosides from *Thevetia peruviana* (Yellow oleander), by Kohls et al.,⁵¹ supports the hypothesis that dehydration is most likely to occur during acid catalysed hydrolysis at the C14-position.

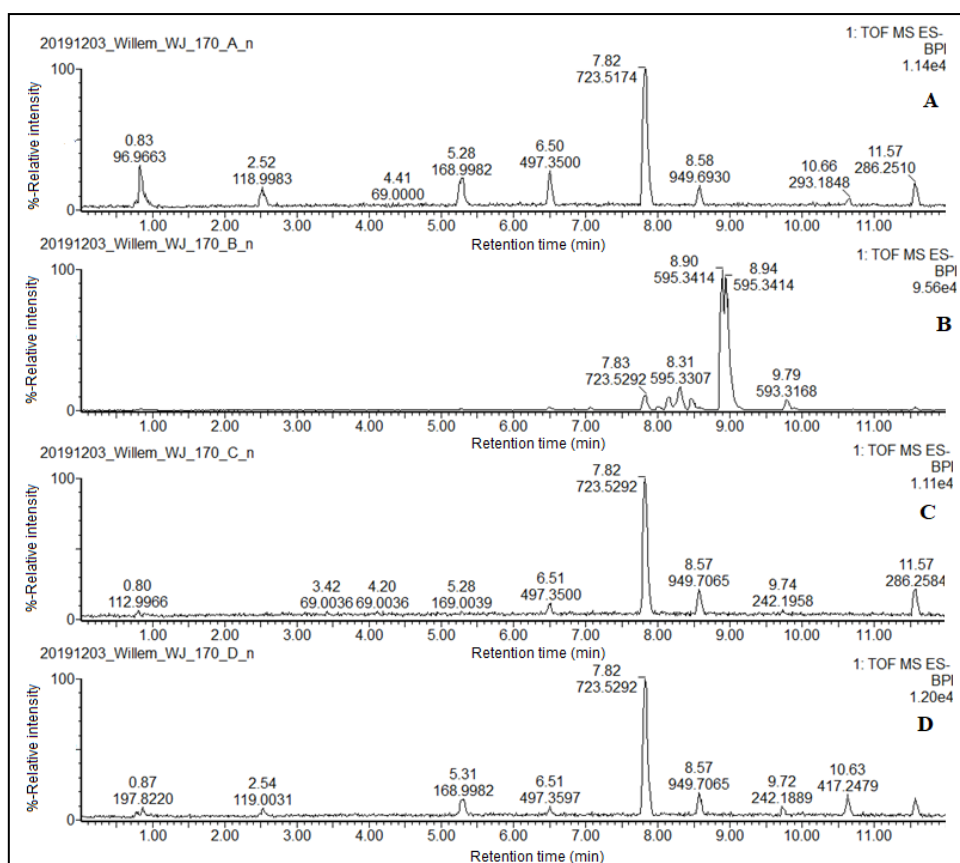


Figure IV-9. UPLC-MS/MS chromatograms of hydrolysed samples containing acovenoside A (**22**) and scillaren A (**7**). From top to bottom: Method blank, enzymatic hydrolysis with β -glucuronidase, hydrolysis with concentrated $HCl_{(aq)}$, hydrolysis with diluted $HCl_{(aq)}$.

Table IV-4. Summary of masses detected in WJ-170-D's additional chromatographic peak at 10.63 min.

m/z	Calculated formula	Fragment/adduct type	Parent molecular formula	Calculated mono-isotopic mass (Da)	Theoretical mono-isotopic mass (Da)
Positive ionisation mode					
373.2376	$[C_{23}H_{33}O_4]^+$	$[M+H]^+$	$C_{23}H_{32}O_4$	372.2303	372.2300
395.2201	$[C_{23}H_{32}O_4Na]^+$	$[M+Na]^+$	$C_{23}H_{32}O_4$	395.2198	372.2300
355.2273	$[C_{23}H_{31}O_3]^+$	$[M-H_2O+H]^+$	$C_{23}H_{30}O_3$	354.2200	354.2195
745.4654	$[C_{46}H_{65}O_8]^+$	$[2M+H]^+$	$C_{23}H_{32}O_4$	745.2291	372.2300
767.4493	$[C_{46}H_{64}O_8Na]^+$	$[2M+Na]^+$	$C_{23}H_{32}O_4$	767.2300	372.2300
Negative ionisation mode					
417.2313	$[C_{24}H_{33}O_6]^-$	$[M+FA-H]^-$	$C_{23}H_{32}O_4$	417.2331	372.2300

GC-MS analysis of silylated hydrolysis products of acovenoside A

In this initial analysis of hydrolysed and silylated acovenoside A (**35**), no internal standard was spiked into the sample. Peak 1 in the gas chromatogram (**Figure IV-10**) is produced by the derivatisation reagent, MSTFA, which was added in excess to the sample during preparation. Since only acovenoside A (**22**) was spiked into an empty test tube when the sample was prepared, Peak 2 is likely produced by the silylated derivatives of the hydrolysis products of acovenoside A. To confirm this assumption, different volumes of a 1.00 mg/mL stock solution of acovenoside A (**22**) were spiked into test tubes and prepared for GC-MS analysis. The chromatograms produced in this experiment are given in **Figure IV-11**.

In **Figure IV-11** the dashed line indicates the position of MSTFA in the chromatogram, and the solid line the peaks suspected of being produced by the derivatisation products of hydrolysed acovenoside A (**22**). Since the intensity of the chromatographic peaks, at the same retention time as Peak 2 in **Figure IV-10**, increase with an increase in the amount of spiked acovenoside A (**22**), Peak 2 is dependent on the mass of acovenoside A spiked into the test tubes. This implies peak 2 (**Figure IV-10**) is produced by the target analytes.

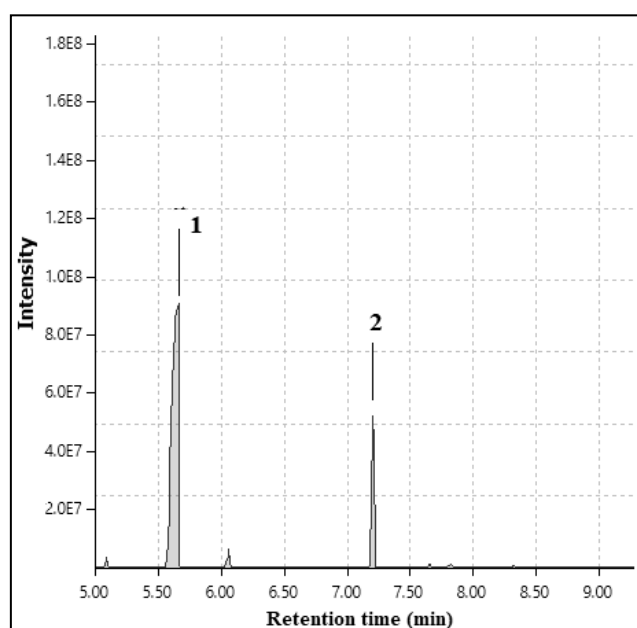


Figure IV-10. GC-MS chromatogram of hydrolysed Acovenoside A (**22**), derivatised by MSTFA. The peaks are labelled: (1) MSTFA, (2) Derivatised analyte.

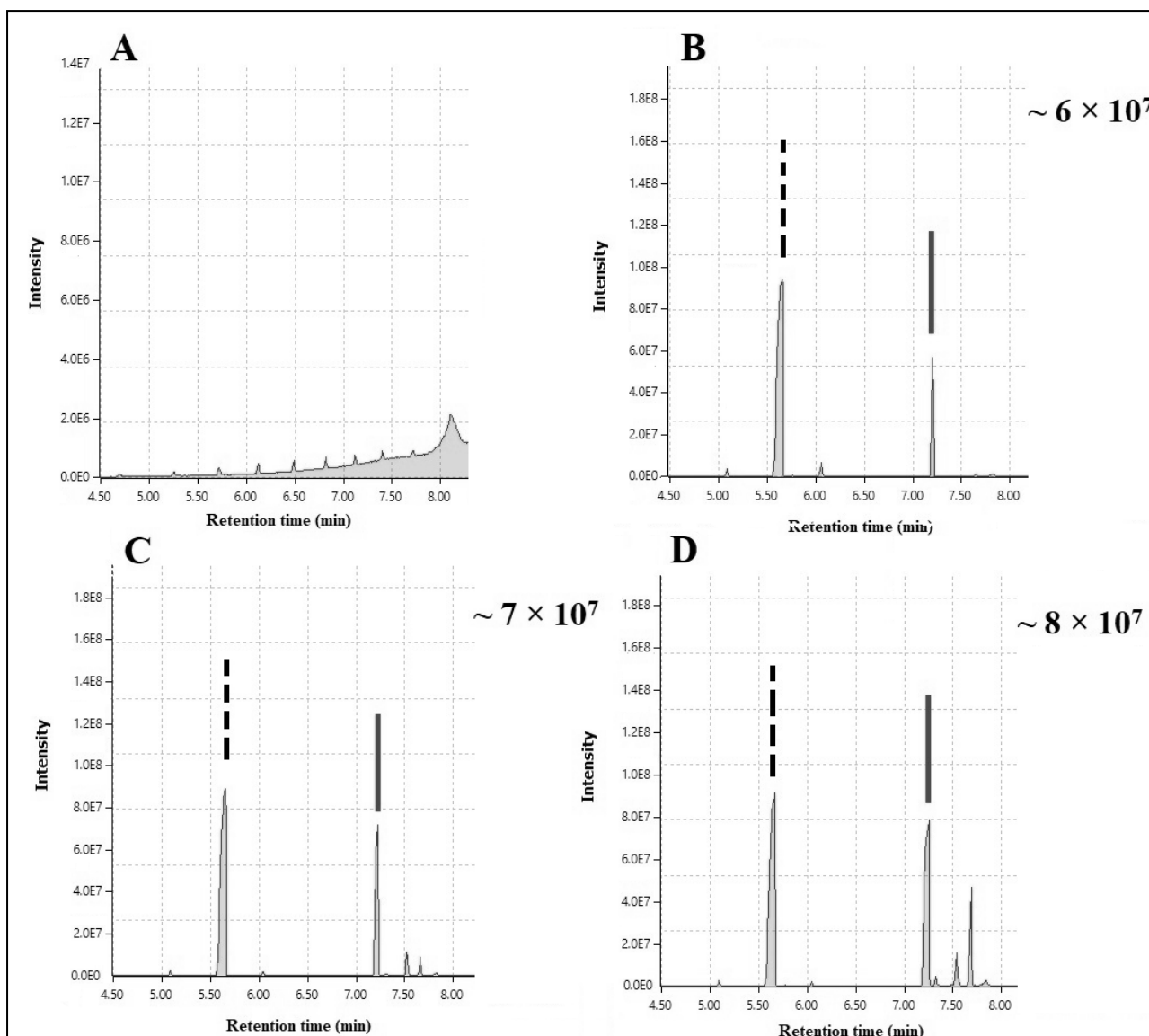


Figure IV-11. Gas chromatographs showing the comparison between (A) an *n*-hexane blank, (B) 25.0 µg acovenoside A (**22**) spiked sample, (C) 50.0 µg acovenoside A (**22**) spiked sample and (D) a 100.0 µg acovenoside A (**22**) spiked sample. The dashed line indicates the position of MSTFA, and the solid line the derivatised analytes.

Multiple hydrolysis products can form from the microwave assisted hydrolysis of acovenoside A. Each of these can be derivatised to a different extent. This produces multiple chromatographic peaks, all of which can be attributed to acovenoside A (**22**) (**Figure IV-12**). To determine which hydrolysis products of acovenoside A (**22**) (**35**) are detected by GC-MS, the mass spectra of the detected peaks were analysed (see **Table IV-5**).

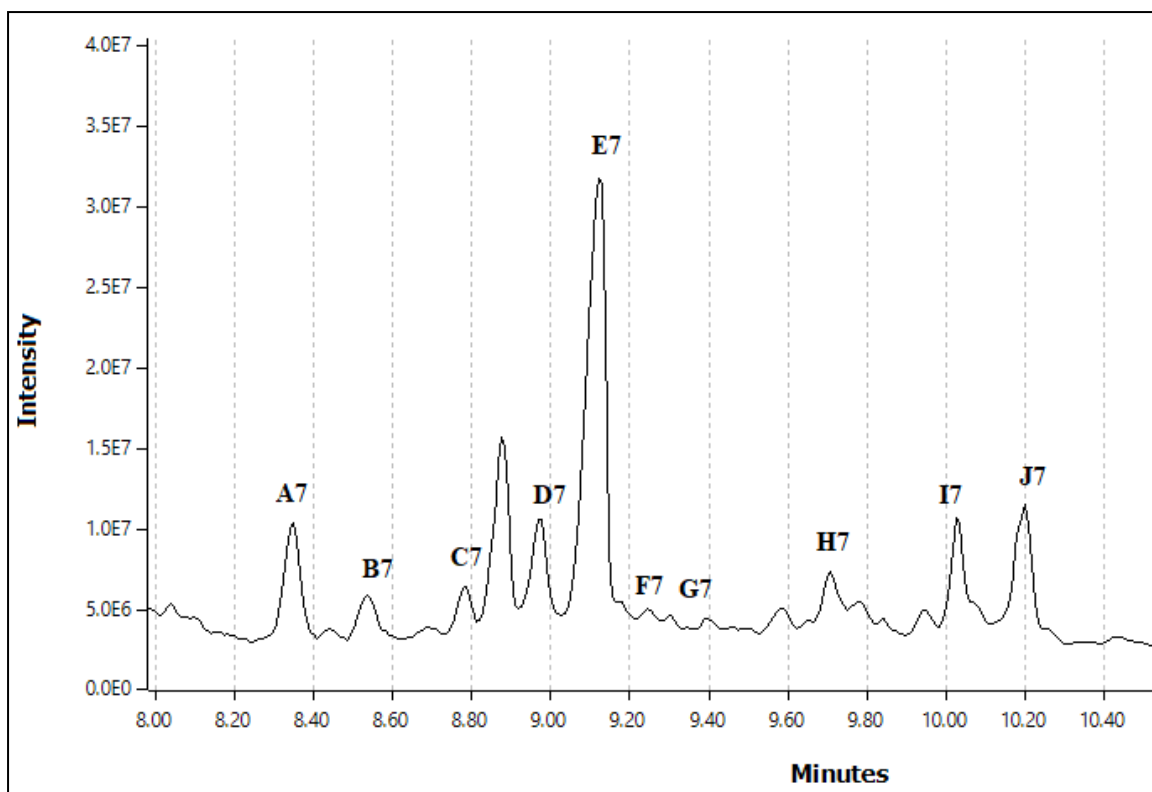


Figure IV-12. A cropped chromatogram recorded for the GC-MS analysis of 100.0 μg of acovenoside A (22), following hydrolysis and derivatisation. Peaks A7 to J7 are suspected silylated hydrolysis products of acovenoside A.

Table IV-5. Analyte peaks in the GC-MS chromatogram with suspected molecular ion m/z -ratio values.

Peak	Retention time (min)	Suspected molecular ion m/z -ratio
A7	8.349	588
B7	8.534	516
C7	8.777	562
D7	8.970	588
E7	9.120	588
F7	9.238	588
G7	9.246	588
H7	9.707	542/516
I7	10.026	588/576
J7	10.202	426

The common denominator among the m/z -ratios of the suspected molecular ions listed in **Table IV-5**, is $m/z = 588$. This nominal mass corresponds to the nominal mono-isotopic mass of a trisilylated derivative produced from the derivatisation of acovenoside A's (**22**) singly dehydrated aglycone (**35**). Under strong acidic conditions, the glycosidic bond in Acovenoside A is readily hydrolysed and dehydrated (Section 3.3.1). There are four possible locations where a double bond may form during dehydration. Since the five-membered lactone ring of cardenolides is readily tautomerized to an enol under acidic conditions, three active hydrogen atoms are available for derivatisation.^{50,51}

If silylation of the dehydrated hydrolysis product is incomplete, that is only two active hydrogen atoms are displaced, an analyte with a nominal mono-isotopic mass of 516 is produced. When TMSOH is lost during fragmentation, the fragment of $m/z = 426$ is produced. Based on the relative abundances of the peaks with molecular ion of $m/z = 588$, peak G7 likely corresponds to the disilylated derivative for the dehydrated hydrolysis product in peaks A7, and D7 to G7.

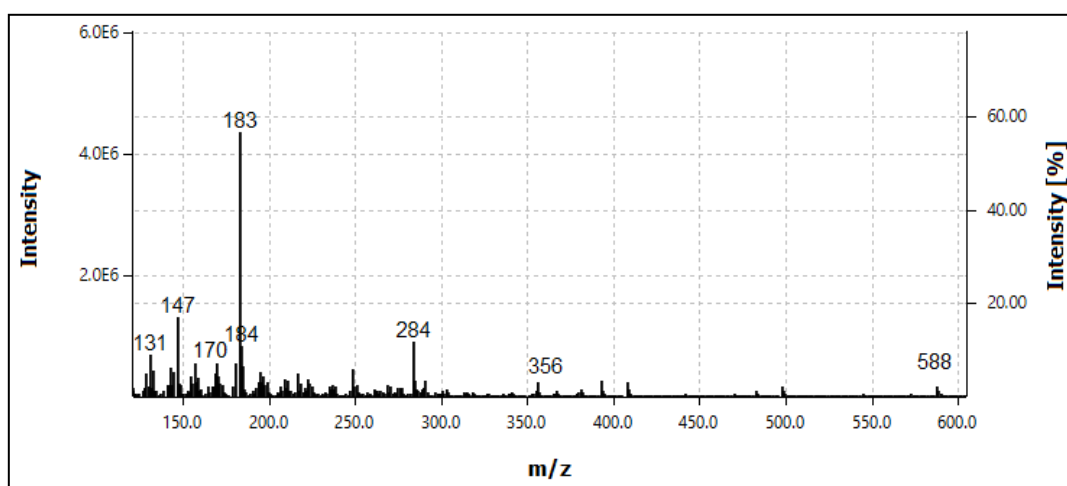


Figure IV-13. Mass spectrum of peak A7 generated by 70 eV electron impact ionisation.

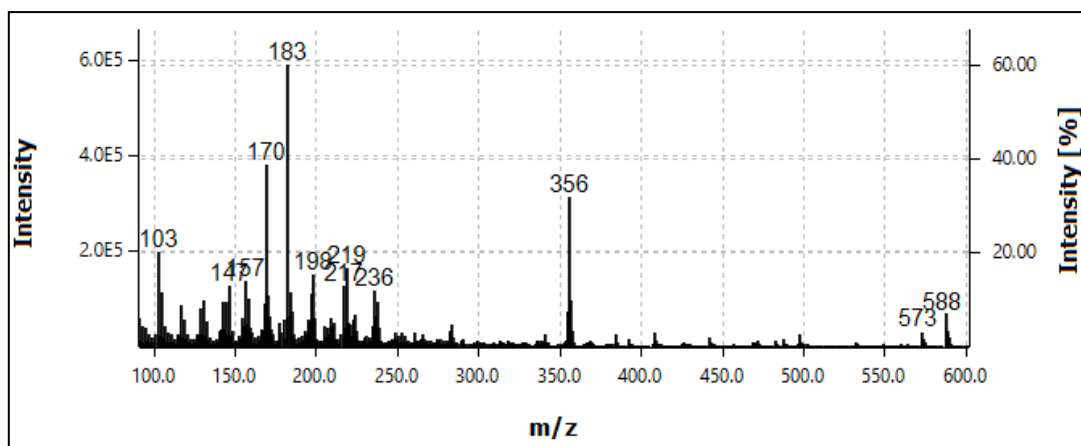


Figure IV-14. Mass spectrum of peak D7 generated by 70 eV electron impact ionisation.

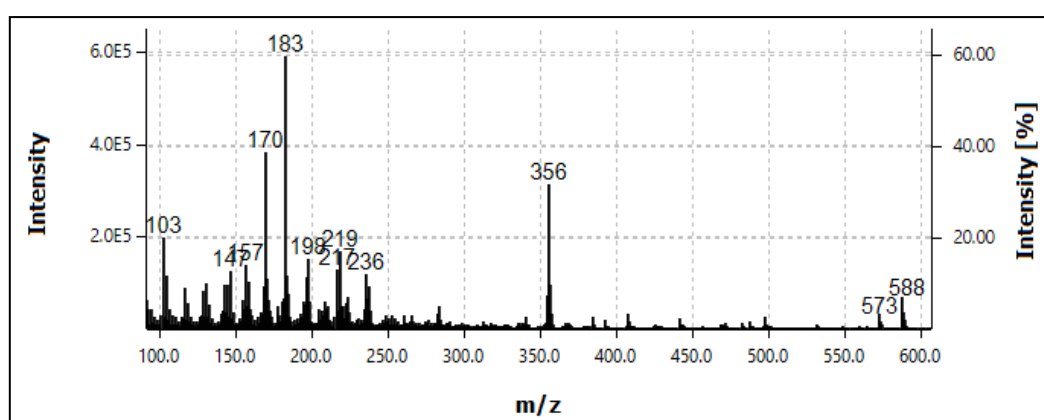


Figure IV- 15. Mass spectrum of peak E7 generated by 70 eV electron impact ionisation.

Comparing the mass spectra obtained for peaks A7, D7, and E7, it is observed that all three contain the ions at $m/z = 588$, 356, 183 and 170, albeit in different ratios. The importance of this is the implied similarity in their structures. In peak A7, the fragment with $m/z = 573$ is obtained from the molecular ion, following the loss of a methyl group (**35**) (**Figure IV-16**). This fragment is also observed in peaks D7 and E7 (See Appendix IV – C: **Figure A (IV)-4**).

The presence of the fragment ion $m/z = 356$ indicates that dehydration during hydrolysis occurred at the C14-position, since this fragment is produced by the loss of $\text{'CH}_2\text{CH(OTMS)CH}_2\text{CH(OTMS)'$ from ring A in the molecular ion (**38**). In the formation of the fragment ions $m/z = 170$ and 183, two hydrogen atoms shift from the C18-methyl group to the C17-position, forming a single fragment ion **Figure IV-16 (39) & (40)**. This shift is observed in the mechanisms proposed by Kohls et al.⁵¹

The likely position of the alkene following dehydration can be deduced from Zaitsev's rule for elimination via an E1-mechanism.³¹ Since the Δ 14,8-unsaturated anhydro-cardenolide aglycone is the most substituted elimination product, it is likely to be the major product corresponding to the analyte in peak E7. A7 would likely be its Δ 14,15-isomer. The change in the position of the double bond will impact the abundance in the formation of the fragment with $m/z = 183$. In the Δ 14,15-alkene there is no conjugated system to stabilise the radical in the steroid skeleton fragment (mass = 405 Da), whereas the Δ 14,8-alkene forms a conjugated allylic radical which would increase the drive behind the formation of the ion $m/z = 183$.

The contradiction revolving around the exact identity of peaks A7 and E7 could be resolved based on the presence of $m/z = 198$ in peak B7. This fragment ion could be formed by the additional loss of the C-15-C-17 chain with the lactone group, via a mechanism like that involved in the formation of the fragment ion $m/z = 183$ (**Figure IV-16 & Figure IV-17**). Such a process is most likely when the double bond is formed between C-14 and C-8. This would imply that Zaitsev's rule is obeyed, and the major product carries the most substituted alkene.³¹ The formation of the fragment ion with $m/z = 170$ remains unchanged and characteristic of cardenolides with a silylated lactone group (see **Figure IV-16**).

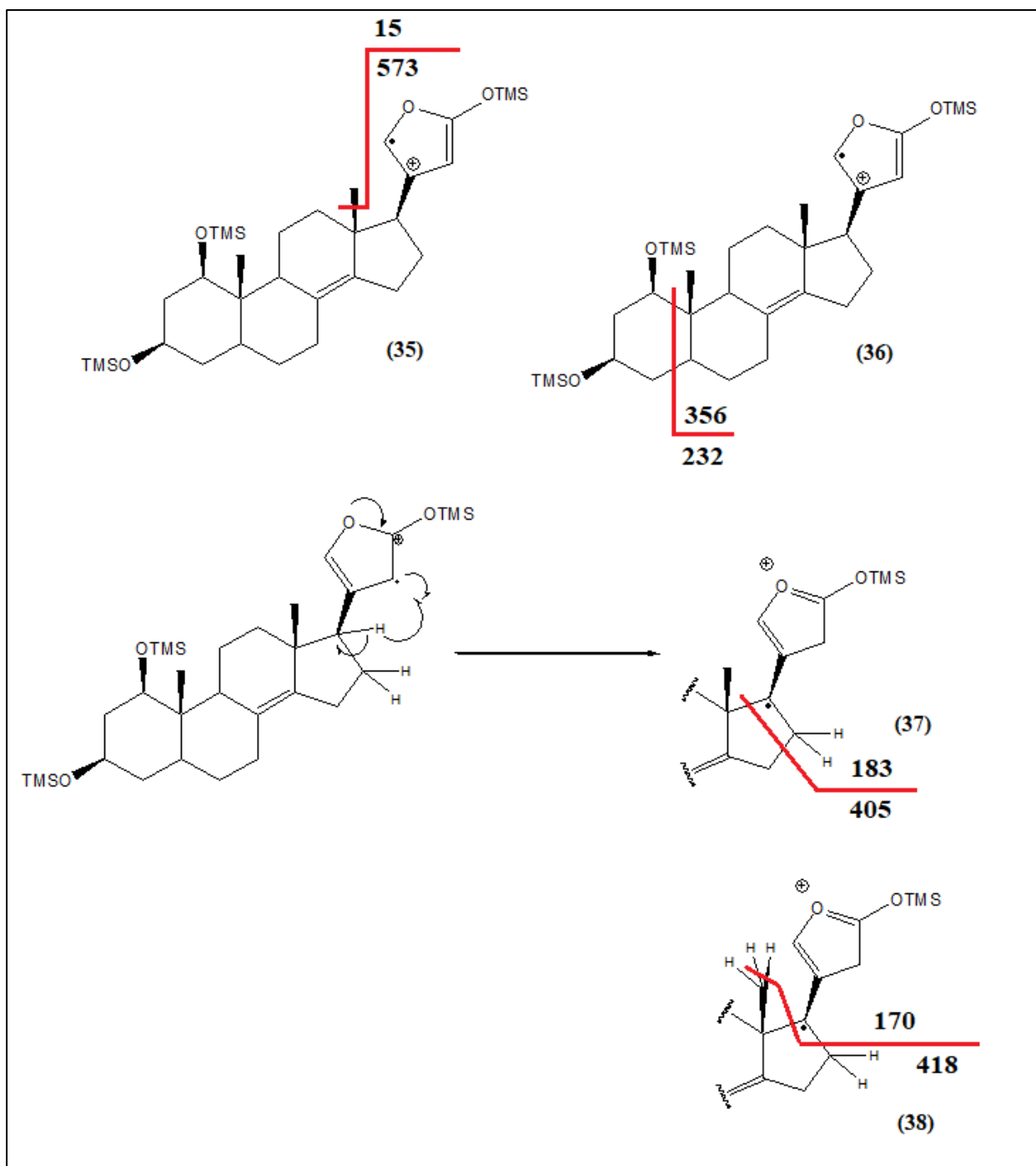


Figure IV-16. Proposed fragmentation pathways for the trisilylated derivative of the hydrolysis product in peak A.^{50,51}

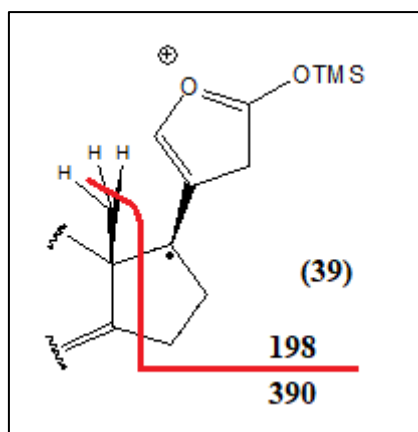


Figure IV-17. Formation of the fragment ion $m/z = 198$.

For quantitative analysis, however, it was opted to use Peaks D7 and E7, since they were well-resolved from the matrix components by the temperature program. D7 is likely one of the trisilylated products formed when dehydration occurred in ring A and not on the ring C/ring D-interface. The absence of a Δ 14,15-dehydro-system in D7 would explain why the $m/z = 198$ is also present.

3.3.2 Inter-ion ratio relationships of fragment ions

For each of the two selected chromatographic peaks of derivatised acovenoside A (Peaks D7 and E7 in **Figure IV-12**), five ion ratios were selected. Since the two peaks contained the same ions, the same five ratios used in one peak were used in the other. The selected ion ratios are given in **Table IV-6**.

Table IV-6. Ion ratios selected for analysis of both fragmentation patterns and the positive identification of the analyte signals in method validation.

Designation	Definition
IR 1	Area $m/z = 588 \div$ Area $m/z = 356$
IR 2	Area $m/z = 588 \div$ Area $m/z = 183$
IR 3	Area $m/z = 356 \div$ Area $m/z = 183$
IR 4	Area $m/z = 356 \div$ Area $m/z = 170$
IR 5	Area $m/z = 170 \div$ Area $m/z = 183$

The ion ratios of the two chromatographic peaks were analysed separately but interpreted concurrently. This was because the simultaneous positive identification of acovenoside A in both chromatographic peaks was required to confirm the presence of acovenoside A. However, the peaks were well resolved, therefore, the associated ratios cannot be treated as if from the

same compound. The two distribution matrices for the chromatographic peaks were calculated from the ion ratios measured at the centroid concentration level (1.311 ppm). For the analysis of the ion ratios, only the those from the urine samples were used since the ideal case of a de-ionised aqueous matrix would not be encountered in routine forensic analysis.

Table IV-7. Correlation matrix for the ion ratios obtained from peak D7, recorded in SIM-mode.

	IR 1	IR 2	IR 3	IR 4	IR 5
IR 1	1,000	-0,212	-0,758	-0,947	-0,370
IR 2	-0,212	1,000	0,789	0,210	0,907
IR 3	-0,758	0,789	1,000	0,696	0,864
IR 4	-0,947	0,210	0,696	1,000	0,241
IR 5	-0,370	0,907	0,864	0,241	1,000

Table IV-8. Correlation matrix for the ion ratios obtained from peak E7, recorded in SIM mode.

	IR 1	IR 2	IR 3	IR 4	IR 5
IR 1	1,000	0,907	-0,790	-0,866	0,832
IR 2	0,907	1,000	-0,461	-0,608	0,771
IR 3	-0,790	-0,461	1,000	0,959	-0,670
IR 4	-0,866	-0,608	0,959	1,000	-0,852
IR 5	0,832	0,771	-0,670	-0,852	1,000

In the signal component from D7 there is a strong correlation between IR 1 and IR 3 and between IR 1 and IR 4. The correlation exists since IR 1, IR 3 and IR 4 contain the signal contribution from $m/z = 356$. The correlation between IR 1 and IR 3 is negative, therefore, if IR 1 increases, IR 3 decreases. This relationship can be attributed to the opposite positions (numerator and denominator) of $m/z = 356$ in the ratios.

Underlying to this relationship is the trivial relationship where a decrease in the molecular ion abundance due to fragmentation, would increase the abundance of the fragment ion. Since the fragment and parent (molecular) ion are in opposing positions in their ratios, a decrease in IR 1, if $m/z = 588$ decreases in abundance, would cause a decrease in IR 3, if $m/z = 356$ increases. This is balanced if fragmentation occurs to produce $m/z = 183$, thereby decreasing IR 3. These three interactions balance out to give the correlation coefficient $r_{1,3} = -0.790$. The same train of thought applies to the relationship between IR 1 and IR 4.

There is a weak positive correlation between IR 2 and IR 3 ($r_{2,3} = 0.789$). This correlation stems from the fragmentation pathways in competition with each other. If IR 2 increases, $m/z = 183$ would have decreased in abundance. This would increase either $m/z = 588$ or $m/z = 356$, or both. Since $m/z = 356$ is produced when ring A is fragmented, it relies on the presence of the lactone to have the nominal mass equal to 356 Da, as well as the positive charge. From $m/z = 356$, subsequent fragmentation to $m/z = 183$ is possible. This parent-daughter ion relationship creates a weak competition during formation.

The correlation between IR 2 and IR 5 shows the competition between the formation of $m/z = 170$ and $m/z = 183$ is similar to the relationship between IR 2 and IR 3. The difference being that $m/z = 170$ is likely *not* a daughter ion of $m/z = 183$ during subsequent fragmentation. The strong correlation suggests that both ratios decrease proportionally when the abundance of $m/z = 183$ increases, and vice versa. During the weak interaction between IR 3 and IR 4, some of this competition is also visible. A decrease in either of the two ions ($m/z = 170$ or 183), induces a small increase in $m/z = 356$.

Besides its relationships to IR 1 and IR 2, IR 3 has a strong positive correlation with IR 5. The correlation is attributed to the direct proportionality between the ratios, with the proportionality constant the inverse of IR 4. Since IR 4 has no significant correlation with IR 5, but a weak correlation with IR 3, the competition between $m/z = 170$ and 183 is not strong. The IR 3-IR 4 relationship exists mainly because of the communal factor of $m/z = 356$. This shows that $m/z = 170$ forms via a pathway independent from those of $m/z = 588$, 356 and 183.

In the correlation matrix from E7, there are additional relationships that appear. IR 1 has a strong positive correlation with IR 2 ($r_{1,2} = 0.907$) in contrast to the absence of correlation for the ratios from D7. The direct proportionality between the ratios is the likely source of this correlation. Its absence from the ratios in D7 shows that the fragmentation pathways had some independence from each other. Theoretically, IR 2 is the product of IR 1 and IR 3. The weak underlying competition for formation between $m/z = 356$ and 183, decreased the correlation between IR 1 and IR 2 since a small increase in $m/z = 356$ causes a proportional change in $m/z = 183$ in the opposite growth direction.

The strong relationship between IR 1 and IR 5 gives some insight into the pathway of fragmentation to form $m/z = 183$ and 170 . Based on the correlation coefficient ($r_{15} = 0.832$), a decrease in IR 1 induces a strong decrease in IR 5. A decrease in IR 1 would imply an increase in all fragment ions. If $m/z = 356$ increases, then IR 5 increases as well. Yet IR 5 is the ratio of $m/z = 170$ and 183 . Since there is some competition between $m/z = 183$ and $m/z = 356$, the correlation coefficient is not unity. It also shows that if $m/z = 170$ forms independently from $m/z = 183$, then a decrease in the molecular ion abundance would increase both $m/z = 170$ and 356 , subsequently fragmenting to $m/z = 183$.

3.4 Validation of quantitative GC-MS method

3.4.1 Linearity and precision in measured data

Linearity and precision in the calibration models of de-ionised aqueous samples

Linear response models were generated as described in Sections 2.4 and 2.5 in both urine and de-ionised water. The response model was generated from the regression of the combined analyte response relative to the response from the internal standard (5- α -cholestane), on the theoretical concentration of acovenoside A (**22**) spiked into the samples. The combined analyte signal was calculated as the sum of the areas under the two adjacent chromatographic peaks ($t_R = 2.062$ min and 2.213 min, w.r.t. the internal standard) for the extracted ion chromatogram of the base peak ion in selected ion mode ($m/z = 183$).

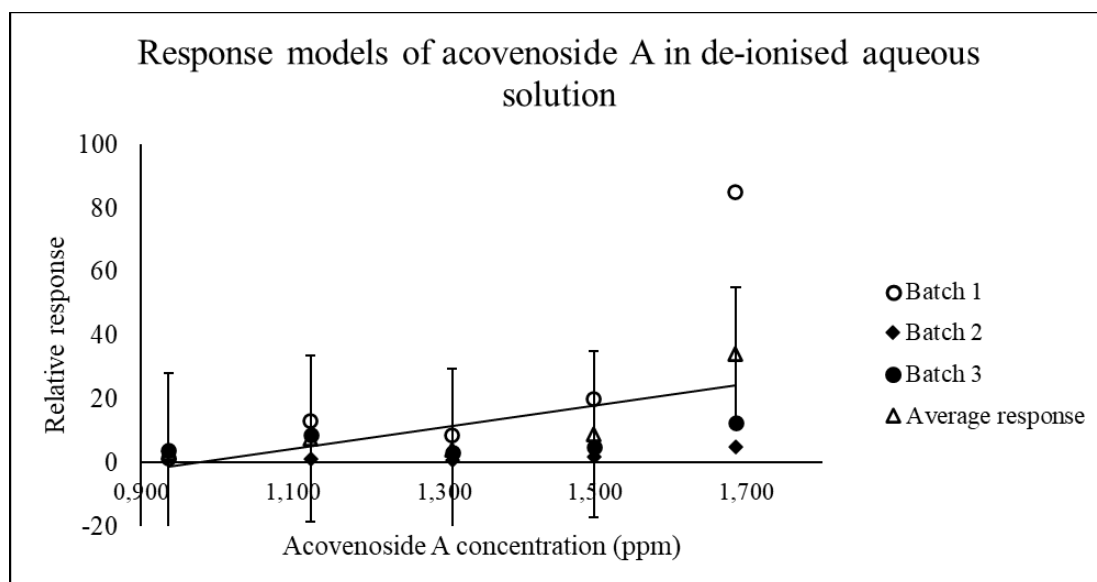


Figure IV-18. A scatter plot showing the three individual batches of duplicate analyses and the mean calibration model (open triangles). Note the strong exponential trend in batch 1 (open circles).

In each of the three batches of de-ionised aqueous samples, the response models for the measured data points did *not* significantly correlate with the corresponding calculated linear trendlines. In the mean response model of the three batches of samples, the observed trend tended towards an exponential model rather than the expected linear model with equation $y = 34.1 \text{ ppm}^{-1} \times x - 33.1$ (**Figure IV-18**). The slope of the regression line had a standard deviation of 15.6 ppm^{-1} and the intercept had a standard deviation equal to 20.9.

A closer analysis of the individual sample batches showed that in Batch 1 the absolute response of the internal standard decreased with an increase in the spiked analyte concentration, whereas the analyte concentration followed a parabolic trend in the combined absolute response. The exponential nature of the trend in the relative response could have been caused by the combination of the decrease in the denominator of the relative response and the parabolic trend in the numerator. In the second batch of duplicate analyses, the relative response follows a clear parabolic trend. This trend is likely caused by the opposite parabolic trend in the absolute response of the internal standard. In the third batch, there is no clear trend visible. The magnitude of the relative response in Batch 1 greatly contributed to the observed exponential trend in the mean calibration model.

The observed trends in the responses of 5- α -cholestane and acovenoside A could have been caused by variation in ionisation efficiency of the ion source. Since acovenoside A and 5- α -cholestane have similar carbon skeletons, their extraction efficiencies are expected to follow similar trends with a change in concentration. Since the internal standard concentration was kept constant, the trend in the relative response should be attributed to the trend in the combined response from acovenoside A's (**22**) signals. This suggests the non-linear trend could also be due to the change in the relative amounts of hydrolysis and derivatisation products produced at different analyte concentrations, during sample preparation.

To assess the suitability of a logarithmic transformation to the data, regression analysis was performed on the relationship between the logarithm (\log_{10}) of the relative response and the theoretical acovenoside A (**22**) concentration (**Figure IV-19**). The mathematical relationship between the relative response and the theoretical acovenoside A (**22**) concentration is given by $y = \log(\text{Relative response}) = 1.18 \times \text{Concentration (ppm)} - 0.65$, where the standard deviation of the slope is 0.42 ppm^{-1} and that of the y-intercept is 0.57.

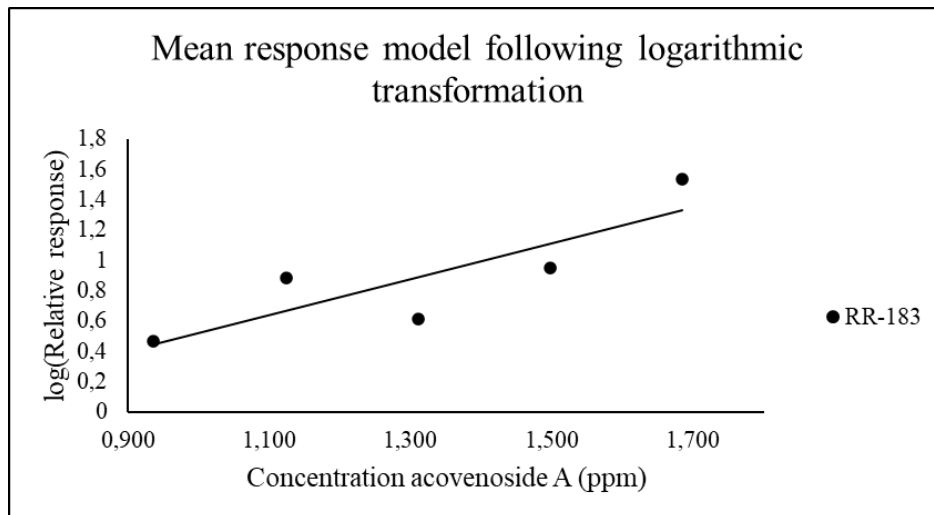


Figure IV-19. Linear response model of the $\log_{10}(\text{relative response})$ vs. the theoretical concentration of acovenoside A.

A comparison of the linear regression model's r^2 -value ($r^2 = 0.6130$) to that of the logarithmically transformed model ($r^2 = 0.7194$) showed a closer, yet *not* significant, correlation in the logarithmic model. This supports the hypothesis to apply non-linear transformations to the data to define a linear best fit line. The improved fit of the logarithmic model can also be seen in the y-residuals plot where the residuals are more randomly distributed than in the case of the linear regression (**Figure IV-20**).

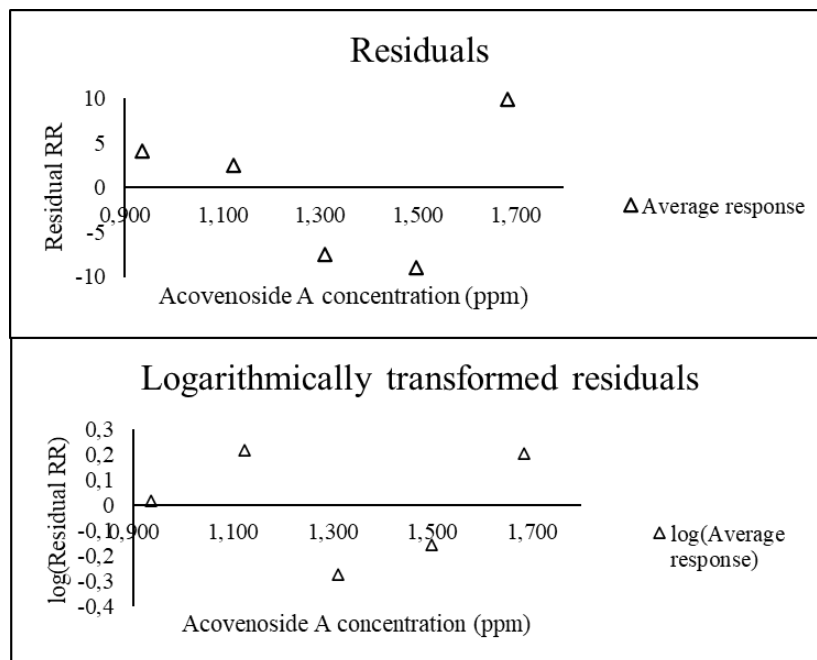


Figure IV-20. A comparison of the residuals for the linear regression models, of the individual batches and the mean calibration model, with the residuals of the transformed residuals.

From the comparison of the residual graphs, a difference in the magnitude of the residuals can also be seen. It must be considered that the y-axis has been transformed to the logarithm of the relative response. These residuals, when transformed back to response units, are close to one. Therefore, there is a small improvement in the magnitude of the residuals when the logarithmic transformation is applied.

Table IV-9. %-RSD values for the linear and log-linear calibration models at each concentration level.

Concentration acovenoside A (ppm)	%-RSD (Linear regression)	%-RSD (Log-linear regression)
0.936	24.6	17.5
1.12	18.3	11.2
1.31	17.0	10.9
1.50	13.5	8.44
1.69	21.6	12.0

For the individual batches, the %-RSD value was frequently above the recommended level from Horwitz's equation (16%).^{74,75} This level of precision carried through to the regression of the average relative responses on the concentration of acovenoside A (**22**) spiked into the de-ionised aqueous samples. The trend observed in the %-RSD values for the linear regression model showed a homoscedastic distribution of variance, centred close to an analyte concentration of 1.50 ppm.

Comparing the log-linear regression model's %-RSD values to that of the linear regression model reveals an improvement in precision of measurement for the log-linear model. In the log-linear model the %-RSD values only exceeded the expected benchmark %-RSD value from the Horwitz equation (16%), at the 0.936 ppm level.⁷⁴ This experimentally limits the analytical range of the method, had correlation between the measured data and the trendline been significant for $\alpha = 0.046$.

Linearity and precision in the calibration models of urine samples

In the analysis of the urine samples, the same two chromatographic peaks were quantified to estimate the total abundance of acovenoside A (**22**) in the spiked urine samples. As was done for the de-ionised aqueous samples, the relative responses of the three batches of samples, analysed in duplicate, were averaged to obtain the mean calibration model. In contrast to the response models developed in de-ionised aqueous samples, the measured data from the quantitative analysis of acovenoside A (**22**) in urine followed a linear-like trend in all three batches (**Figure IV-21**). The trend in the average relative response was described by the linear best fit line with equation $y = 1.20 \text{ ppm}^{-1} \times x - 0.96$, with the standard deviation of the slope 0.56 ppm^{-1} and that of the intercept 0.75 .

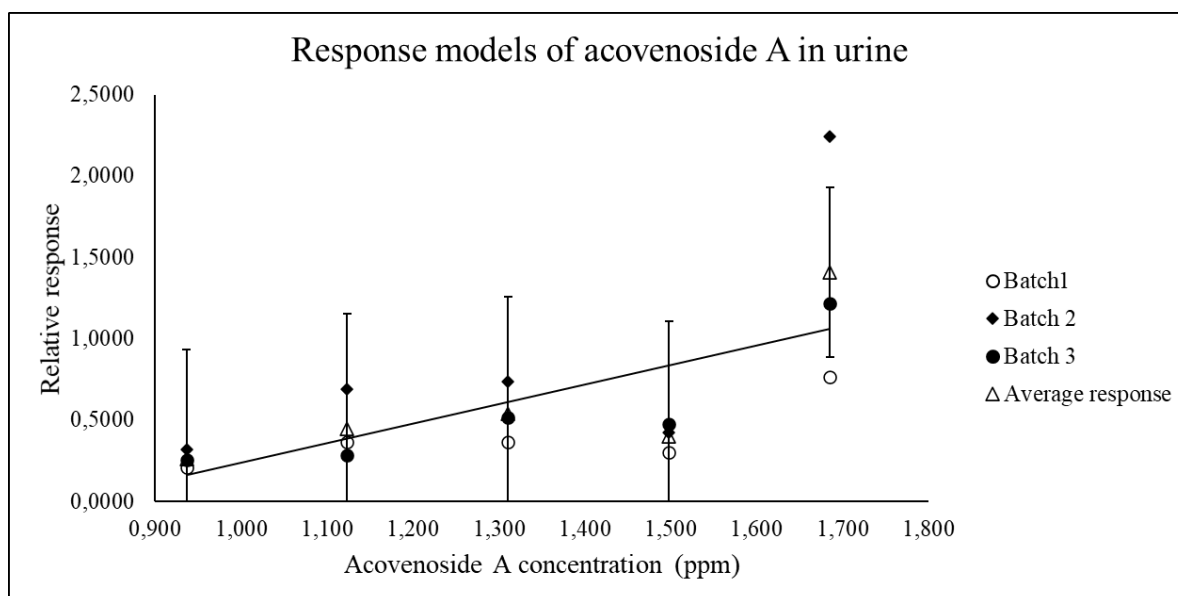


Figure IV-21. The relative responses of the individual batches of duplicate analyses overlaid with the regression model of the mean relative responses at each concentration.

Assessment of the closeness of fit between the linear trendline of the mean calibration model and the measured data showed there is not significant correlation between the data and the trendline ($r^2 = 0.6071$) at the $\alpha = 0.046$ significance level. The greatest deviation from the trendline is observed at concentration levels 4 and 5 (1.50 and 1.69 ppm respectively). These potential outliers were tested by performing Grubb's test for a single significant outlier in the residuals at a significance level of $\alpha = 0.046$.⁷⁶ It was determined, with 95.4% confidence, that neither of these residuals were significant outliers.

Since neither of the two terminal points were outliers, alternative models were considered to mathematically describe the trend in the measured data. The sudden increase in the measured

relative response at 1.69 ppm acovenoside A (**22**), prompted the consideration of an exponential model as was used for the de-ionised aqueous samples. To transform the exponential trend to the form of a linear equation, the logarithm-base 10 (\log_{10}) of the relative response was regressed on the theoretical concentration of acovenoside A (**22**). The logarithmic transformation produced a better correlation, yet not significant at $\alpha = 0.046$, between the measured relative responses and the calculated trendline ($r^2 = 0.6848$). The transformed equation had the form $y = \log(\text{Relative response}) = 0.76 \times x - 1.28$. The slope had a standard deviation of 0.30 ppm^{-1} , and the intercept a standard deviation of 0.40. (See **Figure IV-22**)

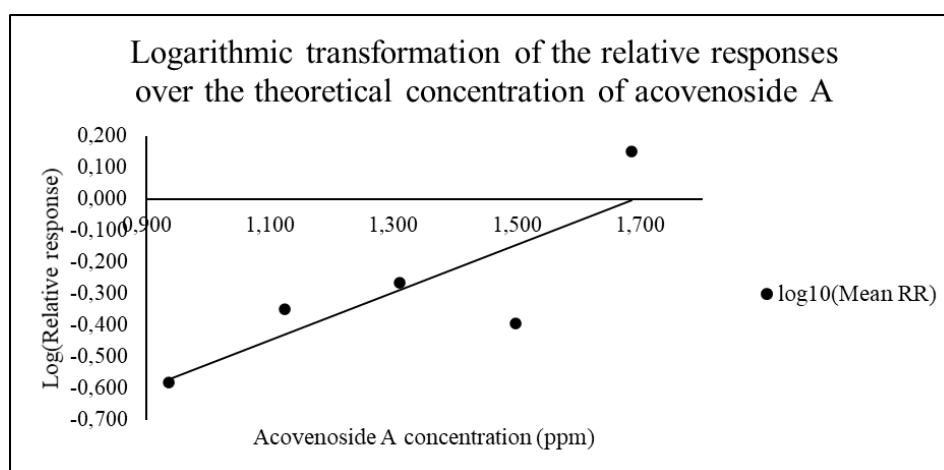


Figure IV-22. Log-linear regression model generated by applying a logarithmic transformation to the mean relative responses.

Despite the improvement in the closeness of fit, the log-linear model showed the same sharp deviation from the trend at a concentration of 1.50 ppm. In both the linear and log-linear models, this point caused a significant decrease in correlation between the measured data and the calculated trendline. For the log-linear model, Grubb's test was again performed on the value of the y -residual at 1.50 ppm.⁷⁶ The test showed the response at 1.50 ppm is not a significant outlier.

In both linear and log-linear models the residuals in the y -direction followed the same trend (**Figure IV-23**). The magnitude of the residuals must not be compared directly since the y -axes of the models are measured in different units. The large variance in the y -values and the absence of significant correlation from either model makes the comparison of the linear model with the log-linear model more complex.

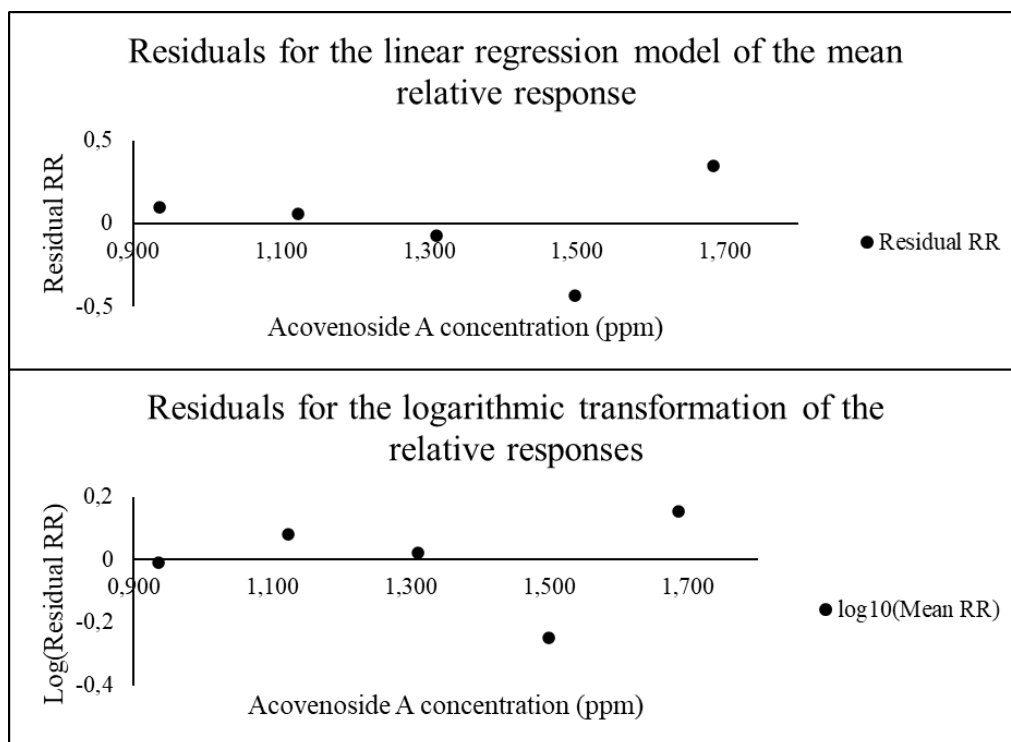


Figure IV-23. Residuals calculated for the linear regression model (Top) and the logarithmically transformed model (Bottom). The y-axis for the transformed model is in logarithmic units.

In terms of the method precision neither the linear, nor the log-linear models showed suitable inter-sample precision for the quantitative analysis of acovenoside A (22). If either method were repeatable at different concentrations, a clear trend would have been obtained and modelled mathematically with significant correlation. Improved repeatability was observed in the log-linear model compared to the linear regression model.

The sudden decrease in the measured relative response at 1.50 ppm, occurred in batches 1 and 2, but not in batch 3. The repetition of the result prompted further investigation into whether the trend can be attributed to random variance within the sample batches, or whether the variation between the batches contributed significantly to the observed variation. This was done by utilising a single factor ANOVA method.

The results of the ANOVA tests, performed at each concentration level for the three batches of duplicate analyses, showed the between-batch variation contributed significantly to the variance between the measured responses at the 1.69 ppm level. The large variation between the measured responses at this concentration level is visible in the graph of the linear regression models calculated for the mean relative response and the three individual batches (**Figure IV-21**).

Table IV-10. Comparison of precision in the estimation of the concentration of acovenoside A in urine samples, via the %-RSD values calculated for each theoretical concentration level.

Concentration (ppm)	%-RSD (Linear model)	%-RSD (Log-linear model)
0.936	25.9	53.7
1.12	18.8	37.6
1.31	15.5	30.1
1.50	14.5	29.2
1.69	21.8	16.0

Precision in calculating concentrations of acovenoside A (**22**) from the linear or the log-linear response model was determined from the calculated standard deviation at each theoretical concentration of acovenoside A (**22**). The %-relative standard deviations were then calculated at each concentration level relative to the theoretical concentration of acovenoside A (**22**) (**Table IV-10**). Neither response model showed suitable repeatability in the estimation of concentration, since the %-RSD values are greater than the expected value estimated at 16% from the Horwitz equation.^{74,75} In exception to this observation, the %-RSD values calculated for the linear regression model at concentration levels of 1.31 and 1.50 ppm, did fall within the expected range of variance based on the Horwitz equation.⁷⁴

In the linear regression model, the %-RSD values indicated a homoscedastic distribution of variance over the regression model. The %-RSD values calculated for the log-linear model, indicated a heteroscedastic distribution of variance over the range of theoretical concentrations in the regression model.

In terms of the repeatability in calculating the concentration of acovenoside A (**22**) in a sample, the linear regression model estimated the concentrations with a lower %-RSD than the log-linear method. However, in both de-ionised aqueous and urine matrices, the log-linear model provided a closer correlation with a random distribution of data points in the y-residuals plot. Therefore, the log-linear regression model should be considered for further investigation in the application to the quantitative analysis of samples.

3.4.2 Limits of analyte detection and quantitation

Applying the same reasoning as in the discussion on linearity, the log-linear models for both matrices' calibration models were utilised in calculating the limits of detection and quantification. Calculation of the limits of detection and quantification from the calculated

response models were done based on the guidelines of the United States Department of Health and Human Services.⁷⁷ The method selected from the guidelines estimated the limit of detection as the concentration of acovenoside A (in ppm) that corresponds to a log(relative response) equal to three times the standard deviation of the logarithm of the blank signal at the analyte retention time.⁷⁷

The limit of detection in urine samples was calculated to be 2.88 ppm with a standard deviation of 1.30 ppm. The one-standard-deviation confidence interval encompasses the upper levels of the concentration range of the spiked samples. Since the limit was calculated from a standard deviation associated with the regression model, the large variance and absence of significant correlation contributed to the unexpectedly high limit. With an improvement in repeatability the limit of detection is expected to decrease.

In de-ionised aqueous samples, the limit was 0.952 ppm with a standard deviation of 0.197 ppm. This limit differs significantly from the detection limit in the urine samples at the $\alpha = 0.046$ significance level. The significantly lower limit of detection in de-ionised aqueous samples can be attributed to the fewer matrix components present in de-ionised water, compared to urine.

In both matrices the limits of detection fell well within the range of theoretical concentrations of acovenoside A (**22**) that were analysed in the development of the calibration models. Since neither regression model correlated significantly with the measured data, an alternative approach that does *not* rely on the variance of the measured relative responses for calculating the limit of detection, must be considered.

Applying the same method of calculation, the limits of quantification were estimated from the log-linear regression models at ten standard deviations of the logarithm of the blank signal. In de-ionised aqueous samples, the limit was calculated to be 3.17 ppm with a corresponding standard deviation of 0.73 ppm. The limit of quantification in urine was calculated to be 9.60 ppm. The limit had a standard deviation of 3.92 ppm. Both these limits are significantly greater than the concentration levels analysed in the development of the calibration models. This result can be attributed to the problematic correlation in the response model and the deficiency in method repeatability.

3.4.3 *Selectivity (Specificity) of the analytical method*

The hydrolysis and derivatisation of acovenoside A (**22**) produced multiple products that elute at different retention times in the chromatogram – a case that is not ideal in any manner. Since most of the analyte signal was attributed to two chromatographic peaks, only these peaks were analysed to quantify and identify acovenoside A (**22**) in a sample. Despite both chromatographic peaks containing the same ions, the baseline resolution in retention time distinguished between these peaks as different compounds, possibly isomers. Their ion ratios should therefore be treated as two independent sets of variables.

Despite being treated as two independent sets of variables, the vectors of ratios measured for a test sample must simultaneously fall within the 99.7% confidence interval around the corresponding centroids for positive identification. This criterion is based on the co-existence of the two chromatographic peaks that were employed in the quantification of acovenoside A (**22**).

The sets of ion ratios that have been used for identification were the same in both chromatographic peaks since the corresponding mass spectra contained the same ions (**Figure IV-13** & **Figure IV-14**). These ratios are defined in **Table IV-6**.

3.4.4 *Recovery of the analyte and accuracy in measurement*

The accuracy of the method and its level of analyte recovery were evaluated by plotting the concentration of acovenoside A (**22**), calculated from the linear regression models of each matrix, against the theoretical concentration of acovenoside A (**22**) in the samples (**Figure IV-24**). In the accuracy response model for de-ionised aqueous samples, the calculated gradient was 1.00 and the y-intercept was calculated to be naught. For the urine samples, the model generated for the regression of the calculated concentration on the theoretical concentration had a slope of 1.00 and a y-intercept, at -9×10^{-16} ppm, that does not differ significantly from naught for $\alpha = 0.046$ (**Figure IV-24**).

The results of the accuracy study showed that in both matrices the concentration can be measured accurately from the linear response model. However, the problematic repeatability of the method in either regression model (linear and log-linear) of both matrices, must be addressed before the method can be applied in routine analyses.

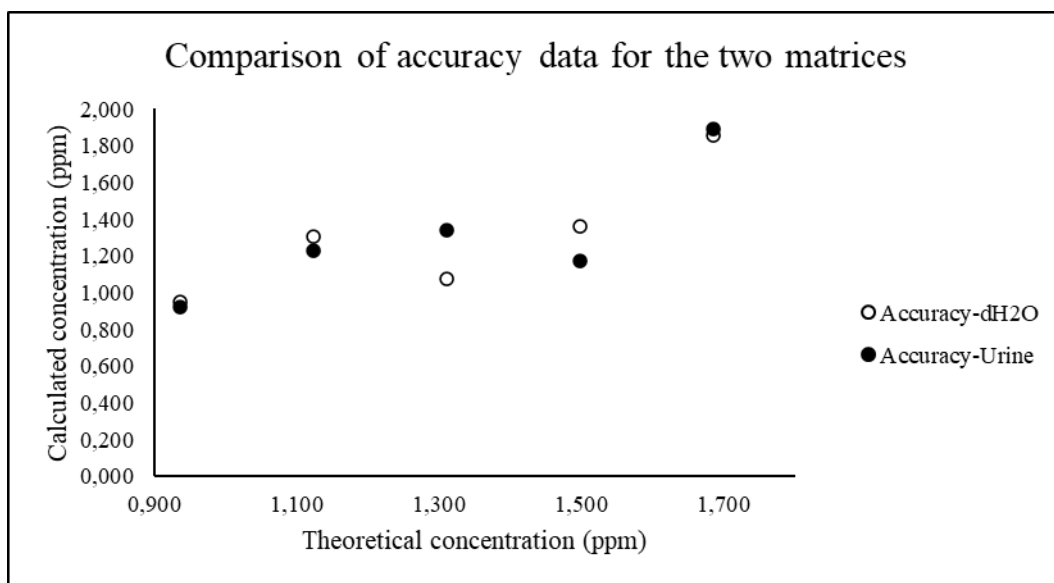


Figure IV-24. A comparison of the accuracy data for urine and de-ionised water samples. The linear equation and r^2 -coefficient for both matrices' accuracy models are adjacent to the related trendlines.

It was expected that the accuracy would decrease in the urine samples relative to the de-ionised aqueous samples, since the matrix components might influence the retention of the analyte in the SPE-cartridges. That would severely impact the recovery of analyte from the samples and produce a negative bias. Since neither response model's accuracy regression line deviated significantly from the $y = x$ line, it can be assumed neither response model was subjected to significant bias.

3.5 Validation of qualitative figures of merit in the analytical method

The analysis of ion ratios and the comparison of them between matrices is an integral part of positive analyte identification in sample matrices when low resolution mass spectrometry is employed. In the positive identification of acovenoside A (**22**) from its ion ratios, in either matrix, two chromatographic peaks must be considered simultaneously. In this discussion, the peak that elutes at 2.062 min (relative to the internal standard signal) will be denoted as AA-LHS. The peak that elutes at 2.213 min (relative to the internal standard signal) will be denoted AA-RHS.

For positive identification of acovenoside A (**22**) the ion ratios, selected as in Section 3.3.3 (Table IV-6) were utilised. Positive identification was assumed when all ten ion ratios, five per chromatographic peak, were within the 99.7% confidence interval of the centroids of ratios for the respective peaks. The centroids were calculated as the average ion ratios detected within a chromatographic peak for samples of a single matrix, spiked with an acovenoside A (**22**)

concentration of 1.311 ppm. The centroids of all the ratios in the two respective peaks detected in the de-ionised aqueous samples were:

$$\overline{m}_{HLHS} = \begin{bmatrix} 0.1754 \\ 0.1064 \\ 0.6373 \\ 0.8165 \\ 0.7936 \end{bmatrix} \text{ with } \overline{s}_{HLHS} = \begin{bmatrix} 0.0641 \\ 0.0264 \\ 0.1226 \\ 0.1638 \\ 0.1522 \end{bmatrix}$$

$$\overline{m}_{HRHS} = \begin{bmatrix} 0.1544 \\ 0.0842 \\ 0.5444 \\ 0.8371 \\ 0.6504 \end{bmatrix} \text{ with } \overline{s}_{HRHS} = \begin{bmatrix} 0.0308 \\ 0.0185 \\ 0.0309 \\ 0.0475 \\ 0.0063 \end{bmatrix}$$

In the urine samples the centroids of the ion ratios in the respective peaks were:

$$\overline{m}_{ULHS} = \begin{bmatrix} 0.1771 \\ 0.1064 \\ 0.6582 \\ 0.7840 \\ 0.8284 \end{bmatrix} \text{ with } \overline{s}_{ULHS} = \begin{bmatrix} 0.0586 \\ 0.0241 \\ 0.2748 \\ 0.1864 \\ 0.2360 \end{bmatrix}$$

$$\overline{m}_{URHS} = \begin{bmatrix} 0.1757 \\ 0.0797 \\ 0.4654 \\ 0.7081 \\ 0.4907 \end{bmatrix} \text{ with } \overline{s}_{URHS} = \begin{bmatrix} 0.0502 \\ 0.0143 \\ 0.0618 \\ 0.1373 \\ 0.0582 \end{bmatrix}$$

3.5.1 Variation of ion ratios over the modelled calibration range in de-ionised aqueous samples

In AA-LHS, each of the measured ion ratios (Section 3.3.3) remains within the 99.7% confidence interval about the centroid across the entire calibration range. The ion ratios recorded for the chromatographic peak AA-RHS in the aqueous samples fall within the corresponding limits (at $\alpha = 0.003$) for each concentration, except at 0.936 ppm. At this concentration level, IR 5 was significantly different from the centroid (**Figure IV-25**). Since the criterium for positive identification requires both chromatographic peaks to be positively identified simultaneously, this significant deviation places a limit on the detection of acovenoside A (**22**) at 1.12 ppm.

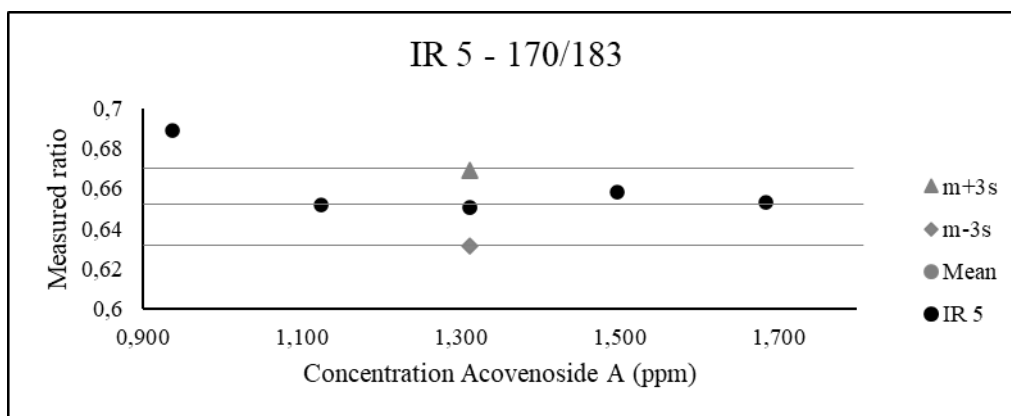


Figure IV-25. The distribution of ion ratio 5 in AA-RHS for the de-ionised aqueous samples. At 2.341 ppm the ratio significantly deviates from the centroid confidence interval for the ratio.

The ion ratios in both models' mass spectra remained quite constant over the higher levels of the concentration range of spiked acovenoside A (**22**) samples, except for the significant deviation observed in IR 5 of AA-RHS. This consistency in the ion ratios does not allow forecasting by forward or backward extrapolation to find a possible concentration where the ion ratio is expected to significantly deviate from the centroids. The point of significant deviation is more likely to appear after a sharp, significant change in one, or more, ion ratios as was seen for IR 5 in AA-RHS.

Precision in the measurement and calculation of the ion ratios were evaluated between the individual batches and within the batches, over the concentration range. Precision over the concentration range, for each individual ion ratio, was evaluated from the %-RSD values calculated relative to the mean of the ion ratio's distribution over concentration. Comparing the %-RSD values of the ion ratios showed which ion ratios were the most reliable for the identification of acovenoside A (**22**) at different concentration levels.

In the AA-LHS component only two ratios, IR 4 and IR 5, had %-RSD values less than 20%. The third lowest %-RSD value was associated with IR 2. A possible contributing factor to the large variance is the low chromatographic intensity and magnitude of the signal area for the AA-LHS component. This increases the relative contribution of background signal to the recorded mass spectra and, thus, to the ion ratios. In AA-RHS, the ratios all had %-RSD values less than 20%, and therefore, better precision in measurement than the ratios in AA-LHS. The three ratios with the lowest %-RSD value were IR 3, IR 4, and IR 5 (**Table IV-11**).

Table IV-11. %-RSD values calculated for each ion ratio in both chromatographic peaks.

Concentration (ppm)	%-RSD (AA-LHS)	%-RSD (AA-RHS)
IR 1	35,62	17,90
IR 2	24,32	19,77
IR 3	24,47	5,415
IR 4	15,94	5,966
IR 5	19,31	4,348

3.5.2 Variation of ion ratios over the modelled calibration range in urine samples

The analysis of the distribution of measured ion ratios from the urine samples over the range of spiked acovenoside A (**22**) concentrations, showed all the measured ratios were within the 99.7% confidence limit around the centroids. Thus, acovenoside A (**22**) can be positively identified, with 99.7% confidence, in urine samples at each theoretical concentration level in the calibration model. For the urine samples the limit of detection, based on the ion ratios, is lower than for samples in a de-ionised aqueous matrix. A possible limit of detection for the spiked urine samples was estimated based on the measured ion ratios for samples spiked at concentrations below the calibration range.

Three urine samples were spiked at concentrations of 0.187 ppm, 0.373 ppm and 0.560 ppm acovenoside A (**22**) respectively and analysed in duplicate. Significant deviation of the measured ion ratios from the centroid region was evaluated with Hotelling's T^2 -test at the $\alpha = 0.003$ significance level. Only the AA-LHS chromatographic peak, for the urine samples, was analysed at first. If no significant deviations were observed, AA-RHS would also be analysed. If a significant deviation was confirmed in the AA-LHS signal component, then the limit of detection can be estimated without further analysis of the AA-RHS component. The results for Hotelling's T^2 -test are summarised in **Table IV-12**.

Table IV-12. Results from performing Hotelling's T^2 -test to compare the ion ratios from low concentrations acovenoside A to the centroid confidence interval.

Concentration (ppm)	T^2	F-stat (n = 6; p = 5)	F (5, 1)*
0.187	1.734E+07	6.937E+05	0.03460
0.373	5.987E+06	2.395E+05	
0.560	3.043E+04	1.217E+03	

* $\alpha = 0.003$ for a two-tailed distribution

Hotelling's T^2 -test showed that the ion ratios measured at an acovenoside A (**22**) concentration of 0.5595 ppm in urine, significantly deviated from the ratios in the centroid region at a significance level of $\alpha = 0.003$. Since the ion ratios measured for the concentrations in the calibration model, all lie within the confidence region, the experimental limit of detection lies between 0.560 ppm and 0.936 ppm. This supports the hypothesis that the significant deviation in the ion ratios would occur after a sudden change in the measured ratios rather than along a linear trend.

Table IV-13. %-RSD values calculated for the individual ion ratios, distributed over the concentration range of the calibration model.

Ion ratio	%-RSD (AA-LHS)	%-RSD (AA-RHS)
IR 1	35,62	17,90
IR 2	24,32	19,77
IR 3	24,47	5,415
IR 4	15,94	5,966
IR 5	19,31	4,348

Analysis of the %-RSD values calculated for each individual ion ratio in the AA-LHS component, showed a different trend than for the de-ionised aqueous samples. For the urine samples, the %-RSD values were greater in magnitude and the lowest values were associated with IR 1, IR 2, and IR 5 (**Table IV-13**). The greater magnitude of relative variance can be attributed to the additional background signal produced by the urine matrix.

In the AA-RHS component, the magnitude of the calculated %-RSD values was also greater than in the samples with a de-ionised aqueous matrix. Comparing these %-RSD values to those for the AA-LHS component for the urine samples, showed better precision in the ion ratios of

the AA-RHS component than in those of the AA-LHS component. This was also observed for the samples in the de-ionised aqueous matrix. The relative effect of the background noise on the measured signal areas is less in the high intensity AA-RHS component than in the lower intensity AA-LHS component (See **Table IV-13**).

3.5.3 Between-batch variation of ion ratios at a single concentration

To evaluate the contribution of between-batch variation to the variance between the individual measurements for each respective ion ratio, a MANOVA-analysis was performed. The ratios analysed were measured at the centroid concentration of acovenoside A. The analyses were done via the IBM® SPSS® Statistics Software suite (ver. 26). The contributing components to the total analyte signal, AA-LHS and AA-RHS, were analysed independently.

The ion ratios for the AA-LHS component of the analyte signal for samples in de-ionised water, was analysed first. A Wilks' Lambda (Λ) value of 0.022 was obtained from the distribution of the ratios. This corresponded to an F-value of 1.916 for 6 degrees of freedom in the numerator and 2 in the denominator. At a significance level of $\alpha = 0.003$, this F-value was less than the critical F-value of 332.666, thus, there is no significant contribution to the variance by the between-batch variation in the ion ratios for the AA-LHS component.

In the AA-RHS component of the samples in the de-ionised aqueous matrix, the MANOVA analysis of the ratios generated a Λ -value of 0.202 and a corresponding F-value of 0.408. For 6 degrees of freedom in the numerator and 2 in the denominator, the calculated F-value is less than the one-tailed critical F-value for these degrees of freedom at $\alpha = 0.003$. The between-batch variation does, therefore, not significantly contribute to the variance within the respective sets of measured ion ratios.

From the results of the MANOVA analysis, the between-batch variation for the total analyte signal does not significantly contribute to the variance within any specific ion ratio. Therefore, across multiple batches the method can be expected not to produce additional variance.

For the urine samples, the same approach was employed. The AA-LHS signal component was calculated to have a Λ -value of 0.004. With six degrees of freedom in the numerator and two in the denominator, the calculated F-value was 4.743. The same critical F-value (one-tailed at $\alpha = 0.003$) applies as in the de-ionised water samples. For the specified confidence level, the calculated F-value was less than the critical value, thus, the between batch variation does not make a significant contribution to the variance within the measured values of any tested ion ratio.

Analysis of the ratios in the AA-RHS component produced the same result with a Λ -value of 0.001 and corresponding F-value, with the same degrees of freedom, of 9.597. Therefore, in neither de-ionised water, nor in urine, did the between-batch variation significantly contribute to the variance within the measured values for a specific ion ratio. The method can be applied to multiple batches of samples in a specific matrix without producing additional variance due to variation in measurement between the batches.

4. Conclusion to Chapter IV

Through the work described in this chapter, a method was developed for the preparation and subsequent analysis of urine samples for the presence of the mono-dehydrated aglycone of acovenoside A. The developed method could separate two prominent chromatographic peaks of the analyte from the signals in the urine matrix and confirm the presence of acovenoside A's mono-dehydrated aglycone in the urine sample. By calculating the mean vectors of ion ratios at the centroid concentration level, with a 99.7% confidence interval for both chromatographic signals in the analyte signal, a control range was set up for the identification of the trisilylated dehydrated derivative of acovenoside A (35).

$$\text{For } \bar{m} = \begin{bmatrix} m_{IR1} \\ m_{IR2} \\ m_{IR3} \\ m_{IR4} \\ m_{IR5} \end{bmatrix} \pm 3\bar{s}: \bar{m}_{ULHS} = \begin{bmatrix} 0.1771 \\ 0.1064 \\ 0.6582 \\ 0.7840 \\ 0.8284 \end{bmatrix} \pm \begin{bmatrix} 0.1759 \\ 0.0724 \\ 0.8244 \\ 0.5592 \\ 0.7079 \end{bmatrix} \text{ and } \bar{m}_{URHS} = \begin{bmatrix} 0.1757 \\ 0.0797 \\ 0.4654 \\ 0.7081 \\ 0.4907 \end{bmatrix} \pm \begin{bmatrix} 0.1506 \\ 0.0430 \\ 0.1853 \\ 0.4120 \\ 0.1746 \end{bmatrix}$$

Sample preparation and analytical methods were also applied to generate a calibration model for the quantitative analysis of urine samples, spiked with acovenoside A (22). The aim being application of the developed method in routine setting. The limits of the method were determined by following method validation procedures. By modelling the measured relative response values as a log-linear trend, a closer correlation was obtained than with a linear regression model. The calculated line of best fit is described by the equation:

$$y = 0.76 \text{ ppm}^{-1} \cdot x - 1.28$$

where y is the logarithm (base 10) of the measured relative response, and x is the concentration of acovenoside A (22) in parts per million ($\mu\text{g/mL}$). The standard deviation of the slope was calculated to be 0.30 ppm^{-1} and that of the intercept 0.40.

The log-linear model had ideal accuracy, with a regression line, for the calculated concentration vs. the theoretical concentration of acovenoside A (22), that did not significantly differ from

the $y = x$ line. However, the precision in the log-linear regression model was not ideal since there was no significant correlation between the logarithm of the measured relative response values and the calculated trendline. The log-linear model's correlation was better than that of the linear model.

The precision of the calibration model in calculating the theoretical concentrations of acovenoside A (**22**) was determined through calculation of the %-RSD value at each theoretical concentration. In the log-linear model the %-RSD values were all greater than or equal to the 16% expected value, from the Horwitz equation.

The research described in this chapter opens the door to further research into improving the precision and correlation of the calibration model for urine samples, containing acovenoside A (**22**). Factors that should be addressed include the development of a more efficient sample preparation method and the optimisation of the hydrolysis and derivatisation of acovenoside A (**22**). This optimisation should focus on decreasing the number of products formed by each reaction step to improve the precision and the method accuracy. An alternative would be to include more chromatographic peaks in calculating the signal strength of the analyte. In this project only two peaks were used since they were the best resolved and had similar mass spectra with similar ion ratios.

Further investigation into the analysis of trends in the ion ratios can be done. However, further laboratory experiments should be considered to thoroughly investigate the sudden change in ion ratios that define the limit of detection at the fundamental level of positive identification.

References

- (1) Neuwinger, H. D. 1996. *Acokanthera* spp. *African Ethnobotany - Poisons and Drugs*. Weinheim: Chapman & Hall GmbH, pp. 60-80.
- (2) Hutchings, A., Scott, A. H., Lewis, G. & Cunningham, A. B. 1996. *Acokanthera oppositifolia* (Lam.) Codd. *Zulu Medicinal Plants - An Inventory*. South Africa: University of Natal Press, pp. 243.
- (3) Botha, J. & Weiersbye, I. 2010. Ethnobotanic and forage uses of plants on mine properties in the Witwatersrand basin gold fields, South Africa. *Fourie, A. Tibbett, M. and Wiertz, J.(eds) Mine closure*, 2010.
- (4) Van Wyk, B.-E., Van Heerden, F. & Van Oudtshoorn, B. 2014. *Acokanthera oppositifolia*. In: Ferreira, R. (ed.) *Poisonous plants of South Africa*. 1st ed. ed. Pretoria: Briza Publications, pp. 34-35.
- (5) Van Wyk, B.-E. & Gericke, N. 2018. Women's Health. *People's Plants - A guide to useful plants of southern Africa*. 2nd ed. Pretoria: Briza Publications, pp. 215-232.

- (6) Steenkamp, V. 2003. Traditional herbal remedies used by South African women for gynaecological complaints. *Journal of Ethnopharmacology*, 86, 97-108.
- (7) Wink, M. & Van Wyk, B.-E. 2008. *Acokanthera oppositifolia*. In: Pearson, D. (ed.) *Mind-altering & Poisonous Plants of the World*. First ed. Pretoria: Briza Publications, pp. 39.
- (8) Van Wyk, B.-E. & Gericke, N. 2018. Dental Care. *People's Plants - A guide to useful plants of southern Africa*. 2nd ed. Pretoria: Briza Publications, pp. 247-256.
- (9) Van Wyk, B.-E. & Gericke, N. 2018. Hunting & Fishing. *People's Plants - A guide to useful plants of southern Africa*. 2nd ed. Pretoria: Briza Publications, pp. 287-295.
- (10) Neuwinger, H. D. 1974. Pflanzliche Pfeilgifte. *Afrikanische Pfeilgifte*. Stuttgart: Wissenschaftliche Verlagsgesellschaft m.b.H., pp. 29-31.
- (11) Hauschild-Rogat, P., Weiss, E. K. & Reichstein, T. 1967. Die Cardenolide von *Acokanthera oppositifolia* (LAM.) CODD. 3. Mitteilung . Isolierung weitere Cardenolide und teilweise Strukturaufklärung. Glykoside und Aglykone, 301. Mitt. *Helvetica Chimica Acta*, 50, 2299-2321.
- (12) Saeed, M. E., Meyer, M., Hussein, A. & Efferth, T. 2016. Cytotoxicity of South-African medicinal plants towards sensitive and multidrug-resistant cancer cells. *Journal of Ethnopharmacology*, 186, 209-223.
- (13) El Gaafary, M., Ezzat, S. M., El Sayed, A. M., Sabry, O. M., Hafner, S., Lang, S., Schmiech, M., Syrovets, T. & Simmet, T. 2017. Acovenoside A Induces Mitotic Catastrophe Followed by Apoptosis in Non-Small-Cell Lung Cancer Cells. *Journal of Natural Products*, 80, 3203-3210.
- (14) Ezzat, S. M., El Gaafary, M., El Sayed, A. M., Sabry, O. M., Ali, Z. Y., Hafner, S., Schmiech, M., Jin, L., Syrovets, T. & Simmet, T. 2016. The Cardenolide Glycoside Acovenoside A Affords Protective Activity in Doxorubicin-Induced Cardiotoxicity in Mice. *Journal of Pharmacology and Experimental Therapeutics*, 358, 262-270.
- (15) Stafford, G. I. 2009. *Southern African plants used to treat central nervous system related Disorders*. University of KwaZulu-Natal, Pietermaritzburg.
- (16) Bethwell, O. O. 2007. *Acokanthera oppositifolia* (Lam.) Codd. [Online]. Wgeningen: PROTA (Plant Resources of Tropical Africa / Ressources végétales de l'Afrique tropicale). Available: [https://www.prota4u.org/database/protav8.asp?g=pe&p=Acokanthera+oppositifolia+\(Lam.\)+Codd](https://www.prota4u.org/database/protav8.asp?g=pe&p=Acokanthera+oppositifolia+(Lam.)+Codd) [Accessed 2020-04-27].
- (17) Chaboo, C. S., Biesele, M., Hitchcock, R. K. & Weeks, A. 2016. Beetle and plant arrow poisons of the Ju|'hoan and Hai||om San peoples of Namibia (Insecta, Coleoptera, Chrysomelidae; Plantae, Anacardiaceae, Apocynaceae, Burseraceae). *ZooKeys*, 9-54.
- (18) Van Den Berg, H., Schultz, R. & Kellerman, T. 2005. The role of fluorescence polarization immuno-assay in the diagnosis of plant-induced cardiac glycoside poisoning livestock in South Africa. *Onderstepoort Journal of Veterinary Research*, 72, 189-201.
- (19) Hankey, A. 2001. *Acokanthera oppositifolia* (Lam.) Codd [Online]. Pretoria: SANBI (South African National Biodiversity Institute). Available: <http://pza.sanbi.org/acokanthera-oppositifolia> [Accessed 2020-04-27].

- (20) Van Wyk, B.-E., Van Heerden, F. & Van Oudtshoorn, B. 2014. Animal poisoning in South Africa. In: Ferreira, R. (ed.) *Poisonous Plants of South Africa*. 1st ed. ed. Pretoria: Briza Publications, pp. 10-11.
- (21) Neuwinger, H. D. 1974. Die Giftpflanzen und ihre Wirkstoffe. *Afrikanische Pfeilgifte*. Stuttgart: Wissenschaftliche Verlagsgesellschaft m.b.H., pp. 9-27.
- (22) Timbrell, J. 2009. 3.2 Absorption. *Principles of Biochemical Toxicology*. 4th ed. New York: Informa Healthcare USA, Inc., pp. 35-43.
- (23) El-Seedi, H. R., Khalifa, S. A., Taher, E. A., Farag, M. A., Saeed, A., Gamal, M., Hegazy, M.-E. F., Youssef, D., Musharraf, S. G. & Alajlani, M. M. 2018. Cardenolides: Insights from chemical structure and pharmacological utility. *Pharmacological research*.
- (24) Evans, W. C. 2009. Saponins, cardioactive drugs and other steroids. In: Evans, D. (ed.) *Trease and Evans Pharmacognosy*. 16 ed. New York: Saunders Elsevier, pp. 304-332.
- (25) Bartnik, M. & Facey, P. C. 2017. Glycosides. In: Badal, S. & Delgoda, R. (eds.) *Pharmacognosy: Fundamentals, Applications and Strategy*. London: Elsevier Inc., pp. 101-161.
- (26) Sticher, O. 2010. Triterpene einschließlich Steroide. In: Hänsel, R. & Sticher, O. (eds.) *Pharmakognosie — Phytopharmazie*. Berlin, Heidelberg: Springer Berlin Heidelberg, pp. 833-938.
- (27) El-Seedi, H. R., Khalifa, S. a. M., Taher, E. A., Farag, M. A., Saeed, A., Gamal, M., Hegazy, M.-E. F., Youssef, D., Musharraf, S. G., Alajlani, M. M., Xiao, J. & Efferth, T. 2019. Cardenolides: Insights from chemical structure and pharmacological utility. *Pharmacological research*, 141, 123-175.
- (28) Smith, J. G. 2017. Other Facts About the Diels-Alder Reaction. In: Timp, T., Pellerito, A. & Murdzek, J. (eds.) *Organic Chemistry*. 5th ed. New York: The McGraw-Hill Companies Inc., pp. 627-630.
- (29) Doherty, J. E. 1973. Digitalis glycosides: Pharmacokinetics and their clinical implications. *Annals of internal medicine*, 79, 229-238.
- (30) Haustein, K. O. 1982. Digitalis. *Pharmacology & Therapeutics*, 18, 1-89.
- (31) Smith, J. G. 2017. Dehydration of Alcohols to Alkenes. In: Timp, T., Pellerito, A. & Murdzek, J. (eds.) *Organic Chemistry*. 5th ed. New York: The McGraw-Hill Companies Inc., pp. 345-348.
- (32) Wink, M. & Van Wyk, B.-E. 2008. Main classes of toxins and psychoactive compounds. In: Pearson, D. (ed.) *Mind-altering & Poisonous Plants of the World*. First ed. Pretoria: Briza Publications, pp. 252-337.
- (33) Kang, Y. J. 2008. Toxic Responses of the Heart and Vascular System. In: Klaassen, C. D. (ed.) *Casarett & Doull's Toxicology - The Basic Science of Poisons*. 7th ed. New York: The McGraw-Hill Companies, Inc., pp. 699-739.
- (34) 2015. *Lanoxin (digoxin) tablets* [Online]. St. Michael, Barbados: Concordia Pharmaceuticals Inc. Available: https://www.accessdata.fda.gov/drugsatfda_docs/label/2018/009330s0331bl.pdf [Accessed 2020-07-14].
- (35) Raven, P., Johnson, G., Mason, K., Losos, J. & Singer, S. 2014. Muscle Contraction. *Biology*. 10th ed. New York: The McGraw-Hill Companies Inc., pp. 969-975.

- (36) Hall, J. E. & Guyton, A. C. 2011. Cardiac Muscle; The Heart as a Pump and Function of the Heart Valves. *In: Gruliow, R. (ed.) Guyton and Hall Textbook of Medical Physiology*. 12 ed. Philadelphia: Saunders, Elsevier Inc., pp. 101-113.
- (37) Guyton, A. C. 1991. Heart Muscle; The Heart as a Pump. *Textbook of Medical Physiology*. 8th ed. Philadelphia: W. B. Saunders Company, pp. 98-110.
- (38) Todorovic, M. & Barton, M., 2018. *Digoxin - Mechanism of Action*, Dr Matt & Dr Mike. Available: <https://www.youtube.com/watch?v=Xm0vsJ8IU9c> [Accessed 2020-04-23].
- (39) Sampson, K. J. & Kass, R. S. 2011. Anti-Arrhythmic Drugs. *In: Brunton, L. L., Chabner, B. A. & Knollmann, B. C. (eds.) Goodman & Gilman's The Pharmacological Basis of Therapeutics*. 12th ed. New York: The McGraw-Hill Companies, Inc., pp. 815-848.
- (40) Van Der Merwe, D. 2009. Poisons of Plant Origin. *In: Ballantyne, B., Marrs, T. C. & Syversen, T. (eds.) General and Applied Toxicology*. 3rd ed. West Sussex: John Wiley & Sons Limited, pp. 3449-3466.
- (41) Raven, P., Johnson, G., Mason, K., Losos, J. & Singer, S. 2014. Vision. *Biology*. 10th ed. New York: The McGraw-Hill Companies Inc., pp. 927-933.
- (42) Chao, M.-W., Chen, T.-H., Huang, H.-L., Chang, Y.-W., Huangfu, W.-C., Lee, Y.-C., Teng, C.-M. & Pan, S.-L. 2017. Lanatoside C, a cardiac glycoside, acts through protein kinase C δ to cause apoptosis of human hepatocellular carcinoma cells. *Scientific Reports*, 7, 46134.
- (43) Khalid, M., Suliman, R., Ahmed, R., Salim, H. & Clarke, R. J. 2014. The High and Low Affinity Binding Sites of Digitalis Glycosides to Na,K-ATPase. *Arabian Journal for Science and Engineering*, 39, 75-85.
- (44) Hutchison, J. S., Ward, R. E., Lacroix, J., Hébert, P. C., Barnes, M. A., Bohn, D. J., Dirks, P. B., Doucette, S., Fergusson, D. & Gottesman, R. 2008. Hypothermia therapy after traumatic brain injury in children. *New England Journal of Medicine*, 358, 2447-2456.
- (45) Smith, J. G. 2017. Carbohydrates. *Organic Chemistry*. 5th ed. New York: McGraw-Hill Education, pp. 1106-1151.
- (46) Hayward, R. 1987. Digitalis: the present position. *In: Hamer, J. (ed.) Drugs for Heart Disease*. Dordrecht: Springer Science+Business Media, pp. 145-193.
- (47) Frey, W. A. & Vallee, B. L. 1980. Digitalis metabolism and human liver alcohol dehydrogenase. *Proceedings of the National Academy of Sciences*, 77, 924-927.
- (48) Tzou, M.-C., Sams, R. & Reuning, R. 1995. Specific and sensitive determination of digoxin and metabolites in human serum by high performance liquid chromatography with cyclodextrin solid-phase extraction and precolumn fluorescence derivatization. *Journal of pharmaceutical and biomedical analysis*, 13, 1531-1540.
- (49) Tor, E. R., Holstege, D. M. & Galey, F. D. 1996. Determination of oleander glycosides in biological matrices by high-performance liquid chromatography. *Journal of Agricultural and Food Chemistry*, 44, 2716-2719.
- (50) Kiouisi, P., Angelis, Y., Koupparis, M., Kouretas, D., Diakakis, N., Desiris, A. & Georgakopoulos, C. 2004. Gas Chromatographic–Mass Spectrometric Cardiotonic Glycosides Detection in Equine Urine Doping Analysis. *Chromatographia*, 59, S105-S108.

- (51) Kohls, S., Scholz-Böttcher, B. M., Teske, J., Zark, P. & Rullkötter, J. 2012. Cardiac glycosides from Yellow Oleander (*Thevetia peruviana*) seeds. *Phytochemistry*, 75, 114-127.
- (52) Guan, F., Ishii, A., Seno, H., Watanabe-Suzuki, K., Kumazawa, T. & Suzuki, O. 1999. Identification and quantification of cardiac glycosides in blood and urine samples by HPLC/MS/MS. *Analytical chemistry*, 71, 4034-4043.
- (53) Aderjan, R., Buhr, H. & Schmidt, G. 1978. Investigation of cardiac glycoside levels in human post mortem blood and tissues determined by a special radioimmunoassay procedure. *Archives of toxicology*, 42, 107-114.
- (54) Brock, A. 1974. A radioimmunoassay for Digoxin in serum, urine and myocardial tissue. *Acta pharmacologica et toxicologica*, 34, 198-204.
- (55) Molina, D. K. 2010. Alphabetical Listing of Drugs. In: Geberth, V. J. (ed.) *Handbook of Forensic Toxicology for Medical Examiners*. Boca Raton: CRC Press, pp. 11-335.
- (56) Haynes, B. E., Bessen, H. A. & Wightman, W. D. 1985. Oleander tea: Herbal draught of death. *Annals of Emergency Medicine*, 14, 350-353.
- (57) Adamowicz, P. & Chudzikiewicz, E. 2002. Digoxin in a forensic laboratory—an analysis of cases. *On the issues of Forensic Science*, 49, 114-127.
- (58) Melo, P., Machado, R. & Teixeira, H. M. 2012. Analysis of digoxin and metildigoxin in whole blood using solid-phase extraction and liquid chromatography tandem mass spectrometry. *International journal of analytical chemistry*, 2012, 975824-975824.
- (59) Frommherz, L., Köhler, H., Brinkmann, B., Lehr, M. & Beike, J. 2008. LC-MS assay for quantitative determination of cardio glycoside in human blood samples. *International Journal of Legal Medicine*, 122, 109-114.
- (60) Kohls, S., Scholz-Böttcher, B., Rullkötter, J. & Teske, J. 2012. Method validation of a survey of thevetia cardiac glycosides in serum samples. *Forensic Science International*, 215, 146-151.
- (61) Øiestad, E. L., Johansen, U., Opdal, M. S., Bergan, S. & Christophersen, A. S. 2009. Determination of digoxin and digitoxin in whole blood. *Journal of analytical toxicology*, 33, 372-378.
- (62) Gault, M. H., Charles, J. D., Sugden, D. L. & Kepkay, D. C. 1977. Hydrolysis of digoxin by acid. *Journal of Pharmacy and Pharmacology*, 29, 27-32.
- (63) Toribio-Delgado, A. F., Maynar-Mariño, M., Caballero-Loscos, M. J., Robles-Gil, M. C., Olcina-Camacho, G. J. & Maynar-Mariño, J. I. 2012. Qualification and Quantification of Seventeen Natural Steroids in Plasma by GC-Q-MS and GC-IT-MS/MS. *Journal of chromatographic science*, 50, 349-357.
- (64) Deber, C. M., Stone, J. & Soldin, S. J. 1989. Deuterated digoxin. *Analytical letters*, 22, 2783-2790.
- (65) Yamaki, H., Nonaka, A., Tani, M. & Watanabe, M. 1999. GC/MS analysis for Strophanthidin and Digitoxigenin in Moroheiya (*Corchorus olitorius* L.). *Nippon Shokuhin Kagaku Kogaku Kaishi*, 46, 255-261.
- (66) Knapp, D. R. 1979. Derivatives of Digitalis Steroids. *Handbook of Analytical Derivatisation Reactions*. New York: John Wiley & Sons, Inc., pp. 511-514.

- (67) Vetticaden, S. J. & Chandrasekaran, A. 1990. Chromatography of cardiac glycosides. *Journal of Chromatography B: Biomedical Sciences and Applications*, 531, 215-234.
- (68) Bekker, L. 2004. *Development and validation, of a gas chromatographic method for the analysis of urinary endogenous steroid metabolites, and its diagnostic applications in the clinical laboratory*. MSc Dissertation, University of Pretoria, University of Pretoria.
- (69) Thurman, E. M. & Mills, M. S. 1998. Overview of Solid-Phase Extraction. In: Winefordner, J. D. (ed.) *Solid-Phase Extraction - Principles and Practice*. New York: John Wiley & Sons, Inc., pp. 1-23.
- (70) Agilent-Technologies 2009. Integration. *Agilent ChemStation - Understanding Your ChemStation*. 07/09 ed. Waldbronn: Agilent Technologies Inc., pp. 67-112.
- (71) European Commission: Directorate General for Health and Food Safety. 2017. *SANTE/11945/2015: Guidance document on analytical quality control and method validation procedures for pesticides residues analysis in food and feed*. European Commission: Directorate General for Health and Food Safety. Available: https://ec.europa.eu/food/sites/food/files/plant/docs/pesticides_mrl_guidelines_wrkdoc_2017-11813.pdf [Accessed 2020-08-26].
- (72) 2007. *Dictionary of Natural Products*. Boca Raton: Chapman and Hall/CRC.
- (73) European Commission: Directorate General for Health and Food Safety. 2020. *SANTE/12682/2019: Guidance document on analytical quality control and method validation procedures for pesticide residues analysis in food and feed*. European Commission: Directorate General for Health and Food Safety. Available: https://ec.europa.eu/food/sites/food/files/plant/docs/pesticides_mrl_guidelines_wrkdoc_2017-11813.pdf [Accessed 2020-08-26].
- (74) Rivera, C. & Rodríguez, R. 2014. Horwitz equation as quality benchmark in ISO/IEC 17025 testing laboratory. *Private communication*.
- (75) Massart, D. L., Smeyers-Verbeke, J. & Heyden, Y. 2005. Benchmarking for analytical Methods: The Horwitz curve. *LC GC Europe*, 18, 528-531.
- (76) Grubbs, F. E. 1969. Procedures for detecting outlying observations in samples. *Technometrics*, 11, 1-21.
- (77) Center for Drug Evaluation and Research. 1996. *Guidance for Industry - Q2B Validation of Analytical Procedures: Methodology*. Rockville: Center for Drug Evaluation and Research. Available: https://ec.europa.eu/food/sites/food/files/plant/docs/pesticides_mrl_guidelines_wrkdoc_2017-11813.pdf [Accessed 2020-08-26].

Chapter V

Urginea sanguinea (Schinz) Jessop

1. Background and information

1.1 Ethnic applications of *Urginea sanguinea*

In ethnic medicine, the cardio-activity of extracts from *U. sanguinea* is utilised for the treatment of blood circulation and cardiac ailments.^{1,2} *U. sanguinea* is used in a variety of forms – decoctions,¹ poultices,³ pastes,⁴ snuff powder,⁵ and juices from the bulb scales. When a decoction made from the extracts of the bulb is consumed, it triggers an emetic response.⁶ This has led to the use of *U. sanguinea* as a blood ‘purifier’ and to treat persistent coughing.^{4,7} Pastes made from *U. sanguinea* extracts are used in disinfecting and dressing wounds.⁴

1.2 Toxic chemical constituents of *U. sanguinea*

U. sanguinea is infamous in the agricultural sector for its contribution to livestock fatalities.⁸ Similar to *A. oppositifolia*, *U. sanguinea*’s primary bioactive compounds are cardiac glycosides, however, they are of the bufadienolide class, and not cardenolides.^{4,8,9} This difference is easily identified by a six-membered lactone group at the C-17 β -position, instead of the five-membered lactone group characteristic to the cardenolides, as seen in **Figure V-1**.⁹

The most abundant bufadienolide in *U. sanguinea* is expected to be scillaren A (**40**) (**Figure V-3**).^{1,5} It also contains a reduced derivative of scillaren A (**40**), 4,5-dihydroscillaren A (**41**) (the aglycone of scillaren A (**40**)), scillarenin (**42**), and scillaredin A (**43**), the 2,3-dehydrated aglycone (**Figure V-3**).^{1,4,9} Unlike the cardioactive cardenolides of *A. oppositifolia*, the connection between rings A and B in scillaren A is planar between C-5 and C-10, and between C-5 and C-6.⁹ Since ring D is *cis* with respect to ring C, the substituents on C-3 and C-14 are β -oriented relative to the steroid skeleton and the lactone group is fully conjugated and scillaren A (**40**) remains cardioactive.^{9,10}

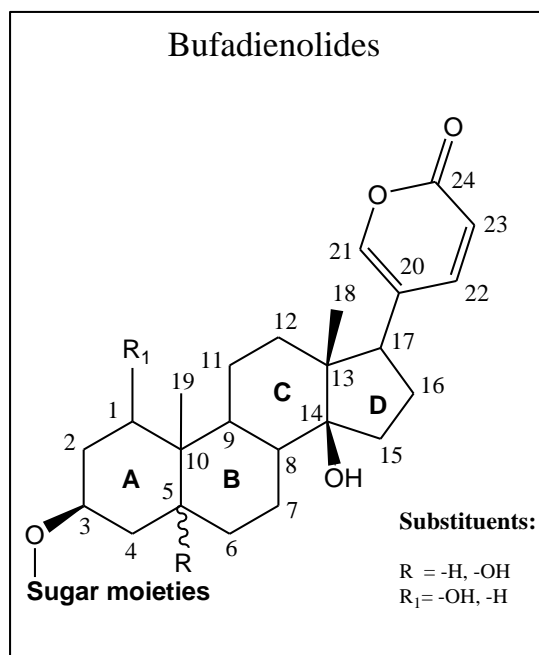


Figure V-1. General structure of bufadienolide cardiac glycosides.¹¹⁻¹⁴

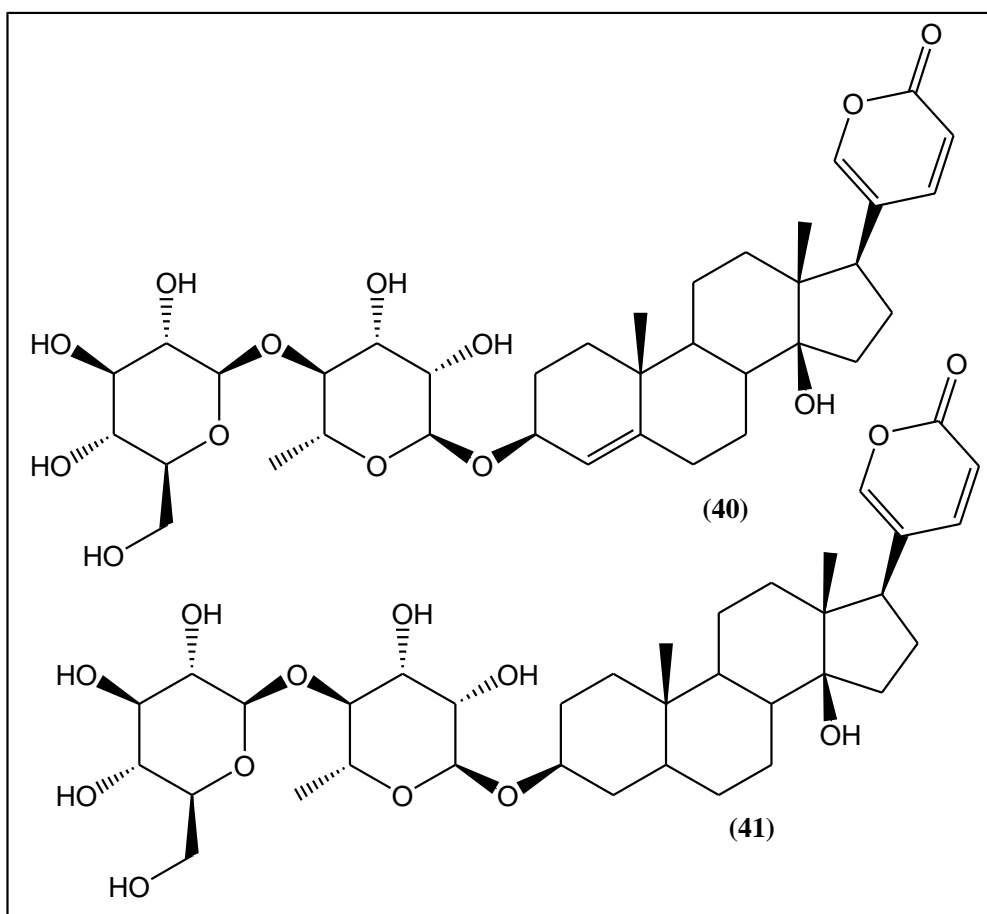


Figure V-2. Bufadienolide glycosides reported to be present in *U. sanguinea*: scillaren A (40), 4,5-dihydroscillaren A (41)

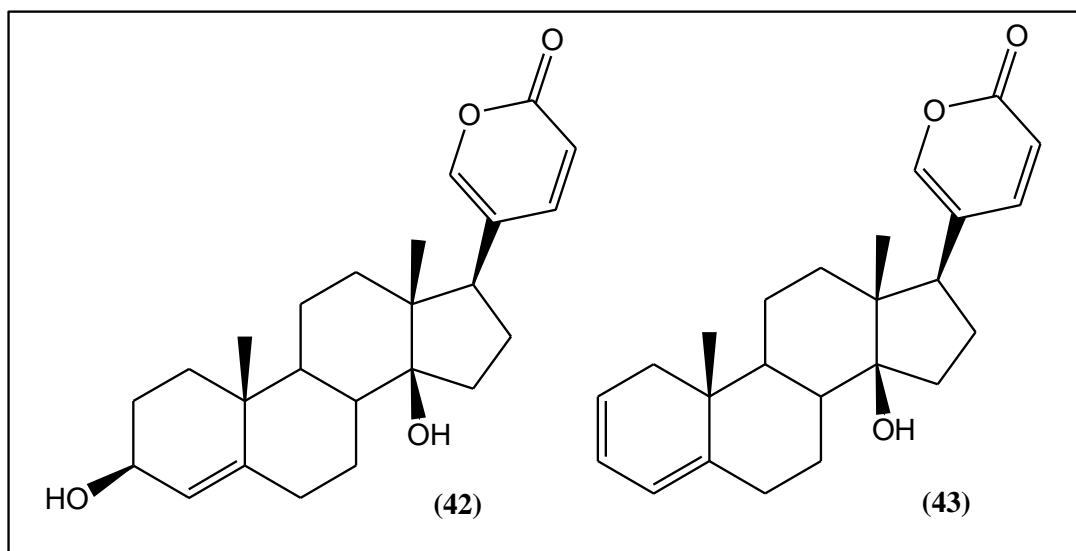


Figure V-3. Aglycone bufadienolide constituents reported to be present in *U. sanguinea*.: scillarenin (42), scillaredin A (43).^{1,9}

1.3 Physiological effects following intoxication

Like cardenolides, bufadienolides induce a positive inotropic effect in the cardiac muscle.⁵ Compounds of this class also, like the cardenolides, induce emetic effects; especially when consumed orally. As described by Marx et al.,⁵ neurotoxicity may also manifest in cases of severe overdose. McVann et al.³ describes a part of this neurotoxicity when describing the source of the induced emetic effect as central stimulation of the chemo-emetic trigger zone in the brain. This would imply the emetic effect is produced irrespective of the mode of cardiac glycoside absorption into the body, provided it enters the blood stream and is transported to the brain.

Bufadienolides induce neurotoxicity through inhibition of the sodium-potassium pumps ($\text{Na}^+/\text{K}^+\text{-ATPase}$) in neurons, and binding to the iso-enzyme digitalis receptors in the brain.⁵ Inhibition of $\text{Na}^+/\text{K}^+\text{-ATPase}$ in the brain affects neurotransmission by altering both the calcium and sodium ion intracellular concentrations. This, in turn, impacts the regulation of serotonin release in the synaptic cleft. The re-uptake of glutamate from the synaptic cleft is also affected by the sodium and calcium ion currents in the brain.⁵

A study by Kawahara et al.,¹⁵ mentioned by Marx, et al.⁵, indicated severe neuropathy induced by glutamate neurotoxicity when *in vitro* cell cultures were exposed to the cardenolide ouabain. Marx et al.⁵ suggests this neurotoxicity, induced by cardiac glycosides, as a cause for the induction of abortion in pregnant women who use *U. sanguinea* medicinally.⁵

Following the ingestion of bufadienolide-containing plant material by an animal, symptoms of cardiac glycoside toxicosis may take as long as two days before appearing.¹⁶ If greater quantities of material is ingested, symptoms may appear sooner. Bufadienolides may also induce cardiac toxicosis following chronic consumption of the poisonous plant by the animal. The type of poisoning (acute or chronic) can be deduced from the symptoms observed in the animals.⁸

In ruminants, acute cardiac toxicity is accompanied by ceasing of peristalsis in the rumen, causing bloatedness or constipation, watery diarrhoea, bruxism and abnormal respiratory rates.^{16,17} Accompanying neurotoxicity may manifest as muscle weakness in the hind quarters of the affected animal.¹⁶ This symptom is less prevalent in acute toxicosis than the cardiac and gastro-intestinal symptoms.⁸

Bufadienolides with a cumulative effect induce toxicosis, following chronic consumption of the plant causing a condition known as *krimpsiekte*.⁸ In these cases, the cardiac and gastro-intestinal symptoms are less severe. However the neurotoxic action becomes more prevalent and posterior paresis more severe – especially in small stock such as sheep and goats.⁸ A diagnosis of *krimpsiekte* is of great importance, since the meat of the affected animal may not be safe for consumption.⁸ Botha et al.¹⁸ noted that cases of fatal secondary poisoning has occurred in carnivores that consumed the flesh of animals that have succumbed to *krimpsiekte*.

According to Kellerman et al.⁸, bufadienolides from plants of the genus *Urginea* spp. are not expected to show cumulative action. This is corroborated by the acute nature of the symptoms observed in animals following consumption of plant material from *U. sanguinea*.² Both Marx et al.⁵ and Joubert and Schultz,¹⁶ however, state that the chronic consumption of small amounts of material from *U. sanguinea* has a cumulative effect that may lead to toxicosis.

1.4 Proposed metabolic pathways of scillaren A

Multiple pathways exist for the metabolism of scillaren A (**40**) in the human body. Bufadienolides, like cardenolides, undergo systematic cleavage of the glycosidic bonds present in the glycone molecule.^{10,19} In the case of scillaren A (**40**), enzymatic cleavage of the glycosidic bond in the disachcharide chain produces D-glucose and Proscillaridin A (**44**).^{1,5,20} Proscillaridin A can be further hydrolysed enzymatically, or under acidic conditions in the stomach, to produce the aglycone, Scillarinin (**42**).^{20,21}

Based on Han et al.'s study²² on the metabolism of bufalin (4,5-dihydroscillarenin) (**41**), the main pathways of bufadienolide aglycone metabolism in the liver are hydroxylation and dehydrogenation. Due to the double bond between C4 and C5, epimerisation of the C3-hydroxyl group during metabolism, as suggested by Han et al.²², might not occur.

Han et al.'s in depth study²² on the metabolism of bufalin by human hepatic microsomes, indicates that the dehydrogenation of bufalin occurs at the C3-position. This oxidises the hydroxyl functional group to a ketone, producing an oxo-metabolite. It is likely that this same process may occur in the hepatic metabolism of scillaren A (**45**) (**Figure V-4**).

According to the literature, phase II metabolism (conjugation reactions) is not often observed for bufadienolides in mammalian species.²² Based on Han et al.'s extensive study²² on the metabolism of bufalin, the characteristic six-membered lactone moiety remains unaffected by *hepatic* metabolism. In contrast, the five-membered lactone ring of cardenolides is readily hydrogenated to detoxify the glycoside.^{10,19}

Incubation under acidic conditions within the stomach, could lead to extensive dehydration of the aglycone, which readily forms within the stomach (**Figure V-4 (46) & (47)**).²⁰ This dehydration produces unsaturated systems that are susceptible to further metabolism, such as epoxidation and spontaneous subsequent hydroxylation.²³ Based on the observed metabolic pathways of bufalin it is, however, unlikely that phase II metabolism will proceed via human liver microsomes, following the phase I metabolism of both glycone and aglycone.²²

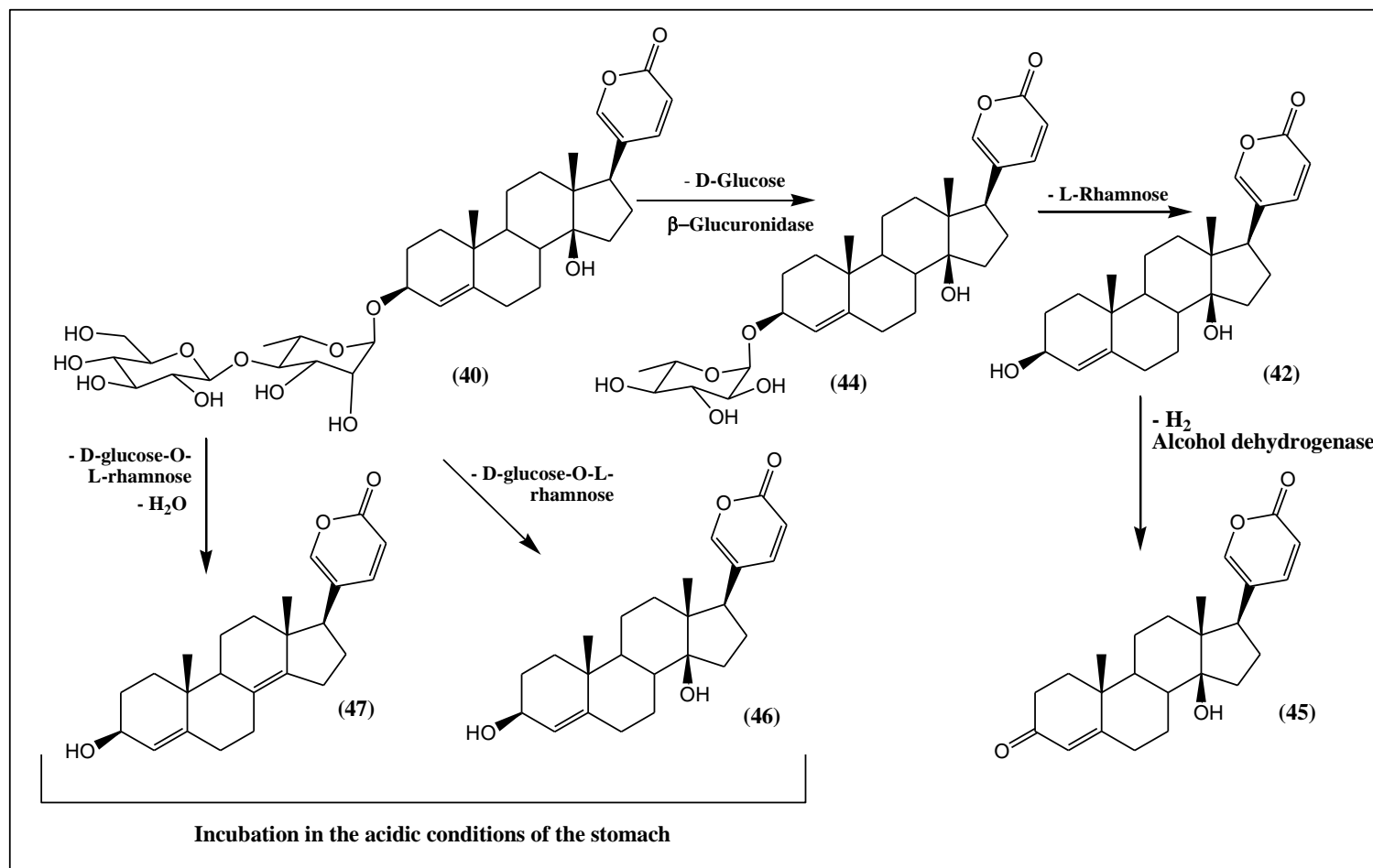


Figure V-4. Proposed metabolic pathway for scillaren A (40).^{22,24}

1.5 Cases and statistics of *U. sanguinea* poisoning

1.5.1 Cases and statistics regarding bufadienolide poisoning in humans

The high level of cardiac glycosides present in all components of the plant creates a great risk for overdose in patients who use *U. sanguinea* for medicinal purposes. The toxic nature of the plant is well known by ethnic herbalists (*amanyanga*) and is generally prescribed with great caution. Despite the caution of the herbalists, many patients self-medicate or determine their own dosage. This can lead to cardiac glycoside intoxication and possibly death.^{3,5}

In the 1987 to 1992 period, ten of the 313 reported cases of poisoning by plant material at the Ga-Rankuwa hospital were suspected of being caused by *U. sanguinea*. In a further four cases in the same period, poisoning with *U. sanguinea* was confirmed.² According to Marx et al.⁵ no records were available regarding poisoning with herbal medicines at Ga-Rankuwa hospital for the period 1992 to 2005.

1.5.2 Cases and statistics regarding bufadienolide poisoning in animals

A statistical survey, conducted by Kellerman et al.⁸ on the distribution of plant poisonings among small livestock and cattle in South Africa during 1995, indicates that bufadienolide-type cardiac glycosides are among the leading causes of mortality in livestock. Data from this survey shows that ~33% of cases where cattle were mortally poisoned by plants, were caused by the ingestion of bufadienolides. Among small livestock ~10% of plant poisoning cases were accounted for by fatal toxicosis from bufadienolide-containing plants.⁸

1.6 Methods for the detection of bufadienolides cited in literature

1.6.1 Radioimmuno assay

As with cardenolides, radioimmuno assays with broad-spectrum cardiac glycoside antibodies, can be used to diagnose bufadienolide poisoning.²⁵ RIA is a very sensitive technique; however, it is hampered by the cross-reactivity of cardiac glycosides.²⁶ This cross-reactivity does not allow for the easy identification of the responsible cardiac glycosides and, subsequently, the source of the glycoside.¹⁹ This information would be of great value to a farmer, who would want to eradicate the plant from his pastures.

Radford et al.²⁷ illustrates the application of antibodies with a broad-spectrum sensitivity to cardiac glycosides, in the RIA-analysis of biological material. This decreases the possibility of a false negative test for a general cardiac glycoside, but broadens the range of cross-reacting cardiac glycosides.²⁷

1.6.2 Fluorescence polarisation immunoassay

An alternative immunoassay to RIA-analysis is the fluorescence polarisation immunoassay. In this analytical method a sample is spiked with a known amount of a fluorescent internal standard that competes with the xenobiotic, suspected of being present in the sample, for the binding sites of antibodies present in the sample. When the internal standard binds to the antibody, its emission wavelength changes, thus altering the fluorescence polarisation of the sample. The extent of internal standard-antibody binding is inversely related to the concentration of the xenobiotic in the sample.^{28,29}

This method was used extensively by van den Berg et al.²⁵ in diagnosing cardiac glycoside poisoning in cattle and small livestock. To confirm the source of the cardiac glycoside, the investigators had to determine which poisonous plants were present on the affected farms, and confirm which plants showed signs of being consumed by the animals. As in the case of RIA, FPIA cannot selectively quantify a specific cardiac glycoside.³⁰ Instead, cardiac glycosides are quantified as digoxin-equivalents. FPIA did, however, aid the investigators in narrowing down the possible causes of poisoning, and was able to do so with great sensitivity (in the range of nanomoles per litre).²⁵

1.6.3 Liquid chromatography-Mass spectrometry

Mass spectral analysis of analytes addresses the shortcomings of DAD as detection system in identifying eluted analytes from the HPLC-system. By hyphenating an HPLC-system (or UPLC) as separation mechanism with a time-of-flight (TOF) mass analyser, accurate mass analysis can be performed on the eluted species. LC-MS methods employed in the detection, identification, and quantification of digoxin, and other cardenolides, were described in Section 1.6.2 of Chapter IV in this thesis.

For the analysis of physiological samples for the presence of bufadienolides, similar methods to those used for cardenolides have been investigated. Both solid phase extraction and liquid-liquid extraction techniques were investigated for the preparation of physiological samples for cardiac glycoside analysis. Bagrov et al.³¹ developed such a method, utilising liquid-liquid extraction techniques for the analysis of urine samples suspected of containing bufadienolides.

In 2007, Cao et al.³² developed a method for the detection and quantification of bufadienolides in canine blood plasma via HPLC-TOF/MS analysis. The sensitivity of the method was similar to that of LC-MS methods utilised for the detection and quantification of cardenolides (Chapter IV). It has a limit of detection equal to 0.15 ng/mL and a quantification limit at

0.45 ng/mL.³² A similar method developed by Tao et al.³³ in 2016 for the quantification of bufadienolides in rat plasma, was not as sensitive. It had a limit of quantification at 12.5 ng/mL.³³

2. Experimental methods

2.1 List of reagents and chemicals utilised in the experimental work

Table V-1. List of chemicals and reagents used in the experimental work of Chapter V.

Chemical	% Purity	Company	City[†]
5-α-Cholestane	99.9 (HPLC)	Sigma Life Sciences	St. Louis, USA
Acetic Acid	99.9 (GC)	Sigma-Aldrich Chemie GmbH	Schnelldorf, DEU
β-Glucuronidase from <i>Helix pomatia</i> (112173 units)[†]	99.2	Sigma-Aldrich Chemie GmbH	Schnelldorf, DEU
Chloroform	>99.0 (GC)	Merck KGaA	Darmstadt, DEU
De-ionised water	20. Ω .m [‡]	Merck (Pty) Ltd.	Modderfontein, ZA
Diethyl ether	\geq 98.0	Merck KGaA	Darmstadt, DEU
Dichloromethane	\geq 99.8 (GC)	Merck KGaA	Darmstadt, DEU
Dichloromethane	>99	Radchem	Johannesburg, ZA
Disodium hydrogen orthophosphate dihydrate	\geq 99.5 (A)**	Merck (Pty) Ltd.	Modderfontein, ZA
Ethyl acetate	99.9	Radchem	Johannesburg, ZA
Ethyl acetate	99.98 (GC)	Sigma-Aldrich Chemie GmbH	Schnelldorf, DEU
Formic acid	98.2	Sigma-Aldrich Chemie GmbH	Schnelldorf, DEU
Hydrochloric acid	32.7 (A)	Aldrich	St.Louis, USA
Isopropanol	99.99 (GC)	Sigma-Aldrich Chemie GmbH	Schnelldorf, DEU
Methanol	99.98 (GC)	Sigma-Aldrich Chemie GmbH	Schnelldorf, DEU
Methanol	99.9	Radchem	Johannesburg, ZA
Methanol	>99.9	ROMIL via Microsep	Johannesburg, ZA

MSTFA	99.2 (GC)	Sigma-Aldrich Chemie GmbH	Schnelldorf, DEU
n-Hexane	>98.0 (GC)	Merck KGaA	Darmstadt, DEU
n-Hexane	>99	Radchem	Johannesburg, ZA
Pyridine	99.99 (GC)	Sigma-Aldrich Chemie GmbH	Schnelldorf, DEU
Scillaren A	100	Sigma-Aldrich Chemie GmbH	Schnelldorf, DEU
Sodium Acetate	< 99 (A)	Merck (Pty) Ltd.	Modderfontein, ZA
Sodium hydroxide	≥99.0 (A)	Merck (Pty) Ltd.	Modderfontein, ZA
Sodium sulphate	≥99.0 (A)	Merck (Pty) Ltd.	Modderfontein, ZA
Water	18 Ω.m	ROMIL via Microsep	Johannesburg, ZA

†The number β-glucuronidase enzymatic units per millilitre solution.

‡Resistivity assay: A resistivity of ~18.5 Ω.m in water indicates the %-ionic content is near naught

**Acidimetric assay via acid/base titration

2.2 Preparation of a crude extract from *U. sanguinea*

U. sanguinea bulbs were purchased from the Faraday Muti Market, Johannesburg. One bulb was cultivated in a greenhouse at the University of Pretoria and was later submitted as voucher specimen to the H.G.W.J. Schweikerdt Herbarium (UP) for identification. Another bulb was peeled and dried in a laboratory oven (~40.0 °C) after the bulb scales were cut into smaller pieces. The dried bulb scales were milled to a fine powder with a Lasec® Polymix grinding mill, and a portion of the material (50 g) was weighed out for extraction.

The material was extracted by maceration in a dichloromethane/methanol extraction solvent system (Radchem® solvents, 500.0 mL, 1:1) for 24 h with continuous stirring, whereafter the extract was filtered through Whatman Grade 1 filter paper with the aid of a vacuum. The extract volume was reduced *in vacuo* by rotary-evaporation. The process was repeated twice and the extracts combined. One milligram of the combined extract was analysed via UPLC-qTOF-MS.

A de-fatted fraction was prepared from the crude extract by solubilising the extract in distilled water (50.0 mL) and diethyl ether (Merck®, 50.0 mL). The container of the extract was rinsed into a separating funnel with a diethyl ether/water solvent system (150.0 mL, 1:1). Two more aqueous extracts (200.0 mL each) were prepared from the organic phase and dried with the aid of an SP Scientific EZ-2 Plus Genevac®-evaporator.

Further purification of the cardiac glycosides from the de-fatted extract was done by liquid-liquid extractions from the reconstituted extract (in 50.0 mL distilled water). Three repetitions of the extraction were performed with an ethyl acetate (Radchem®)/chloroform (Merck®) extraction solvent (100.0 mL, 1:1). The organic phases were combined and dried with the aid of an SP Scientific EZ-2 Plus Genevac®-evaporator.

2.3 UPLC-qTOF-MS analysis of the crude extract

A sample of crude extract from *U. sanguinea* (1. mg) was prepared by dissolving it in methanol (ROMIL® Ultra-pure Solvent (UpS)®, 1.0 mL). The sample was solubilised with the aid of sonication in an ultrasonic bath for ca. 30 min. To remove any undissolved material, the sample was centrifuged in a Baygene® Micro Centrifuge (BG-Qspin™) for 5 min. The supernatant was transferred to a clear glass HPLC-vial (2 mL) and diluted ten-fold into an identical vial.

UPLC-analysis was performed with a generic gradient solvent system (**Table V-2**). The eluted analytes were analysed by quadrupole-time-of-flight (qTOF) accurate mass analysis, in both the positive and negative ionisation mode. The UPLC-system consisted of a Waters® Aquity™ Binary Solvent Manager, a Sample Manager, and an Aquity® UPLC-column (2.1 × 100 mm) with a BEH C18-type stationary phase adsorbed onto 1.7 µm particles. Accurate mass analysis of the eluting compounds was performed with a Synapt™ G2 High Definition Mass Spectrometry system (resolution ~18 000 FWHM) with a mass scan range of 50 to 1 200 Da. Ionisation and mass correction parameters for the UPLC-qTOF-MS analyses are described in Chapter II, Section 2.2.2.

Table V-2. Generic gradient solvent system employed in UPLC-qTOF-MS analysis

Time (min)	Flow rate (ml/min)	% (H₂O + 0.1% FA)	% (MeOH + 0.1% FA)
Initial	0.300	97.0	3.0
0.10	0.300	97.0	3.0
14.00	0.300	0.0	100.0
16.00	0.300	0.0	100.0
16.50	0.300	97.0	3.0
20.00	0.300	97.0	3.0

To confirm the identity of scillaren A (**40**) ($\geq 99\%$) in the chromatogram of the crude extract, a certified reference standard was prepared for analysis by UPLC-qTOF-MS. A GC-vial was spiked with scillaren A (**40**) stock standard solution (10.00 μL , 1.00 mg/mL) and dried in a heating block (40.0 $^{\circ}\text{C}$) under a stream of dry air. The residue was reconstituted in UpS[®]-grade methanol (ROMIL[®], 100.0 μL) and transferred to a conical insert for UPLC-qTOF-MS analysis. The same instrument system and conditions were used as for the sample of the crude extract.

2.4 Sample preparation method for the GC-MS analysis of physiological samples

2.4.1 Preparation of a scillaren A stock solution and an internal standard stock solution

A certified reference standard of scillaren A (**40**) was purchased from Sigma-Aldrich[®]. The mass of scillaren A (**40**) in the bought vial was assumed to be as indicated (1 mg). The scillaren A present in the vial was solubilised in HPLC-grade methanol (1.000 mL) by vortex mixing. The required volume of this 1 mg/mL stock solution was spiked into the corresponding samples for analysis.

Throughout the project the same stock solution was utilised as internal standard. This solution was prepared by weighing 5- α -cholestane (Sigma[®] Life Sciences, 10.04 mg) into a volumetric flask (10.00 \pm 0.04 mL) and filling the flask to the calibration mark with HPLC-grade ethyl acetate (Sigma-Aldrich[®]). The stock solution was homogenised by shaking and vortex mixing. The resulting stock solution had a concentration of 1.004 mg/mL.

2.4.2 Spiking of urine and de-ionised aqueous samples for analysis

Routine samples were simulated by measuring 25.00 mL of blank matrix with an Eppendorf[®] Multipette[®] M4 into a polypropylene urine collection cup. Each sample was spiked with the required volume of scillaren A stock solution (1 mg/mL). Each sample was subsequently spiked with the 5- α -Cholestane stock solution (30.0 μL , 1.004 mg/mL) and the acetate buffer (5.00 mL, 1 M, pH \sim 4.5), prepared according to the process described in Section 2.5.3 of Chapter IV.

2.4.3 Solid phase extraction of scillaren A from samples

Scillaren A (**40**) was extracted from the matrices by solid phase extraction with Agilent[®] C18-BondElut[®] SPE cartridges (6 cc, 500 mg sorbent mass, 4 μm particle diameter), prepared as for application in the extraction of aovenoside A (**22**) from sample matrices. The samples were applied to the cartridges with the aid of a small pressure differential (vacuum \leq 1 “Hg). The loaded cartridges were eluted with dichloromethane (Merck[®] (Pty) Ltd, 5.00 mL), without the

aid of a pressure differential, and aspirated to dryness with a 5 “Hg vacuum. Each cartridge was spiked with the 5- α -cholestane stock solution (30.0 μ L, 1.004 mg/mL) and eluted with methanol (5.00 mL) without applying a pressure differential. To remove residual extraction solvent, a 5 “Hg pressure differential was applied for ~30 s.

2.4.4 Preparation of eluted samples and temperature program for GC-MS analysis

Hydrolysis of eluted analytes

After aspiration through the cartridge, the collected methanol was dried under a stream of dry air at 40 °C. Hydrolysis of the dried residues was achieved by reconstituting the samples in concentrated aqueous hydrochloric acid (500. μ L, 6 M). To promote hydrolysis, the samples were irradiated in a microwave oven for three minutes at a 50% power setting (corresponding to 500 W).

Extraction of hydrolysis products from the reaction mixture

The hydrolysed samples were buffered to an alkaline pH by addition of disodium hydrogen orthophosphate buffer (500. μ L, 0.8 M, pH ~ 11.5) to each sample, followed by the required volume of aqueous concentrated sodium hydroxide (10 M) to obtain a pH of ca. 11. The hydrolysis products were extracted from the buffered solution with an ethyl acetate (Sigma-Aldrich®)/n-hexane (Merck® (Pty) Ltd) extraction solvent (2.000 mL, 1:1). The organic phase of each sample was transferred to a corresponding amber glass GC-vial (2 mL) and dried in a heating block with the aid of a stream of dried compressed air. The extraction process was repeated to improve analyte recovery.

Derivatisation of hydrolysis products

Since active hydrogen atoms (in hydroxyl groups) might be present in the hydrolysis products, the dried residues were exposed to the same derivatisation conditions as in the case of acovenoside A (**22**). The samples were reconstituted in pyridine (Sigma-Aldrich®, 20.0 μ L) and MSTFA (Sigma-Aldrich®, 20.0 μ L) and vortex mixed to improve analyte recovery from the vial walls. To facilitate the derivatisation reaction the samples were irradiated for 6 min in a microwave oven set to a 50% power level (equivalent to 500 W). The derivatised samples were vortex mixed and transferred to a conical glass insert in a vial, for GC-MS analysis.

GC-MS analysis of the samples

GC-MS analysis was performed via a system consisting of an Agilent® 7890B GC-oven system, an Agilent® 7693 Autosampler and Auto-injector, and a Hewlett-Packard® 5973 Mass Selective Detector. For the GC-MS analysis, 2 µL of the reconstituted sample volume was applied to the GC-column (Phenomenex® ZB-5 MSi, 15 m length, 0.25 mm internal diameter, 0.25 µm film thickness) through a deactivated glass inlet liner (temperature set to 280 °C). Separation of the sample constituents was achieved with a gradient temperature program initiated at a temperature of 180 °C and maintained for three minutes. A temperature ramp, with gradient 30 °C/min, was applied to reach the plateau at 230 °C. The temperature was held constant for two minutes before it was ramped at 15 °C/min to 290 °C. After two minutes the final temperature ramp, 30 °C/min, was applied to reach 310 °C. The final temperature was maintained for 1.5 min.

The vapor phase of the eluting analytes was sustained between the GC-oven and the ion source by passing the column through a 230 °C transfer line system. In the ion source the primary electron beam was accelerated to a kinetic energy of 70 eV and the temperature maintained at 230 °C. The quadrupole mass analyser was heated to 150 °C to prevent sample condensation on the analyser.

During chromatographic analysis with the mass analyser in the scan mode, all m/z -ratios in the range of $m/z = 50$ -800 were selected for detection by the quadrupole analyser. In the selected ion mode, the analyser was set to select only $m/z = 149, 217, 357, 372$ between the end of the solvent front (at 2.50 min) and 6.50 min. The range of ions was then changed to $m/z = 147, 170, 183, 356, 573, \text{ and } 588$ for the detection of silylated hydrolysis products of acovenoside A (**22**), (**35**). At 9.60 min the ion m/z -ratio range was changed to $m/z = 169, 197, 211, 226, \text{ and } 348$ for the detection of the derivatised hydrolysis products of scillaren A (**40**). Throughout the analysis the dwell time of the mass analyser was set to 100 ms.

2.5 Validation of qualitative analysis of urine samples for scillaren A

2.5.1 Evaluation of the method linearity and precision

Linearity was assessed by evaluating the descriptive regression statistics, calculated from replicate response models. These response models were generated from the duplicate GC-MS analyses of samples spiked at five concentration levels, excluding the matrix blank sample analysed with each batch. In the assessment of linearity, one batch of each sample matrix was

simultaneously spiked with equal amounts of acovenoside A (**22**) and scillaren A (**40**). In this manner the analytical method was validated for both analytes simultaneously.

In the batches where both acovenoside A (**22**) and scillaren A (**40**) were present, scillaren A (**40**) was spiked into the samples after acovenoside A (**22**). The samples were spiked with volumes of scillaren A (**40**) stock solution (1 mg/mL) such that the respective concentrations in the samples were 1.00, 1.20, 1.40, 1.60, and 1.80 µg/mL (ppm). To each sample 5- α -cholestane stock solution (30.0 µL, 1.004 mg/mL) was aliquoted.

By analysing a single batch of concentration levels in both urine and de-ionised water in duplicate, the within-batch repeatability could be estimated. There was not sufficient reference standard solution available to conduct further replicate analyses. An estimation of the limits of detection and quantification could be made for each sample matrix based on the regression data obtained. These theoretical limits of detection were compared to the limits determined experimentally.

2.5.2 Evaluation of the method accuracy and recovery

A comparison of the theoretical and experimental concentrations detected for each respective sample matrix, was performed. This comparison provided an indication of the analyte recovery from the samples, the accuracy of the analytical method and the effect of a physiological matrix on these figures of merit.

2.5.3 Selection of ion ratios for the identification of analytes

For the identification of the possibly derivatised hydrolysis product of scillaren A, five ion ratios were selected. Positive identification was assumed when all five ratios simultaneously lie within the 99.7% confidence interval of the ion ratio centroid. This centroid is a vector variable with the mean of each ion ratio as its elements. Since only two batches of samples spiked with scillaren A (**40**) were analysed, one in de-ionised water and the other in urine, the centroid vector was calculated as the mean of the sample vectors at each concentration.

The five ion ratios selected took into consideration the most abundant ions formed during fragmentation as well as the molecular ion. Comparing the ratios between the fragment and molecular ions was expected to provide information on the mechanism of fragmentation and the competition of different fragmentation pathways.

Table V-3. Definition of ion ratios for the qualitative analysis of derivatised hydrolysis products from *scillaren A*.

Designation	Definition of the ion ratio
IR 1	Area m/z = 348 ÷ Area m/z = 226
IR 2	Area m/z = 226 ÷ Area m/z = 211
IR 3	Area m/z = 348 ÷ Area m/z = 211
IR 4	Area m/z = 211 ÷ Area m/z = 197
IR 5	Area m/z = 226 ÷ Area m/z = 197

3. Results and discussion

One of the bulbs bought under the name *sekanama* was cultivated in the University of Pretoria's greenhouses. This plant was submitted as voucher specimen to the H.G.W.J. Schweickerdt Herbarium on campus for identification. It was catalogued with the reference number PRU 126147.

3.1 UPLC-qTOF-MS analysis of the crude extract

In this project, UPLC-analysis was performed with a generic gradient solvent system that employed formic acid as a buffer to aid in ionisation efficiency. Under these conditions, cardiac glycosides tend to form a formic acid adduct, following the loss of a proton. In the ESI (-)-mode chromatogram of the crude extract from *U. sanguinea*, shown in **Figure V-5**, four chromatographic peaks of high intensity were observed. These peaks were tentatively identified, as shown in **Table V-4**, within the 5 ppm tolerance range and with the aid of the Dictionary of Natural Products.^{34,35}

Peak 3 in **Figure V-5** was of particular interest since it is the most intense peak in the ESI (-) chromatogram of the crude extract. The base peak ion in the first order mass spectrum of Peak 3, given in **Figure V-6**, was $m/z = 737.3389$. Also present in this mass spectrum is an ion with accurate mass $m/z = 691.3344$. Elemental composition analysis of the two ions produced the formulae $[C_{37}H_{53}O_{15}]^-$, with 82.66% confidence (isotopic fit ratio = 37.0), and $[C_{36}H_{51}O_{13}]^-$, with 82.3% certainty (isotopic fit ratio = 35.), respectively for the two detected ions. The former composition corresponds to the formula for the formic acid adduct of scillaren A (**40**), and the latter to the quasi-molecular ion ($[M-H]^-$) of scillaren A (**40**). Both these ions did not differ more than 5 ppm from the theoretical masses of the detected ions. This tentatively confirms the identity of Peak 3 as scillaren A (**40**).³⁴

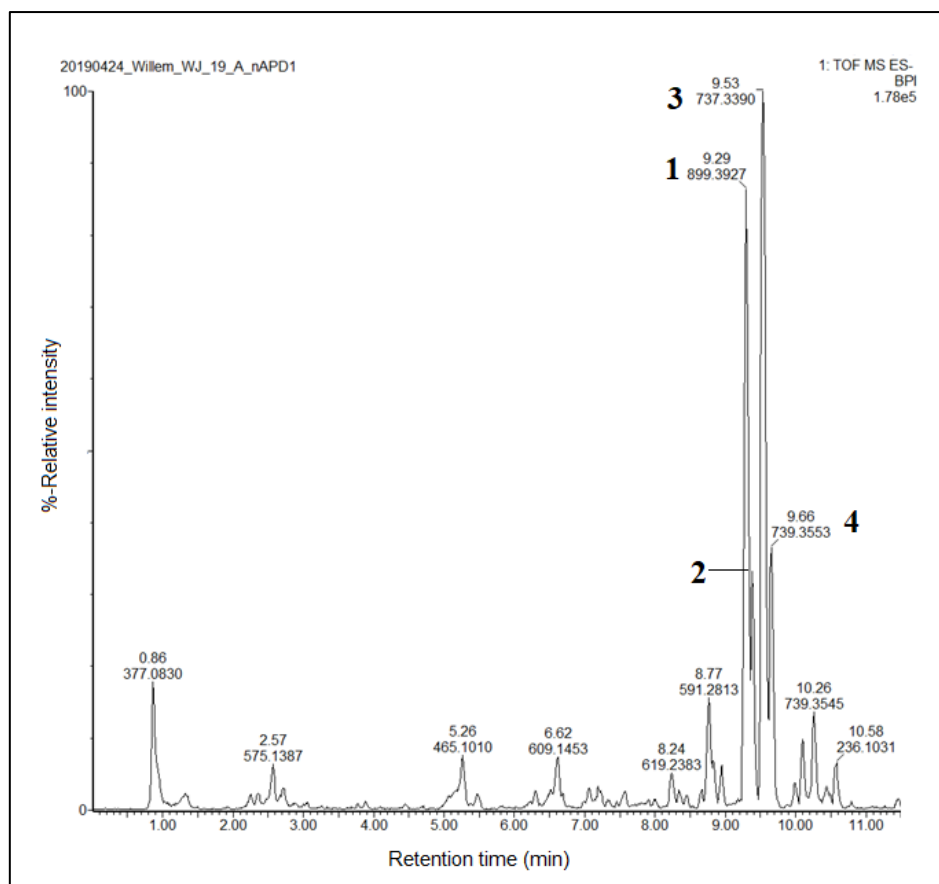


Figure V-5. ESI (-)-mode UPLC chromatogram of the crude extract from *U. sanguinea*.

Table V-4. Compounds detected in the ESI (-) mode for the UPLC-qTOF-MS analysis of the *U. sanguinea* crude extract (Peaks described from TIC).

Peak no.	t_R (min)	m/z ([M-H+FA] ⁻)	Calc. accurate mass (Da)	Formula	Theoretical monoisotopic mass (Da)	Tentative identification
1	9.287	899.3927	854.3945	C ₄₂ H ₈₂ O ₁₈	854.3936	Glucoscallaren A
2	9.384	901.4064	856.4082	C ₄₂ H ₆₄ O ₁₈	856.4093	Cardenolide B3 (<i>N.o.</i>)* Oleaside F (<i>N.o.</i>)* Thevetioside F (<i>T.n.</i>) [‡] Thevetioside H (<i>T.n.</i>) [‡]
3	9.533	737.3389	692.3407	C ₃₆ H ₅₂ O ₁₃	692.3408	Scillaren A
4	9.660	739.3553	694.3571	C ₃₆ H ₅₄ O ₁₃	694.3564	4,5-Dihydro-scillaren A

[‡]Constituent of *Thevetia neriiifolia*

*Constituent of *Nerium oleander*

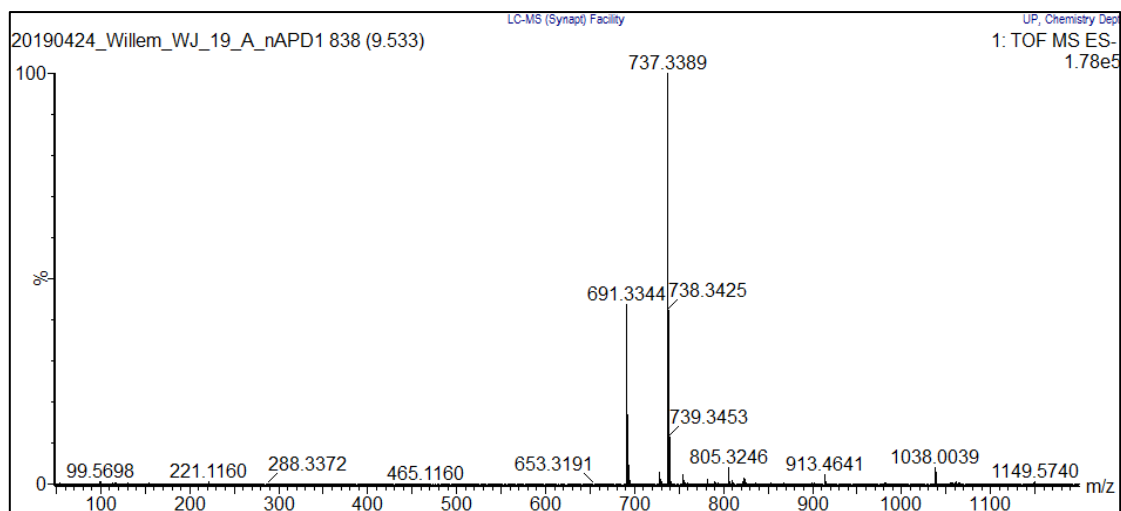


Figure V-6. First order ESI (-)-mass spectrum, detected at 9.533 minutes, tentatively identified as belonging to scillaren A (**40**).

Further confirmation of the identity of the compound that produced chromatographic Peak 3, at 9.533 min, was obtained by comparing the chromatogram of the crude extract with a chromatogram for the certified reference sample of scillaren A (**40**). Relative to the background signal with base peak ion $m/z = 311.1777$ and a retention time of 13.55 min, the peak tentatively identified as scillaren A (**40**), eluted 4.01 min before the reference peak. In the certified reference sample, scillaren A (**40**) was detected at a relative retention time of 4.34 min (before the background signal with $m/z = 311.1853$ – See **Figure V-7**). The closely spaced relative retention times support the tentative identification of peak 3 as scillaren A.

In the certified reference sample, the formic acid adduct of scillaren A was detected with an accurate mass of $m/z = 737.3301$. Between this accurate mass and that detected in Peak 3 of the chromatogram for the crude extract, in **Figure V-5**, there exists a 11.9 ppm mass difference. The $[M-H]^-$ -quasi-molecular ion was detected in the certified reference sample at $m/z = 691.3262$, which also differs by 11.9 ppm from the measured accurate ion mass in the crude extract. Since the mass difference is greater than the tolerance limit of 5 ppm, Peak 3 remains only tentatively identified as scillaren A (**40**).

Of the compounds detected and identified by Majinda et al.,⁹ possibly both scillaren A (**40**) and its 4,5-dihydro derivative (**41**) were present in the crude extract (Peaks 3 and 4 in **Figure V-5** & **Table V-4**). Chromatographic Peak 1 can be attributed to glucoscillaren A, based on the accurate masses calculated from the formic acid adduct (854.3945 Da from $m/z = 899.3927$) and the $[M-H]^-$ -quasi molecular ion (854.3968 Da from $m/z = 853.3895$). Both accurate masses corresponded to the molecular formula $C_{42}H_{82}O_{18}$ within 5 ppm. Glucoscillaren A was the most

likely compound fitting this formula, since it is a known constituent of a species of squill (*Scilla maritima*) related to *Drimia* spp., according to the Dictionary of Natural Products.³⁵⁻³⁷

Chromatographic Peak 2, at 9.384 min, could be attributed to a cardenolide with the molecular formula of $C_{42}H_{64}O_{18}$. This formula's monoisotopic mass correlated with the measured accurate mass (of the parent molecule) with a 1.2 ppm and -0.8 ppm mass difference for the formic acid and $[M-H]^-$ -quasi molecular ion, respectively. Cardenolides were not expected to be present in the extract of *U. sanguinea* since literature cites the cardiac glycoside components of the extract as primarily bufadienolides.^{1,5,9}

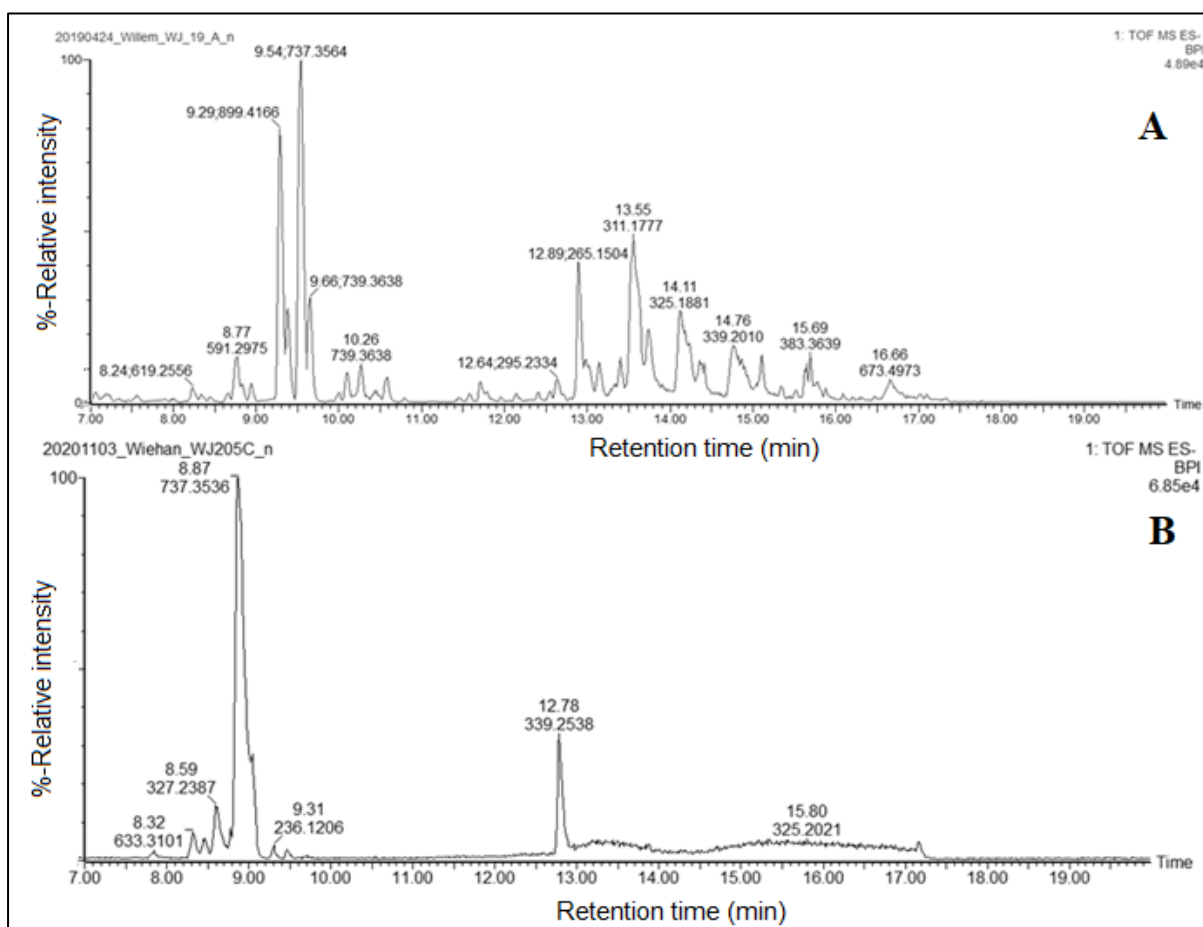


Figure V-7. Comparison of the negative mode chromatograms for the crude extract from *U. sanguinea* (A) and the certified reference material for scillaren A (B). Note the consistency in relative retention time to the background signal with $m/z = 311.1777$ as base peak ion. In the CRM (B) this signal is the small hump adjacent to the peak at 12.78 min.

3.2 GC-MS analysis of samples for scillaren A

3.3.1 Identification of the derivatised hydrolysis products of scillaren A

Comparing the recorded chromatogram for a reference sample of scillaren A (**40**) with that of a method blank, prepared identically to the sample, clearly shows the chromatographic peaks that are generated by the sample components. These chromatographic peaks do not have a corresponding signal in the method blank. What also stands out is the difference in retention time between the peaks produced by the derivatisation reagent in the respective chromatograms. Correcting for the shift in retention time in the sample containing scillaren A (**40**), the overlay in **Figure V-9** is obtained.

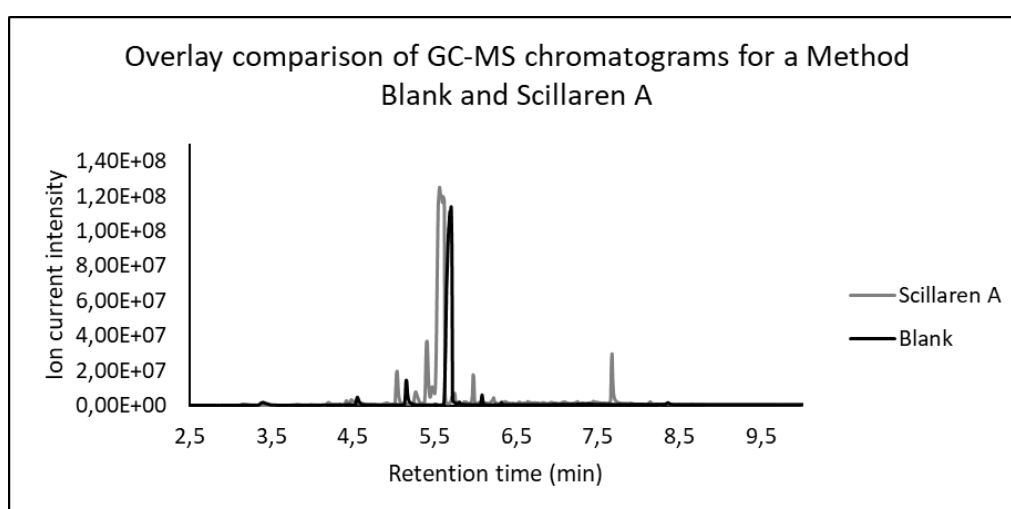


Figure V-8. A GC-MS chromatogram recorded for 50.0 μg silylated scillaren A in water (grey), overlaid with a chromatogram for a method blank prepared identically to the scillaren A sample (black).

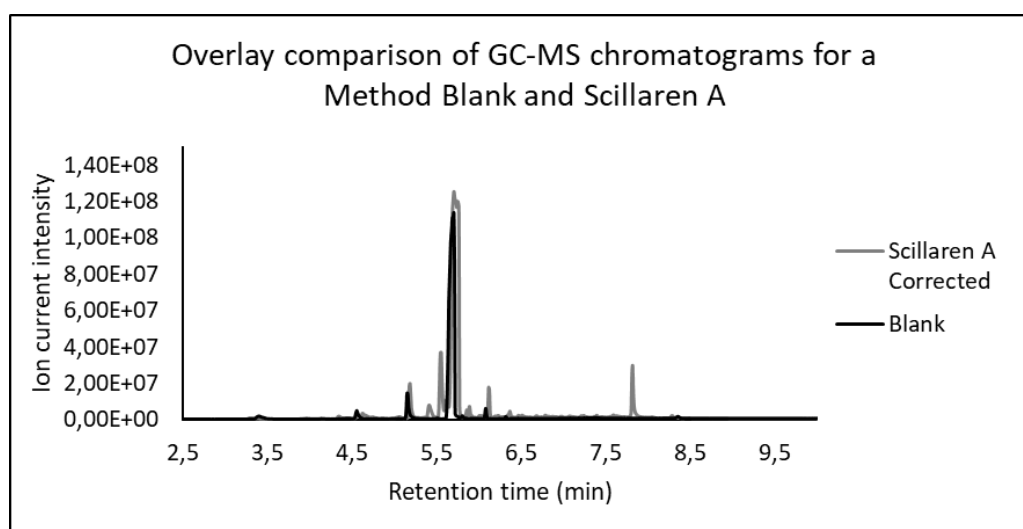


Figure V-9. Overlay of the chromatogram for scillaren A (grey), versus corrected retention time, with the chromatogram for a method blank (black).

Based on these chromatograms, three chromatographic peaks stand out at retention times of 5.273, 5.407 and 7.679 min. The mass spectrum recorded at 7.679 min corresponded to a proposed fragmentation pattern of the dehydrated derivative of scillarenin ($\Delta 2,3$ - $\Delta 8,14$ -dehydroscillarenin (**48**)), with a molecular ion at $m/z = 348$ (**Figure V-10**). In the mass spectrum, the detected base peak ion has a m/z -ratio of 211. This ion corresponds to the loss of a methyl group and the simultaneous loss of the lactone group and C16. This corresponds to the loss of 137 nominal mass units (**Figure V-11**).

Further analysis of the fragmentation pattern shows fragmentation of dehydrated scillarenin (**48**) occurs mostly in ring D of the steroid skeleton. The ion, with $m/z = 197$, is produced when ring D and a methyl group, likely on C13, and the six-membered underivatized lactone simultaneously undergoes fragmentation off the analyte. A notable fragment ion is $m/z = 226$. This fragment corresponds to the component of the steroid skeleton, following the loss of the bufadienolide six-membered lactone bound to an ethene group (See **Figure V-11**).

The characteristic fragments produced by the loss of the lactone group of either glycoside class, could aid in identification of the glycoside class. As an example, Kohls et al.³⁸ studied the fragmentation pattern of hydrolysed cardiac glycosides from *Thevetia peruviana*, following derivatisation by silylation.³⁸

In Kohls et al.,³⁸ and in Chapter IV, characteristic fragments lost from silylated cardenolides had m/z -ratios 183 and 170. These respectively corresponded to the loss of the silylated enol tautomer of the five-membered lactone ring bound to either an ethene group or a methylene radical (CH_2^\bullet). Had the five-membered ring not been tautomerized, a characteristic ion of m/z -ratio of 111 would have been detected.³⁸ The loss of the ionised cardenolide fragment with $m/z = 183$, corresponds to the loss of the unsilylated lactone from scillarenin bound to an ethene group (total mass loss = 122) to produce the fragment ion with $m/z = 226$.

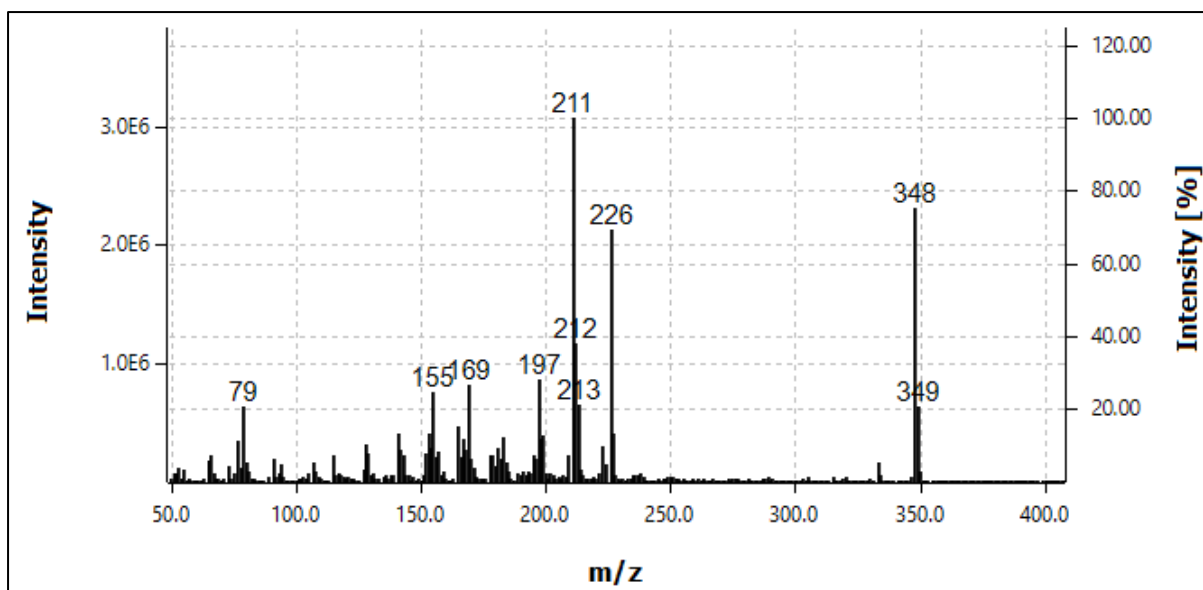


Figure V-10. Electron impact mass spectrum of dehydrated scillarenin (48)-(50).

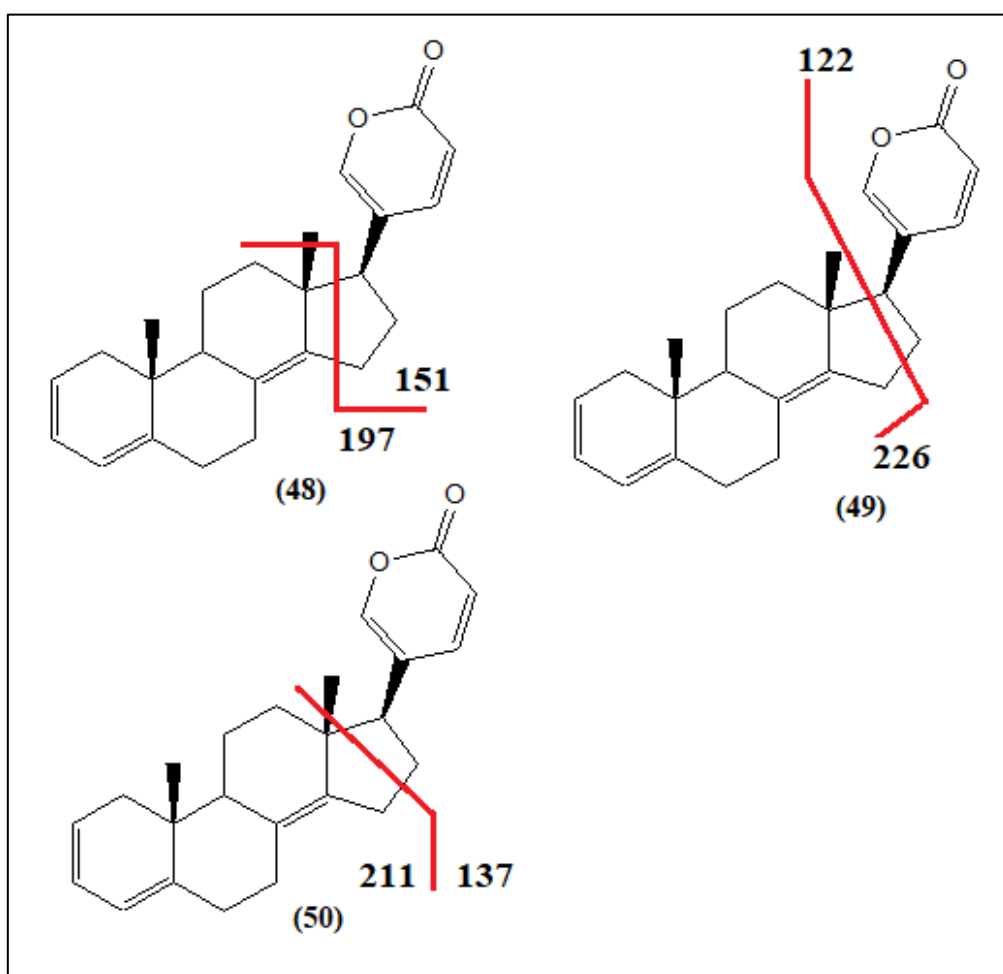


Figure V-11. Fragmentation of scillarenin in a 70 eV electron impact ion source.

3.3.2 Ion ratio relationships observed for urine samples spiked with scillaren A

Four ion ratios were selected and calculated for the analysis of inter-ion ratio relationships. Of these, three will be selected during validation for the identification of dehydrated scillarenin (48). The ratios account for the molecular ion abundance, the abundance of the characteristic ion with $m/z = 226$, and the base peak ion at $m/z = 211$. The ratios were defined as:

$$\text{Ratio 1} = (\text{Area } m/z = 348) \div (\text{Area } m/z = 226)$$

$$\text{Ratio 2} = (\text{Area } m/z = 226) \div (\text{Area } m/z = 211)$$

$$\text{Ratio 3} = (\text{Area } m/z = 348) \div (\text{Area } m/z = 211)$$

$$\text{Ratio 4} = (\text{Area } m/z = 211) \div (\text{Area } m/z = 197)$$

$$\text{Ratio 5} = (\text{Area } m/z = 211) \div (\text{Area } m/z = 226)$$

$$\text{Ratio 6} = (\text{Area } m/z = 197) \div (\text{Area } m/z = 211)$$

Applying multivariate Gaussian analysis, the unbiased correlation matrix (**R**) was calculated for these ratios and is shown in **Table V-5**.

Table V-5. Correlation matrix (**R**) for the ion ratios describing the relationships between ions in the fragmentation of the analyte.

	IR 1	IR 2	IR 3	IR 4	IR 5	IR 6
IR 1	1.000	-0.685	0.994	-0.752	0.697	0.835
IR 2	-0.685	1.000	-0.603	0.552	-1.000	-0.556
IR 3	0.994	-0.603	1.000	-0.739	0.615	0.831
IR 4	-0.752	0.552	-0.739	1.000	-0.559	-0.986
IR 5	0.697	-1.000	0.615	-0.559	1.000	0.566
IR 6	0.835	-0.556	0.831	-0.986	0.566	1.000

From the unbiased estimation of the correlation matrix, a strong positive correlation between ratios 1 and 3 was observed, with a correlation coefficient of 0.99397. This correlation is trivial since both ratios are directly proportionate to the area of the ion with $m/z = 348$. There is a weak negative correlation between ratios 2 and 3.

Since both ratios 2 and 3 are inversely proportionate to the area of the base peak ion, the correlation is indicative of the relationship between the ions with m/z -ratios 348 and 226. A negative correlation indicates that a change in one signal area produces a change in the opposite

direction in the second signal area. Thus, an increase in the area of $m/z = 348$ would produce a decrease in the area of $m/z = 226$. Such a relationship implies that $m/z = 226$ is a daughter ion of the molecular ion. Since the correlation coefficient, $r_{23} = -0.60266$, is small, there are likely other contributing factors to the abundance of $m/z = 226$.

Comparing the inverse of ratio 2 (ratio 5) to ratio 1, an indication of the relationship between $m/z = 348$ and $m/z = 211$ was obtained. The correlation coefficient, $r_{15} = 0.69684$, implies that there exists a weak positive correlation between the change in abundance of $m/z = 348$ and $m/z = 211$, and a weak negative correlation between the change in abundance of $m/z = 211$ and $m/z = 226$. Therefore, the abundance of $m/z = 211$ will increase if the abundance of $m/z = 226$ decreases.

From the correlation matrix it is observed that ratio 6 is strongly correlated to ratio 3 in the positive direction ($r_{63} = 0.83067$). However, it is weakly correlated to ratio 2 in the negative direction ($r_{62} = -0.55625$). These correlations imply that the ion with $m/z = 197$ competed for formation with the ion at $m/z = 226$.

From these observations, a fragmentation mechanism is proposed, starting from the molecular ion with $m/z = 348$. This ion fragments to produce the ion $m/z = 226$. This ion fragment may undergo further degeneration to $m/z = 211$ or $m/z = 197$. Therefore, the fragment ions $m/z = 211$ and 197 are daughter ions of $m/z = 226$. It is likely that these two ions compete for formation since the abundance of $m/z = 197$ is characteristically less than that of $m/z = 211$ as can be seen from the observed values for ratio 4.

3.3 Assessment of quantitative figures of merit in the generated response model

For accurate quantification, the purity of the reference material was obtained from the certificate of analysis provided by Sigma-Aldrich® for the product lot number. The purity is cited at 100% based on LC/MS-ELSD (evaporative light scattering detection).³⁹

Evaluation of linearity in the response models

In the response model set up for scillaren A (**40**), samples were spiked at five concentration levels as described in Section 2.4.2 of this chapter. Two batches were analysed in this study – one batch was prepared in urine and the other in de-ionised water. Each batch was analysed in duplicate on the same instrument. The response models generated as the average of each respective duplicate set, are summarised in **Table V-6** and illustrated in **Figure V-12**. Response models were generated for the relative response of the base peak ion signal area of dehydrated

scillarenin ($m/z = 211$), with respect to the base peak ion signal area of the internal standard ($5\text{-}\alpha\text{-Cholestane} - m/z = 217$).

Table V-6. Summary of figures of merit in determining the linearity of the response models.

Matrix	r^2	Slope (b)	Intercept (a)	s_b	s_a	$S_{y/x}$
Urine	0,08277	0,0074	0,005	0,0142	0,020	0,008975
dH ₂ O*	0,06974	0,011	-0,003	0,024	0,034	0,015043

*dH₂O = De-ionised water

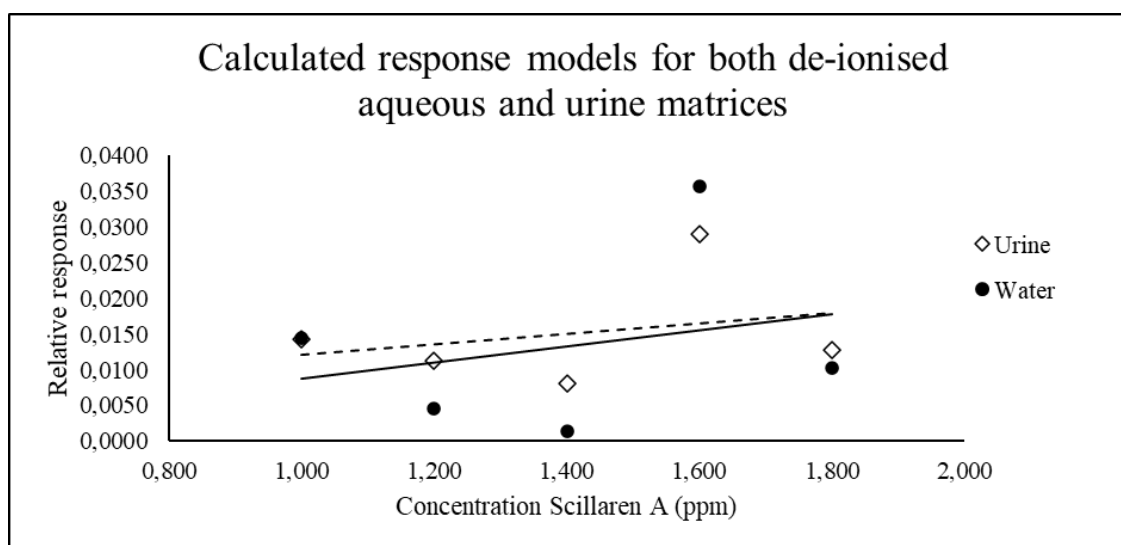


Figure V-12. Overlaid response models for scillaren A (40), spiked into urine and de-ionised water, respectively.

Based on the calculated product-moment correlation coefficients (r^2 -values in **Table V-6**), there is no significant correlation between the measured data and the calculated regression models. However, there could be a non-linear trend in the measured relative responses since the distribution of relative responses, over concentration, follows the same trend in both matrices (**Figure V-12**). The absence of significant correlation between the measured relative responses could, therefore, be attributed to the inadequate suitability of a linear model in describing the trend in the data.

A closer examination of the relative responses of the individual batches revealed a possible polynomial or exponential trend in the data. This, however, is contradicted by the sudden decrease in relative response at 1.80 ppm. A trend that was observed in one replicate of each batch of samples in the respective matrices. This sudden decrease was observed in the absolute responses measured for the hydrolysis product of scillaren A (48). Combined with a sharp

increase in the absolute response of the internal standard, the relative response sharply decreases at 1.80 ppm.

The repeated occurrence of this sharp decrease in both matrices does not support the occurrence of gross error. Since the combined absolute response of acovenoside A's (**22**) signals increases sharply at the highest concentration level, it is unlikely that extraction efficiency from liquid-liquid extraction or application of the sample to the column, caused the sudden decrease in relative response. The factors that could influence the absolute response of scillaren A's hydrolysis product (**48**), are expected to be independent from those that influence the absolute response of acovenoside A's derivatised hydrolysis products (**35**).

A scenario where multiple factors selectively influence the absolute response of scillaren A's hydrolysis product (**48**) should also be considered. The factors that could influence this absolute response include the repeatability of pipetting during spiking of the samples, sample stability on the autosampler, and the repeatability of the solid phase extraction process. Regarding the SPE-process, the selectivity of dichloromethane and methanol for scillaren A (**40**) was observed to change for different sample matrices, however, the overall trend in the data remained the same for both matrices.

An evaluation of method repeatability

At each concentration level, the %-relative standard deviation (%-RSD) was calculated for the *x*-direction. The extreme %-RSD values indicate that the method is not suitable for the quantitative analysis of scillaren A neither in urine nor in de-ionised aqueous samples, when modelled by a linear regression equation (see **Table V-7** and **Table V-8**). When the ideal case of a linear model for the data was investigated, regression analysis of variance indicated that the variation in the measured values, across concentration levels, can be attributed to random variation. This result follows from the observation that the between-concentration variation does not significantly contribute to the change in relative response.

Since only one batch of samples was analysed for each sample matrix, the contribution of random variation to the observed variance could not be determined. The number of analyses performed was limited by the availability of the reference standard for scillaren A (**40**).

Table V-7. Table of %-RSD values in the x-direction for samples prepared in urine.

ppm	%-RSD_x
1,00	104,3
1,20	117,7
1,40	148,1
1,60	235,8
1,80	66,03

Table V-8. %-RSD values (x-direction) of the analytical method for samples prepared in de-ionised water.

ppm	%-RSD_x
1,00	178,61
1,20	346,78
1,40	389,66
1,60	620,25
1,80	120,17

Evaluation of method accuracy

The accuracy and analyte recovery of the method were investigated by examining the experimental concentrations of analyte as calculated at each concentration level via a linear best-fit line versus the theoretical analyte concentration levels. The analysis of the data showed that analyte recovery during sample preparation was the same for the two sample matrices. However, the trend in the accuracy of measurement did not correlate with the $y = x$ line for samples of either matrix.

Since this accuracy is dependent on the regression model applied to the data, a suitable mathematical equation for the trend in the data would improve the accuracy in interpolation from the measured relative response to the corresponding concentration. Addressing the factors that contribute to the measured relative responses deviating from a linear trend, could also improve the accuracy of interpolation via a regression model.

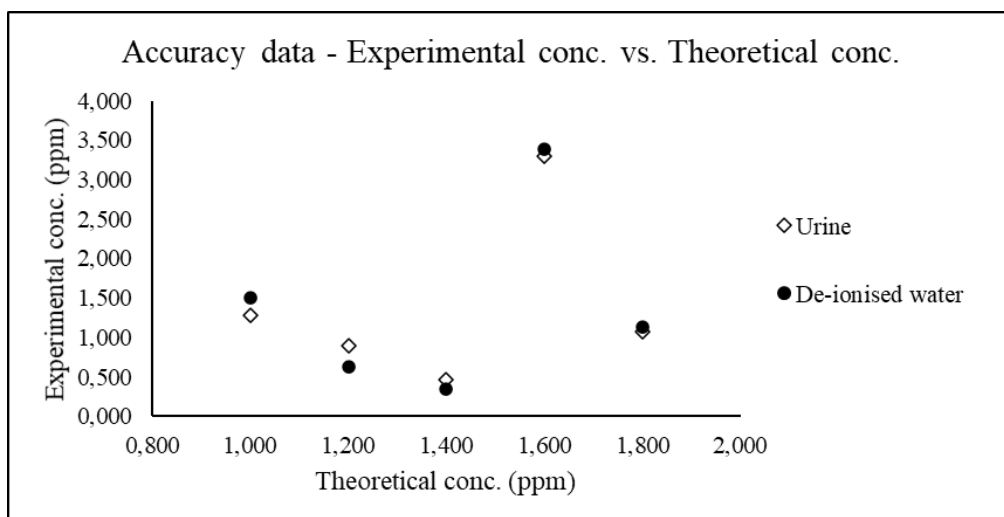


Figure V-13. Evaluation of the accuracy of the sample and analytical methods by plotting the experimentally calculated concentration of analyte against the theoretical concentration.

3.4 Assessment of qualitative figures of merit in the generated response model

Four of the six ratios in Section 3.3.2 and one additional ion ratio, defined as $IR5 = (\text{Area } 226) \div (\text{Area } 197)$, were selected for the qualitative analysis of the Δ^3 -dehydro- Δ^{14} -dehydro derivative of scillarenin (**48**). The ratios selected from Section 3.3.2 were ratios 1 to 4. Ratios 5 and 6, in Section 3.3.2, were not used since they were the inverse ratios of ratios 2 and 4. The selected ratios were then designated as in Section 2.6.3.

3.4.1 Change in ion ratios over the concentration range

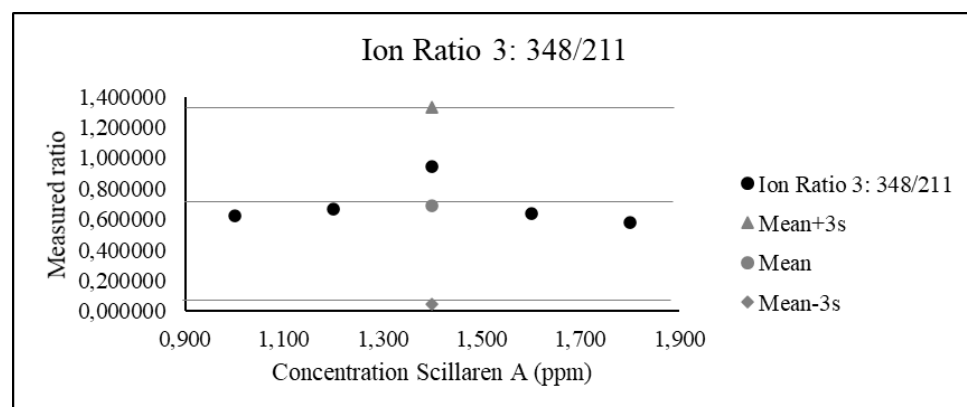
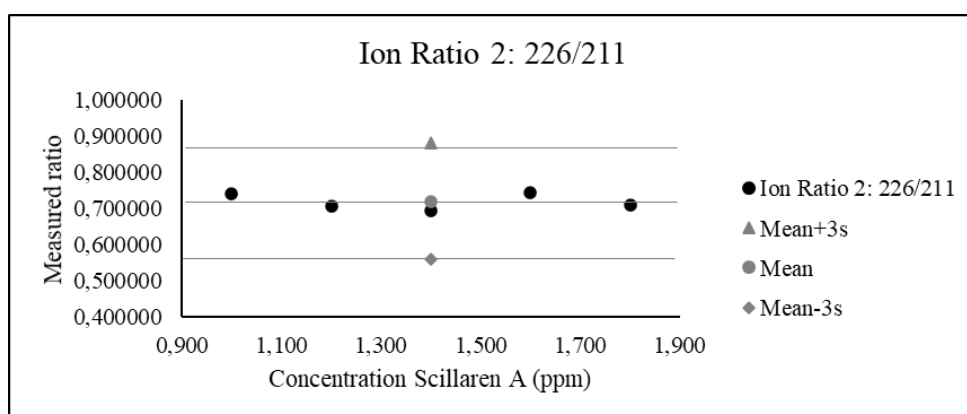
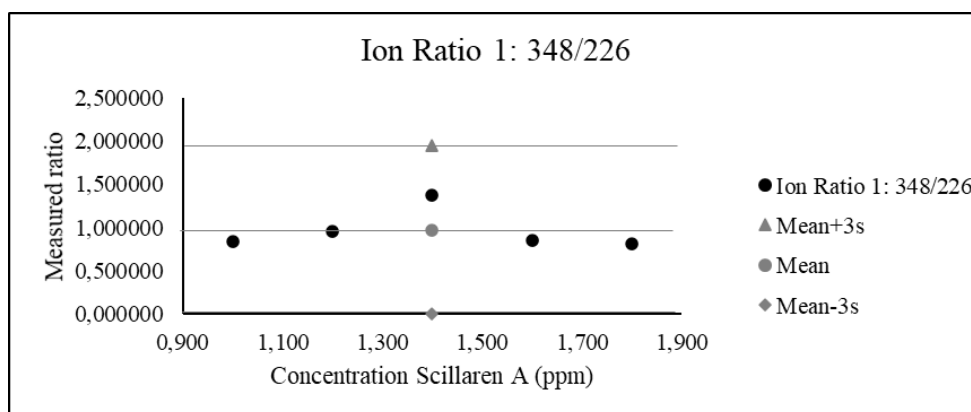
A centroid vector of the ion ratios was calculated for both the samples in urine and the de-ionised aqueous matrices. The 99.7% confidence interval around the centroid vector defined the multidimensional control region for the ion ratios. If, at $\alpha = 0.003$, a single ion ratio falls outside the control region, the vector of measured ratios deviates significantly from the centroid. The standard deviations of the ion ratios were calculated from the diagonal elements of the unbiased distribution matrix for the ion ratios. The centroid for urine samples was calculated to be:

$$\overline{m}_U = \begin{bmatrix} m_{IR1} \\ m_{IR2} \\ m_{IR3} \\ m_{IR4} \\ m_{IR5} \end{bmatrix} \pm 3 \times \bar{s} = \begin{bmatrix} 0.9677 \\ 0.7198 \\ 0.6917 \\ 2.620 \\ 1.909 \end{bmatrix} \pm \begin{bmatrix} 0.9790 \\ 0.1612 \\ 0.6413 \\ 2.656 \\ 2.154 \end{bmatrix}$$

For samples in the de-ionised aqueous matrix, the centroid was calculated to be:

$$\bar{m}_H = \begin{bmatrix} m_{IR1} \\ m_{IR2} \\ m_{IR3} \\ m_{IR4} \\ m_{IR5} \end{bmatrix} \pm 3 \times \bar{s} = \begin{bmatrix} 0.9669 \\ 0.6585 \\ 0.6413 \\ 2.136 \\ 1.409 \end{bmatrix} \pm \begin{bmatrix} 1.0358 \\ 0.1367 \\ 0.7431 \\ 1.958 \\ 1.387 \end{bmatrix}$$

To determine whether there were such significant deviations within the calibration range (1.000 to 1.800 ppm), the distribution, of the means of the duplicate analyses of ion ratios were plotted against concentration (See the graphs in **Figure V-14** & **Figure V-15**).



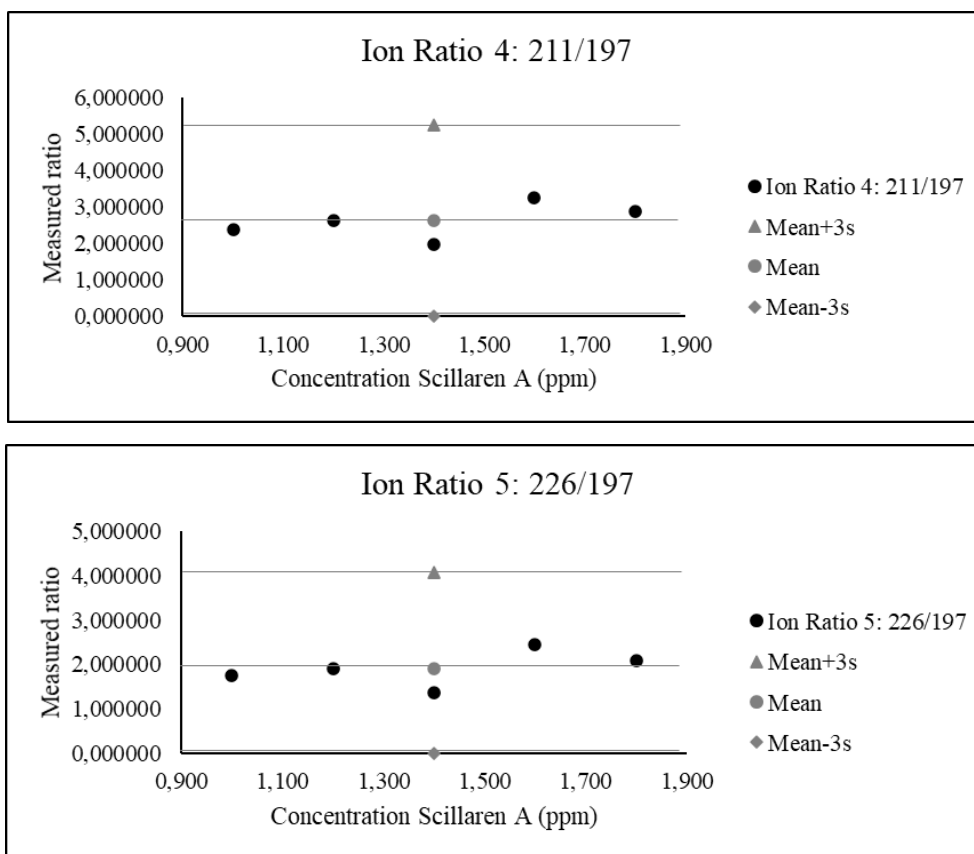


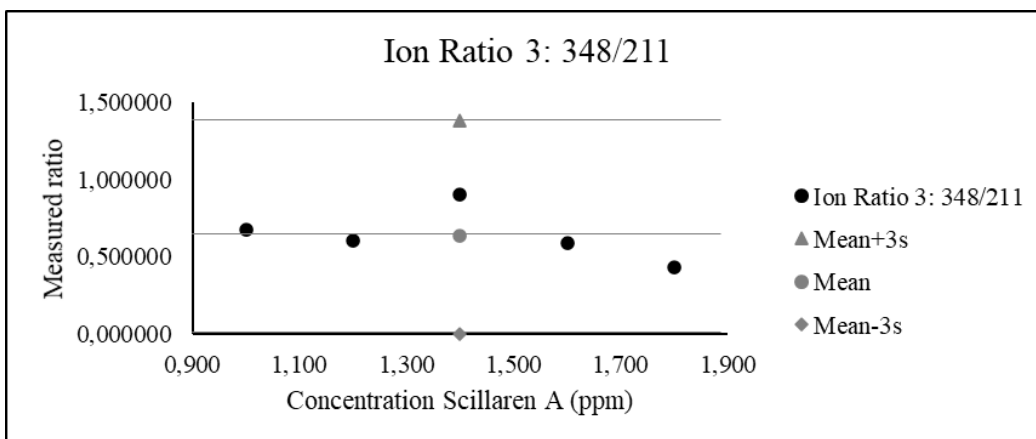
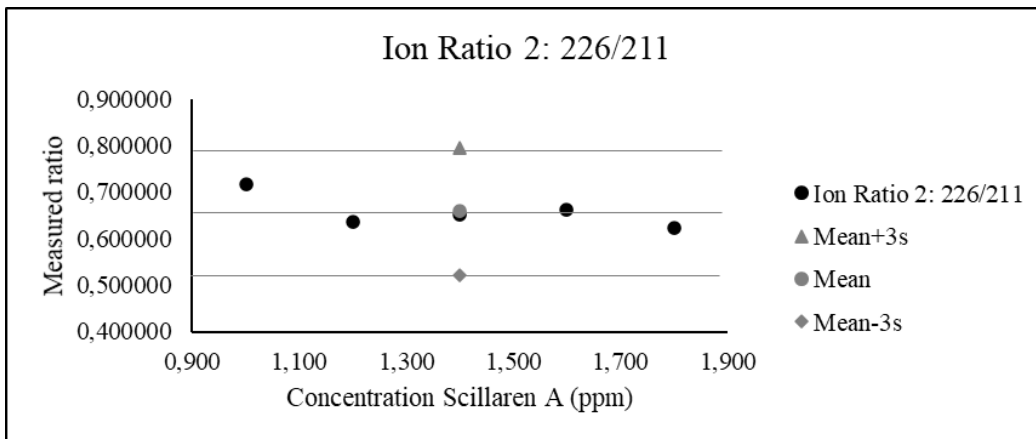
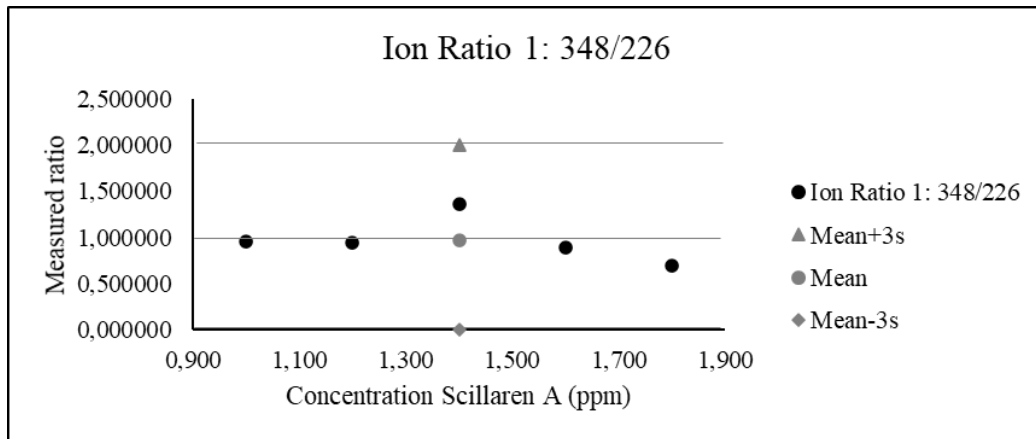
Figure V-14. Distribution of ion ratios in urine samples over the calibration range. The grey markers indicate the centroid and associated control ranges.

Within the concentration range of the calibration model, the ion ratios remained within the $\alpha = 0.003$ significance limits of the control range (**Figure V-14**). Therefore, the Δ^3, Δ^{14} -dehydro derivative of scillarenin (**48**) could be positively identified from its ion ratios in the mass spectra recorded in selected ion mode (SIM) at each concentration level in the calibration model. The limit of detection, based on the measured ion ratios, does not lie within the concentration range of the calibration model.

Since there was not enough certified reference material for further analysis due to logistical issues, the limit of detection could not be estimated experimentally via the analysis of samples spiked at low ppm-levels (low concentration). It was observed in the qualitative analysis of the other analytes studied in the project, that the ion ratios did not necessarily follow a modelled trend, which can be extrapolated to where the ratios reach the control limits. In some cases, the ratios underwent a sudden dramatic change within a very narrow concentration range.

The ion ratios measured from the de-ionised water samples (**Figure V-15**), were also analysed for the occurrence of significant deviation within the calibration range. In these distributions no significant deviation from the control range occurred. There were, however, stronger trends

away from the centroid ratios in the aqueous samples than in the urine samples where the distributions were more random. The correlation of the ion ratios to the calculated linear regression lines was, however, not significant enough so that the calculated regression model could be effectively applied in the estimation of a possible limit of detection.



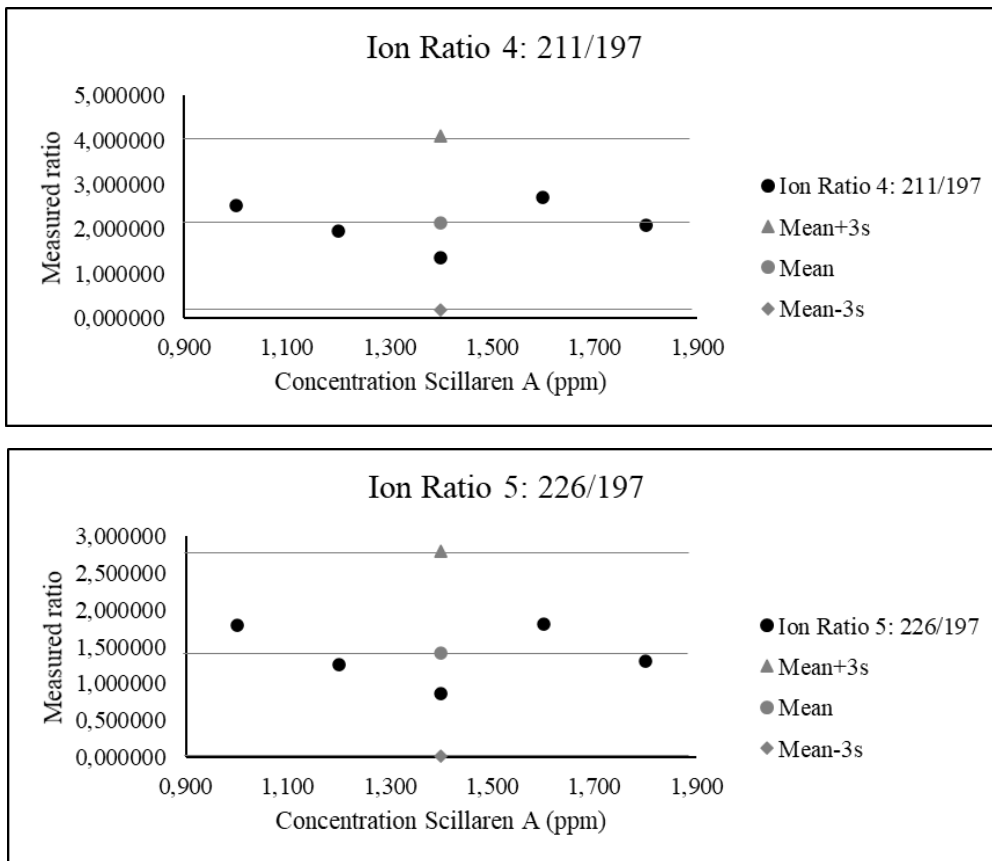


Figure V-15. Distribution of ion ratios in de-ionised water samples, over the concentration range in the calibration model. The grey markers indicate the centroid and associated control ranges.

3.4.2 Comparison of precision in ion ratios from two matrices

Table V- 9. %-RSD values for the ion ratios measured in de-ionised water and urine samples.

Ion ratio	%RSD	
	(De-ionised water)	(Urine)
IR 1	35.71	33.72
IR 2	6.917	7.464
IR 3	38.63	30.90
IR 4	30.56	33.80
IR 5	32.81	37.61

Both matrices are observed to produce the same level of precision in the measurement of the ion ratios. The calculated %-RSD values in either matrix is very high for four of the five measured ion ratios. A notably high precision was observed in the estimation of IR 2, where the %-RSD was less than 10.00% for samples in either matrix. The loss of precision in the

estimation of the centroid vector of ion ratios could be attributed to the variance in ion ratios between concentration levels. To determine whether this hypothesis is valid, multivariate analysis of variance (MANOVA) was performed on the duplicate measurement of ion ratios within each of the two batches at a significance level of $\alpha = 0.003$. The MANOVA calculation was performed on the IBM® SPSS® Statistics software suite (version 26).

In the MANOVA-calculation for urine samples, the degrees of freedom in the denominator of the F-distribution were five, and that of the numerator were 20. The Wilks' Lambda (Λ) value for the analysis was calculated to be 0.002, corresponding to an F-statistic of 1.160. Compared to a critical F-value of $F_5^{20} = 16.038$, the variation in ion ratios between the concentration levels did not significantly contribute to the total variance between the measured ion ratio vectors.

For the same number of degrees of freedom, the MANOVA-test was repeated for the de-ionised water samples. Λ was found to be equal to 0.057, corresponding to an F-statistic equal to 0.291. This value is less than the critical F-value for a one-tailed distribution at $\alpha = 0.003$. Therefore, the variation in the measured vectors of ion ratios did not significantly contribute to the total variance between the ion ratios.

Since the large variance between the measured vectors of ion ratios could not be attributed to inter-concentration level variation, it can alternatively be interpreted as a large variance in the selectivity of fragmentation pathways. This indicates that the ratio of the signal area of $m/z = 226$, to the signal area of $m/z = 211$ is a consistent characteristic of the Δ^3, Δ^{14} -dehydro derivative of Scillarenin.

4. Conclusion to Chapter V

In this chapter, scillaren A (**40**) was tentatively identified in the negative ion mode UPLC-chromatogram based on accurate mass and elemental composition analysis of the measured masses in the recorded mass spectra. The formic acid adduct's parent molecule had an accurate mass that correlated with the theoretical monoisotopic mass, with a mass difference of -0.1 ppm. The mass difference calculated for the quasi-molecular ion's neutral parent molecule, compared to the theoretical mass, was 1.3 ppm. Further confirmation of the identity of the peak as scillaren A was obtained by comparison of the relative retention times of the analyte peak with that of a reference sample of scillaren A (**40**).

The study explored the application of the analytical method developed for the quantitative analysis of acovenoside A (**22**) in Chapter IV, in quantifying scillaren A (**40**) in aqueous and

urine samples. The response models generated in the two matrices did not show any correlation with the linear models calculated from the regression of the relative response of the base peak ion (w.r.t. the base peak ion in the internal standard) over concentration. Without any correlation, the model could not be applied in estimating theoretical limits of detection and quantification.

Comparing the response models from the two matrices showed the similarity in the trends of the measured relative responses. This similarity indicates good repeatability of the method for different sample matrices, implying the problematic correlation of the measured data to the regression model cannot be attributed to variation caused by matrix effects. Factors that could selectively impact the absolute and, therefore, the relative analyte response include the repeatability of elution from SPE-cartridges for scillaren A (**40**) and the repeatability of pipetting of the scillaren A (**40**) stock solution into the samples.

Further development of the sample preparation method is, therefore, suggested. To address the problematic inter-sample repeatability of the method, attention should be given to the optimisation of the solid-phase extraction process by choosing an internal standard that mimics the extraction chemistry of scillaren A (**40**) better. The observation that the selectivity of dichloromethane and methanol as extraction solvents is not repeatable, indicates other elution solvents should be considered. The elution solvent system should be able to elute both cardenolides and bufadienolides, together with suitable internal standard, from the SPE-sorbent bed. By utilising different extraction solvents in multiple elution steps, the repeatability of the method may have been decreased, since different extraction efficiencies were produced.

Evaluation of the qualitative analysis of Δ^3 -dehydro- Δ^{14} -dehydroscillarenin (**45**), produced during hydrolysis of scillaren A (**40**) showed large variance in the estimation of ion ratios from the areas of analyte ions in extracted ion chromatograms. In each matrix the centroid vector of ion ratios, and its associated 99.7% confidence interval was calculated. For urine samples the centroid vector was:

$$\bar{m}_U = \begin{bmatrix} m_{IR1} \\ m_{IR2} \\ m_{IR3} \\ m_{IR4} \\ m_{IR5} \end{bmatrix} \pm 3 \times \bar{s} = \begin{bmatrix} 0.9677 \\ 0.7198 \\ 0.6917 \\ 2.620 \\ 1.909 \end{bmatrix} \pm \begin{bmatrix} 0.9790 \\ 0.1612 \\ 0.6413 \\ 2.656 \\ 2.154 \end{bmatrix}$$

The centroid vector of ion ratios for de-ionised water samples was:

$$\bar{m}_H = \begin{bmatrix} m_{IR1} \\ m_{IR2} \\ m_{IR3} \\ m_{IR4} \\ m_{IR5} \end{bmatrix} \pm 3 \times \bar{s} = \begin{bmatrix} 0.9669 \\ 0.6585 \\ 0.6413 \\ 2.136 \\ 1.409 \end{bmatrix} \pm \begin{bmatrix} 1.0358 \\ 0.1367 \\ 0.7431 \\ 1.958 \\ 1.387 \end{bmatrix}$$

Despite the large %-RSD values, all five ion ratios remained within the 99.7% control range around the centroid vector of ion ratios in both respective matrices across the whole concentration range of the calibration model. Δ^3 -dehydro- Δ^{14} -dehydroscillarenin (**48**) can, thus, be positively identified from its characteristic ion ratios at each point in the concentration range at which the samples were spiked. The variation between the measured vectors of the ion ratios over the concentration range, was found not to contribute significantly to the total variance between the measured vectors.

The absence of multiple replicate batches in the estimation of the limits of the method, negatively impacted the quality of the results. Future work should include more repeats of measurements, which would provide a better representation of the limits and capabilities of the method. The number of replicate analyses in this chapter were severely limited, due to the small amount of reference material available. High monetary cost and a restricted timeline did not allow for further purchase of the reference material.

Since the ion ratios remained within the control ranges, further research into the limit of detection for scillaren A (**40**) (via Δ^3 -dehydro- Δ^{14} -dehydroscillarenin (**48**)) is suggested. This would also entail further development of the analytical and sample preparation methods to optimise the accuracy and precision of the calculated response models. To determine the limits of detection and quantification, the optimised calibration model can be used and the results compared to the experimentally determined limits obtained by performing the same limit of detection study as for acovenoside A (**22**).

References

- (1) Neuwinger, H. D. 1996. *Drimia sanguinea* (Schinz) Jessop. *African Ethnobotany - Poisons and Drugs*. Weinheim: Chapman & Hall GmBH, pp. 548-551.
- (2) Foukaridis, G. N., Osuch, E., Mathibe, L. & Tsipa, P. 1995. The ethnopharmacology and toxicology of *Urginea sanguinea* in the Pretoria area. *Journal of Ethnopharmacology*, 49, 77-79.
- (3) Mcvann, A., Havlik, I., Joubert, P. & Monteagudo, F. 1992. Cardiac glycoside poisoning involved in deaths from traditional medicines. *South African Medical Journal*, 81, 139-141.

- (4) Van Wyk, B.-E., Van Heerden, F. & Van Oudtshoorn, B. 2014. *Urginea sanguinea*. In: Ferreira, R. (ed.) *Poisonous plants of South Africa*. 1st ed. ed. Pretoria: Briza Publications, pp. 214-215.
- (5) Marx, J., Pretorius, E., Espag, W. & Bester, M. 2005. *Urginea sanguinea*: medicinal wonder or death in disguise? *Environmental toxicology and pharmacology*, 20, 26-34.
- (6) Van Wyk, B.-E. & Gericke, N. 2018. General Medicines. *People's Plants - A guide to useful plants of southern Africa*. 2nd ed. Pretoria: Briza Publications, pp. 138-164.
- (7) Van Wyk, B.-E., Van Oudtshoorn, B. & Gericke, N. 2017. *Drimia elata*. *Medicinal Plants of South Africa*. Pretoria: Briza Publications, pp. 126-127.
- (8) Kellerman, T. S., Naudé, T. & Fourie, N. 1996. The distribution, diagnoses and estimated economic impact of plant poisonings and mycotoxicoses in South Africa.
- (9) Majinda, R. R., Waigh, R. D. & Waterman, P. G. 1997. Bufadienolides and other constituents of *Urginea sanguinea*. *Planta medica*, 63, 188-190.
- (10) Haustein, K. O. 1982. Digitalis. *Pharmacology & Therapeutics*, 18, 1-89.
- (11) El-Seedi, H. R., Khalifa, S. A., Taher, E. A., Farag, M. A., Saeed, A., Gamal, M., Hegazy, M.-E. F., Youssef, D., Musharraf, S. G. & Alajlani, M. M. 2018. Cardenolides: Insights from chemical structure and pharmacological utility. *Pharmacological research*.
- (12) Evans, W. C. 2009. Saponins, cardioactive drugs and other steroids. In: Evans, D. (ed.) *Trease and Evans Pharmacognosy*. 16 ed. New York: Saunders Elsevier, pp. 304-332.
- (13) Ezzat, S. M., El Gaafary, M., El Sayed, A. M., Sabry, O. M., Ali, Z. Y., Hafner, S., Schmiech, M., Jin, L., Syrovets, T. & Simmet, T. 2016. The Cardenolide Glycoside Acovenoside A Affords Protective Activity in Doxorubicin-Induced Cardiotoxicity in Mice. *Journal of Pharmacology and Experimental Therapeutics*, 358, 262-270.
- (14) Bartnik, M. & Facey, P. C. 2017. Glycosides. In: Badal, S. & Delgoda, R. (eds.) *Pharmacognosy: Fundamentals, Applications and Strategy*. London: Elsevier Inc., pp. 101-161.
- (15) Kawahara, K., Hosoya, R., Sato, H., Tanaka, M., Nakajima, T. & Iwabuchi, S. 2002. Selective blockade of astrocytic glutamate transporter GLT-1 with dihydrokainate prevents neuronal death during ouabain treatment of astrocyte/neuron cocultures. *Glia*, 40, 337-349.
- (16) Joubert, J. & Schultz, R. 1982. The treatment of *Urginea sanguinea* Schinz poisoning in sheep with activated charcoal and potassium chloride. *Journal of the South African Veterinary Association*, 53, 25-28.
- (17) Nel, P., Jordaan, P., Anderson, L., Kellerman, T. S., Reid, C. & Schultz, R. A. 1987. Cardiac glycoside poisoning in sheep caused by *Urginea physodes* (Jacq.) Bak. and the isolated physodine A. *Onderstepoort Journal of Veterinary Research*, 54, 641-644.
- (18) Botha, C. & Penrith, M.-L. 2008. Poisonous plants of veterinary and human importance in southern Africa. *Journal of Ethnopharmacology*, 119, 549-558.
- (19) Vetticaden, S. J. & Chandrasekaran, A. 1990. Chromatography of cardiac glycosides. *Journal of Chromatography B: Biomedical Sciences and Applications*, 531, 215-234.

- (20) Tobyn, G., Denham, A. & Whitelegg, M. 2011. CHAPTER 15 - *Drimia maritima*, squill. In: Tobyn, G., Denham, A. & Whitelegg, M. (eds.) *Medical Herbs*. Edinburgh: Churchill Livingstone, pp. 155-164.
- (21) Sato, N. & Muro, T. 1974. Antiviral activity of scillarenin, a plant bufadienolide. *Japanese journal of microbiology*, 18, 441-448.
- (22) Han, L., Wang, H., Si, N., Ren, W., Gao, B., Li, Y., Yang, J., Xu, M., Zhao, H. & Bian, B. 2016. Metabolites profiling of 10 bufadienolides in human liver microsomes and their cytotoxicity variation in HepG2 cell. *Analytical and bioanalytical chemistry*, 408, 2485-2495.
- (23) Gibson, G. G. & Skett, P. 1994. Pathways of drug metabolism. In: Professional, B. A. (ed.) *Introduction to Drug Metabolism*. 2nd ed. Dordrecht: Springer Science+Business Media, pp. 1-34.
- (24) Ning, J., Wu, T.-H., Tian, Y., Wang, C.-Y., Tian, G., Zhang, B.-J., Liu, K.-X. & Ma, X.-C. 2010. Identification of cinobufagin metabolites in the bile of rats. *Xenobiotica*, 40, 48-54.
- (25) Van Den Berg, H., Schultz, R. & Kellerman, T. 2005. The role of fluorescence polarization immuno-assay in the diagnosis of plant-induced cardiac glycoside poisoning livestock in South Africa. *Onderstepoort Journal of Veterinary Research*, 72, 189-201.
- (26) Guan, F., Ishii, A., Seno, H., Watanabe-Suzuki, K., Kumazawa, T. & Suzuki, O. 1999. Identification and quantification of cardiac glycosides in blood and urine samples by HPLC/MS/MS. *Analytical chemistry*, 71, 4034-4043.
- (27) Radford, D. J., Gillies, A. D., Hinds, J. A. & Duffy, P. 1986. Naturally occurring cardiac glycosides. *Medical Journal of Australia*, 144, 540-544.
- (28) Jameson, D. M. & Croney, J. C. 2003. Fluorescence polarization: past, present and future. *Combinatorial chemistry & high throughput screening*, 6, 167-176.
- (29) Nielsen, K., Lin, M., Gall, D. & Jolley, M. 2000. Fluorescence polarization immunoassay: detection of antibody to *Brucella abortus*. *Methods*, 22, 71-76.
- (30) Lippolis, V., Pascale, M., Valenzano, S., Porricelli, A. C. R., Suman, M. & Visconti, A. 2014. Fluorescence polarization immunoassay for rapid, accurate and sensitive determination of ochratoxin A in wheat. *Food Analytical Methods*, 7, 298-307.
- (31) Bagrov, A. Y., Fedorova, O. V., Dmitrieva, R. I., Howald, W. N., Hunter, A. P., Kuznetsova, E. A. & Shpen, V. M. 1998. Characterization of a urinary bufadienolide Na⁺, K⁺-ATPase inhibitor in patients after acute myocardial infarction. *Hypertension*, 31, 1097-1103.
- (32) Cao, Y., Zhao, L., Liang, Q., Bi, K., Wang, Y. & Luo, G. 2007. Study of the determination and pharmacokinetics of bufadienolides in dog's plasma after administration of Liu-Shen-Wan by high performance liquid chromatography time-of-flight mass spectrometry. *Journal of Chromatography B*, 853, 227-233.
- (33) Tao, J., Mao, L., Zhou, B., Liu, Q., Yang, A., Wei, G., Liu, R., Zhang, W.-D., Xu, W. & Ye, J. 2017. Simultaneous determination of ginsenosides and bufadienolides in rat plasma after the oral administration of Shexiang Baixin Pill for pharmacokinetic study by liquid chromatography tandem mass spectrometry following solid-phase extraction. *Biomedical Chromatography*, 31, e3816.

- (34) European Commission: Directorate General for Health and Food Safety. 2017. *SANTE/11945/2015: Guidance document on analytical quality control and method validation procedures for pesticides residues analysis in food and feed*. European Commission: Directorate General for Health and Food Safety. Available: https://ec.europa.eu/food/sites/food/files/plant/docs/pesticides_mrl_guidelines_wrkdoc_2017-11813.pdf [Accessed 2020-08-26].
- (35) 2007. Dictionary of Natural Products. Boca Raton: Chapman and Hall/CRC.
- (36) Stoll, A., Kreis, W. & Von Wartburg, A. 1952. Die hydrolytische Spaltung von herzwirksamen Glykosiden der weissen Meerzwiebel. 33. Mitteilung über Herzglykoside. *Helvetica Chimica Acta*, 35, 2495-2519.
- (37) Von Wartburg, A. 1966. 6. Die Herzglykoside der roten Meerzwiebel (*Scilla maritima*): Scillirubrosid 54. Mitteilung über Herzglykoside [1]. *Helvetica Chimica Acta*, 49, 30-42.
- (38) Kohls, S., Scholz-Böttcher, B. M., Teske, J., Zark, P. & Rullkötter, J. 2012. Cardiac glycosides from Yellow Oleander (*Thevetia peruviana*) seeds. *Phytochemistry*, 75, 114-127.
- (39) 2020. *Certificate of Analysis - Scillaren A* [Online]. Darmstadt: Sigma-Aldrich. Available: <https://www.sigmaaldrich.com/catalog/CertOfAnalysisPage.do?symbol=SMB00229&LotNo=12222845V&brandTest=SIGMA&returnUrl=%2Fproduct%2FSIGMA%2FSMB00229> [Accessed 2020-11-04].

Chapter VI

Conclusion

1. Isolation of a reference standard of buphanidrine from *B. disticha*

Through the research and experimentation done in this project, a suitable reference standard of buphanidrine (**1**) was purified and isolated from the bulb of *B. disticha* by liquid-liquid extraction and chromatography. The standard was isolated from plant material since buphanidrine (**1**) was not readily available commercially. The identity of the isolated analyte was confirmed by NMR (^1H -, ^{13}C - and 2D-HSQC-NMR), accurate mass analysis, and comparison of its 70-eV electron impact mass spectrum with the Wiley-NIST Registry (11th-edition). Buphanidrine (**1**) was isolated with a 90.36% purity based on UPLC-qTOF MS analysis in the positive ion mode.

This isolated standard was successfully used in the validation of an analytical method for its detection *and* quantification in urine by GC-MS.

2. Limitations of developed quantitative analytical methods

2.1 Linearity of the developed methods

Through method validation of the developed analytical methods, the limitations of the methods were defined. In terms of the suitability of a linear regression model in describing the data, only the method developed for the analysis of samples containing buphanidrine (**1**) showed significant correlation between the data and the calculated trendline. The relative responses measured for colchicine (**7**) and acovenoside A (**22**) were better described by log-linear regression models. In these models the logarithm (base 10) of the relative responses were regressed on the concentration of analyte in the samples. Despite the improved correlation, the response models did not show significant correlation with the respective calculated trendlines. The relative responses of scillaren A (**40**) spiked into either de-ionised water or urine, showed no clear trend and could not be modelled with any degree of correlation to a calculated linear trend line.

For buphanidrine (**1**), limits of detection and quantification could be inferred from the calculated linear regression model. In the case of acovenoside A (**22**) and colchicine (**7**), hypothetical limits of detection and quantification were suggested. These limits can, however, not be applied in a routine laboratory setting since the suitability of the log-linear models in describing the trend in the relative responses is not within acceptable limits. The complete

absence of a clear trend in the data for scillaren A (**40**) made it impossible to infer the limits of detection and quantification, even hypothetically, from an associated regression model.

The calculated limits of detection and quantification were compared to the limits of identification, experimentally determined from the distribution of ion ratios over concentration. For each analyte, the centroid vector of characteristic ion ratios was calculated at the centroid concentration level. Around these centroid vectors, a 99.7% confidence level was defined and used as a control range at the $\alpha = 0.003$ significance level for positive identification of the analytes. By monitoring the distribution of the measured vectors of ion ratios for each analyte at concentration levels below the respective corresponding concentration ranges, the limits of identification could be inferred experimentally. These limits were compared to the calculated limits of detection to determine if the experimental limit is significantly greater than the calculated limit.

2.2 Precision in measurement and analysis

The repeatability of sample preparation and analysis across the concentration range of the response model was evaluated through the %-RSD estimates at each concentration level. These %-RSD values also indicated experimental limits of quantification where the coefficient of variation exceeded the expected level for the concentration order of magnitude from the Horwitz equation. For the analysis of samples spiked with buphanidrine (**1**) or acovenoside A (**22**), the precision was, as expected, not as good in urine samples than in de-ionised water samples. The precision in the analysis of samples that were spiked with colchicine (**7**), showed the opposite trend.

Analysing the contributions to total variance in the measurement of relative responses at each concentration level, showed the between-batch variation can be expected to significantly contribute at the lower concentration levels in the response models. This observation was attributed to the relatively strong background signals detected in the samples. The additional contribution to the variance at low concentration levels induced a heteroscedastic distribution of variance over the respective response models.

By applying multivariate unbiased-Gaussian statistics, the precision in measurement across batches of samples was evaluated. For none of the four analytes did the between-batch variation in measurement significantly contribute to the total variance between the measured vectors of ion ratios at a single concentration level. This shows the developed methods were repeatable over multiple batches of samples in positively identifying the analytes in the sample matrices.

3. Applicability of developed quantitative methods in the routine setting

Through the research done in this project, a first step has been taken in developing analytical methods conforming to standardised quality for the routine analysis of physiological samples suspected of containing toxins originating from plants. The precision in positively identifying the toxins spiked into urine, provided a degree of initial application of the developed methods. Further development and optimisation may produce methods with acceptable levels of inter-batch *and* inter-concentration repeatability.

4. Planned and suggested future research on the topic of this project

The application of the limit of *identification* and its mathematical definition has been selected as a topic for further investigation following this project. It provides a more fundamental limitation to the analytical range of a quantitative method than the theoretical limits calculated from the regression model. The effect of poor precision in measurement on the calculation of detection and quantification limits from the regression model can be seen in the results obtained for acovenoside A (**22**) and colchicine (**7**) where the calculated limit of detection reached the high concentration levels on which the response model was defined, yet the limit of *identification* was at a lower concentration level than the definition of the response model.

Several factors remain that should be investigated further in future research. Attention should be given to the improvement of precision in generating response models by optimising the sample preparation procedures developed in this project. The limitations in sample stability and method robustness should be thoroughly investigated and optimised. For scillaren A (**40**), the limit of identification should be investigated by analysis of lower levels of concentration.

Further research on the metabolism of the toxins should also be conducted. Ideally such a study should involve case studies of patients poisoned by the plants and toxins covered in this project. Since poisoning with *U. sanguinea* often involves livestock, analysis of physiological fluids from poisoned animals may provide valuable information on the distribution and metabolism of bufadienolides in animals. As an alternative to *in vivo* case studies, *in vitro* investigation was considered where the toxins would be incubated with liver microsomes to induce the hepatic metabolism expected *in vivo*. Here time limitation prevented the inclusion of the experiment in the project thesis.

Appendix to Chapter I

A. Additional molecular structures

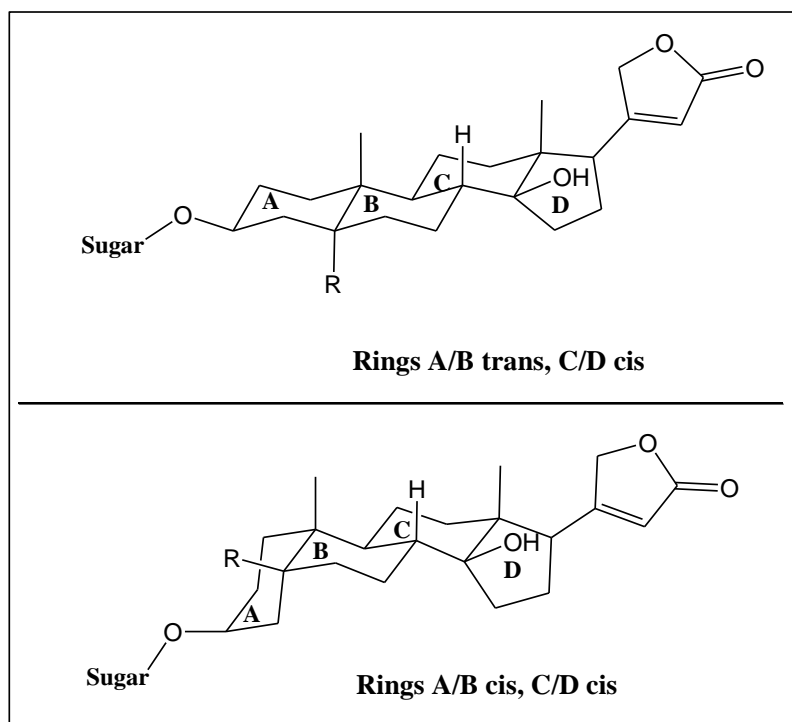


Figure A (I)-1. Stereoisomers of cardenolide structures. For cardio-activity, the cis-cis conformation is required.

B. Gas chromatography-Mass spectrometry diagrams

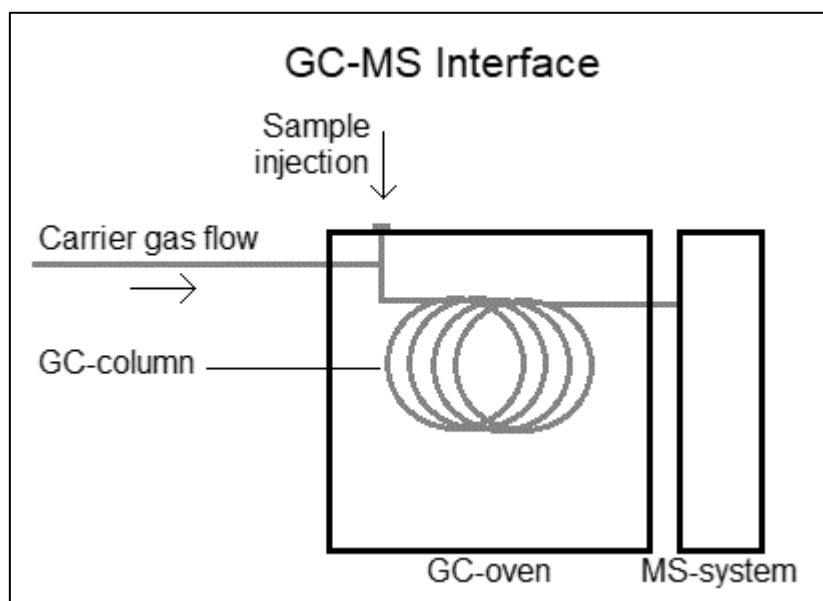


Figure A (I)-2. Basic gas chromatography (GC) system.

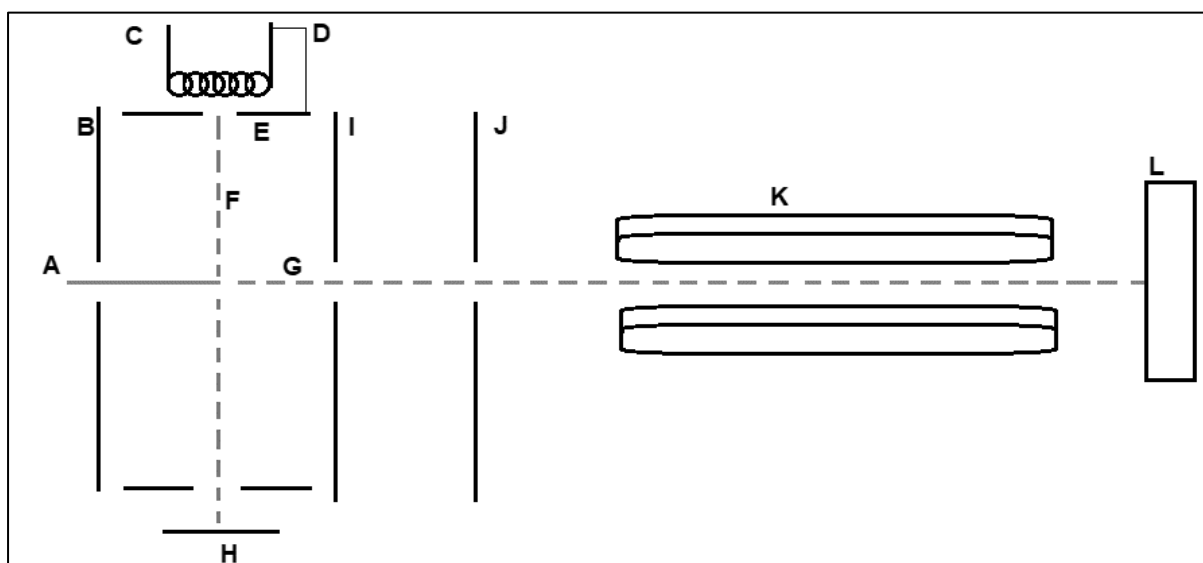


Figure A (I)-3. An electron impact (EI) ion source connected to a quadrupole mass analyser.

(A) Outflow from GC-column, (B) Repelling plate, (C) Tungsten filament (electron source), (D) 70 V potential difference applied between the filament and accelerator lens, (E) Accelerator plate, (F) Beam of high energy (70 eV) electrons, (G) Beam of molecular ions and fragments, (H) Cathode for capturing electrons, (I) Ion accelerator lens, (J) Ion lens, (K) Quadrupole mass analyser, (L) Detector and signal amplifier.

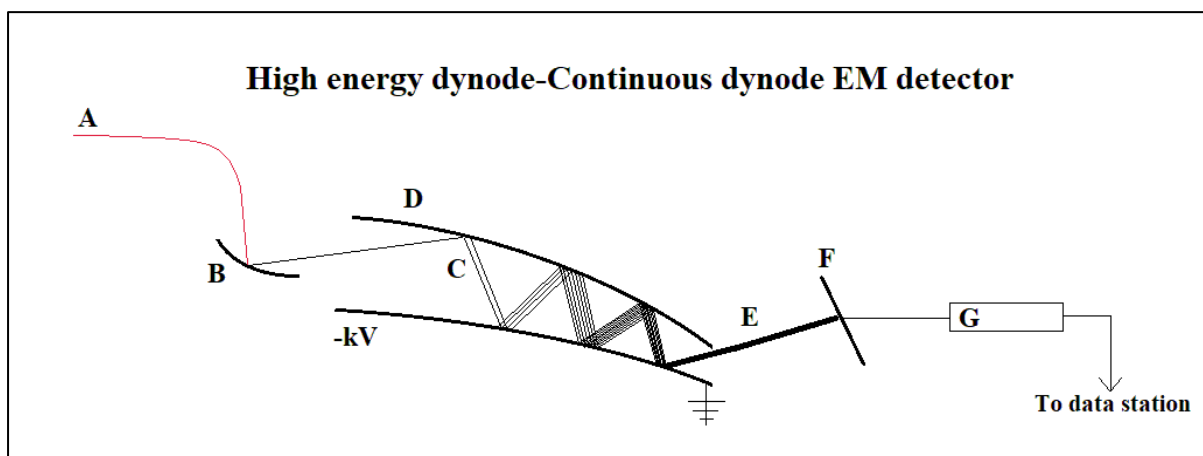


Figure A (I)-4. Off-axis high energy dynode (HED) Electron multiplier (EM) detector. (A) Incident ion beam of specific nominal m/z -ratio from mass analyser, (B) High energy conversion dynode, (C) Electrons generated by collision of high energy secondary electrons, accelerated to less negative dynode, (D) Continuous dynode; a large negative voltage is applied to the wide opening and a positive or earth potential is applied to the narrow exit, (E) Beam of secondary electrons emitted from multiplier, (F) Detection plate connected to signal amplifier leading to (G) the data station.

C. Liquid chromatography-High Resolution Mass Spectrometry diagrams

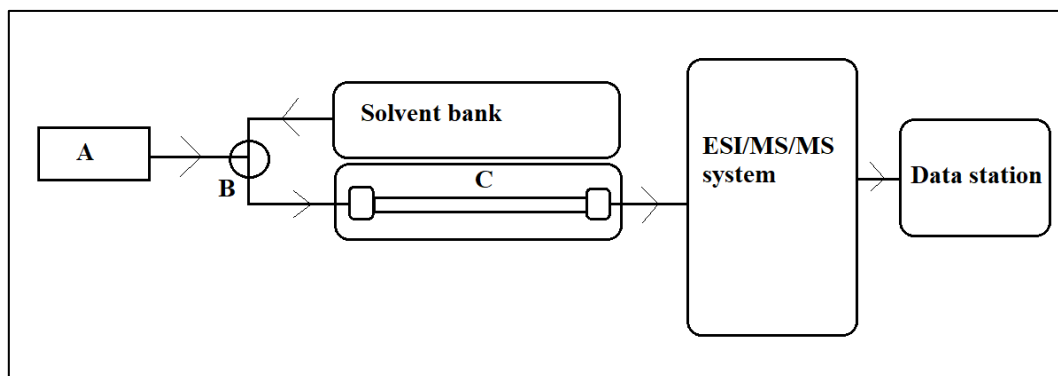


Figure A (I)-5. LC-MS/MS system. (A) Sampling system, (B) Valve combining sample and mobile phase flow, (C) UPLC/HPLC-column. The arrows indicate the direction of flow.

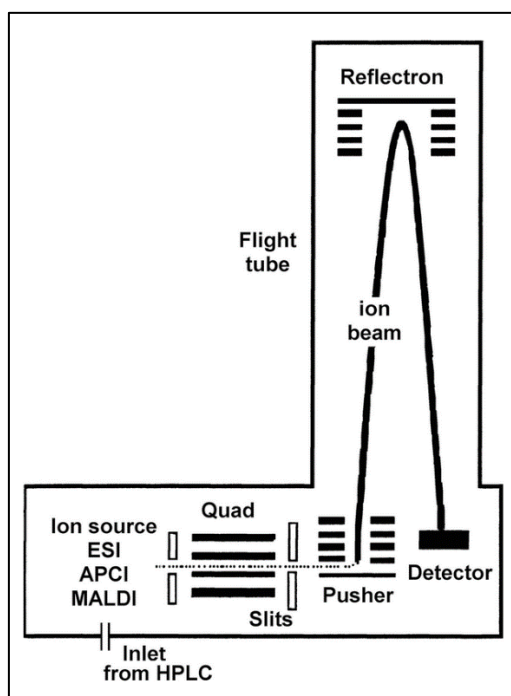


Figure A (I)-6. Basic qTOF system with a single quadrupole and a single reflectron (ion mirror).

D. Additional formulas used in statistical data analysis

Student's t-test ($N < 30$):

$$t = \frac{|x_i - \mu|}{s\sqrt{N}} \quad (\text{AI-1})$$

z-test ($N \geq 30$):

$$z = \frac{|x_i - \mu|}{\sigma\sqrt{N}} \quad (\text{AI-2})$$

t-test for significant correlation:

$$t = \frac{|r|\sqrt{N-2}}{\sqrt{1-r^2}} \quad (\text{AI-3})$$

F-test:

$$F = \frac{s_1^2}{s_2^2}; s_1^2 > s_2^2 \quad (\text{AI-4})$$

$$F_{CRIT} = F_{v_2}^{v_1}; v_1 \text{ for } s_1^2, v_2 \text{ for } s_2^2$$

T^2 -statistic:

$$T^2 = N(\bar{m} - \bar{\mu})^T \mathbf{D}^{-1}(\bar{m} - \bar{\mu}) \quad (\text{AI-5})$$

$$F_{N-p}^p = \frac{N-p}{p} \left(\frac{T^2}{N-1} \right)$$

Standard deviation of the calculated concentration x_0 :

$$s_{\frac{y}{x}} = \sqrt{\frac{\sum_{i=1}^n (y_i - \hat{y}_i)^2}{n-2}}$$

(AI-6)

$$s_{x_0} = \frac{s_{\frac{y}{x}}}{b} \sqrt{\frac{1}{m} + \frac{1}{n} + \left(\frac{(y_0 - \bar{y})^2}{b^2 \sum_{i=1}^n (x_i - \bar{x})^2} \right)}$$

Appendix to Chapter II

A. Library mass spectra from the Wiley-NIST spectral registry

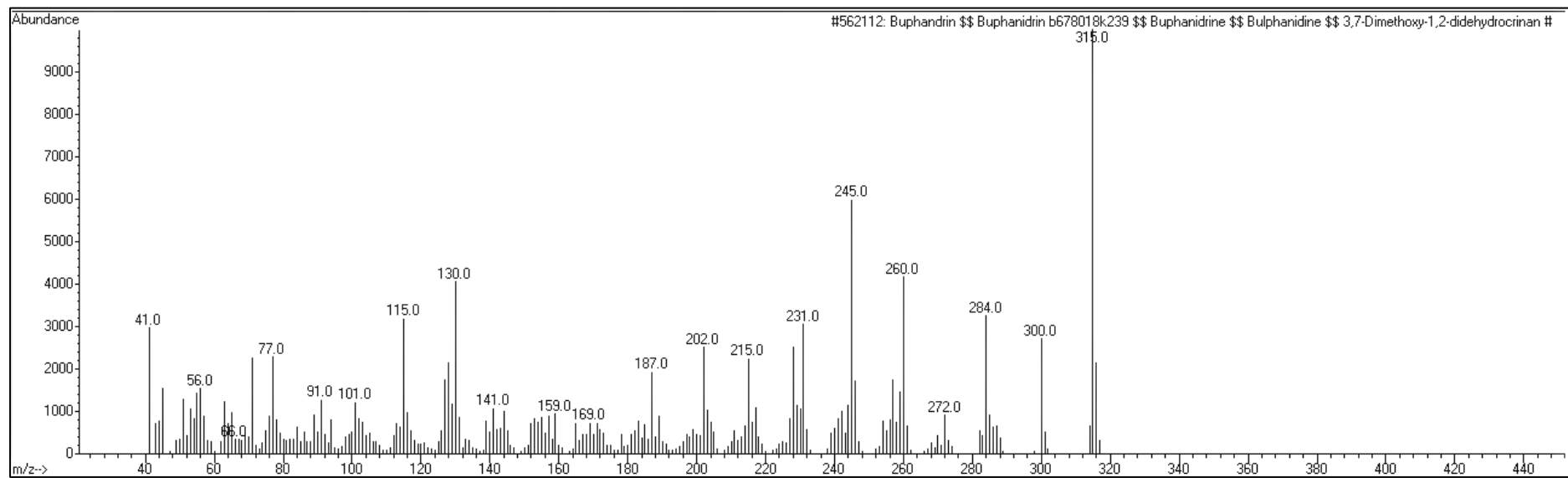


Figure A (II)-1. Library EI-mass spectrum for buphanidrine.

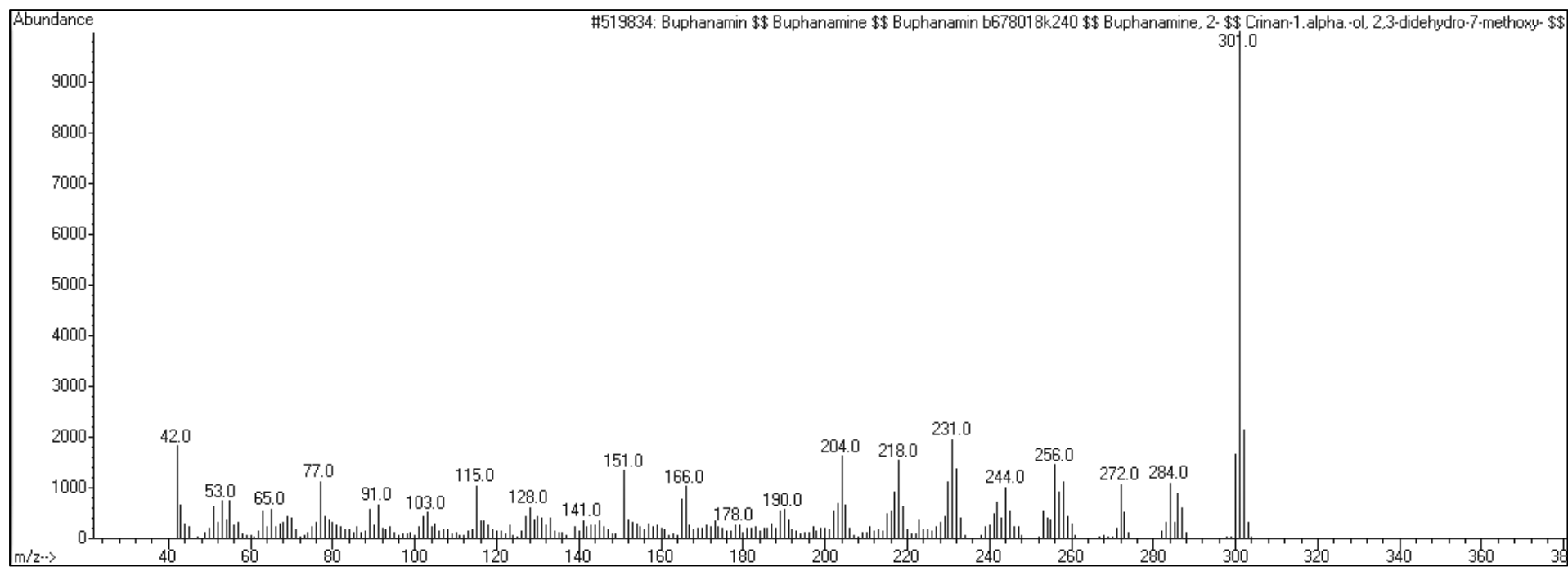


Figure A (II)-2. Library EI-mass spectrum for buphanamine.

B. NMR-spectra recorded for isolated buphanidrine

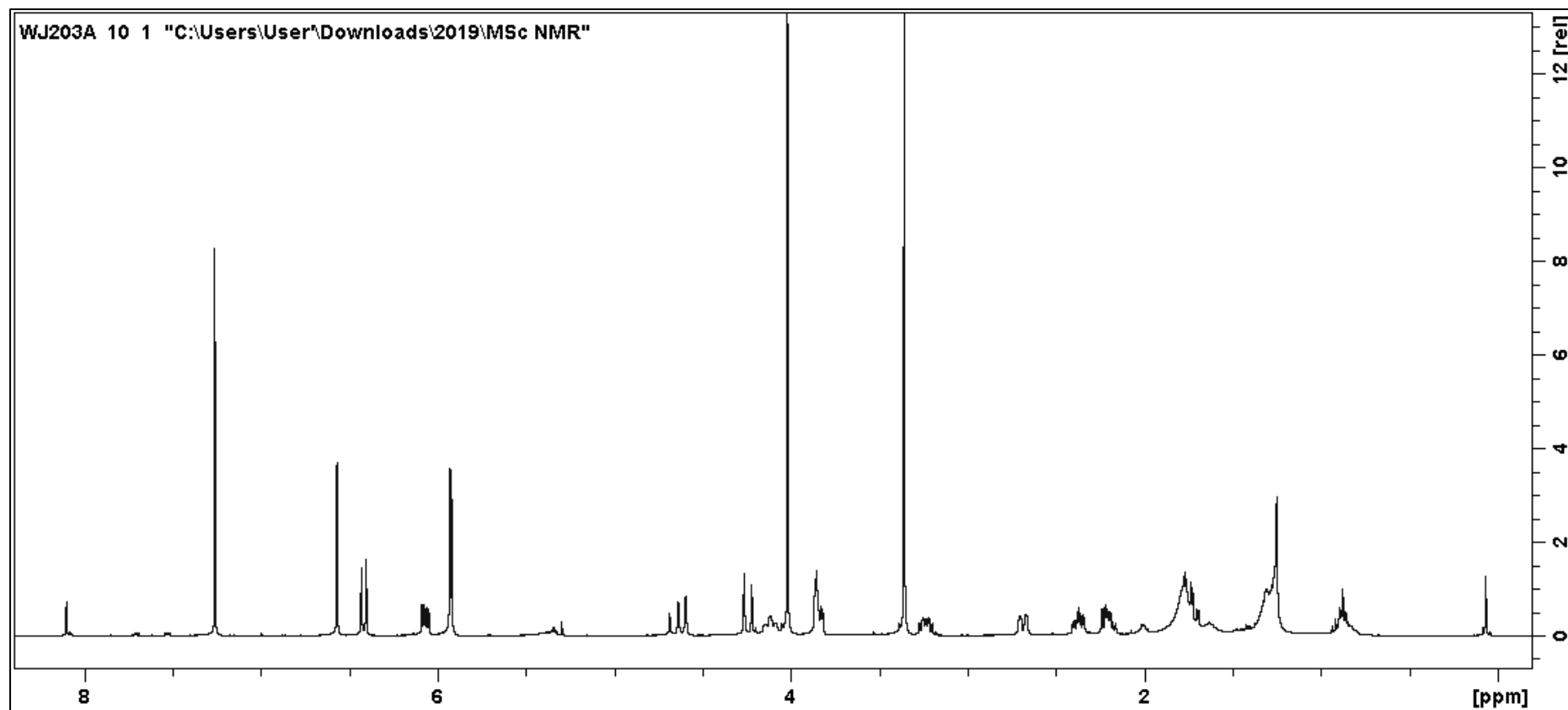


Figure A (II)-3. ¹H-NMR spectrum for buphanidrine, recorded in CDCl₃ with a 400 MHz spectrometer.

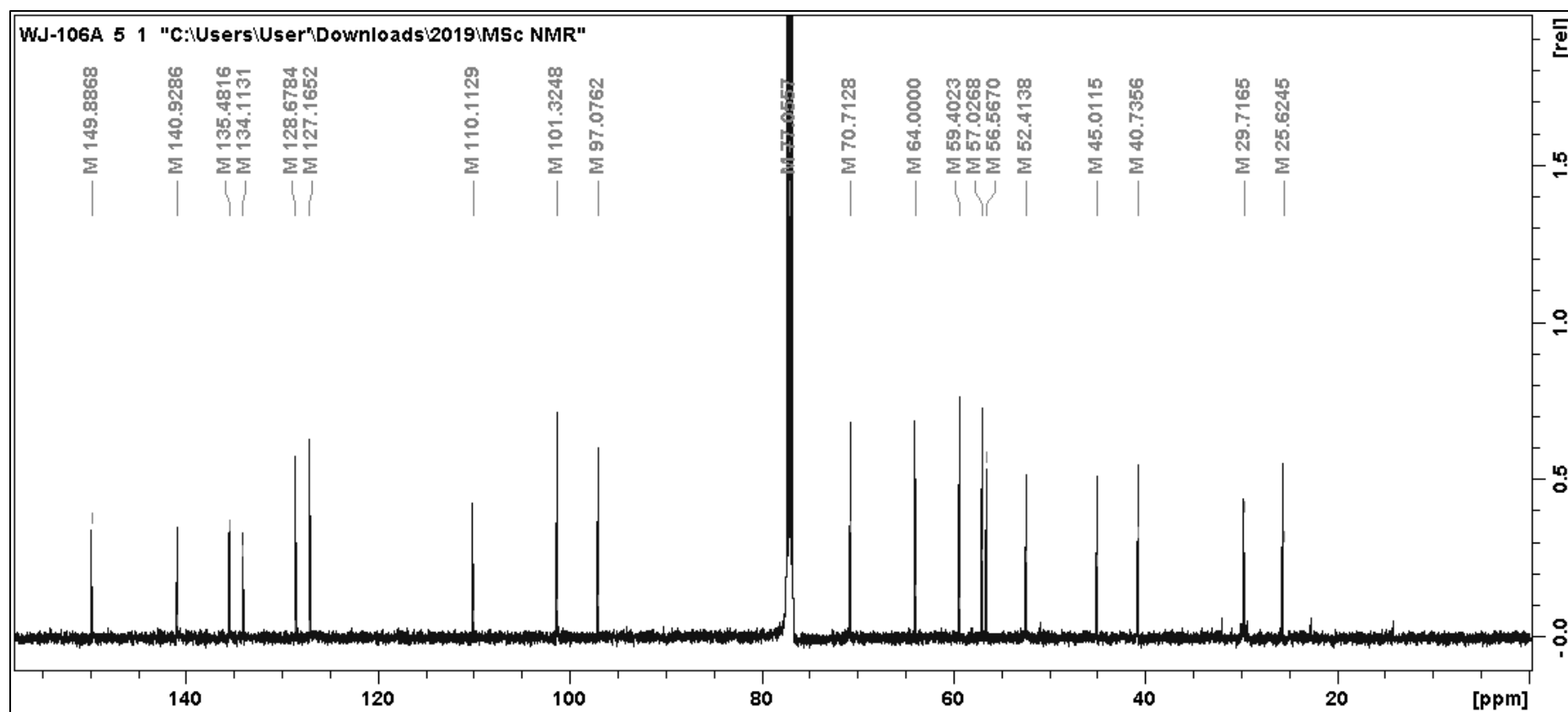


Figure A (II)-4. ^{13}C -NMR spectrum of buphanidrine, recorded in CDCl_3 . A 500 MHz spectrometer was used for this analysis.

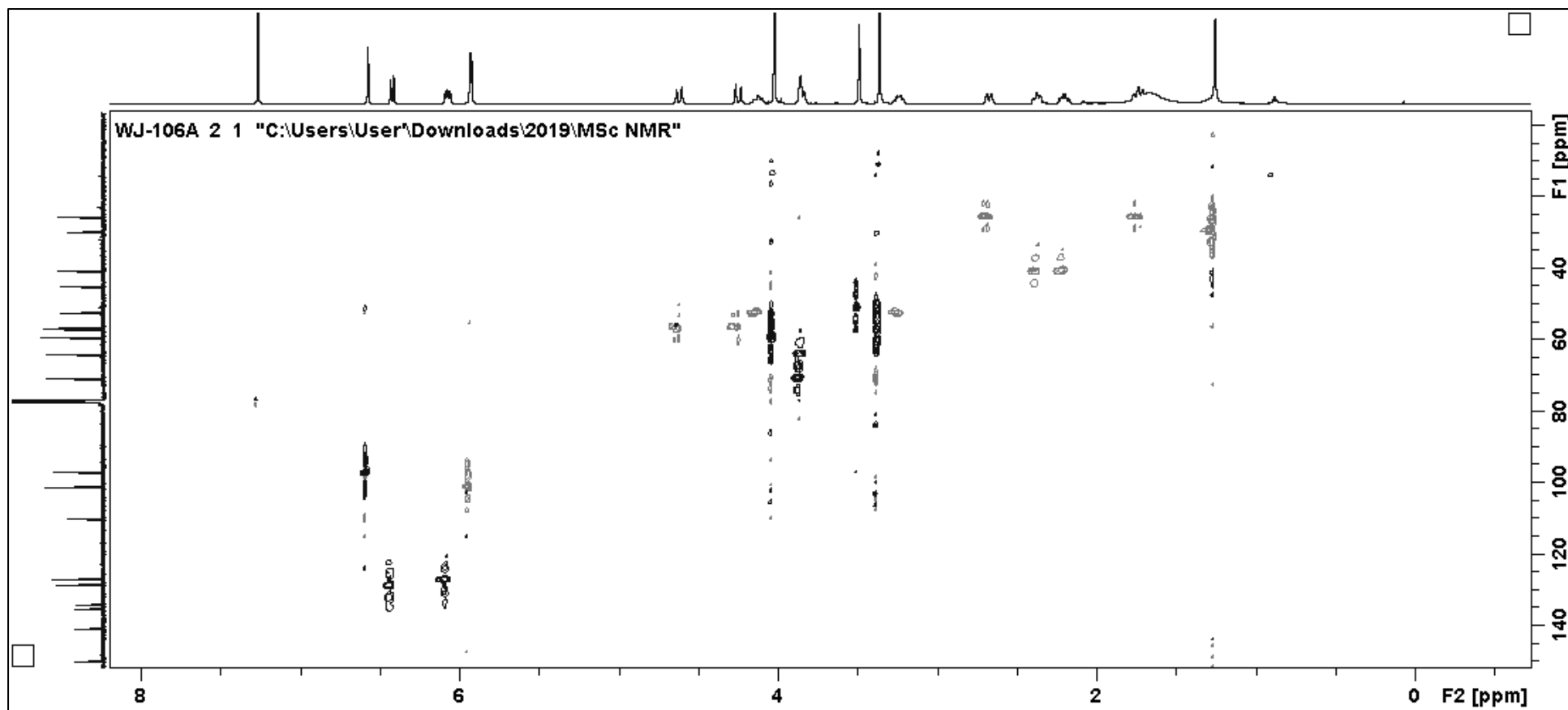


Figure A (II)-5. A Heteronuclear single quantum coherence spectroscopy (HSQC) 2D-NMR spectrum for buphanidrine, recorded with a 500 MHz spectrometer.

C. Photographs of *B. disticha*



Figure A (II)-6. (1) A juvenile bulb of *B. disticha* with trimmed leaves. The green ruler is 15.0 cm in length. (2) *B. disticha* in its natural habitat.

D. Method for the preparation of Dragendorff reagent

A stock solution (200 mL) of Dragendorff reagent is prepared by mixing bismuth oxynitrate (1.7 g) with distilled water (80 mL). The volume is brought to 100 mL with glacial acetic acid (20 mL). An aqueous potassium iodide solution (50 % m/v, 100 mL) is mixed in with the bismuth oxynitrate. The mixture is homogenised by shaking and then stored in a dark bottle.

To prepare a working solution of the reagent, the stock solution (100 mL) is diluted with glacial acetic acid (200 mL). This solution is made up to a volume of 1 litre with distilled water (800 mL).

Appendix to Chapter III

A. Photographs of *G. superba*

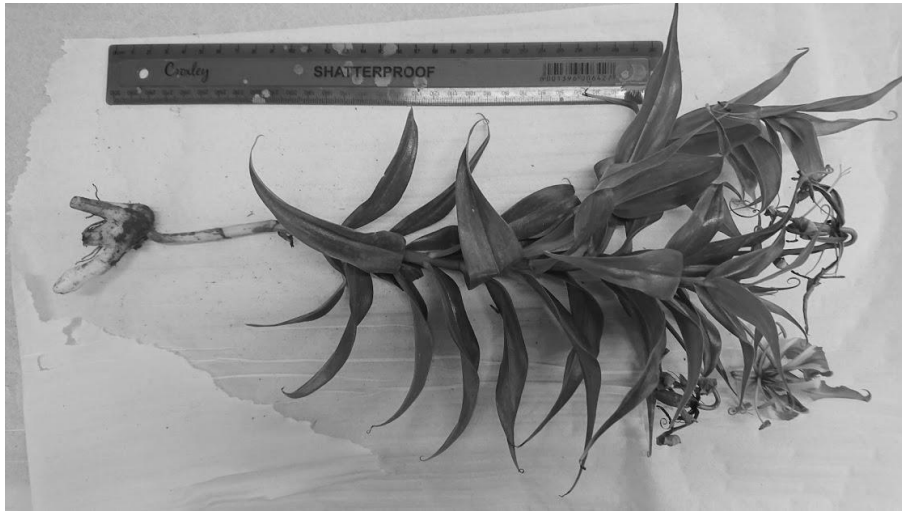


Figure A (III)-1. A full plant specimen of *G. superba*. The ruler in the image is 30.0 cm in length.



Figure A (III)-2. Rhizomes of *G. superba* that were bought at the Faraday Muti Market, Johannesburg. The label at the bottom of the bag reads “uhlamvu”, the isiZulu name for *G. superba*.

B. Library mass spectrum from the NIST mass spectral library

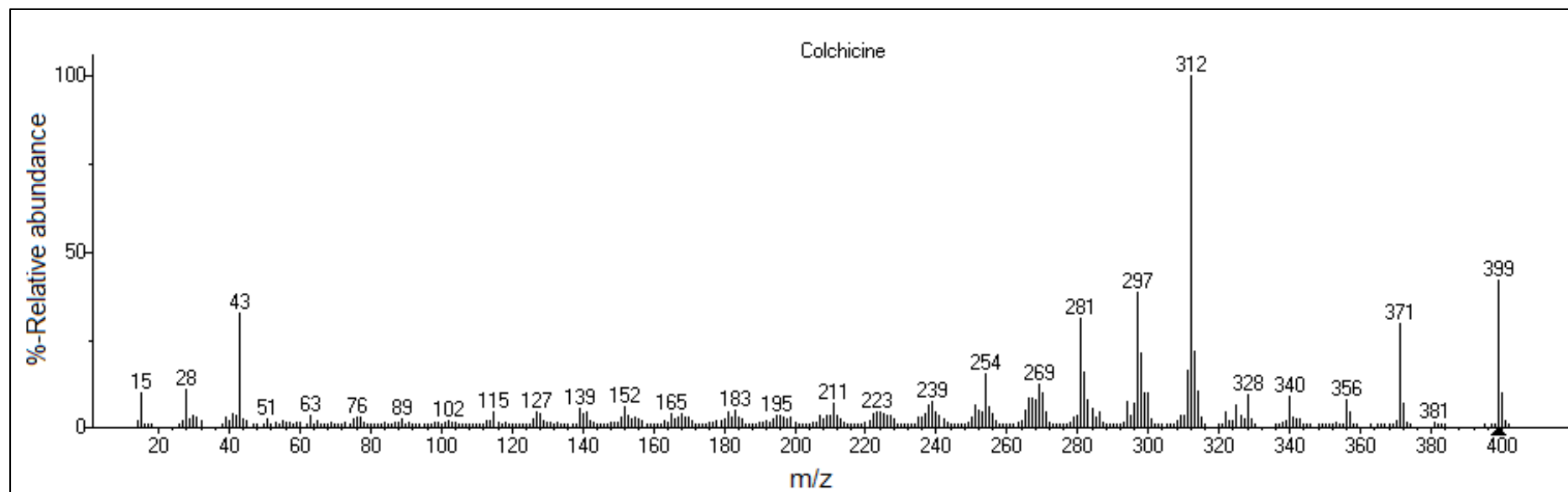


Figure A (III)-3. Electron impact ionisation (EI) mass spectrum of Colchicine from the NIST mass spectral library.

Appendix to Chapter IV

A. Methods for preparing arrow poison from *A. oppositifolia*

Table A (IV)-1. Tabulated methods for the preparation of poison from *A. oppositifolia*.

Region	Tribe (Application)	Plant components used	Method of preparation
Eastern South Africa	Zulu (poison spears for killing hyenas and feral dogs)	Root bark, wood, fruits and seeds	Pieces of wood are boiled in water. Latex from regional <i>Euphorbia</i> spp. were added. The mixture was boiled to a paste and applied to the weapons.
Zimbabwe	Masurwa, Ndebele (poison arrows for hunting)	Wood, extracted plant juices	<p>Poison glands from cobras or mambas are dried and milled to a powder. This is added to an aqueous extract of the plant and slowly boiled to a concentrated paste.</p> <p>Pieces of <i>A. oppositifolia</i> wood is also used in a similar manner to the Zulu of eastern South Africa. A paste made from <i>B. disticha</i> extracts is sometimes also mixed into the poison.</p>
Northern Cape (RSA)	Various regional indigenous tribes	Extracted plant juices	As in Zimbabwe, the venom from a snake's poison glands is used, but here it is left to concentrate by drying in the sun. The paste obtained is mixed with the paste made from the aqueous extract of <i>A. oppositifolia</i> .
Eastern Cape (RSA) & Kalahari	San (poison arrows for hunting) – The poison is specifically applied <i>behind</i> the arrowhead to prevent accidental poisoning.	Plant cuttings (wood and leaves)	Cuttings are made from the plant and immersed in water. The preparation is boiled for at least ten hours to obtain a viscous paste.



Figure A (IV)-1. A typical hunting kit used by the San of KwaZulu-Natal.

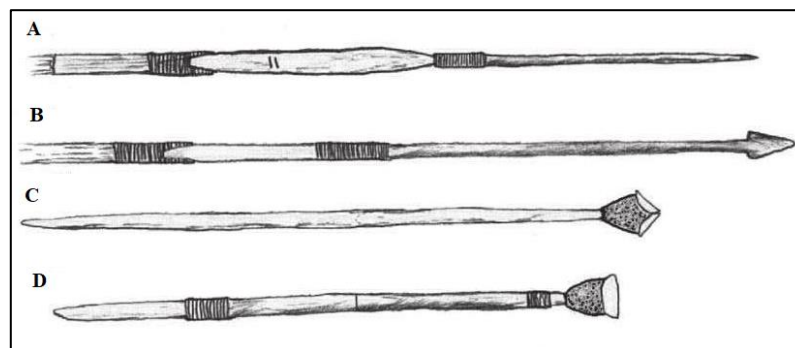


Figure A (IV)-2. Arrowheads used by various groups of San-hunters. (A) Reversible bone point (less risk of stabbing the hunter with a poisoned arrow accidentally); (B) Bone arrowhead with tang; (C & D) Sharpened stone mounted on bone.

B. Photographs of *A. oppositifolia*



Figure A (IV)-3. (1) *A. oppositifolia* bought at the Faraday Muti Market, (2) *A. oppositifolia* cut from a tree on the UP Hatfield Campus. The bar is 15.0 cm in length.

C. GC-MS data related to the analysis of derivatised hydrolysis products

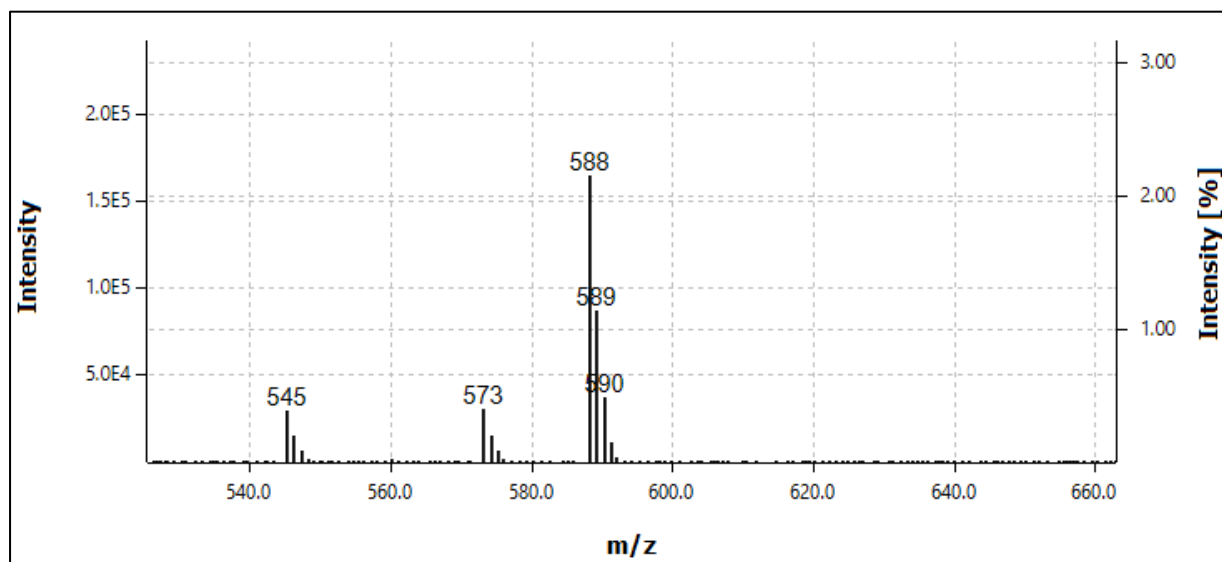


Figure A (IV)-4. Close-up of the mass spectrum measured for band D7 in the analysis of a reference standard for Acovenoside A.

Appendix to Chapter V

A. Photographs of *U. sanguinea*

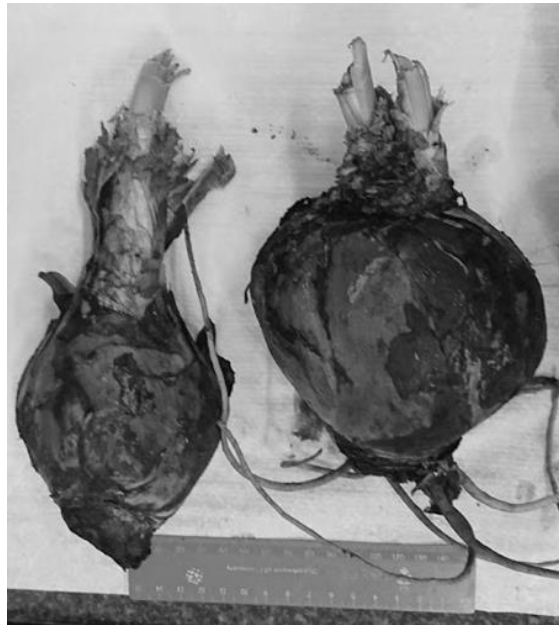


Figure A (V)-1. Two *U. sanguinea* bulbs sourced from the Faraday Muti Market in Johannesburg, ZA. The green ruler in the image is 15.0 cm in length.



Figure A (V)- 2. A specimen of *U. sanguinea* prior to flowering. This specific specimen was cultivated as voucher specimen for this study.